High Throughput Screening to Identify, Develop and Analyse Inositol Phosphorylceramide Synthase Inhibitors as Novel Antileishmanials

NORCLIFFE, JENNIFER,LOUISE

High Throughput Screening to Identify, Develop and Analyse Inositol Phosphorylceramide Synthase Inhibitors as Novel Antileishmanials

A thesis submitted in partial fulfilment of the requirements for the degree of Doctor of Philosophy from the University of Durham by

Jennifer Louise Norcliffe

October 2015

Department of Chemistry

Abstract

Leishmaniasis and Human African trypanosomiasis are tropical diseases caused by kinetoplastid parasites that together affect over 12 million people, with an estimated 400 million at risk worldwide. Both are potentially fatal, yet the current treatments available are expensive and many have toxic side effects. Emerging resistance to many current drugs is also a concern; novel therapeutic agents are therefore urgently required.

One novel target for drug discovery previously identified in the group is sphingolipid synthesis. Sphingolipids are ubiquitous biomolecules found in nature and are both structural membrane components and signalling molecules. Inositol phosphorylceramide synthase (IPCS) is an essential enzyme involved in kinetoplastid sphingolipid synthesis that has no mammalian equivalent, making it an attractive drug target. Whilst specific inhibitors of the fungal IPCS are known, they are unsuitable as pharmaceuticals. The overall aim of this project was to identify novel inhibitors of this enzyme that could be further investigated as potential antikinetoplastid drugs.

The first stage involved the construction of *Saccharomyces cerevisiae* strains as expression systems of the kinetoplastid IPCS enzymes. The strain complemented with the *Leishmania major* enzyme was subsequently used in the development and optimisation of a robust high throughput screening (HTS)-compatible assay. This was used to screen the 1.8 million compound library stored at the GlaxoSmithKline research site in Tres Cantos in what is believed to be the largest screening project undertaken by an academic group to date. 500 compounds were identified as selective inhibitors of the *L. major* IPCS enzyme, and 216 of these were selected for additional investigation.

Further compound triage was achieved by means of a screening process involving multiple *in cellulo* assays against both *Leishmania* parasites and mammalian cells. Six compounds demonstrating both high potency and selectivity were identified. Following additional biochemical testing, the two most potent compounds were found to share a common benzazepane chemical structure. Investigation of analogues of these compounds permitted the identification of preliminary structure-activity relationship data, which identified several possible avenues for further investigation.

Acknowledgements

First and foremost I would like to thank my supervisors Dr Paul Denny and Prof. Patrick Steel for the opportunity to work on a fantastic project. Their guidance and support have been unfaltering, even when things didn't go to plan and life got in the way. I am also grateful to Durham University for the financial support of a Durham Doctoral Scholarship, without which I wouldn't be here, and to the Tres Cantos Open Lab Foundation and the Wellcome Trust for backing the project.

This project would not have been possible without our collaborators, so my thanks go to: Pepe Fiandor, Silvia Gonzalez and the team at GSK; Vanessa Yardley and the team at the London School of Hygiene and Tropical Medicine; and Monica Delpogetto and the team at Aptuit. Thanks also to everyone who made my trip to GSK possible, in particular to Beatriz Cosme for giving up evenings and weekends to help me during boiler breakdowns and electrical emergencies. My research there would not have been possible without the help of the group – Julio Martin, Emilio Alvarez, Ana Bardera, Paco De Dios and Vanessa Barroso – as well as the Biological Reagent and Assay Development (BRAD) and Sample Management and Technology (SMTech) groups. I am eternally grateful to you all. Special thanks also to Gonzalo Colmenarejo of the Computational and Structural Chemistry group for sparing me the task of 1.8 million data points worth of number crunching.

I would also like to thank all members, both past and present, of Lab 229 and office 231 for their continued support, patience and baked goodies throughout the years – I will miss our Thursday morning Bake Off chat immensely. I am especially grateful to Hayley and Julie, who were there when things were at their worst. Special thanks also to: John Mina, for providing extensive training in cell culture and molecular biology techniques; Frances Chadbourne, for teaching me the ins and outs of working with parasites; and Chris Brown, for enduring the dreaded microsome prep with me on a number of occasions. I must also thank Gina and Becky – I couldn't have asked for better undergraduate students to work with. I wish you both the best of luck in your own PhD endeavours.

Last but by no means least, I am eternally grateful to my family:

To my granddad, Peter Drake, who used to make the best birthday cakes and now gives the best hugs.

To auntie Louise and uncle Paul, who always knew when I needed a postcard through the letterbox to cheer me up, and when I needed help were always ready with cocktails / power tools as required.

To my brother Gareth and new sister-in-law Fiona, who put up with me being the third wheel and tagging along on everything from cinema trips and games nights to house viewings and car buying excursions.

And finally, to my mum and dad, Caroline and Martyn. You never lost faith in me, even when I lost faith in myself. I'll never be able to put into words how much your endless support means to me.

Dedication

To my grandparents, who saw me start but didn't see me finish.

Kathleen Norcliffe

7th June 1939 – 29th March 2014

~

Ronnie Norcliffe

21st July 1936 – 15th August 2014

~

Olwyne Drake

5th April 1935 – 12th November 2014

I miss you every day. I hope I've made you proud.

Declaration

The work presented herein was carried out by the author in the Department of Chemistry at the University of Durham between October 2011 and August 2015, and in el Centro de Investigación Básica at GlaxoSmithKline, Tres Cantos between February 2012 and June 2012. Additional work was completed by our collaborators at GSK, Tres Cantos and The London School of Hygiene and Tropical Medicine, and is stated and acknowledged within. No part of this work has been submitted for any other degree at this or any other University.

Statement of Copyright

Contents

Abbreviations

5FOA	5-Fluoroorotic acid
α-AUR1	α *ade*$^{-}$.*lys*$^{-}$.*leu*$^{-}$.Δ*aur1*$^{-}$ complemented with pEL.*ScAUR1*$^{+}$
α-*Lmj*	α *ade*$^{-}$.*lys*$^{-}$.*leu*$^{-}$.Δ*aur1*$^{-}$ complemented with pEL.*LmjIPCS*$^{+}$
α-*Tb*1	α *ade*$^{-}$.*lys*$^{-}$.*leu*$^{-}$.Δ*aur1*$^{-}$ complemented with pEL.*TbSLS1*$^{+}$
α-*Tb*4	α *ade*$^{-}$.*lys*$^{-}$.*leu*$^{-}$.Δ*aur1*$^{-}$ complemented with pEL.*TbSLS4*$^{+}$
AbA	Aureobasidin A
AFU	Arbitrary fluorescence units
AmB	Amphotericin B
ATP	Adenosine triphosphate
BBB	Blood-brain barrier
BSA	Bovine serum albumin
CHAPS	3-[(3-Cholamidopropyl)dimethylammonio]-1-propanesulphonate
CL	Cutaneous leishmaniasis
CL_{int}	Intrinsic clearance
cLogP	Calculated logarithm of the 1-octanol−water partition coefficient
CoA	Coenzyme A
DAG	Diacylglycerol
DMSO	Dimethyl sulphoxide
DNA	Deoxyribonucleic acid
DNAUC	Dose normalised area under the curve
DNDi	Drugs for Neglected Diseases initiative
ED_{50}	Half maximal effective dose
eGFP	Enhanced green fluorescent protein
ELISA	Enzyme-linked immunosorbent assay
ER	Endoplasmic reticulum
F+	False positive
F−	False negative
FAD	Flavin adenine dinucleotide (oxidised form)
$FADH_2$	Flavin adenine dinucleotide (reduced form)
FDGlu	Fluorescein di-(β-D-glucopyranoside)
FLIPR	Fluorescent imaging plate reader
FRET	Fluorescence resonance energy transfer
GFP	Green fluorescent protein
GPCR	G-protein coupled receptor
GSK	GlaxoSmithKline
HAT	Human African trypanosomiasis

HBSS	Hank's balanced salt solution
HIV	Human immunodeficiency virus
HPTLC	High performance thin layer chromatography
HTS	High throughput screening
IC_{50}	Half maximal inhibitory concentration
IPC	Inositol phosphorylceramide
IPCS	Inositol phosphorylceramide synthase
LDL	Low-density lipoprotein
LHS	Left hand side
*Lmj*IPCS	*Leishmania major* inositol phosphorylceramide synthase
LogP	Logarithm of the 1-octanol−water partition coefficient
LPP	Lipid phosphate phosphatase
LS-BSF	Long slender bloodstream form
LSHTM	London School of Hygiene and Tropical Medicine
MCL	Mucocutaneous leishmaniasis
MCS	Multiple cloning site
MW	Molecular weight
$NADP^+$	Nicotinamide adenine dinucleotide phosphate (oxidised form)
NADPH	Nicotinamide adenine dinucleotide phosphate (reduced form)
NECT	Nifurtimox-eflornithine combination therapy
NTD	Neglected tropical disease
OD	Optical density
PCR	Polymerase chain reaction
PDB	Protein Data Bank
pED_{50}	$-\log_{10}(ED_{50})$
pEL	pESC-LEU
PFI	Property forecast index
PI	Phosphatidylinositol
pIC_{50}	$-\log_{10}(IC_{50})$
PKDL	Post-kala-azar dermal leishmaniasis
R_f	Retardation factor
RFP	Red fluorescent protein
RHS	Right hand side
SAR	Structure-activity relationship
SI	Selectivity index
SLS	Sphingolipid synthase
SMS	Sphingomyelin synthase
SODA	Statistical online data analysis
SS-BSF	Short stumpy bloodstream form
*Tb*SLS1	*Trypanosoma brucei* sphingolipid synthase isoform 1

*Tb*SLS4	*Trypanosoma brucei* sphingolipid synthase isoform 4
Tm	Melting temperature
TPP	Target product profile
uHTS	Ultra-high throughput screening
VL	Visceral leishmaniasis
WHO	World Health Organisation
Z′	Z-prime factor

Chapter 1

Introduction

1.1 Thesis Synopsis

The aim of this work is to identify novel small molecule inhibitors of the inositol phosphorylceramide synthase (IPCS) enzyme from trypanosomatid parasites, with a particular focus on *Leishmania major*. This enzyme represents a promising drug target against the diseases caused by these parasites. This chapter presents a review of the areas of work central to this project, beginning with an overview of the diseases leishmaniasis and human African trypanosomiasis, which are caused by trypanosomatid parasites. The structure and function of sphingolipids will subsequently be summarised, along with the differences in metabolism observed between different kingdoms; these differences form the basis of this project. Finally, the process of drug discovery by high throughput screening (HTS) will be discussed.

Chapter 2 reports the construction and testing of yeast strains engineered to produce the trypanosomatid IPCS enzymes, whilst the development and implementation of the HTS-compatible assay is covered in chapter 3. Chapter 4 reports the identification of a lead compound family following further screening, with structure-activity relationships (SARs) being explored in chapter 5. Conclusions and future work are discussed in chapter 6, whilst materials and methods are described in chapter 7.

1.2 Neglected Tropical Diseases

The neglected tropical diseases (NTDs) are a group of infections which currently affect more than 1 billion people globally,[1] with the majority of those affected living in developing countries characterised by poverty, poor sanitation and a lack of education

and appropriate medical care.[2, 3] It is estimated that NTDs cause in the region of 500,000 deaths per annum,[4] as well as being responsible for approximately 48 million disability-adjusted life years lost each year.[5] NTDs have also been linked to an increased susceptibility to the human immunodeficiency virus (HIV), with widespread co-infections observed across sub-Saharan Africa.[6]

Of the diverse group of NTDs, 17 have been prioritised by the World Health Organisation (WHO); these diseases are endemic in 149 countries and cost developing economies billions of dollars each year.[1] These 17 diseases are collectively caused by four distinct types of infective pathogen; helminth worms, viruses, bacteria and protozoa. In this last group, the three diseases – leishmaniasis (*Leishmania* spp.), human African trypanosomiasis (HAT, *Trypanosoma brucei*) and American trypanosomiasis (Chagas disease, *Trypanosoma cruzi*) – are caused specifically by trypanosomatid parasites.

Trypanosomatids belong to the phylogenetic class Kinetoplastida, a group of single-cell, flagellated parasites that are distinguished by the presence of a region containing a large mass of mitochondrial DNA, termed the kinetoplast, in their single mitochondrion.[7] There are two separate orders within the Kinetoplastida class (Figure 1–1): Trypanosomatidae, which are characterised by possessing only a single flagellum and a small kinetoplast; and Bodonidae, which are biflagellate and possess a larger kinetoplast.[8] Another feature of the trypanosomatid parasites is that they are dixenous in nature, meaning they require two obligatory hosts to complete their life cycle.[9]

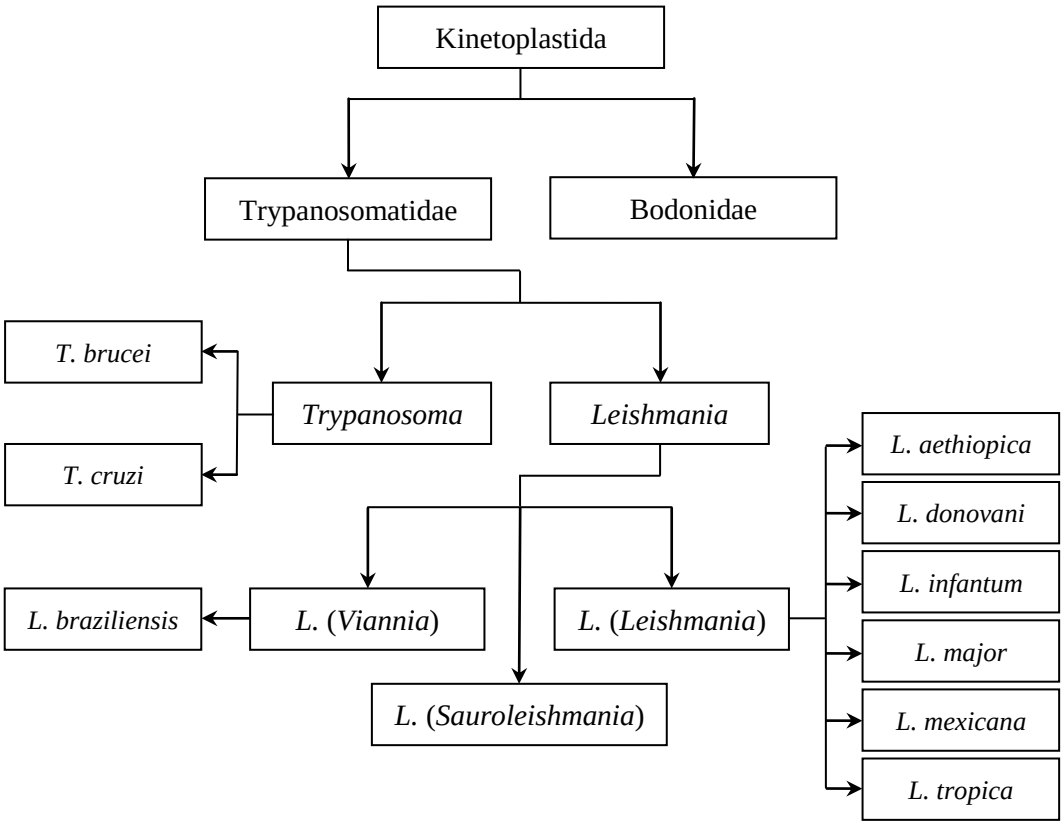

Figure 1–1: The taxonomy of Kinetoplastida (for clarity, the only species of *Leishmania* shown are those of major medical importance to humans)

1.2.1 Leishmaniasis

1.2.1.1 Introduction and Clinical Manifestations

There are more than 30 known species of *Leishmania*; these can be classified into 3 distinct subgenera (Figure 1–1). *L*. (*Leishmania*) spp. and *L*. (*Viannia*) spp. differ slightly in their colonisation of the insect host, whilst *L*. (*Sauroleishmania*) spp. infect reptile rather than mammalian hosts.[10] In total, 20 species are known to be pathogenic to humans; these are distributed across 98 countries on 5 continents (Figure 1–2)[11, 12] and in total 310 million people are currently at risk of infection. It is estimated that there are approximately 1.3 million new cases annually, although less than half of these are officially recorded with data from Africa being especially sparse.[13] There are three distinct forms of leishmaniasis, with the clinical manifestations differing according to the infective *Leishmania* species.

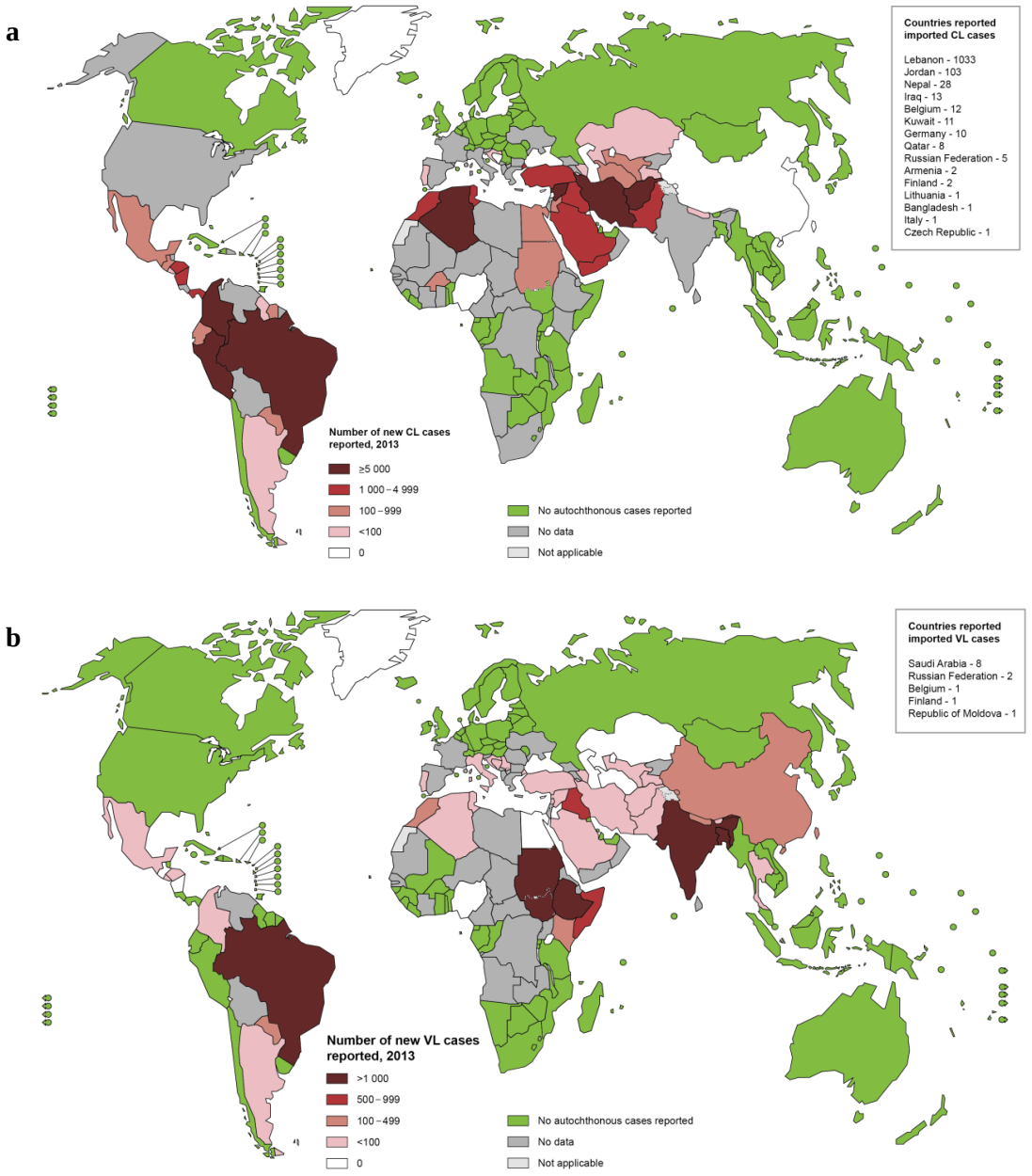

Figure 1–2: The global distribution of (a) cutaneous leishmaniasis (reproduced from WHO[11] with permission) and (b) visceral leishmaniasis (reproduced from WHO[12] with permission)

Cutaneous leishmaniasis (CL) is the most common and least severe form of leishmaniasis and is predominantly caused by the Old World species *L. aethiopica*, *L. major* and *L. tropica* in the Eastern hemisphere, and by the New World species *L. braziliensis* and *L. mexicana* in the Western hemisphere.[14] The disease first presents, often after two weeks to two months, as a papule at the site of infection which is commonly the exposed skin of the face, arms or legs. This then evolves to form a nodular plaque before progressing to a large, ulcerative lesion;[15] although this is usually painless, it can become uncomfortable if it is located close to a joint or if it becomes infected. It is not uncommon for satellite papules or lesions, as well as subcutaneous

induration, to develop around the site of the primary lesion.[16] The majority of cases of CL regress and cure spontaneously, although this often takes in excess of 12 months. As a result, patients are often left with permanent scarring which, whilst not generally debilitating, can be highly disfiguring.

Mucocutaneous leishmaniasis (MCL) is predominantly a disease associated with New World species of *Leishmania* with the majority of cases occurring in Brazil, Bolivia and Peru; however, cases due to the Old World species *L. donovani*, *L. infantum* and *L. major* have also been reported.[17] The disease usually manifests several years after the presentation of the primary lesions of CL as an infection of the mucosal membranes. The progression of the disease is slow in comparison to CL, with the mucosal lesions developing over a period of several years.[18] Eventually these lesions can lead to the destruction of the mucosa and cartilage of the mouth, nose and throat which can, in some cases, be fatal if left untreated.[14] Even if treated successfully, patients can be left with severe disfigurement of the face which may result in social stigmatism.[19]

Visceral leishmaniasis (VL), also known as kala-azar, is the most severe form of the disease and is usually fatal within 2 years if left untreated.[20] The primary causative agents of the disease are *L. donovani*, which is prevalent in Africa and the Indian subcontinent, and *L. infantum*, which is responsible for cases in Mediterranean regions and the New World.[21] New World cases of VL were historically attributed to *L. chagasi*, but this species is now known to be *L. infantum* and the names are used synonymously.[22] Visible symptoms include prolonged fever and drastic weight loss, although the major damage occurs internally. Enlargement of the liver and spleen (hepatomegaly and splenomegaly respectively) and pancytopenia are the major clinical characterisations.[23] Gastrointestinal bleeding and liver or heart failure are the most common causes of death in patients,[21] with the disease presenting an estimated annual death toll of 40,000–50,000.[24] Even if treated successfully, a common outcome of VL caused by *L. donovani* is the development of the chronic disease post-kala-azar dermal leishmaniasis (PKDL), which manifests as a maculopapular and nodular rash. The disease acts as a reservoir for *Leishmania* parasites and usually requires an additional course of treatment.[25] In addition, VL is the form of the disease most closely associated

with HIV co-infection, with the parasite acting as an opportunistic pathogen of immunocompromised patients.[26]

1.2.1.2. Life Cycle

The life cycle of the *Leishmania* species is shown in Figure 1–3.[27] It can be described as both dixenous, meaning the life cycle is split between two different host species, and dimorphic, with the parasite exhibiting morphologically distinct forms in the different hosts. The cycle can proceed anthroponotically (utilising only human reservoirs) or zoonotically (utilising multiple mammals as reservoirs).[28]

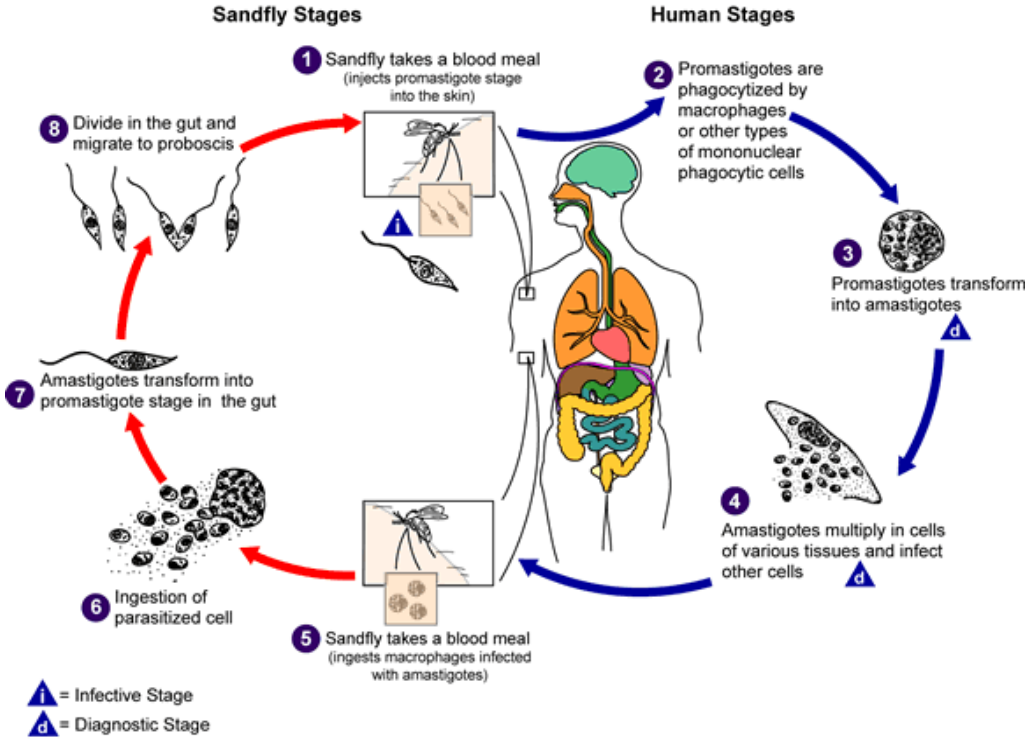

Figure 1–3: The life cycle of *Leishmania* spp. (reproduced from CDC[27] with permission)

The cycle begins with the transfer of metacyclic (infective or stationary phase) promastigote parasites to the human host (1) via a bite from a female phlebotomine sandfly, the genus of which is dependent on the geographical location. Old World leishmaniasis in the Eastern hemisphere is spread by sandflies of the genus *Phlebotomus* whilst the New World disease in the Western hemisphere (primarily in South America although cases have been reported as far north as Texas) is transmitted by sandflies of the genus *Lutzomyia*.[10, 29] The parasites are passed into the bloodstream along with saliva and promastigote secretory gel, which synergistically recruit

macrophages to the site of infection.[30] Promastigotes are subsequently phagocytosed by the recruited macrophages and skin dendritic cells (2)[31] and, within 72 hours, undergo metamorphosis to the amastigote form (3) induced by the increase in temperature and acidity (in comparison to the sandfly midgut).[32, 33] The amastigote form, which is the cause of the disease in humans, is smaller and more ovoid in shape with a severely diminished flagellum. This flagellum is non-motile and is thought instead to be involved in host-parasite signalling.[34] Intramacrophage amastigotes proliferate by binary fission, eventually resulting in macrophage rupture and the release of amastigote parasites, leaving them free to infect other cells (4).

Infected macrophages and free parasites can also be ingested by a sandfly during the taking of a blood meal (5, 6). The decrease in temperature and increase in pH in the sandfly midgut (or hindgut in the case of *L.* (*Viannia*) spp.) triggers the transformation of amastigotes into flagellated procyclic (non-infective or log phase) promastigotes,[10] which are able to adhere to the midgut epithelial cells and rapidly proliferate (7).[35] Once stationary phase has been achieved procyclic promastigotes differentiate to metacyclic promastigotes (metacyclogenesis), which have an elongated body and longer flagellum. The metacyclic promastigotes subsequently migrate via osmotaxis to the proboscis (8) in preparation for transmission to a mammalian host during the sandfly's next blood meal.

1.2.1.3. Currently Available Treatments

The preferred treatment for leishmaniasis depends primarily on the form of the disease contracted and the identity of the infective species,[36] with several possible therapies (both single drug treatments and drug combinations) available. The most common of the current antileishmanials are shown in Figure 1–4.

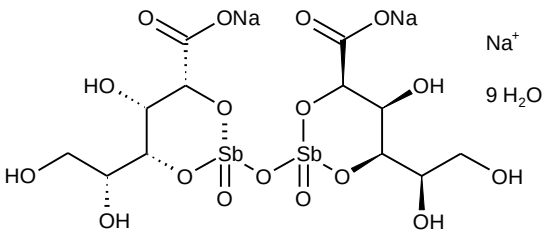

Sodium stibogluconate (**1**)

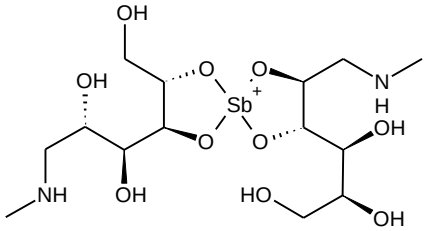

Meglumine antimoniate (**2**)

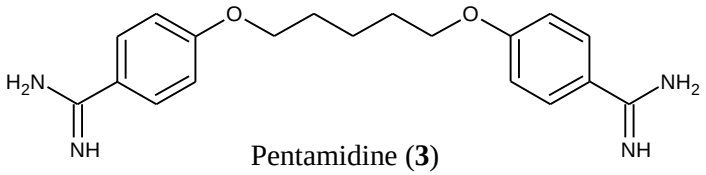

Pentamidine (**3**)

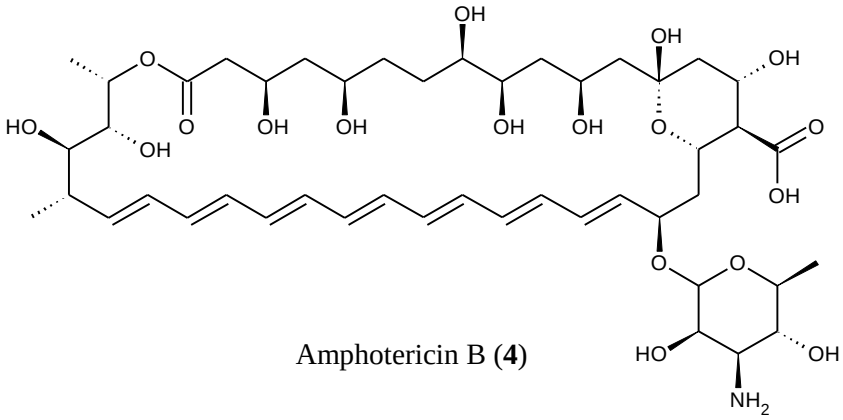

Amphotericin B (**4**)

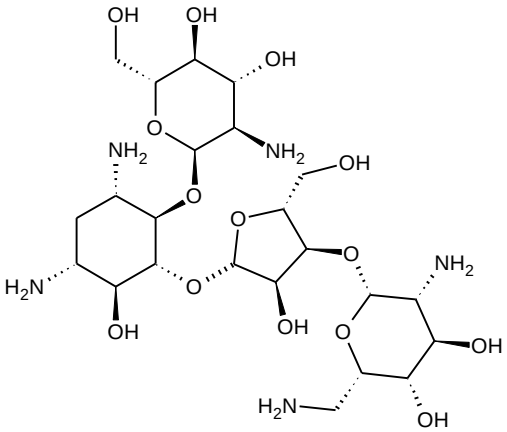

Paromomycin (**5**)

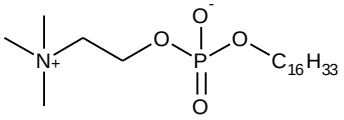

Miltefosine (**6**)

Figure 1–4: The structures of currently used antileishmanial drugs

1.2.1.3.1. Pentavalent Antimonials

Trivalent antimonial compounds were first reported for the treatment of CL and VL in 1912 and 1915 respectively.[37, 38] These compounds, however, displayed acute

toxicity and in 1922 a superior pentavalent antimonial named urea stibamine was first utilised by Brahmachari as a chemotherapeutic agent against VL.[39] Further progress over the next couple of decades resulted in the discovery of sodium stibogluconate (**1**) in 1945 and later meglumine antimoniate (**2**) which have been the primary treatments for both CL and VL for over 60 years.[40]

Despite being the preferred front line drug for the majority of *Leishmania* infections, pentavalent antimonials display an extremely poor safety profile. Common side effects range in intensity from headaches and joint or muscle pain to pancreatitis and cardiotoxicity that may be fatal.[41, 42] Both drugs also require intravenous administration at a dosage of 20 mg of Sb(V)/kg/day for 20 days and treatment is therefore lengthy, costly and painful.[43]

The mode of action of pentavalent antimonial drugs has been extensively studied but is still not thoroughly understood; there are, however, two proposed mechanisms. The first is a prodrug model and suggests that Sb(V) is biologically reduced to Sb(III), and this is the species that exhibits antileishmanial activity.[40] This reduction has been observed to be stage specific (which would explain the observation that amastigotes are more sensitive to Sb(V) than promatigotes) with parasite susceptibility to Sb(V) correlating with the level of Sb(V) reducing activity.[44] The second proposed mode of action suggests that Sb(V) possesses intrinsic biological activity; sodium stibogluconate has been shown to specifically inhibit type 1 DNA topoisomerase in *L. donovani*, whilst Sb(III) does not.[45]

As with many antimicrobials, one of the major challenges facing pentavalent antimonials is resistance. The current recommended dosage is now much greater than in historic cases (up to the 1970s, a dosage of 10 mg of Sb(V)/kg/day for 10 days was utilised)[40] and in the year 2000 it was observed that up to 60% of cases in India did not respond to pentavalent antimonial treatment due to resistance.[46] Multiple studies of antimonial resistance have suggested the mechanisms to be multifactoral, meaning it is not a problem that will be easily overcome.[47]

1.2.1.3.2. Pentamidine

Pentamidine (**3**) was first reported as a treatment for VL in India in 1949.[48] Typically administered as a formulation, treatment requires intramuscular or intravenous injection at a dosage of 4 mg/kg/day for pentamidine methanesulphonate or 7 mg/kg/day for pentamidine isethionate.[49] There are a number of side effects, the most serious of which is the irreversible condition diabetes mellitus type 1.[50] Other side effects include fever, myalgia, myocarditis, hypotension, hypoglycaemia and renal toxicity.[51]

The mode of action of pentamidine is not fully understood, although the mitochondrion is known to be involved. This is demonstrated by the observation that resistant *Leishmania* parasites show a reduction in pentamidine accumulation in the mitochondrion compared to wild types due to an increase in drug efflux.[52] The drug has also been shown to bind preferentially to the kinetoplast DNA due to the high adenine-thymine content, which could result in disrupted replication or transcription.[51, 52]

As mentioned above, pentamidine, like the pentavalent antimonials, faces problems due to resistance. In the 1990s, pentamidine was abandoned as the second line treatment for VL in India due to the declining response, high costs and numerous side effects.[53, 54] However, the drug remains the first line treatment for CL caused by *L. guyanensis* in French Guiana, where a single injection of pentamidine isethionate results in a cure rate above 75%.[55]

1.2.1.3.3. Amphotericin B

Amphotericin B (AmB, **4**) is a polyene antibiotic first isolated from *Streptomyces nodosus* in 1955,[56, 57] and was first used to treat patients with VL in Brazil in 1963.[58] Treatment requires intravenous injection, and the drug is usually administered as a complex with deoxycholate. Due to the multiple side effects (which include fever, renal failure and potentially fatal cardiovascular issues)[59] AmB has historically been used as a second line treatment for leishmaniasis; however, increased resistance to pentavalent antimonials and pentamidine resulted in the adoption of AmB as the first line treatment

against VL in India in the 1990s.[60] AmB deoxycholate is highly efficacious, displaying a 99% cure rate when administered at 1 mg/kg/day for 20 days.[61]

AmB can also be administered as a liposomal formulation. This exhibits milder side effects than AmB deoxycholate due to an increased uptake of the drug by the reticuloendothelial system; this formulation targets the drug to the cells harbouring the parasite and reduces renal uptake of the drug, resulting in lower levels of nephrotoxicity.[53, 62] When it first came onto the market the high cost of this formulation precluded its use in the majority of countries where it was needed the most, meaning the cheaper but more toxic AmB deoxycholate was still generally used.[63] An agreement made in 2005 between the WHO and the manufacturer, however, has lowered the cost significantly and made the drug much more widely accessible.[64]

AmB functions by binding ergosterol, the predominant sterol component in *Leishmania* plasma membranes,[65] for which it has a higher affinity than the cholesterol that is predominant in mammalian membranes.[66] This initially results in the formation of non-aqueous pores which cause an increase in permeability of the cell membrane for monovalent cations, resulting in uneven ionic distribution.[67] At larger concentrations of AmB aqueous pores form and allow greater movement of ions, protons and salts across the membrane, resulting in osmotic lysis.[68] It has also been reported that the interaction of AmB with sterols in macrophage membranes actively prevents the entry of *Leishmania* parasites into the cell, which would help prevent the spread of the infection in the patient.[65]

In comparison to the other antileishmanial drugs, there has been little evidence over the years to suggest *Leishmania* resistance. However, in 2012 an AmB-resistant clinical isolate of *L. donovani* was identified and was observed to have membranes completely devoid of ergosterol.[69] This, along with the increased usage of liposomal formulations of AmB that have longer half lives, means that the increase of AmB resistance in the near future is a real possibility.[66]

1.2.1.3.4. Paromomycin

Paromomycin (**5**) is an aminoglycoside first isolated in the 1950s from *Streptomyces krestomuceticus*,[70] and has been used to treat CL since the 1960s and VL since 1990.[71, 72] Whilst CL can be treated by topical application of creams containing paramomycin,[73] when treating VL the drug must be administered parenterally at a dosage of 11 mg/kg/day for 21 days.[74] Compared to other antileishmanials paromomycin exhibits few side effects, the most common of which are injection site pain (or itching/tenderness if topically applied), mild bleeding and, rarely, ototoxicity.[54]

The mode of action of paromomycin is thought to be complex. It has been shown to bind to the parasite ribosome and drastically increase the levels of misreading of mRNA during protein synthesis, whilst mammalian systems are affected at a much lower level;[75] this could result in the formation of defective proteins which could hinder, or be actively detrimental to, parasite survival. The drug has also been shown to affect vesicle-mediated trafficking, lipid metabolism and membrane fluidity.[76, 77]

Paromomycin has not been as widely utilised as the other major antileishmanials and hence widespread resistance has not yet been observed, although clinical isolates of *L. aethiopica* from patients given the drug showed decreased sensitivity *in vitro* following treatment.[78] This acquired, or secondary, resistance is of concern for patients with VL/HIV co-infection due to the high relapse rate.[70] Resistance is also readily inducible *in vitro*.[79]

1.2.1.3.5. Miltefosine

The final drug of choice for treating leishmaniasis is the phospholipid-like compound miltefosine (**6**), which was originally developed to prevent the spread of breast cancer.[80] However, in 1996 it was shown to possess antileishmanial activity and in 2002 was first orally-available drug approved to treat VL in India.[54, 81] A dosage of 100 mg/kg/day for 28 days results in cure rates up to 94%,[82] whilst a dosage of 2.5 mg/kg/day for 28 days can be used to treat CL, although the effectiveness is species dependent.[83] The most common side effects of the drug are gastrointestinal symptoms such as nausea, vomiting, abdominal pain and diarrhoea, and less frequent effects

include hepatotoxicity and nephrotoxicity.[84] Miltefosine is also teratogenic and therefore cannot be administered to pregnant women.[85]

As with many of the antileishmanials, the mode of action of miltefosine is not fully understood. Evidence of apoptosis-like cell death, including nuclear condensation and DNA fragmentation, has been observed in both promastigotes and amastigotes in response to the drug; however, the mechanism by which it achieves this remains unclear.[86] Another hypothesis suggests that miltefosine inhibits the synthesis of phosphatidylcholine (PC), an integral membrane component that is also involved in cell signalling.[84] Other suggestions for possible effects include perturbation of lipid metabolism, mitochondrial dysfunction and, controversially, immunostimulation.[87]

As with paromomycin, resistance to miltefosine can easily be induced by drug pressure *in vitro*, but clinical cases are rare.[88] However, it is possible for susceptibility to decrease during treatment, especially in HIV co-infection cases where relapse occurs.[89] The long half life of miltefosine also encourages resistance and this fact, combined with the expense of treatment, suggests that miltefosine may be short lived as an effective antileishmanial drug.[90]

1.2.1.3.6. Additional Treatments

Whilst the treatments described above are by far the most commonly utilised therapies against leishmaniasis, there are several additional drugs that are used on a smaller scale. These include, but are not limited to: ketoconazole, an orally available antifungal agent primarily used in the treatment of CL;[91] sitamaquine, an orally available compound that showed high efficacy against VL in recent clinical trials;[92] dapsone, an orally available drug originally used to treat leprosy and repurposed for CL;[93] and imiquimod, a topically-applied drug that is highly effective when used as part of a combination therapy against antimonial-resistant CL.[94]

To date, however, there is no singular 'wonder drug' for the treatment of leishmaniasis, with all of those discussed above either displaying critical levels of human toxicity or being inaccessible, either geographically or financially, to those who most require them. Although numerous drug targets in various *Leishmania* species have

been proposed, there have been relatively few medicinal chemistry campaigns to investigate these further;[54] for example, the Drugs for Neglected Diseases initiative (DNDi) is only investigating 3 new compounds as potential preclinical candidates whilst the rest of the projects are based on using new combinations of currently available drugs.[95] Whilst this approach may produce improved treatment regimens in the short term, the long term aim is to produce novel drugs which better fit the proposed target product profiles (TPPs) that have been published by the DNDi. These are lists of essential and desirable attributes for novel drugs, with requirements including oral administration (or topical for CL), a short (< 14 day) treatment schedule, zero fatalities from the treatment itself and activity against multiple species.[96, 97] No current drug comes close to meeting most of these criteria and this fact, combined with the expanding emergence of resistance and lack of suitable vaccines,[98] highlights the urgent necessity for novel, potent antileishmanial drugs.

1.2.2 Human African Trypanosomiasis

1.2.2.1 Introduction and Clinical Manifestations

Trypanosoma brucei, the causative agent of HAT (also known as African sleeping sickness), was first discovered by Bruce in 1894 and subsequently named in his honour in 1899.[99] Later work identified two distinct subspecies that are geographically isolated; *T. brucei gambiense* is prevalent in central and Western Africa,[100] whilst *T. brucei rhodesiense* is dominant in Eastern and Southern Africa (Figure 1–5).[101] More than 60 million people are at risk of infection in 36 sub-Saharan African countries, with actual numbers of cases varying drastically over the years.[102] The disease was brought under control in the 1960s; however, this was followed by an epidemic that lasted until the late 1990s, and at the height of this it was estimated that up to 300,000 new cases arose each year. This trend was reversed in the early 21st century, and in 2009 the number of reported cases dropped below 10,000 for the first time in 50 years. Even fewer cases are reported today, although not all cases are documented and it is estimated that around 20,000 cases occur annually.[103]

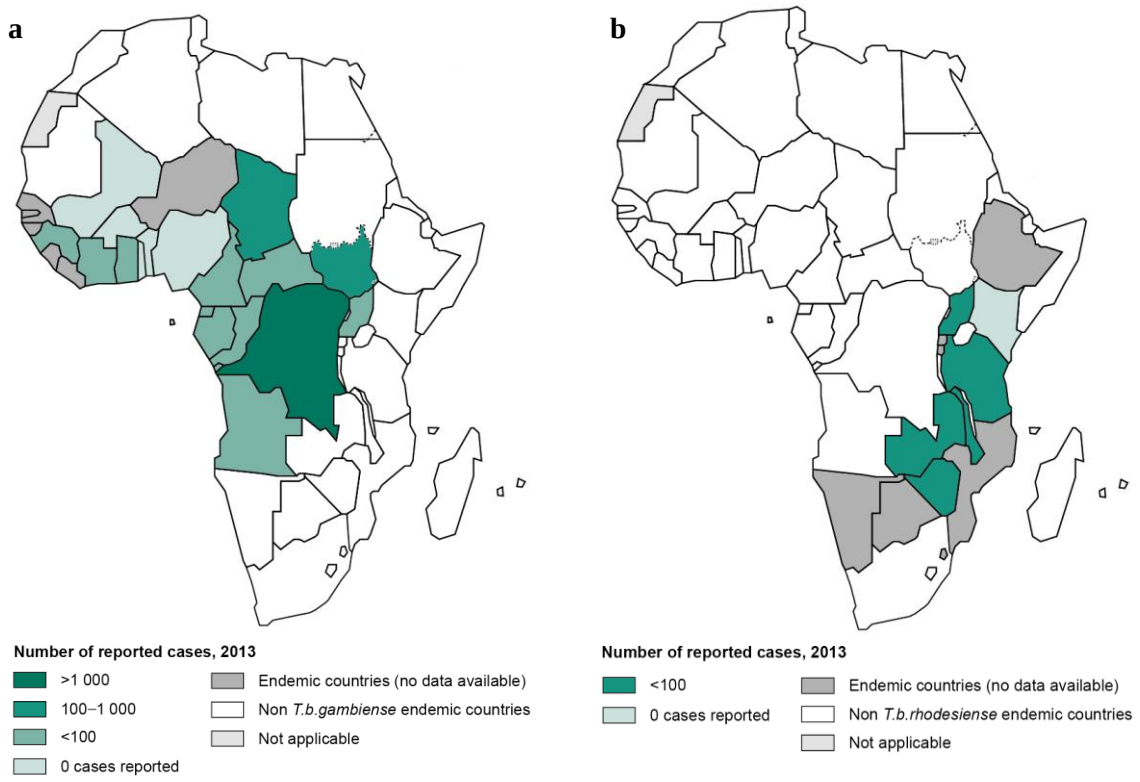

Figure 1–5: The distribution of HAT caused by (a) *T. brucei gambiense* (reproduced from WHO[100] with permission) and (b) *T. brucei rhodesiense* (reproduced from WHO[101] with permission)

The disease manifests in two forms depending on the infective species. *T. brucei gambiense*, which is responsible for more than 98% of cases, results in a chronic illness which may be a- or pauci-symptomatic for months or even years, whilst *T. brucei rhodesiense* causes acute illness with more than 80% of untreated cases resulting in death within 6 months of infection.[104] Both forms of the disease are ultimately fatal if left untreated; however, cases where infected individuals have remained asymptomatic for up to 15 years have been reported.[105]

Despite their differing rates of progression, both diseases are clinically presented in the same two recognised stages. The first, known as the early or hemolymphatic stage, usually occurs 1–3 weeks after infection and entails fatigue, malaise, headaches, arthralgia and weight loss as the parasites invade the lymph and systemic organs. In addition, fever and vomiting may also occur and frequently result in the disease being misdiagnosed as malaria.[106] If left untreated, the parasites will eventually cross the blood-brain barrier (BBB) and invade the central nervous system, marking the onset of the late (or encephalitic) stage of the disease. This results in a broad spectrum of symptoms including: psychiatric disturbances ranging from mild conditions, such as

lassitude and irritability, to violence and hallucinations; loss of motor function including, in many cases, the ability to walk and talk; and sensory involvement such as pruritus and hyperaesthesia, with the latter being particularly common in European sufferers.[102, 107, 108] Finally, the patient descends into the characteristic sleep disturbances that give the disease its name. This is accompanied by seizures, cerebral oedema, coma, systemic organ failure and eventually death.

1.2.2.2. Life Cycle

The life cycle of *T. brucei gambiense* and *T. brucei rhodesiense* is shown in Figure 1–6.[109] As with *Leishmania* spp., the life cycle is dixenous involving both an insect and mammalian host. Due to the chronic nature of the disease caused by *T. brucei gambiense* the main reservoir of the parasites is likely to be human, whereas *T. brucei rhodesiense* requires a bovid reservoir because of the acute nature of the infection.[110]

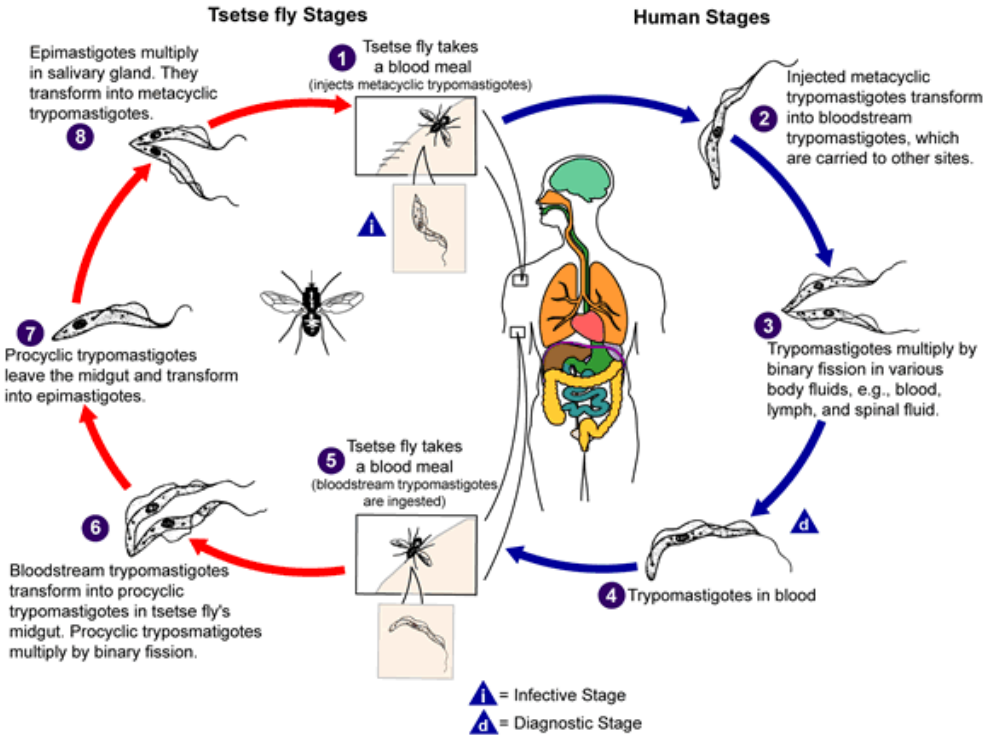

Figure 1–6: The life cycle of *T. brucei gambiense* and *T. brucei rhodesiense* (reproduced from CDC[109] with permission)

As with *Leishmania* spp., the cycle begins with the transfer of metacyclic trypomastigote parasites to the human victim via a bite from an insect vector (1) which, in this case, is a tsetse fly of the genus *Glossina*. More than 20 species of *Glossina* are responsible for disease transmission; these species have adapted to a wide range of

habitats which accounts for the highly endemic nature of the disease.[111] In addition, the disease can be transmitted in a handful of other ways such as a prick from a contaminated needle or a mother to child infection during pregnancy.[103]

Following the bite, the inoculated metacyclic trypomastigotes transform into long slender bloodstream form (LS-BSF) trypomastigotes (2). Unlike *Leishmania* spp., the parasites circulate freely in the bloodstream and lymph and are able to evade clearance by the host immune system by switching between variant surface glycoproteins.[112] LS-BSF trypomastigotes divide rapidly by binary fission (3); upon reaching a certain density the accumulation of a differentiation inducing factor produced by the parasites stimulates differentiation to short stumpy bloodstream form (SS-BSF) trypomastigotes (4).[113, 114] SS-BSF trypomastigotes have a short half life (estimated between 24 and 72 hours) and are non-proliferative in the mammalian host; instead, they are pre-adapted for the vector midgut and, following a blood meal by a tsetse fly (5), it is the SS-BSF trypomastigotes that continue the life cycle.[115]

In the tsetse fly midgut, the SS-BSF trypomastigotes transform into procyclic trypomastigotes which subsequently divide by binary fission (6). Following midgut colonisation, which takes up to 6 days, the procyclic trypomastigotes migrate through the foregut and proboscis to reach the salivary glands; they also transform into an adherent epimastigote form during this time (7).[116] Epimastigotes subsequently divide and multiply in the salivary gland before transforming into a detached metacyclic form (8) which is capable of being transmitted to a new host during the next blood meal.[117]

1.2.2.3. Currently Available Treatments

The drug of choice for the treatment of HAT depends on both the infective subspecies and the stage of the disease, with those effective in the encephalitic stage being required to cross the BBB. The number of drugs approved for HAT is therefore very limited, with those currently in use shown in Figure 1–7 (with pentamidine, also being used to treat leishmaniasis, previously shown in Figure 1–4).

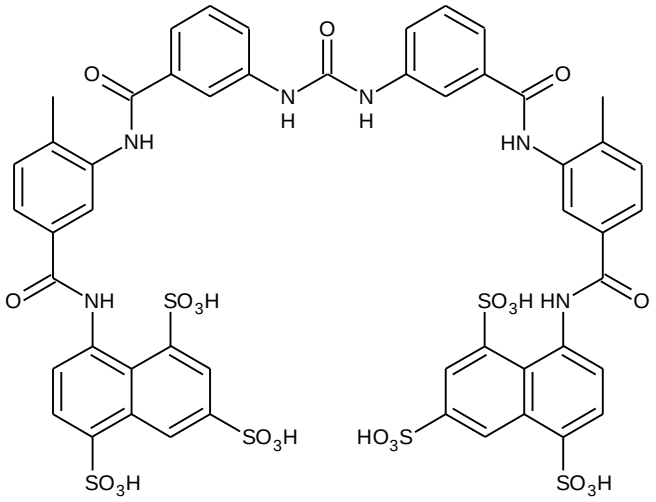

Suramin (**7**)

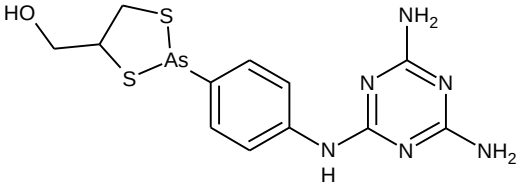

Melarsoprol (**8**)

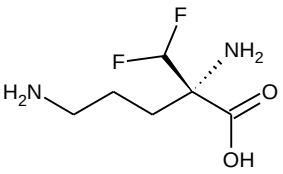

Eflornithine (**9**)

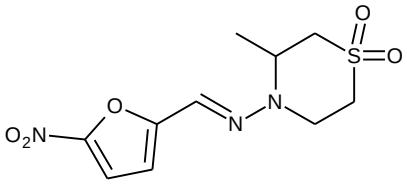

Nifurtimox (**10**)

Figure 1–7: The structures of currently used antitrypanosomal drugs

1.2.2.3.1. Pentamidine

Pentamidine (**3**) was first developed and used to treat HAT in the 1930s.[118] To this day it remains the drug of choice against hemolymphatic stagec *T. brucei gambiense* infections,[119] but it shows only limited efficacy against *T. brucei rhodesiense* infections and is completely ineffective against encephalitic stage disease.[120] Administered either intramuscularly or intravenously at the same dosage as against *Leishmania* infections, a course of 7–10 treatments results in cure rates up to 94% with the same side effects being observed.[121, 122]

As discussed in section 1.2.1.3.2, the mode of activity of pentamidine is not fully understood. However, it has been observed that *T. brucei* parasites possess a number of transporters with a high affinity for pentamidine, allowing accumulation of the drug to very high intracellular levels resulting in selective toxicity for the parasite over mammalian cells.[123] Unlike *Leishmania* infections, resistance of *T. brucei* to pentamidine is extremely rare in the field,[120] although overuse as a chemoprophylactic in some regions has led to decreased sensitivity to the drug.[119, 124]

1.2.2.3.2. Suramin

Suramin (**7**), first used to treat HAT in 1922, is perhaps the oldest antimicrobial drug still in use today.[125] It is the first line treatment for hemolymphatic stage *T. brucei rhodesiense* infections and is typically administered at a dosage of 20 mg/kg (up to a maximum of 1 g per treatment) by slow intravenous infusion every 5–7 days for 4 weeks.[122, 126] Although it is effective against *T. brucei gambiense* infections, suramin is generally avoided due to the high risk of co-infection with *Onchocerca volvulus* (the causative agent of onchocerciasis, or 'river blindness') against which it has high activity and can lead to severe adverse reactions including shock.[127] It is also unable to cross the BBB so cannot be used to treat encephalitic stage disease. Side effects from suramin use are frequent but generally mild and include fever, rash, nausea and reversible nephrotoxicity.[54]

Due to the multiple negative charges on suramin at physiological pH it is able to bind to numerous serum proteins, including low-density lipoprotein (LDL), which facilitate its uptake into the parasites by endocytosis.[125] Accumulation of the drug is relatively slow, but at high enough concentrations there are a number of enzymes which have been reported to be inhibited by suramin including certain kinases, acid phosphatase and phospholipase A_1.[128] Perhaps key, however, are the numerous glycolytic enzymes located in the trypanosome glycosome. Many of these carry a high positive charge and have been shown to be sensitive to micromolar levels of suramin,[129] whilst homologous enzymes from other organisms, including mammals, are less positively-charged and are insensitive to suramin.[128]

As with pentamidine, field resistance to suramin is rare. One possible reason for this is that LDL is essential for parasite proliferation and therefore its uptake into the parasites (and hence the uptake of suramin) cannot be drastically reduced if they are to remain viable.[130] Despite this, clinical instances of decreased suramin sensitivity have been reported,[131] and resistance can be readily selected for in the laboratory.[132]

1.2.2.3.3. Melarsoprol

Melarsoprol (**8**) is an organoarsenical compound which has been used in the treatment of HAT since 1949.[133] Whilst active against both stages of the disease in both *T. brucei* subspecies it is typically only used to treat the encephalitic stage due to its high toxicity, and it remains the only treatment available for late stage *T. brucei rhodesiense* infections.[134] Historically the drug was administered intravenously as a series of three or four daily injections (at a dosage of up to 3.6 mg/kg per injection, although this varied between countries) followed by a rest period of 7–10 days, repeated up to four times; however, more recent studies have shown that a treatment regime of 10 daily injections at a dosage of 2.2 mg/kg produces comparable cure rates.[135, 136] Melarsoprol is the most toxic of the antitrypanosomal drugs with a myriad of side effects including fever, vomiting, abdominal pain, polyneuropathy and thrombocytopaenia;[137] by far the most dangerous, however, is encephalopathy which occurs in 5–10% of all patients and proves fatal in up to 70% of these cases.[138]

The mechanism by which melarsoprol kills trypanosomes is not fully understood, although it has been observed that the drug rapidly metabolises in the body to form melarsen oxide, which is thought to be the species responsible for trypanocidal activity.[139] One observation is that the drug has the ability to interact with thiol groups and disulphide bonds in proteins, which could lead to a loss of function; this would explain the acute toxicity to the patient's own cells.[63, 140] Another is that melarsen oxide reacts with trypanothione to form a stable adduct which inhibits trypanothione reductase, ultimately leading to parasite death.[141]

In addition to its high toxicity, melarsoprol also exhibits a high treatment failure rate in comparison to the two aforementioned trypanocidal drugs. During the first 50 years of its use melarsoprol treatment was unsuccessful in 5–8% of cases, but over the

last 15 years this figure has risen alarmingly.[142] This is particularly evident in the Democratic Republic of Congo, where the failure rate reached 20% in 2003 rising to 57% in recent years, casting doubt on the future use of melarsoprol as a trypanocidal drug.[143, 144]

1.2.2.3.4. Eflornithine

Eflornithine (**9**) was originally developed as an anticancer drug but was observed to be active against trypanosomes *in vivo* in 1980, and was first utilised in the field the following year.[145] The drug is an irreversible inhibitor of ornithine decarboxylase, which is an integral enzyme in polyamine biosynthesis. Inactivation of the enzyme results in arrested trypanosome division and transformation to the metacyclic form, which the immune system is capable of eliminating.[146] However, this mode of action means that eflornithine is only effective against *T. brucei gambiense* given that the target enzyme has a very high turnover rate in *T. brucei rhodesiense* (as it also does in mammals).[147]

Although its primary use is as a safer alternative to melarsoprol for encephalitic stage disease, eflornithine still displays a variety of frequent side effects including fever, gastrointestinal symptoms, pneumonia, seizures and depression of bone marrow function.[148] The major drawback of eflornithine, however, is that it has a half life of only 3–4 hours, meaning it has to be administered intravenously at intervals of 6 hours for 14 days. Additionally, the required dose is extremely high (100 mg/kg in each injection for adults, or 150 mg/kg for children), hence the overall cost of treatment – both the drug price and extended hospitalisation – makes it inaccessible to many people.[149]

1.2.2.3.5. Nifurtimox

Nifurtimox (**10**) was marketed in the 1960s as a treatment for Chagas disease (caused by the kinetoplastid parasite *T. cruzi*) and was first utilised as a treatment for arseno-resistant *T. brucei* in the 1980s.[150] Its mechanism of action involves the reduction of the nitrofuran to produce free radicals which subsequently bind to, and disrupt, proteins and DNA.[151] Although the drug shows limited efficacy as a

monotherapy,[152] it is much more widely utilised in nifurtimox-eflornithine combination therapy (NECT) for the treatment of encephalitic stage disease caused by *T. brucei gambiense*.

NECT therapy was approved for use in 2009 and involves a treatment regime of intravenous eflornithine (200 mg/kg) every 12 hours for 7 days combined with oral nifurtimox (5 mg/kg) every 8 hours for 10 days.[153] Although hospitalisation is still required, the burden on the patient is reduced by the increased dosing frequency and shorter total treatment time; furthermore, the treatment cost is roughly half that of eflornithine monotherapy.[154] In addition, whilst some side effects (nausea, dizziness and tremors) were more common with NECT, the treatment displayed a more favourable overall safety profile with the incidence of major adverse effects being halved.[155, 156] Finally, the prospect of resistance emerging is much reduced for a combination therapy compared to a monotherapy, and hence NECT could prove to be a long-lived antitrypanosomal treatment.[157]

Despite the encouraging development of NECT, however, it is far from a perfect treatment. A TPP proposed by the DNDi, including requirements such as oral bioavailability, multi-target activity and activity against both *T. brucei* subspecies, highlights the large gap between currently available HAT drugs and what is perceived to be ideal.[158] Ongoing efforts include novel combination testing and repurposing from the Malaria Box,[159] and it is crucial that additional drug discovery programmes for HAT continue the search for potent, non-toxic drugs against both hemolymphatic and encephalitic stage disease.

1.2.3 Towards New Antikinetoplastid Drugs

Historically, drug discovery efforts for tropical diseases have been underwhelming, hence the term ‘neglected’. Between 1975 and 1999, only 1.1% of new chemical entities were for NTDs despite them being accountable for 11.5% of global disease burden.[160] The situation failed to improve over the next decade; whilst 4% of new therapeutic products registered between 2000 and 2011 were for neglected tropical diseases, these were predominantly new indications or formulations. Only 1%

of the new chemical entities registered during this time period were for NTDs, and clinical trials for NTDs also only made up 1% of the total number registered.[161]

A major step forwards was made in January 2012 with the launch of the London Declaration on NTDs.[162] This declaration, with 22 original endorsers, committed to working towards eliminating five diseases (including HAT) and controlling another five (including VL) by 2020, and diverges from the classical viewpoint that drug discovery and development is the sole responsibility of pharmaceutical companies and instead requires collaborations such as product development partnerships and public-private partnerships.[163] Thanks to this new initiative, the future of drug discovery for NTDs looks brighter than it has in years; however, in order to achieve this goal, new druggable targets first need to be identified and investigated.

1.3 Sphingolipids

Sphingolipids are a class of natural molecules first identified in 1884 by Thudichum, who isolated three related compounds from human brain tissue.[164] This category of compounds is now known to encompass thousands of structurally diverse molecules, and one of the major challenges in the field is keeping up with the rapid growth in understanding and knowledge.[165]

1.3.1 Structural Features

The sphingolipid family has a common core structure that is distinguishable from other classes of lipids by the presence of an amide bond which links the amine group of a sphingoid base backbone to the acyl group of a fatty acid (Figure 1–8). Sphingoid bases are aliphatic amino alcohols that are structurally similar to sphingosine (**11**) but may differ by a number of factors including alkyl chain length, saturation and modifications such as hydroxyl or methyl groups situated at various positions along the chain.[166] Mammals predominantly produce sphingosine along with dihydrosphingosine (**12**, also called sphinganine) and, to a lesser extent, phytosphingosine (**13**) (which is the predominant sphingolipid found in plants and fungi)[167] although smaller quantities of different chain length homologues are also produced.[168] Sphingoid bases are readily

N-acylated *in vivo* to form *N*-acyl-sphingoid bases which are generically termed ceramides (Figure 1–9).[169]

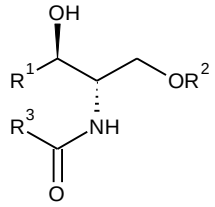

Figure 1–8: The core structure of a sphingolipid. R^1 is usually a saturated or monounsaturated alkyl chain, R^2 is typically a hydrogen or polar hear group and R^3 is classically a saturated alkyl chain

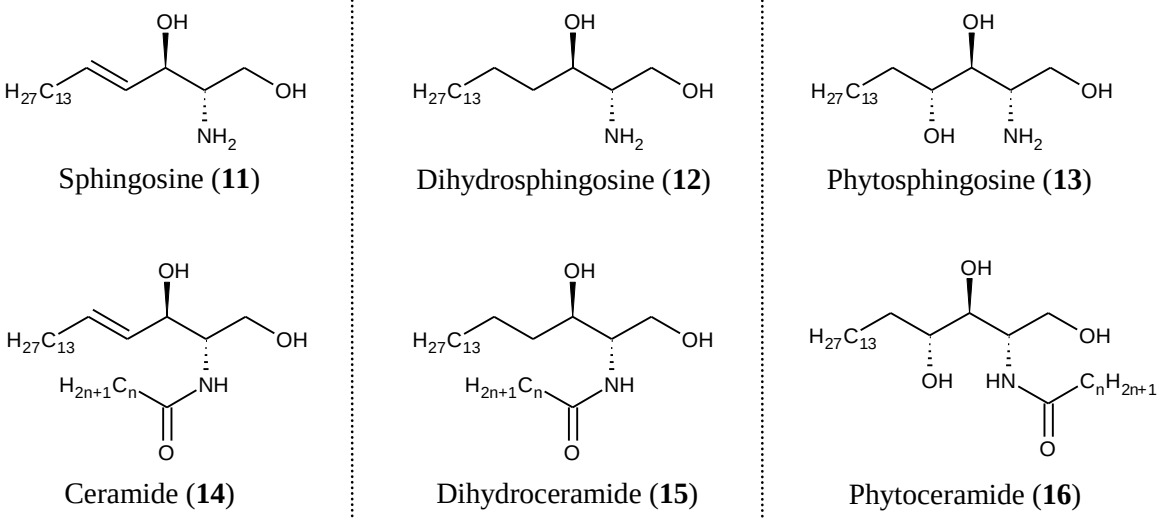

Figure 1–9: The predominant sphingoid bases found in mammals and their respective ceramides

Sphingolipids can be categorised into several major classes. Simple sphingolipids include sphingoid bases and ceramides as discussed above along with basic derivatives such as ceramide-1-phosphates. Complex sphingolipids (Figure 1–10) are extremely varied in nature and comprise molecules in which head groups are attached via phosphodiester linkages (phosphosphingolipids) or glycosidic bonds (glycosphingolipids, which can be either simple cerebrosides or complex gangliosides).[170] Some aquatic organisms produce sphingolipids containing phosphono linkages or 1-arsenate groups,[171] whilst certain bacteria have been shown to produce sulphonosphingolipids.[172]

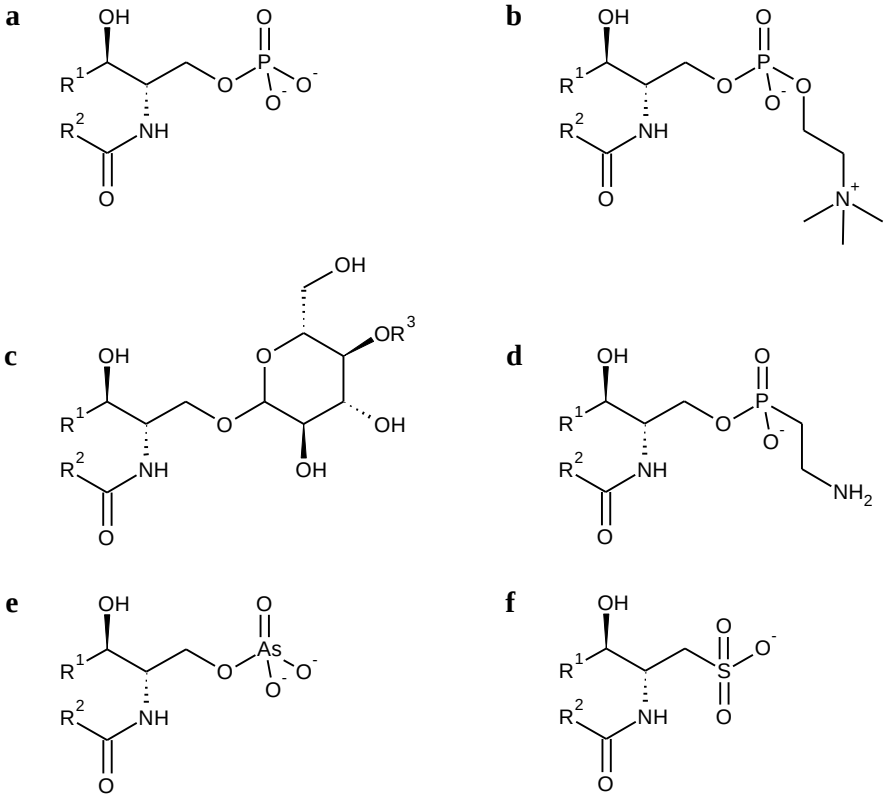

Figure 1–10: Structures of representative examples of the various classes of complex sphingolipids, where R^1 and R^2 are alkyl chains. (a) ceramide-1-phosphate; (b) phosphosphingolipid; (c) cerebroside glycosphingolipid when R^3 = H or ganglioside glycosphingolipid when R^3 = mono- or polysaccharide; (d) phosphonosphingolipid; (e) arsenosphingolipid and (f) sulphonosphingolipid

1.3.2 Biological Functions

Sphingolipids are essential and ubiquitous components of eukaryotic membranes,[173] although they have also been identified in some prokaryotes[174] and a marine virus.[175] The acyl chains of sphingolipids tend to be fully saturated, unlike the unsaturated chains generally observed with other membrane lipids; as a result, sphingolipids are able to pack tightly together and increase the structural stability of the membrane.[176] In addition, this packing of sphingolipids, both together and with sterols (thought to be due to the hydrogen bonding ability of the amide functionality),[177] allows the formation of compact zones of condensed bilayer.[178] This results in phase separation between the sphingolipid- and sterol-rich microdomains, known as lipid rafts, and the more disordered domains resulting from the unsaturated fatty acid chains of the membrane phospholipids.[179]

It has been proposed that lipid rafts form in the *trans*-Golgi apparatus and are able to traffic apical and basolateral proteins into separate vesicles for transport to the correct localisation in polarised epithelial cells.[180] This phenomenon was also observed in neurons, with proteins being sorted to either the axonal or dendritic localisation.[181] Lipid rafts have also been implicated in T-cell receptor signalling,[182] as well as the assembly and activation of signal transduction complexes such as the Hedgehog and Ras signalling systems.[183, 184]

Simple sphingolipids have also been observed to possess roles as signalling molecules (second messengers) in cells. For example, ceramide has been identified as an initiator of both apoptosis and autophagy,[185, 186] and sphingosylphosphorylcholine as a stimulator of calcium mobilisation in various cell types.[187] This activity is facilitated by the fact that many sphingolipids are uncharged at physiological pH and so are freely able to cross membranes.[188]

1.3.3 Biosynthetic Pathway

The biosynthesis of sphingolipids is complex and involves an intricate network of interconnected pathways with ceramide, involved in both anabolism and catabolism, acting as a metabolic hub.[189] Given that sphingolipids are essential cellular components, the biosynthetic pathway is largely conserved across organisms. However, it is the mammalian pathway that is the most extensively studied, and an overview is shown in Figure 1–11.

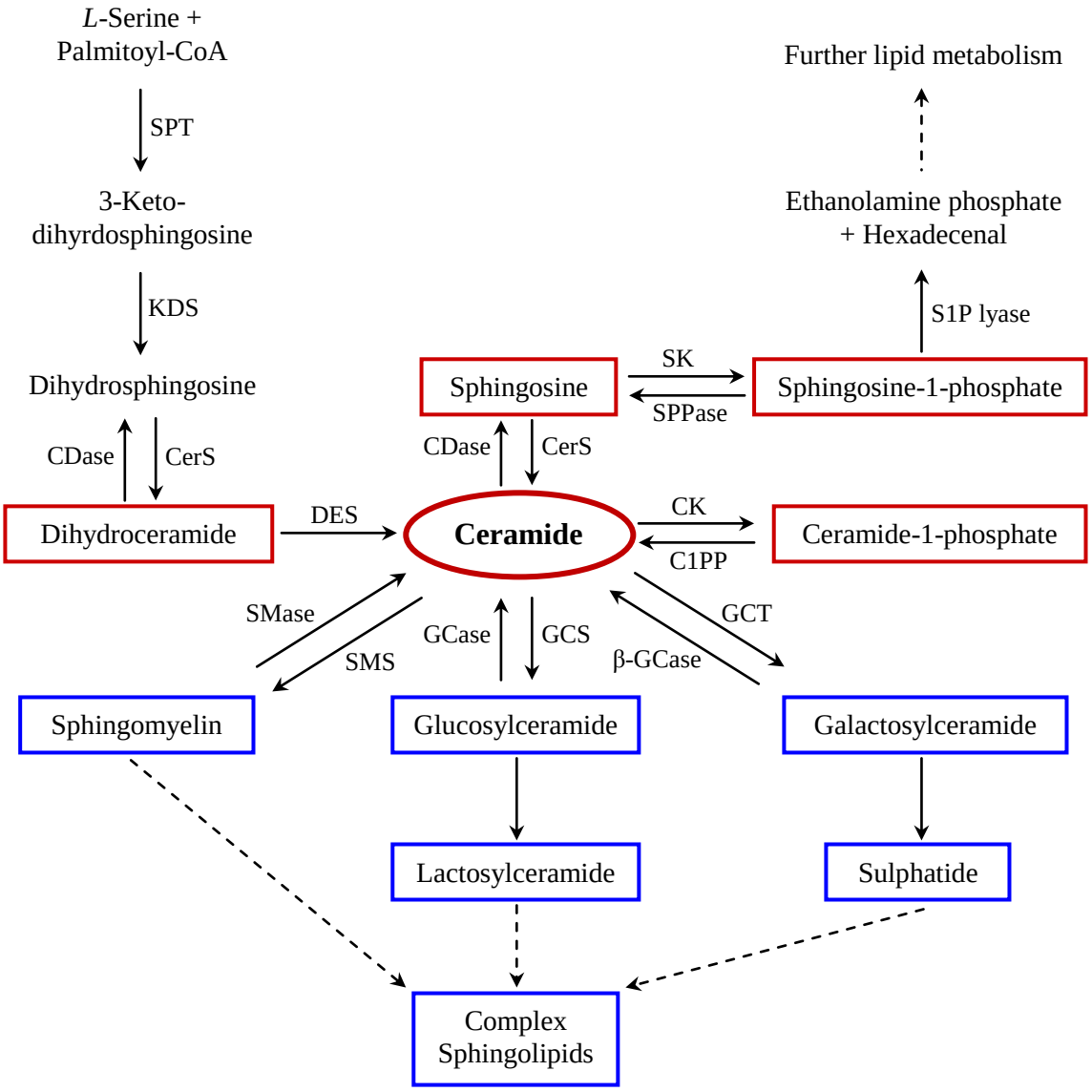

Figure 1–11: An overview of mammalian sphingolipid metabolism (adapted from Bartke and Hannun[189] with permission). Bioactive sphingolipids are outlined in red, whilst those outlined in blue are predominantly membrane components. Enzyme abbreviations are as follows: SPT, serine palmitoyltransferase; KDS, 3-keto-dihydrosphingosine reductase; CerS, ceramide synthase; CDase, ceramidase; DES, dihydroceramide desaturase; SK, sphingosine kinase; SPPase, sphingosine-1-phosphate phosphatase; S1P lyase, sphingosine-1-phosphate lyase; CK, ceramide kinase; C1PP, ceramide-1-phosphate phosphatase; GCT, galactosylceramide transferase; β-GCase, β-galactosylceramidase; GCS, glucosylceramide synthase; GCase, glucosylceramidase; SMS, sphingomyelin synthase and SMase, sphingomyelinase

Sphingolipid biosynthesis is compartmentalised between the endoplasmic reticulum (ER), where synthesis commences, and the Golgi apparatus, where the majority of ceramide metabolism occurs.[190] Synthesis begins in the ER with the condensation of *L*-serine and palmitoyl coenzyme A (CoA) to form 3-keto-dihydrosphingosine; this is the rate-limiting step of sphingolipid synthesis.[191] 3-Keto-dihydrosphingosine is

subsequently reduced to dihydrosphingosine. These first two metabolic steps (Figure 1–12) are highly conserved across eukaryotes.

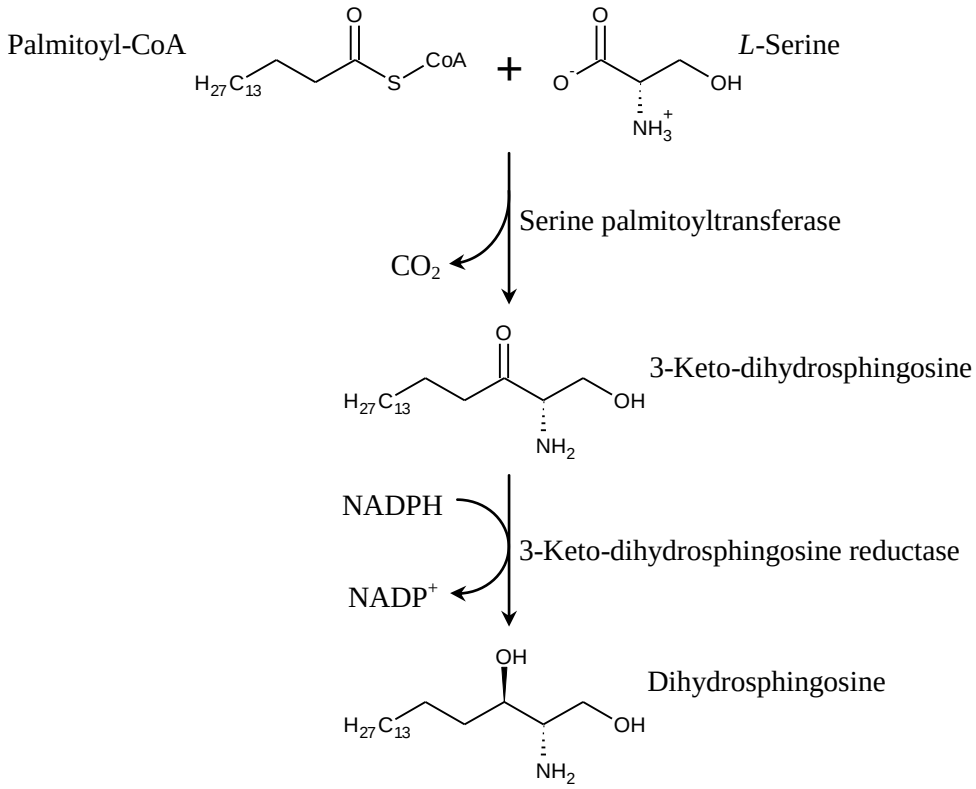

Figure 1–12: Eukaryotic biosynthesis of dihydrosphingosine

Following dihydrosphingosine formation, the metabolic pathways begin to diverge. In animals, dihydrosphingosine is acylated to dihydroceramide before being desaturated to form ceramide. In higher plants and fungi, however, dihydrosphingosine is first hydroxylated to form phytosphingosine before being subsequently acylated to form phytoceramide (Figure 1–13).[192, 193] The products of this synthesis are subsequently transported from the ER to the Golgi apparatus for further metabolism.

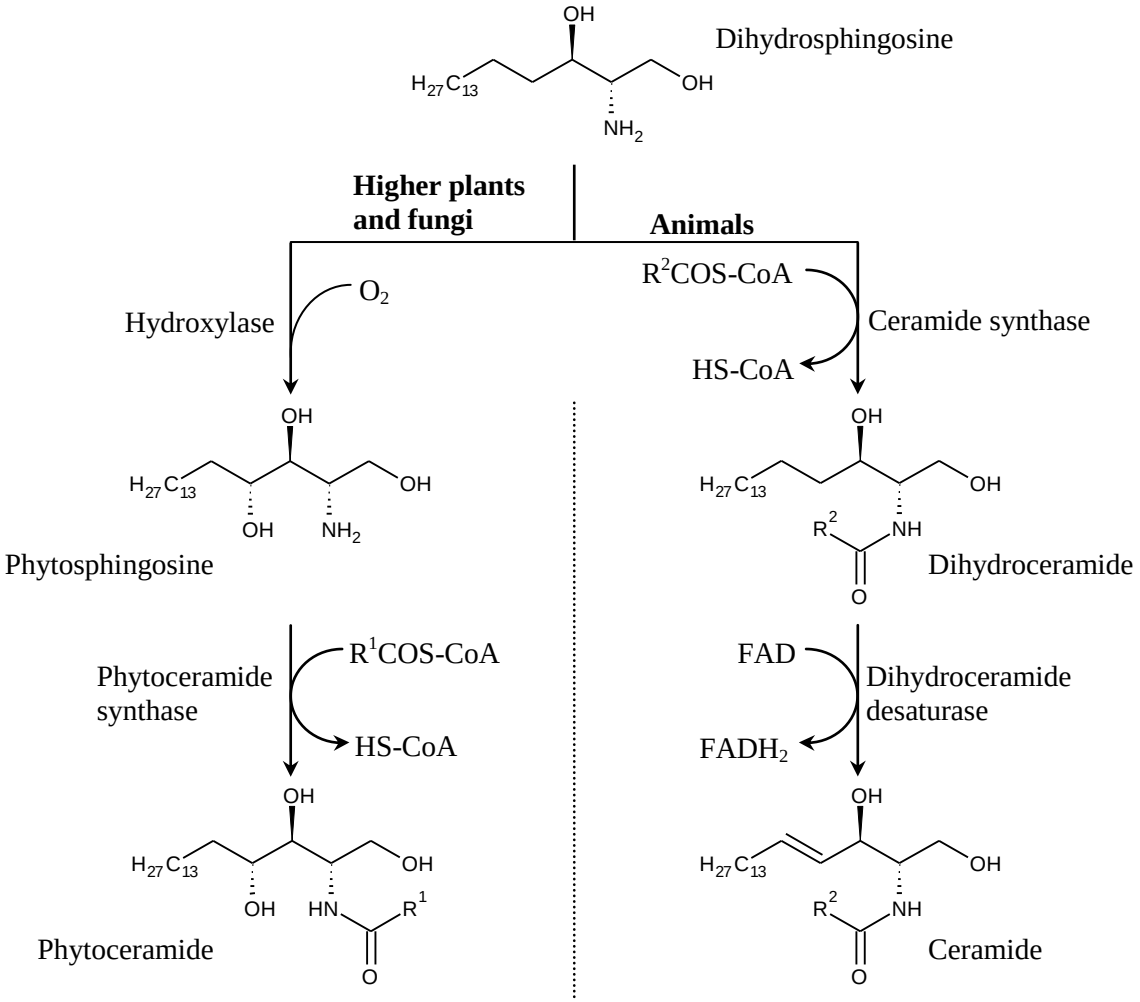

Figure 1–13: Divergent metabolism of dihydrosphingosine in different organisms

Once transported to the Golgi apparatus ceramide (or phytoceramide) can be utilised in a variety of metabolic processes as shown in Figure 1–11. However, the predominant metabolic process is organism-dependent. Mammalian cells possess a sphingomyelin synthase (SMS) enzyme which converts ceramide to sphingomyelin; this is the predominant sphingolipid in animals, forming up to 22% of cellular membranes.[194, 195] In contrast, higher plants and fungi produce inositol phosphorylceramide (IPC) as their prevalent complex sphingolipid using an IPC synthase (IPCS) enzyme.[196] Finally, kinetoplastid parasites form a distinct group and convert ceramide to IPC, also using an IPCS (Figure 1–14).[197]

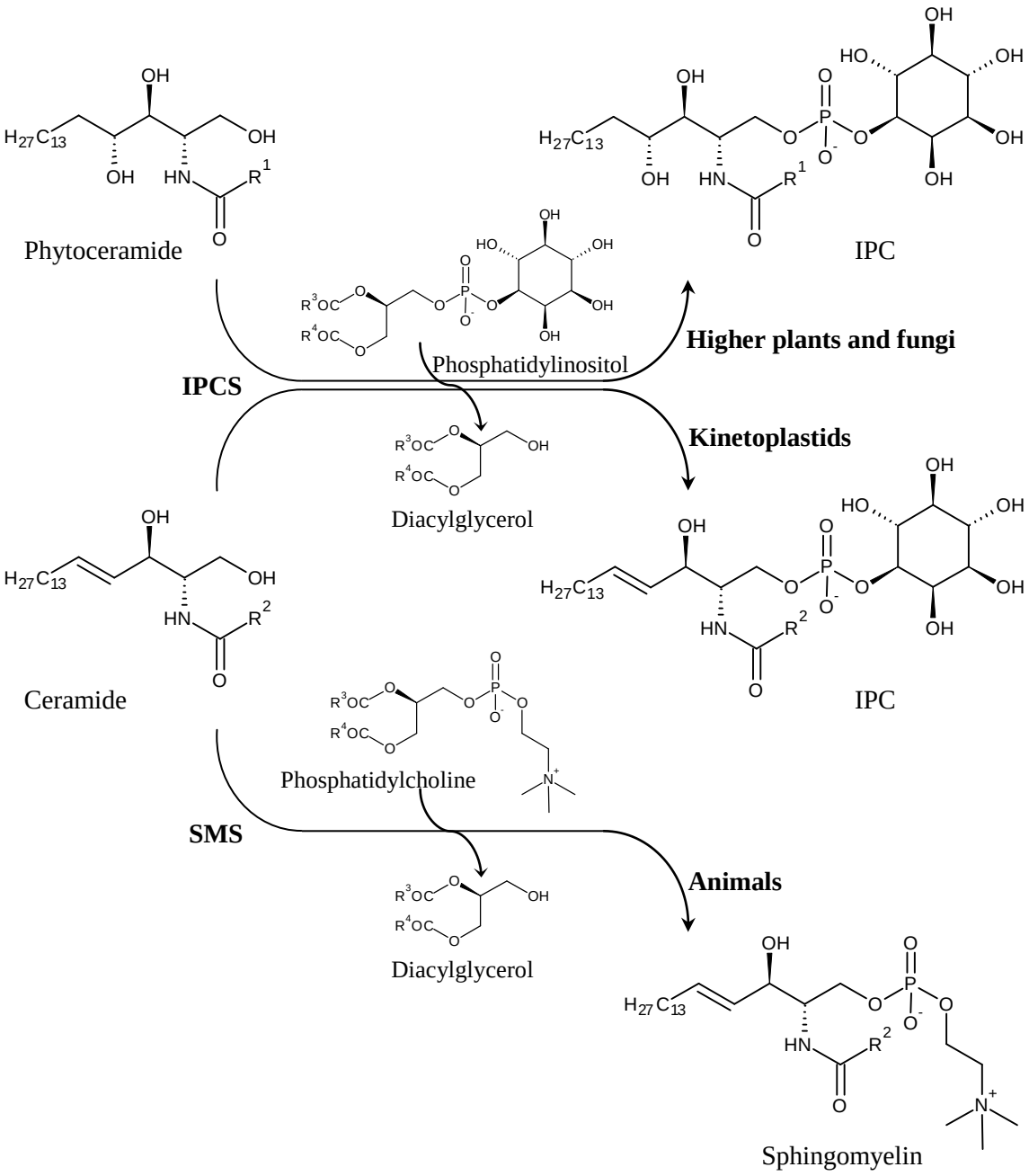

Figure 1–14: Divergent metabolism of ceramide in different organisms

1.3.4 IPCS as a Drug Target

Due to the high levels of conservation across kingdoms in the early stages of sphingolipid synthesis, inhibitors that target enzymes early on in the pathway do not make suitable drugs as they also result in host toxicity.[198] However, given the fact that mammals produce SMS rather than IPCS this enzyme represents an attractive pharmaceutical target. This concept was first demonstrated in yeast in the 1990s. The model yeast *Saccharomyces cerevisiae* was observed to be susceptible to aureobasidin A (AbA, **17**), a cyclic depsipeptide isolated from *Aureobasidium pullulans*.[199]

Subsequent studies on an AbA-resistant strain of *S. cerevisiae* identified a single upregulated gene, which was named *AUR1*, which was responsible for the conference of resistance. Subsequent depletion or deletion of this gene resulted in abnormal morphology and a loss of viability.[200, 201] It was later shown that the *AUR1* gene complemented the IPCS defect present in sphingolipid compensatory yeast strains (which produce glycerophospholipids to compensate for the lack of sphingolipids), hence confirming the identity of the AUR1 protein as an IPCS.[202]

IPCS homologues were later identified in multiple fungal species by polymerase chain reaction (PCR) amplification from genomic DNA libraries using degenerate primers;[203] this resulted in the identification of four conserved domains, two of which were similar to domains present in the lipid phosphate phosphatase (LPP) family.[204] Two additional inhibitors of the fungal IPCS were also subsequently identified; rustmicin (**18**)[205] and khafrefungin (**19**)[206] (Figure 1–15). However, neither of these compounds nor AbA display a favourable pharmacokinetic profile and their highly complex structures present a significant challenge to medicinal chemistry efforts.[207] A recently published three-step method of modifying AbA resulted in the synthesis of a number of compounds which displayed either comparable or slightly improved activity over AbA against two different fungal species;[208] other than this, however, attempts at improving the activities of these compounds have been unsuccessful.

The identification of IPCS in yeast also inadvertently led to the discovery of the mammalian SMS family of enzymes in the early 2000s. Having noted that IPC was the fungal equivalent of SMS, Huitema *et al*. employed a bioinformatics approach to search for mammalian proteins of unknown function possessing a conserved sequence motif ($H(YFWH)X_2D(VLI)X_2(GA)X_3(GSTA)$) shared by LPPs and the IPCS homologues. They identified a family of enzymes containing four highly conserved domains, named D1−D4; D3 and D4 contained the similar sequences shared by LPPs and the IPCS homologues.[209] Despite these regions of similarity in the sequences, it is still acknowledged that IPCS represents an attractive pharmaceutical target; computational systems biology has confirmed this to be the case in *Leishmania*.[210]

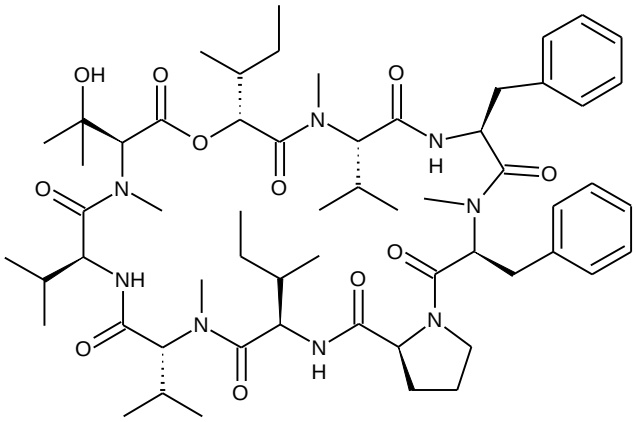

Aureobasidin A (**17**)

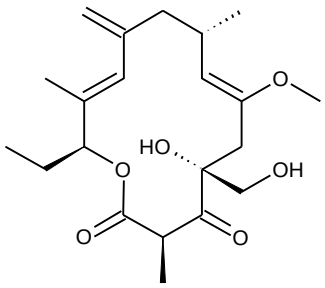

Rustmicin (**18**)

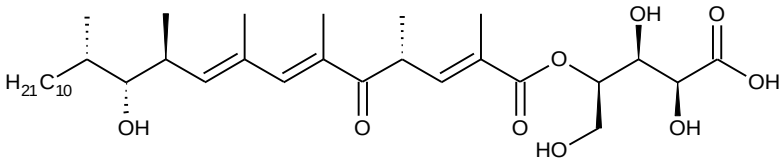

Khafrefungin (**19**)

Figure 1–15: Known inhibitors of the fungal IPCS

1.3.5 The Kinetoplastid IPCS

The kinetoplastid IPCS enzymes were identified by Denny *et al.* in 2006, again by searching the relevant genome databases for the conserved motif given above.[196] All the orthologues displayed two regions that were conserved relative to animal SMSs and similar to AUR1.[203, 209] These regions contain the catalytic triad of His220, His264 and Asp268 (numbered for the *L. major* enzyme) and are located in the luminal domains of D3 and D4 (the conserved regions proposed by Huitema *et al*. for SMS)[209] of IPCS, which is predicted to contain six transmembrane helices (Figure 1–16).[211]

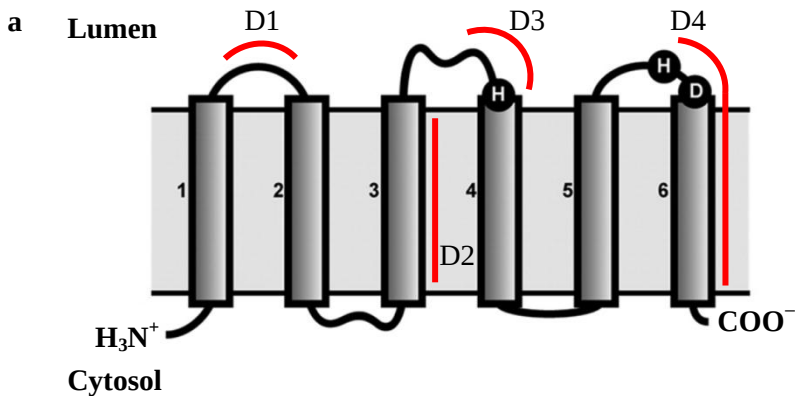

b

		D3				D4	
SMS1_HUMAN	283	CGDYLYSGHT	292		331	AHDHYTVD	338
SMS2_HUMAN	221	CGDFLFSGHT	230		269	AHEHYTID	276
SLS_LEIMA	212	CGDLMFSGHT	221		261	SRSHYTDD	268
SLS1_TRYB2	220	CGDLMYSGHT	229		268	SRSHYTDD	275
SLS2_TRYB2	202	CGDLMYSGHT	211		250	SRFHYTDD	257
SLS3_TRYB2	202	CGDLMYSGHT	211		250	SRFHYTDD	257
SLS4_TRYB2	220	CGDLMYSGHT	229		268	SRFHYTDD	275
		*** ****				*** *	

Figure 1–16: (a) The predicted topology of kinetoplastid IPCS (adapted from Goren *et al.*[211] with permission) with the domains proposed by Huitema *et al.*[209] for SMS shown in red and (b) the alignment of highly conserved regions from human SMS, *L. major* IPCS and *T. brucei brucei* sphingolipid synthases (SLSs). Stars indicated conserved residues and the residues in the catalytic triad are outlined in red

The enzyme has been shown to proceed via a double-displacement mechanism (Figure 1–17).[212] Based on this model, functions for the three amino acids of the catalytic triad have been proposed. In the first step, His264 and Asp268 are thought to operate as a charge relay system which facilitates nucleophilic attack by His264 on the electrophilic phosphorus in the phosphatidylinositol (PI) substrate.[213] His220 is postulated to facilitate nucleophilic attack of the ceramide on the phosphorus in the second step, whilst a conserved arginine (Arg262 in the *L. major* enzyme) is believed to stabilise the transition state (Figure 1–18).[214]

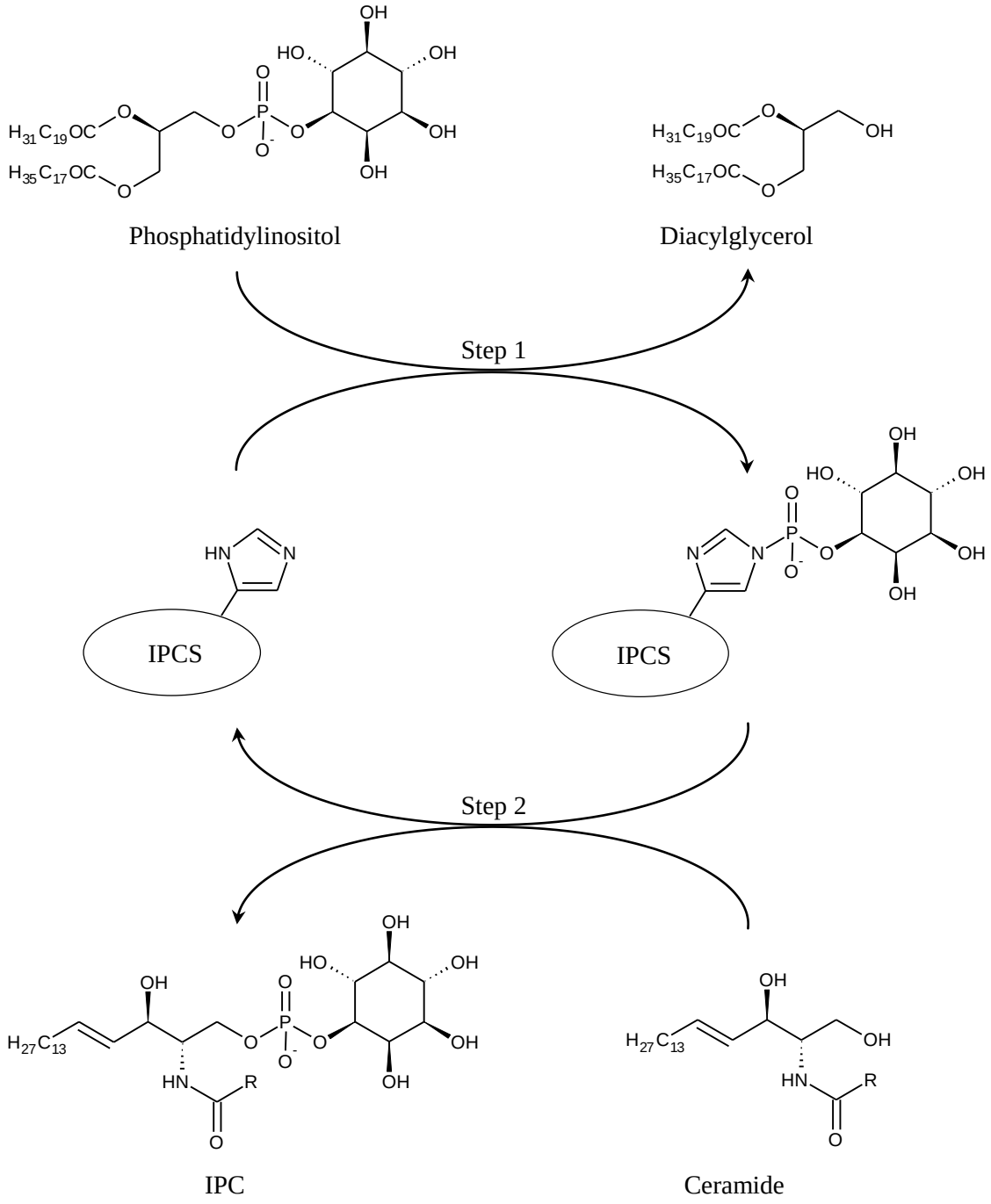

Figure 1–17: The double-displacement mechanism of IPCS. In the first step, the phosphorylinositol group is transferred to the reactive histidine (His264 for *L. major*) with the release of diacylglycerol. In the second step, this group is subsequently transferred to the acceptor substrate ceramide

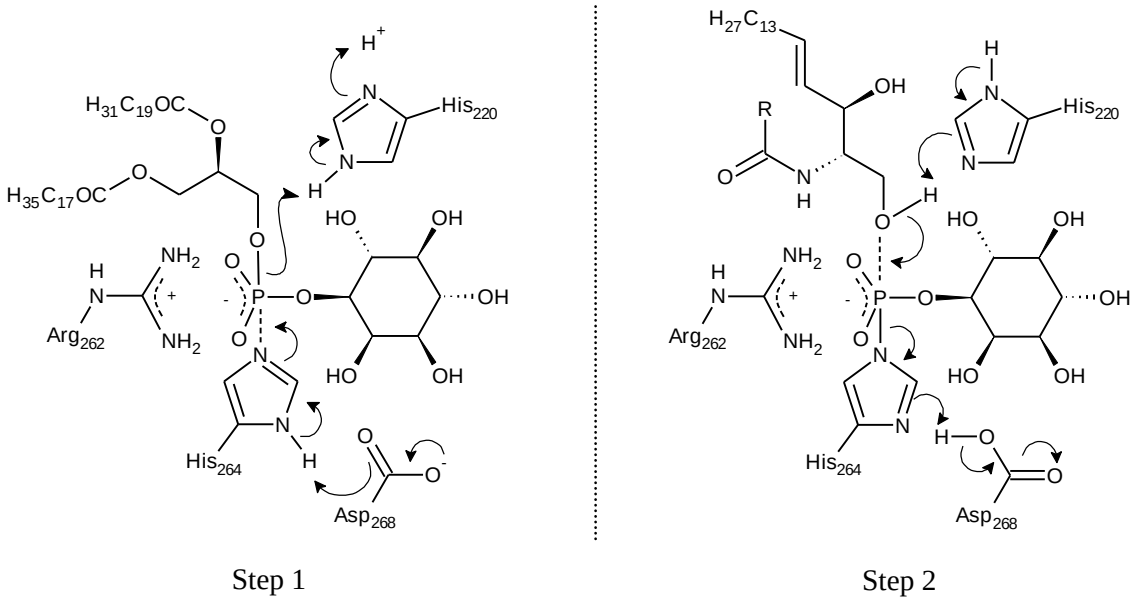

Figure 1–18: The proposed mechanism of action of *L. major* IPCS (adapted from Mina *et al.*[214] with permission)

As can be seen from the mechanism, in addition to regulating the production levels of the essential sphingolipid IPC, this synthetic step also plays a part in controlling the cellular levels of ceramide and diacylglycerol (DAG). This is a crucial observation given that DAG is a mitogenic factor and hence is essential for cell growth,[215] whilst ceramide (as noted in section 1.3.2) induces apoptosis.[185] Therefore, compounds which inhibit IPCS would reduce parasite viability by affecting the levels of three different biomolecules and hence should ideally be highly effective and selective pharmaceutical compounds. The potential for selectivity between closely related IPCS enzymes from different species has already been established; in the case of AbA, inhibitory activity against *L. amazonensis* IPCS[216] and *T. brucei* sphingolipid synthase (SLS) isoform 4 has been described, whilst the *L. major* IPCS is insensitive.[217] As discussed above, however, the only known inhibitors of the fungal IPCS are not suitable drug candidates and hence small molecule inhibitors of this drug target, ideally based on novel chemical scaffolds, need to be identified.

1.4 Introduction to High Throughput Screening and Drug Discovery

The mounting public demand to identify cures for worldwide diseases (including those aforementioned), as well as the development of drug resistance in many infective species,[218, 219] has resulted in high pressure being placed on the pharmaceutical industry to produce new drugs at a rapid rate. The drug discovery process, however, is far from simple, involving many stages that are both time-consuming and costly.[220]

The first stage is the identification of a biological target involved in the disease or pathway of interest. Following this, compounds are tested against this target to uncover some with activity; these compounds have the potential to become drugs and are hence known as leads. Lead optimisation (a process undertaken to increase factors such as solubility and bioavailability) and preclinical studies in animal models to assess biological activity and safety can then last up to five years. Phase I clinical trials (first time in man), where the leads are tested in healthy human volunteers to determine safety and dosage, generally take about a year whilst phase II trials, which evaluate efficacy and adverse effects in patient volunteers, normally last for two years. Any long term adverse effects are identified in phase III, which monitors patient volunteers over a period of three years.[221]

Following this process it can be some years before the drug is registered and approved meaning that, on average, it takes around 12 to 15 years to progress a lead compound to the clinic. The attrition rate of compounds during this period is significant; according to a recent study, over 92% of small molecule drugs that entered phase I clinical trials did not reach approval.[222] As a result, the identification of a large number of high quality leads is of paramount importance for the drug discovery process to be successful, and in the 1990s many pharmaceutical companies began to turn to high throughput screening (HTS) for this stage in the campaign.[223] It is a process that allows large libraries of compounds, ranging from several thousand to a few million, to be tested both rapidly and relatively inexpensively, hence it has the capacity to produce large numbers of potential lead compounds to be progressed further through the drug discovery pipeline.

1.4.1 Evolution of HTS

As with all highly advanced technology, HTS has a very modest background. The foundations were laid in 1950 when Takatsky fashioned the first microtitre plate out of Lucite (a synthetic polymer of methyl methacrylate) in order to provide an easier method of performing low volume serial dilutions.[224] His 72-well invention was well received and by the mid 1950s a moulded plastic version had been commercialised in the United States by Liner, making it a standard piece of equipment for use in immunoassays.[225] This prompted the development of plate readers throughout the 1970s, although these were specific to the biochemical industry. The platform was launched into the standard research laboratory setting following the construction of the laboratory plate reader by BioTek in 1981.[226] This incited an even larger surge in microplate manufacture, and by the mid 1990s the necessity for standardisation of microplate dimensions across manufacturers had been noted.[227] This was eventually finalised in 2004 by the Society for Biomolecular Screening (now the Society for Laboratory Automation and Screening), who published a set of standards covering base (footprint),[228] height[229] and outside flange[230] dimensions in addition to well positions for each of the common formats (96-, 384- and 1,536-well plates).[231]

The first reported attempts at developing HTS assays date to the late 1970s where continuous flow and automation techniques were used to screen blood metabolite levels.[232, 233] These initial assays highlighted many of the problems still associated with HTS such as reagent variability, day-to-day variance of results and the need to carefully validate the assay prior to use. Despite this, assays such as these paved the way for increasingly high throughput experiments, although it was not until the 1990s when standard automatic instrumentation and a choice of plate formats were introduced that HTS as it is known today emerged.[225]

Since that time, HTS has continued to adapt and evolve as required, primarily in the pharmaceutical industry where it has found a niche in drug discovery. As compound libraries grew so did the need for miniaturisation; each well in a 96-well plate typically has an optimal working volume of roughly 200 µl (dependent on well shape), resulting in overly high reagent costs when working with large numbers of compounds. As a result, very few assays carried out in 96-well format are now considered high

throughput, with that label mostly being reserved for those run in 384-well and 1,536-well plates; these typically utilise volumes of 50–70 µl and 5–10 µl respectively.[234, 235] With 1,536-well plates it is possible to screen in excess of 100,000 compounds per day, a screen of this magnitude being termed ultra-HTS (uHTS).[236]

Increasing technological advancement has also resulted in increased availability to the extent that HTS has recently branched out into the academic environment.[237] For example, the University of Dundee has compiled a library of more than 57,000 compounds as a screening tool in drug discovery for neglected diseases;[238] this has been successfully utilised to identify small molecule inhibitors of the *N*-myristoyltransferase from *T. brucei*.[239] Another principle academic use is the identification of chemical probes which can be subsequently used to study biological pathways or targets.[240]

To date, the major drawback of HTS is that the results obtained using *in vitro* assays typically correlate poorly with those obtained in *in vivo* studies, usually due to issues such as off-target toxicity and poor biodistribution.[241] In the past, HTS on animal models has not been practical given the sheer expense and animal numbers that would be required. Recently, however, it was reported that HTS using zebrafish embryos, which can survive in 50 µl of water in 384-well plates, is a possibility;[242] this has since been achieved by a number of research groups in 96-well plates.[243, 244] Given the close genetic and physiological similarities between zebrafish and humans,[245] it is predicted that screening using this model will greatly reduce attrition rates throughout the drug discovery process and increase the number of effective compounds that successfully make it to market.

1.4.2 Stages of HTS

The HTS process encompasses several stages (Figure 1–19), none of which holds a greater importance than any other. Consequently, unless the proper time and attention is spent on each stage of the HTS process the screen will undoubtedly end in failure. As a result, HTS is a highly multidisciplinary process encompassing biologists and biochemists, technology experts, IT personnel and medicinal chemists, all of whom are essential for the screen to be successful and produce the much desired lead compounds.

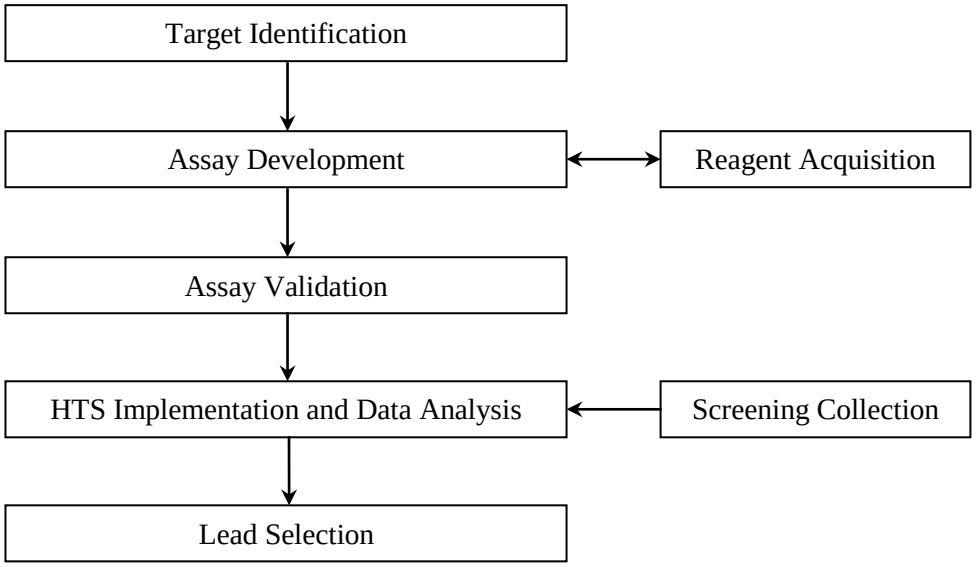

Figure 1–19: The stages of HTS

1.4.2.1 Target Identification

The selection of an appropriate target for HTS involves the consideration of a number of factors, of which the three most important are: how well the target has been linked to the disease (target validity); how facile it would be to utilise or develop a screening assay for the target (assayability); and whether the target is likely to be able to interact with chemically tractable small molecules in a potent and selective fashion to produce a measurable response (druggability).[246] The major issue with target validity is that there is an inverse correlation between this factor and the novelty of the target. Targets that have been well-studied and have established links to a particular disease may well have been previously screened for inhibitors (and hence potential leads could already be patented by another company), whilst highly novel targets are often poorly correlated to disease.[247] The majority of pharmaceutical companies which are large enough to have several projects ongoing will normally study a range of targets which span the risk scale.

On the other hand, if a target is highly validated there is a strong chance that a successful assay format has already been established, or if not, that an existing protocol can be readily modified. Novel targets may require an entirely new assay format to be developed, and the difficulty of this task cannot be predicted prior to commencing the next stage of HTS.[248] However, if the screen can be implemented successfully then these targets are more likely to yield novel classes of compounds.

Druggability assessment of targets is theoretical, with predictions being made using available structural data.[249-251] When tested against known protein/ligand combinations, programmes are capable of identifying binding sites with greater than 80% accuracy.[252] However, predicting druggability of non-protein targets or proteins for which structural information is lacking, such as many membrane proteins,[253] is not possible by these methods; in these cases, druggability usually has to be estimated based on similarity to other members of the same gene family for which more data is known.[249]

Overall, target selection involves balancing the pros and cons of the above range of factors. 'Perfect' targets that satisfy all the criteria for a high quality, successful screen are rare to the point of being non-existent, thus distributing the risk among the various factors is of paramount importance at this stage of the screening campaign.

1.4.2.2 Assay Development

In a typical HTS campaign there is usually not one assay developed and utilised but two. The primary assay is employed during the initial screen against the compound library whilst a second assay, or 'counter screen', is used as a follow-up to validate compounds that act via the desired biological pathway. This is to ensure that any false positives (F+, compounds which produce the same effect via other mechanisms) are excluded from further studies.[240]

In order to achieve this validation primary and secondary assays are typically orthogonal, using either different methodologies or altering the way in which target activity is detected and read. The most common way of achieving this is to develop both a biochemical and a cell-based (phenotypic) assay. These assays study the target in different environments and hence utilise contrasting methods of activity detection; using a combination of both therefore ensures that only worthwhile hits will be taken forward for additional investigation.

1.4.2.2.1 Biochemical Assay

A biochemical assay is defined as one in which the target of interest is isolated from cells and screened *in vitro* in an entirely artificial environment. During the early

1990s, when HTS was established as a component of the drug discovery process, this was by far the preferred format due to the technical difficulties involved in running phenotypic assays on a high throughput scale.[247] However, these initial biochemical assays were themselves far from technically simple.

The majority of assay formats utilised complex separation-based techniques, such as radiofiltration, as a means of detecting target activity. This was a technique originally developed to measure serum immunoglobulin levels[254] before it was adapted for screening purposes such as the search for drugs against human gastric cancer.[255] This technique subsequently evolved into the enzyme-linked immunosorbent assay (ELISA) which superseded the use of radioactive species and is still used today.[256] However, these assay formats are typically both time consuming and labour intensive as several washes have to be conducted between each step, limiting them to being performed in 96-well plates at a comparatively low throughput rate.

The majority of modern assays instead utilise a simple, homogenous format commonly referred to as 'mix and read'. The term was first coined by Toney *et al.* upon their development of an assay for measuring insulin levels in plasma samples that did not rely on the complex separation steps of the previously used ELISA assay but instead only required the mixing of the components in the well.[257] Not only does this cut down on labour and cost, but the potential to use 384-well and 1,536-well plates dramatically increases throughput.[258] For these assays, the majority of detection methods are optical and include absorbance, luminescence and fluorescence. Of these, fluorescence is the most widely used as it is highly sensitive, permitting the use of very small volumes.[259] This sensitivity, though, is also the biggest drawback as the potential for compound interference, either due to compound insolubility or intrinsic fluorescence, is high and can therefore give rise to F+ results.[260] The main strategy for combating this effect is to avoid short excitation wavelengths (below 400 nm) as this is the range at which many small molecule library compounds, such as heterocyclic aromatics and compounds with low levels of conjugation, are also excited, resulting in intrinsic fluorescence in the 400−495 nm region.[261] This can be achieved using a red-shifted fluorophore as demonstrated by Simeonov *et al.*, who screened a library of 71,391 compounds using 8 different fluorophores with a range of excitation and emission values. Whilst 3,643 compounds (5.1%) produced intrinsic fluorescence when

the blue-fluorescent fluorophore AlexaFluor 350 was used, no compounds produced intrinsic fluorescence when the far-red-fluorescent fluorophore AlexaFluor 647 was used.[262]

The major advantage of most biochemical assays is the certainty that the effect measured is due to the target and not to a different mechanism or pathway; however, there are multiple disadvantages. The production and purification of the required protein is often a very time-consuming step and, in many cases, the yields obtained do not provide adequate material for a large HTS campaign,[263, 264] limiting the screening process to smaller libraries. In addition, many small-molecule library compounds are capable of forming aggregates which interfere with protein function, resulting in F+ results; this was demonstrated by McGovern *et al*., who studied 45 reported inhibitors identified by screening and observed that 35 also inhibited unrelated proteins by forming aggregate particles large enough to be observed under a microscope.[265] With respect to screening for new antileishmanials, the major issue is that amastigotes are intracellular parasites localised inside macrophages, hence hit compounds identified *in vitro* often lose efficacy *in cellulo* due to the fact they are required to cross multiple membranes and remain stable in an acidic environment.[266] A study in 2011 eventually suggested that an overreliance on target-based drug discovery was responsible for the high attrition rates and low productivity observed in the pharmaceutical sector over the previous decade;[267] consequently, biochemical assays are now predominantly used as a secondary assay for confirming target specificity, whilst phenotypic assays form the majority of primary screening campaigns.

1.4.2.2.2 Phenotypic Assay

Phenotypic assays were virtually non-existent in the HTS world until 1996, when Schroeder and Neagle reported the construction of a fluorescent imaging plate reader (FLIPR).[268] This instrument was pioneering in the fact that it was capable of reading all the wells in a 96-well plate simultaneously, hence allowing transient signals in cells in response to different conditions to be quantified. Early assays included investigating G-protein coupled receptor (GPCR) activation by measuring the resulting increase in intracellular calcium[269] and the characterisation of potassium channels by measuring changes in membrane potential.[270] Since that time, phenotypic assays using FLIPR

technology have increased rapidly in popularity, resulting in the development of FLIPR machines for use with 384-well and 1,536-well plate formats.[234, 271]

Phenotypic assays can be classified as either target-blind or target-directed. The former simply involves the testing of compounds against the target cells of interest and monitoring cell viability. This type of screen has, in the past, been of particular importance in the discovery of anticancer agents;[272-274] more recently, target-blind phenotypic screening has led to advances in drug discovery for infectious tropical diseases. The Malaria Box, compiled in 2013, is a collection of 400 compounds active against *Plasmodium falciparum* parasites that is now available to researchers free of charge.[275] In addition, three antikinetoplastid compound collections (Leish-Box, Chagas-Box and HAT-Box) have recently been identified by target-blind phenotypic screening and have been provided as an open access resource to, hopefully, further progress research in this area.[276]

The principal advantage of utilising this type of screen is that compounds are tested in a cellular context. As a result, if test compounds act on targets that form part of pathways requiring several additional components to elicit a response, hit compounds will be identified that may have been overlooked using a biochemical format.[277] In addition, the requirement for the production of purified target protein is negated. This type of screening does, however, have one major disadvantage; no information about the target or mode of action is known, hence the investigation of structure-activity relationships (SARs) during the lead optimisation stage can prove more challenging and may require the development of an additional assay.[278] Another downside is that protozoan parasites and mammalian cells can often be difficult, expensive and time-consuming to culture.

The second type of phenotypic assay is cell-based target-directed, which attempts to screen a known target in a cellular context. Perhaps the most prolific use of this type of assay has been in GPCR drug discovery, with a wide variety of assays utilising different technologies to measure different cellular events having been developed over the years.[279] The majority of these assays require some form of cellular engineering or labelling and a wide variety of purpose designed cell lines are now commercially available for use in these assays.[280] Genetic manipulation of protozoan parasites for

NTD drug discovery, however, is relatively challenging, and therefore the target of interest is instead engineered into a different organism, or vehicle, for study. The simplest organisms to manipulate are bacteria; for example, *Escherichia coli* was successfully utilised as a vehicle by Eakin *et al*. in a screen for inhibitors of parasite enzymes involved in purine salvaging.[281] A major drawback of using bacteria is that their cellular machinery for folding proteins is different to that of eukaryotes and misfolding can often occur.[282] As a result, yeast (most commonly *S. cerevisiae* and *Schizosaccharomyces pombe*), which is highly tractable, is gaining increasing recognition as a potential vehicle for HTS.[283]

The most common use of yeast cell-based screening relies upon the substitution of an essential yeast gene with a functional orthologue from the organism of interest. This approach has been widely utilised in the study of both mammalian[284] and parasite[285, 286] proteins. However, the first, and so far only, account of yeast-based HTS for NTD drug discovery was published by Bilsland *et al.* in 2013, whereby they co-expressed the essential dihydrofolate reductase genes from different species with different fluorescent proteins. The fluorescence output could therefore be measured as an indicator of growth, and hence inhibition by test compounds.[287]

Although less common, yeast can also be utilised in different assay formats. One of these is a lethal expression platform, whereby the introduction of a foreign protein results in growth impairment. This was successfully demonstrated by Kurtz *et al.*, who over-expressed an ion-channel forming protein from the influenza virus in *S. cerevisiae* resulting in reduced growth, which was corrected in the presence of enzyme inhibitors.[288] In addition, yeast can also be used as a transactivation platform, whereby modulation of foreign protein activity affects the levels of secondary messenger substrates or products which therefore leads to an altered phenotype. An assay of this type was developed by Middendorp *et al*. in their investigation of human β-secretase, an enzyme thought to be associated with Alzheimer's disease. They engineered a yeast strain in which the gene for histidine was under the control of a GAL promoter and β-secretase was responsible for the activation of invertase, an enzyme that catalyses the hydrolysis of sucrose to glucose. Glucose subsequently repressed the GAL promoter and prevented the production of histidine, meaning the yeast was non-viable on medium lacking this amino acid. On the other hand, in the presence of a β-secretase inhibitor no

invertase and hence no glucose was produced, permitting the growth of the yeast in the absence of histidine.[289]

The main advantage of cell-based target-directed screening is that the identity of the target is known, which makes the progression of hit compounds to the next stage of the drug discovery pipeline much more rapid. Furthermore, yeast-based screening provides several additional advantages including: straightforward genetic engineering, especially with respect to protozoan parasites; low cost of culture; and rapid growth rate.[290] One disadvantage of utilising either type of phenotypic assay is that hit compounds which do not cross the plasma membrane will not be identified, even though a simple resynthesis might solve the problem; this issue is exacerbated in yeast which has the additional barrier of the cell wall. In addition, the target in yeast is tested in its non-native environment which could affect protein function and interaction. As each assay format has its pros and cons, it is therefore necessary to take all of these into consideration when selecting the most suitable format for each individual HTS campaign.

1.4.2.2.3 Assay Optimisation

Once the appropriate assay format has been selected it must be carefully optimised for several parameters, the primary one being cost. The need to lower cost was the driving force behind the miniaturisation process from 96-well plates down to 384-well and 1,536-well plate formats. However, it has been observed that reagent costs may not decrease linearly with the reduction in assay volume as proportionally more material is required in order to obtain the same signal and data quality. For example, in a comparison of different assay formats for Kinase assays, Klumpp *et al.* observed that for luminescence assays, the total volume was reduced eight-fold in 1,536-well format compared to 384-well format but the amount of luminescence reagent could only be reduced four-fold. In contrast, with fluorescence resonance energy transfer (FRET) assays and fluorescence polarisation assays the reduction in reagent required was proportional to the reduction in total volume.[291]

As HTS deals with large numbers of samples, the time required to run the assay on a day-to-day basis is another key factor. Assays that require either a long setup period or exhibit a slow plate readout rate are highly disfavoured as they result in equipment

backlogs.[292] It is also essential to determine the tolerance of the assay to the solvent the test compounds are delivered in, which is usually dimethyl sulphoxide (DMSO). This solvent is utilised in the assay as a negative control, so during assay development it is necessary to check whether different concentrations of the solvent affect the readout;[293] this is particularly important for phenotypic assays as many organic solvents have damaging effects on cell membranes and are therefore toxic.[294] For biochemical assays, buffer composition, pH and concentration is critical and must closely resemble the natural environment of the target to ensure it behaves as expected.[247] Finally, running the assay at the optimum temperature will decrease the time required to obtain a signal of sufficient quality.

Overall, assay development is generally the longest part of the HTS campaign given the sheer number of variables to consider. The process can take anywhere from a few weeks (if a similar screen has been conducted before and only a few modifications are needed) to several months (if an entirely new screening format is required for a novel target). A few trial plates at the selected conditions are tested using a known inhibitor to ensure signal to noise ratio is high enough before progressing to the next stage.

1.4.2.3 Assay Validation

The purpose of validation is to assess how the optimised assay will perform under high throughput conditions. This includes obtaining predictions of hit rate, F+ and false negative (F−) rates as well as determining robustness and day-to-day reproducibility of the assay.

In order to achieve this, a representative sample from the compound library to be screened is selected at random. The size of this sample is typically between 1% and 5% of the total library size; any smaller would reduce the usefulness of validation in predicting the factors mentioned above, whilst any larger would result in a large waste of material should any major problems be identified.[247] These compounds are subsequently dispensed into triplicate sets of plates, with some wells being reserved for the solvent negative control and a known inhibitor as a positive control. Each set is then

run on a different day using the conditions that have been optimised for the HTS assay.[295]

The first check performed upon undertaking assay validation is that there are no technical problems, such as issues with setup, robotics or plate readers, involved in running the assay. One such issue was flagged by Maddox *et al.* during their screen for novel upregulators of the heat shock protein 70 promoter, where a linear trend between the order of plate preparation and the signal to noise ratio was observed. Further investigation revealed that the time the plates were left at room temperature after setup but prior to incubation correlated proportionally with an elevation of background levels of activity, hence batch size had to be reduced to minimise the amount of time between dispensation and incubation.[296]

Upon obtaining numerical results from validation, computational analysis is then required to determine whether the assay is suitable to progress to the primary HTS screen. Primarily, the data allows an estimation of the hit rate for the assay. In order to be classed as a hit the compound must show a percentage activity above the statistically-defined threshold which is calculated as shown in equation 1.1.[297] The ideal hit rate in a primary HTS is about 1%; anything much higher than this will result in many potentially valid compounds having to be discarded at the next step of the screening campaign. One method of reducing a high hit rate is to lower the concentration of test compounds so as to remove those of lower potency; this technique was successfully employed by Urban et *al.* in a screen for chaperones of glucocerebrosidase, a protein which, when mutated, causes Gaucher's disease. Their initial screen produced too many compounds for them to investigate further, but they were able to reduce their hit rate from 4.3% to 0.7% by lowering the compound concentration from 76.7 μM to 15.3 μM.[298] Significantly high hit rates (> 10%) are indicative of a problem with the assay, such as an excessive solvent concentration or elevated temperature affecting the target.

Another important statistical value calculated is the Z-prime factor (Z′), the formula for which is given in equation 1.2.[299] This replaced the previously utilised signal to noise ratio which, whilst measuring the difference between positive and negative samples, does not take result variability into account. Z′, on the other hand, is

calculated using both the means and standard deviations of the samples so is a much more accurate measure of assay robustness. It is essentially a measure of positive and negative population separation, as shown in Figure 1–20. In order to obtain the most reliable Z′, a large number of control wells would ideally be spaced randomly around a test plate to ensure the values obtained were independent of each other. In practice, this is not feasible; dispensing compounds, either manually or robotically, into random wells rather than a common layout would drastically decrease throughput. In addition, the larger the number of control wells, the fewer wells available for test compounds. As a result, two columns per plate are typically reserved – one each for the positive and negative controls – and these are preferably centralised to avoid edge-related bias. Whilst Z′ > 0.5 was originally considered very good,[299] 0.5 is now generally considered to be the minimum Z′ for a high throughput assay to be approved, with Z′ > 0.7 being excellent.[300-302]

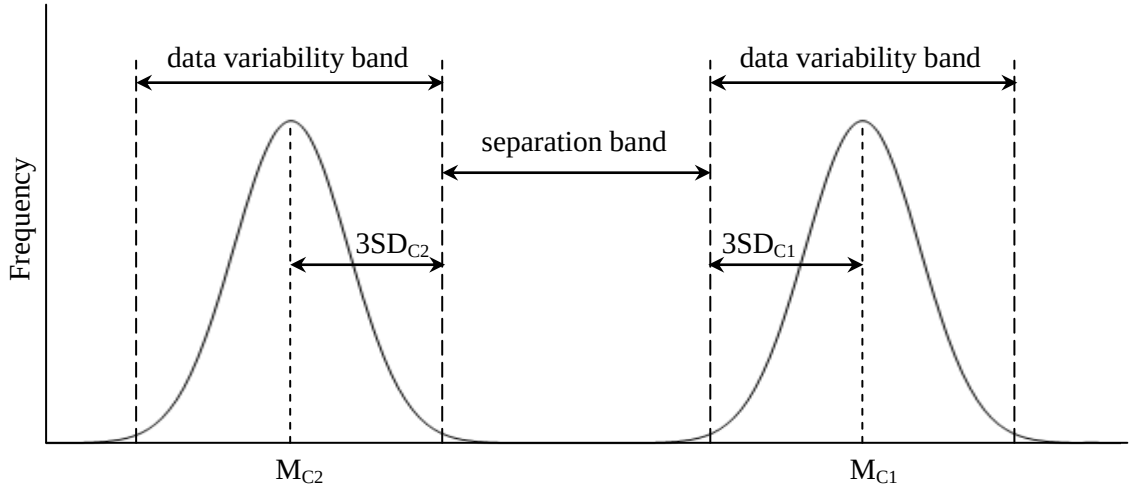

Figure 1–20: Idealised Gaussian distributions of the data and separation bands typically observed in an assay (adapted from Zhang *et al.*[299] with permission). Abbreviations are as in equation 1.2. The variability is 3SD (from the standard threshold calculation, equation 1.1) and encompasses 99.7% of the data points. The greatest separation and highest Z' will occur when the difference between the means is large and the standard deviation is small

$$\text{threshold} = M + (3 \times SD) \tag{1.1}$$

$$Z' = 1 - \frac{3(SD_{C1} + SD_{C2})}{\left|M_{C1} - M_{C2}\right|} \tag{1.2}$$

where: SD = standard deviation
M = mean
C_1 = negative control
C_2 = positive control

Finally, running the validation plates in triplicate allows an estimation of the F+ and F− rates for the assay. Compounds which produce a positive result in one plate and negative in the other two are F+, with compounds that produce a negative result in one plate and positive in two being F−. Of the two, the F− rate is more important; following primary HTS, compounds which are F+ can be identified and discarded after the confirmation screen, whilst compounds which are F− will be lost in the primary screen and have no chance of being recovered. Therefore, whilst the F+ rate can reach as high as 10% without causing alarm, a F− rate greater than 2% is generally considered unacceptable.[303]

1.4.2.4 HTS Implementation and Data Analysis

Following a successful validation the primary screen can finally be undertaken. Given the difficulties that often arise during target selection and assay development, the screen itself is often the easiest part of the whole HTS campaign although it involves several stages and can still be extremely time consuming (Figure 1–21). The most difficult task is ensuring consistency across the entire time period of the screen, so it is preferable that all reagents used are from the same batch and all biological material used originates from the same source. The throughput rate is dependent on the technical parameters of the assay, such as incubation time and plate reading time.

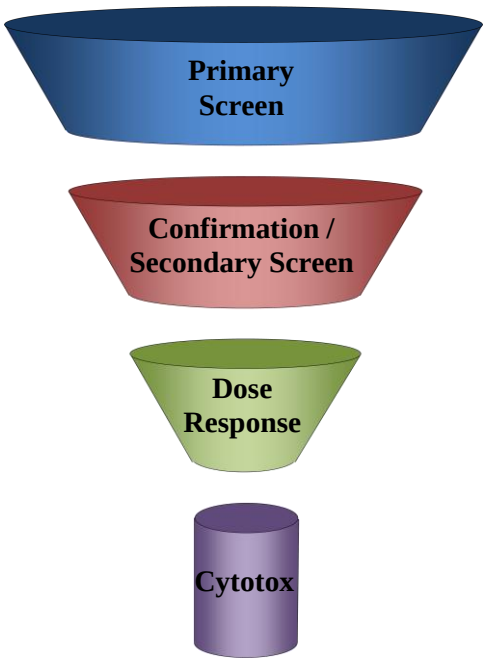

Figure 1–21: Compound attrition through the HTS cascade

Despite the care taken, there is a possibility that systematic errors will be observed in the HTS results.[304, 305] Common causes of this include plate positional effects in either dispensation or reading (where certain rows or columns exhibit consistently high or low values in comparison to the rest of the plate)[306] and uneven temperature or evaporation effects across the plate.[307] The latter has become an increasingly common occurrence as assays have miniaturised; the loss of 1 µl of moisture from a 5 µl assay in a 1,536-well plate has a much more pronounced effect than the loss of the same volume from a 50 µl assay in a 384-well plate.

Compounds which are identified as hits are then screened again, in the same format as the primary HTS, in duplicate. This step is termed confirmation and is used for two purposes: to identify and eliminate any compounds which were F+ in the first screen (as described in section 1.4.2.3); and to obtain average percentage activities for compounds which are true hits.[247] Alternatively, an orthogonal secondary screen can be used at the confirmation stage to validate the hits from the primary screen, before active compounds are progressed to the next stage which is called dose response. Here, compounds are screened in duplicate at a range of concentrations (these vary between screens and pharmaceutical companies but generally range from ~100 µM to ~1 nM) in order to calculate their half maximal inhibitory concentration (IC_{50}).[308] This stage may be carried out used either the primary or secondary assay, although the biochemical assay is generally utilised given that it is directly testing the response of the target.

The final phase of the HTS implementation process is a cytotoxicity assay. This involves screening the hit compounds against human cells in order to check for off-target toxicity.[309] The cells used are usually HepG2 hepatoma cells given that the liver is the organ most commonly damaged by drugs; a study in 2003 showed that drug-induced liver injury accounted for more than 50% of cases of acute liver failure in the United States,[310] with more than 600 drugs being linked to hepatotoxicity.[311] Compounds which are active in this assay are therefore instantly discarded as they are too hazardous to progress further.

1.4.2.5 Lead Selection

Depending on the numbers of compounds which are inactive in the cytotoxicity assay, some or all of them are given lead status. These may not necessarily be the compounds which produce the highest response; compounds with slightly less activity but more favourable pharmacokinetic profiles will be given priority as these are more likely to eventually make better drugs, as was demonstrated by Lipinski *et al.* in 1997.[312] The group studied over 2,000 drugs and drug candidates in clinical trials and found that the best oral drugs, which tended to be membrane permeable and hence readily absorbed by the body, tended to have properties which fell within certain limits. These guidelines are referred to as 'the rule of 5' and cover molecular weight (< 500), LogP (< 5), number of H-bond donors (< 5) and number of H-bond acceptors (< 10).[312] These criteria are commonly used as a measure of drug-likeness, and any screening hits that match (or are close to) these criteria will certainly be considered for lead status.

It is, however, important to note the distinction between drug-like and lead-like candidate compounds. As discussed above, the former display properties common among approved drugs; this does not, however, mean that they are amenable to a lead optimisation campaign. In contrast, lead-like compounds tend to be smaller with simpler chemical structures, which facilitates subsequent modification, whilst retaining the other favourable physiochemical properties.[313] Lead optimisation is therefore generally faster and more cost effective for these compounds. As a result, an assortment of both drug-like and lead-like compounds may be delivered to the medicinal chemists for lead optimisation, marking the end of the HTS phase of the drug discovery process.

1.4.3 Perspectives

In summary, HTS is a process which allows large libraries of compounds, ranging from several thousand to a few million, to be tested against a particular biological target or system. It is therefore of paramount importance to many drug discovery campaigns, allowing the acquisition of large amounts of data in a timescale that would have been inconceivable just a few decades ago. Despite this, its usefulness has been called into question by many groups given the low number of clinical successes that have resulted from this particular method.[314-316] On the other hand, strong proponents of HTS argue

that the high number of lead compounds identified by this method is sufficient proof that it remains one of the most valuable tools in drug discovery.[317, 318]

Irrespective of personal opinion, HTS continues to be the method of choice for the lead generation stage of many current drug discovery campaigns. As such, the field is continually advancing both in terms of technological developments and increasing the quality and diversity of chemical libraries.[319] Consequently, it can be predicted that HTS will continue to play a vital role in drug discovery for many years to come.

1.5 Project Aims

1.5.1 Previous Work

Building on the discovery of the kinetoplastid IPCS enzymes by Denny *et al*., work in the group subsequently focussed on constructing a yeast expression system to produce the *L. major* IPCS (*Lmj*IPCS). This was achieved by bringing the yeast AUR1 enzyme under the control of a GAL promoter which was repressed in the presence of glucose, meaning that the yeast was reliant on the expression of the *Lmj*IPCS from an added plasmid. Following this, further work revolved around formatting an assay to screen the enzyme biochemically, which was subsequently used to screen a synthesised library of substrate analogues. The expression system was also successfully formatted for isoform 4 of the *T. brucei* sphingolipid synthase enzyme (*Tb*SLS4) and plant orthologues.[212, 217, 320, 321]

However, doubt was later cast on the expression system by Sevova *et al*., who observed that *Tb*SLS4 was capable of synthesising sphingomyelin and ethanolamine phosphorylceramide but not IPC.[322] They suggested that this could be due to leaky expression from the GAL promoter, which would result in some AUR1 being produced and hence IPC product being observed. This therefore threw the results obtained thus far in the group into question. In addition, the biochemical assay developed is only suitable for low throughput screening in 96-well plate format due to the numerous manual separation steps that are involved.

1.5.2 Objectives

With the above limitations in mind, the aims of the project were as follows:

1. To establish a new system to produce the *Lmj*IPCS and *T. brucei* orthologues (referred to as sphingolipid synthases (SLSs) given that they are multifunctional)[211] that would eliminate the potential for leaky expression of AUR1 and hence confirm whether they are functional orthologues of the yeast enzyme.
2. To design, develop and implement a novel assay utilising the constructed strains to screen the 1.8 million compound collection at GlaxoSmithKline (GSK) in order to identify novel small molecule inhibitors.
3. To perform secondary screening (both biochemical and *in cellulo* against parasites) in order to determine whether any of the compounds selected were suitable for lead development.
4. To explore SARs for this lead series in order to ascertain whether the efficacy of the lead compound(s) could be enhanced in order to produce the best possible candidate to be progressed further down the drug discovery pipeline.

Chapter 2

Analysis of *Lmj*IPCS and *Tb*SLS Enzymes

2.1 Introduction

As discussed in section 1.5, Sevova *et al*. disputed the previously utilised expression system, citing the potential for leaky expression of the yeast AUR1 protein.[322] In order to address this claim, a novel expression system was required. Rather than keeping AUR1 expression under promoter control, the removal of the AUR1 coding sequence entirely would result in yeast completely dependent on a kinetoplastid SLS for growth. This would therefore completely eliminate the possibility of leaky expression of AUR1. Further characterisation of the kinetoplastid SLSs would hence be possible and would either confirm or disprove the results previously published.

2.2 Construction of Complemented Mutant Yeast Strains

L. major contains a single IPCS enzyme, the gene sequence for which is located in the TriTrypDB genome database with the accession number LmjF.35.4990. With much of the previous work in the group centring around *Lmj*IPCS, this enzyme was the primary focus. The *Tb*SLS4 enzyme also required investigation as, as discussed in section 1.5.1, the ability of this enzyme to function as an IPCS was questioned in the literature. This enzyme was therefore investigated along with *T. brucei* sphingolipid synthase isoform 1 (*Tb*SLS1) in order to confirm this activity. The gene sequences for *Tb*SLS1 and *Tb*SLS4 are located in the TriTrypDB database (http://www.tritrypdb.org/tritrypdb/) for the *T. brucei* Lister 427 strain with the accession numbers Tb427tmp.211.1030 and Tb427tmp.211.1000 respectively.

The coding sequences were cloned into multiple cloning site (MCS) 2 in the pESC-LEU (pEL) plasmid vector (Figure 2–1),[323] bringing the enzymes under the control of a GAL promoter. The plasmids were amplified in *E. coli* before being purified and used to transform the *α ade*$^{-}$*.lys*$^{-}$*.leu*$^{-}$*.Δaur1*::*TRP1*.pRS316.*URA*$^{+}$*.ScAUR1*$^{+}$ *S. cerevisiae* strain. This is a strain in which the genomic *AUR1* has been knocked out and replaced by the *TRP1* gene encoding tryptophan, with the *AUR1* gene, encoding the essential IPCS, being reintroduced on a plasmid. A kind gift from Prof. T. Dunn, this strain had previously been utilised to confirm the function of the *Arabidopsis thaliana* protein ERH1 as an IPCS.[324] In addition to the three kinetoplastid SLSs, the *S. cerevisiae* strain was also transformed with pEL.*ScAUR1*$^{+}$ as a control. The transformants were grown on permissive SGR medium; this contained galactose to induce expression of the IPCSs and raffinose to act as a carbon source, and lacked tryptophan and leucine in order to select for successful transformants.

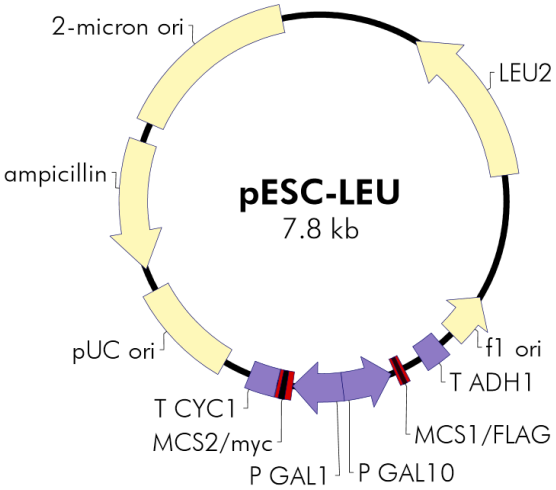

Figure 2–1: The structure of the pEL plasmid.[323] The genes for ampicillin resistance and LEU2 are selectable markers for *E. coli* growth and *S. cerevisiae* growth respectively. The two MCSs are under the control of GAL promoters, so are active in the presence of galactose and repressed in the presence of glucose

In order to cure the yeast of the pRS316.*URA3*$^{+}$*.ScAUR1*$^{+}$ plasmid, the successful transformants were subsequently grown on medium containing 5-fluoroorotic acid (5FOA). In cells maintaining the aforementioned plasmid the gene product of *URA3*, the enzyme orotidine 5′-phosphate decarboxylase, coverts 5FOA to fluorouracil, a toxic analogue of uracil, resulting in cell death (Figure 2–2).[325] This process is known as a plasmid shuffle.

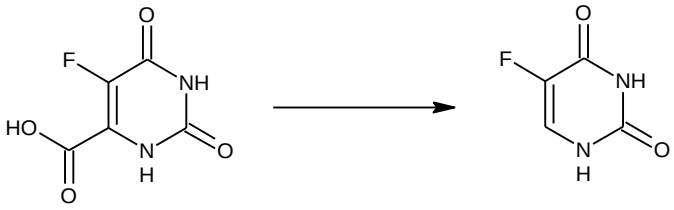

Figure 2–2: The conversion of 5FOA to fluorouracil by orotidine 5′-phosphate decarboxylase

The yeast transformed with pEL.*LmjIPCS*$^{+}$ (α-*Lmj*) was able to grow on 5FOA medium, and a successful plasmid shuffle was confirmed by colony polymerase chain reaction (PCR) (Figure 2–3 (a)). Confirmation of *L. major* IPCS as a functional homologue of AUR1 was subsequently achieved using a complementation assay, in which α-*Lmj* and the control strain complemented with pEL.*ScAUR1*$^{+}$ (α-AUR1) were streaked on both permissive and non-permissive medium (Figure 2–3 (b)). The complemented yeast strains were only capable of growth on permissive medium, verifying that not only are they functionally homologous, but that a functioning IPCS enzyme is essential for yeast growth. This was confirmed by Dr N. Wansadhipathi-Kannangara, who observed that neither of the two human SMS enzymes is capable of rescuing *aur1Δ* yeast.[326]

The yeast transformed with pEL.*TbSLS1*$^{+}$ (α-*Tb*1) or pEL.*TbSLS4*$^{+}$ (α-*Tb*4) both plasmid shuffled successfully, as confirmed by colony PCR (Figure 2–4 (a)). When the strains were tested in the complementation assay they exhibited the same growth pattern as both the previously tested α-*Lmj* and the α-AUR1 control (Figure 2–4 (b)). As the engineered yeast strains are fully dependent on the *T. brucei* SLS enzymes in the absence of endogenous AUR1, this strongly suggests that *Tb*SLS1 and *Tb*SLS4 are functional homologues of AUR1 and are capable of synthesising IPC.

The results obtained thus far are in accord with those previously observed in the group. However, in addition to questioning the expression system, Sevova *et al*. also reported that the *Tb*SLS enzymes were insensitive to the fungal IPCS inhibitor AbA (**17**, Figure 1–15).[322] This contradicts the group's study in which *Tb*SLS4 was observed to be sensitive to AbA.[217] This discrepancy therefore required further investigation.

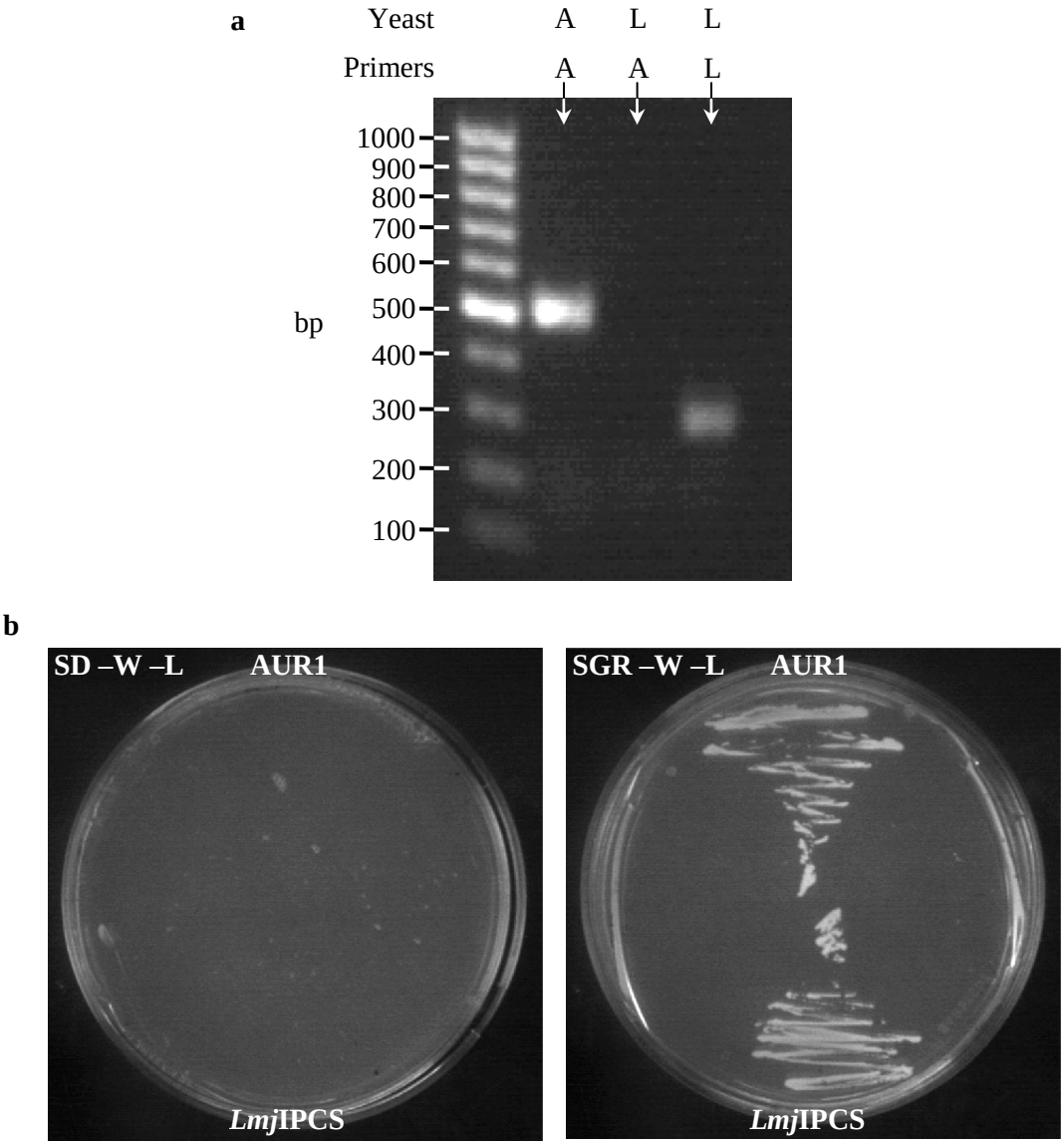

Figure 2–3: (a) Colony PCR of the plasmid shuffled strains, using primers designed to amplify fragments of the inserted coding sequences. A refers to the α-AUR1 strain and *AUR1*-specific primers and L refers to the α-*Lmj* strain and *Lmj*IPCS-specific primers. No PCR product is observed when the α-*Lmj* strain is cycled with *AUR1*-specific primers, indicating that the plasmid shuffle was successful. (b) Complementation of *α ade*$^{-}$*.lys*$^{-}$*.leu*$^{-}$*.Δaur1*::*TRP1* with pEL.*LmjIPCS*$^{+}$ and the control pEL.*ScAUR1*$^{+}$. No growth was observed on glucose-containing medium (SD) due to the repression of expression from the GAL promoter. Both strains displayed growth on galactose-containing medium (SGR) as this induces expression

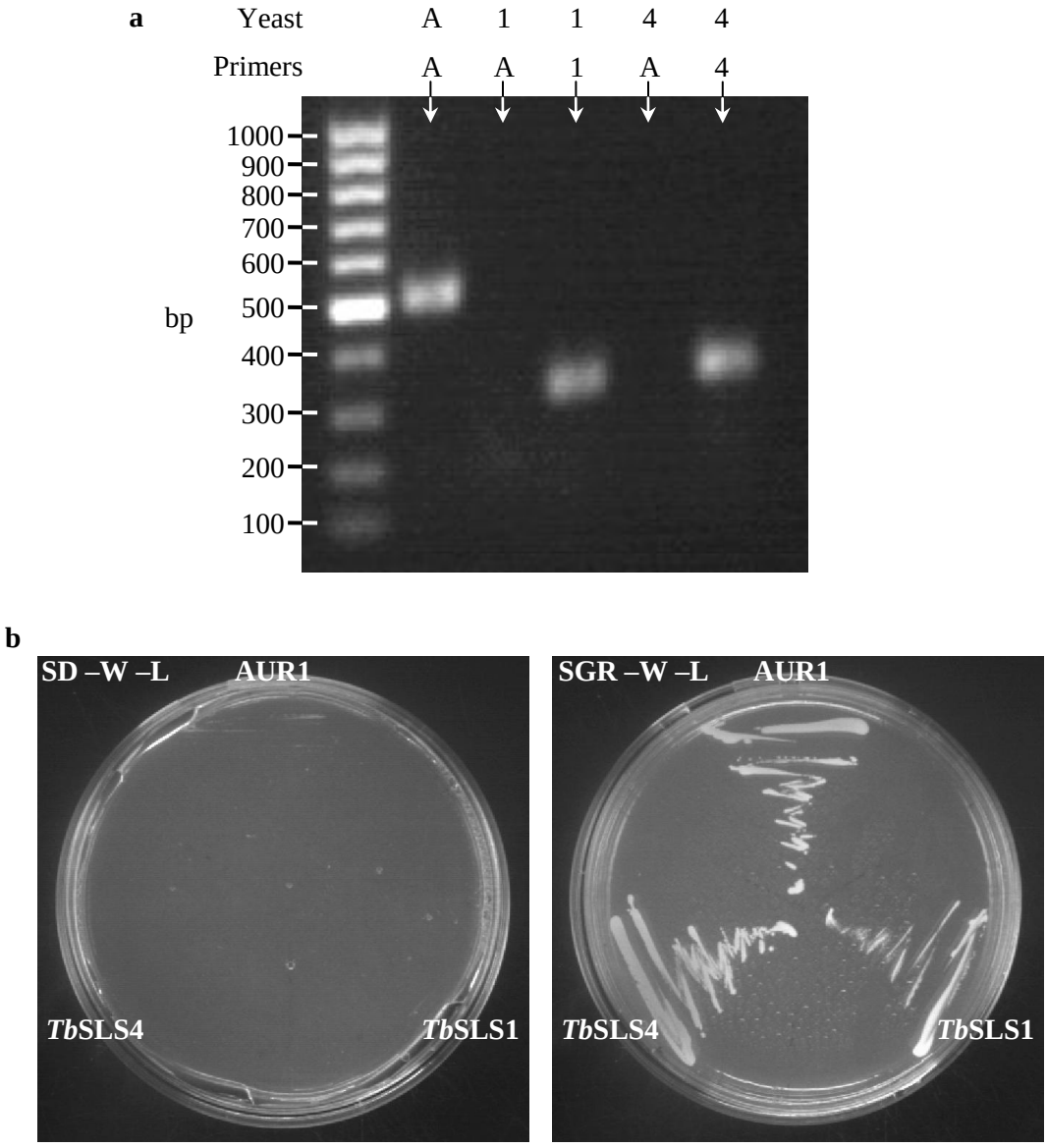

Figure 2–4: (a) Colony PCR of the plasmid shuffled strains, using primers designed to amplify fragments of the inserted coding sequences. A refers to the α-AUR1 strain and *AUR1*-specific primers, 1 refers to the α-*Tb*1 strain and *Tb*SLS1-specific primers and 4 refers to the α-*Tb*4 strain and *Tb*SLS4-specific primers. No PCR product is observed when the α-*Tb*1 or α-*Tb*4 strains are cycled with *AUR1*-specific primers, indicating that the plasmid shuffle was successful. (b) Complementation of *α ade*$^{-}$*.lys*$^{-}$*.leu*$^{-}$*.Δaur1*::*TRP1* with pEL.*TbSLS1*$^{+}$, pEL.*TbSLS4*$^{+}$ and the control pEL.*ScAUR1*$^{+}$. No growth was observed on glucose-containing medium (SD) due to the repression of expression from the GAL promoter. All strains displayed growth on galactose-containing medium (SGR) as this induces expression

2.3 Sensitivity of Kinetoplastid SLSs to AbA

2.3.1 Diffusion Assay

The sensitivity of the complemented yeast strains to 100 µM AbA was first tested in a diffusion assay. This involved embedding the yeast in permissive medium solidified with agarose before applying the inhibitor as a solution in DMSO. This was able to diffuse through the agarose and, if active, produce a clearance zone around the point of application where the yeast would be unable to grow.

The results are shown in Figure 2–5. As expected, α-AUR1 exhibited sensitivity to AbA whilst α-*Lmj* did not, a result which mimics those obtained previously in the group.[212] Notably, the *Tb*SLS strains demonstrated differential sensitivity to AbA with α-*Tb*1 being insensitive and α-*Tb*4 being sensitive. This difference is an extremely interesting observation given the high homology between the two coding sequences (90% identity) and protein sequences (86% identity) and hence a secondary, orthogonal assay was required in order to confirm this result.

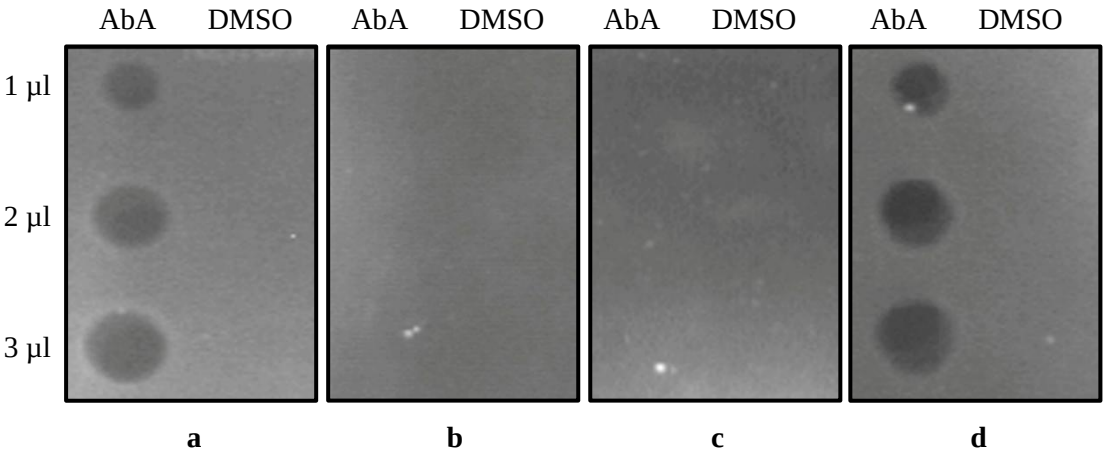

Figure 2–5: Diffusion assay of (a) AUR1, (b) *Lmj*IPCS, (c) *Tb*SLS1 and (d) *Tb*SLS4. AUR1 and *Tb*SLS4 demonstrate sensitivity to 100 µM AbA as can be seen by the formation of clearance zones, whilst *Lmj*IPCS and *Tb*SLS1 do not

2.3.2 Biochemical Assay

In order to verify the results obtained in the diffusion assay, the sensitivities of the kinetoplastid SLSs were investigated biochemically. This necessitated the production of microsomal membrane material, which was undertaken according to the established

protocol.[320] However, low yields of below 0.05% were consistently obtained, which were far lower than those previously reported. Increasing the number of vortexing cycles and the mass of glass beads used resulted in marginal improvements. The crucial factor for increasing the yield was found to be the size of the glass beads; the maximum yield obtained using 212−300 µm beads was 0.08% whilst yields up to 0.45% were obtained using 425−600 µm beads; this therefore suggests that larger beads led to increased disruption of the yeast cells.

With the microsomal membranes in hand, the sensitivities of the kinetoplastid SLSs to 1 µM AbA were tested using the established high-performance thin layer chromatography (HPTLC) assay.[320] This protocol involved the incubation of the crude microsomal membrane fractions (in the absence of additional PI) with NBD-C_6-ceramide, a fluorescent analogue of ceramide, in the presence of an inhibitor. The turnover of this commercially available substrate to the fluorescent product NBD-C_6-IPC, as shown in Figure 2–6, was determined by separating the components of the reaction mixture on a HPTLC plate and visualising using a fluorescence scanner. NBD-C_6-ceramide has an R_f of 0.96 whilst NBD-C_6-IPC has an R_f of 0.57, resulting in well-defined separation and resolution between the two bands.[212]

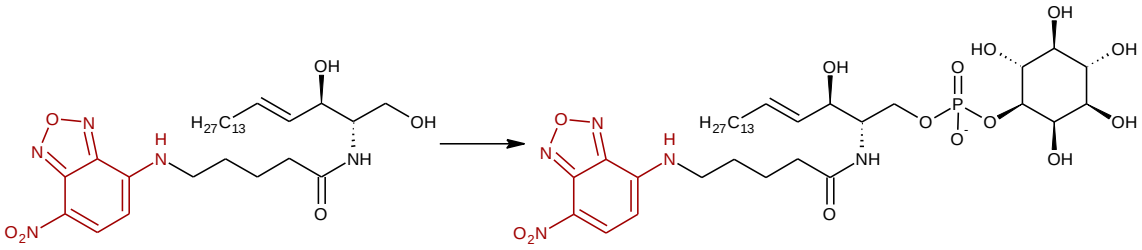

Figure 2–6: The conversion of NBD-C_6-ceramide to NBD-C_6-IPC by IPCS

The results, shown in Figure 2–7, validate what was observed in the diffusion assay, confirming the differential sensitivity of the two *Tb*SLS enzymes to AbA. This observation is even more significant in this assay due to the lower concentration used for testing. Unexpectedly, however, only a single product was observed for *Tb*SLS4. Whilst a single product is the expected case for *L. major*, the SLS enzymes of *T. brucei* have previously been shown to be multifunctional; *Tb*SLS1 synthesises both IPC and sphingomyelin, and different studies suggest that *Tb*SLS4 is capable of synthesising IPC, sphingomyelin and ethanolamine phosphorylceramide.[211, 217] Whilst a faint band for sphingomyelin can be seen for *Tb*SLS1, IPC is the only band observed for *Tb*SLS4.

No explanation can be offered for this observation, although it is possible that additional products are being produced in concentrations too low to be detected.

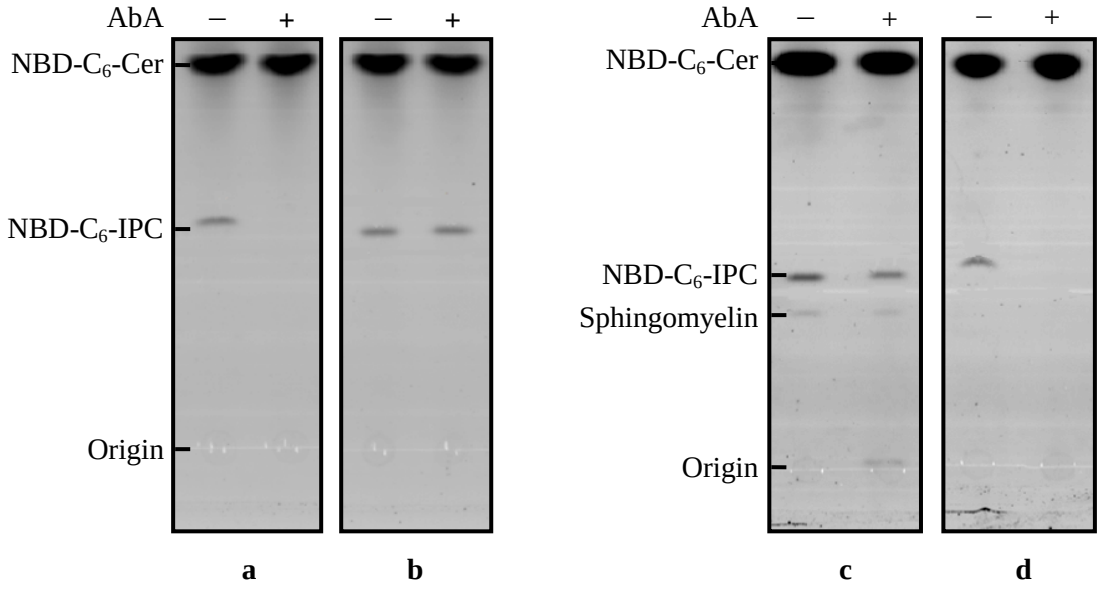

Figure 2–7: HPTLC assay of (a) AUR1, (b) *Lmj*IPCS, (c) *Tb*SLS1 and (d) *Tb*SLS4 in the presence (+) or absence (−) of 1 μM AbA. AUR1 and *Tb*SLS4 demonstrate sensitivity to AbA, as can be seen by the lack of NBD-C_6-IPC formation, whilst *Lmj*IPCS and *Tb*SLS1 do not. The apparent differences in the R_f of NBD-C_6-IPC is likely due to the high volatility of chloroform and hence slight variations in the solvent system used to run the HPTLC plates

Although the reason for the observed differential sensitivity has not yet been determined, there are a few potential explanations. One possibility is that the kinetoplastid SLSs interact differently with KEI1, an AUR1 accessory protein identified by Sato *et al.*[327] Mutant *S. cerevisiae* lacking the KEI1 protein showed decreased IPC production and hypersensitivity to AbA, demonstrating its essentiality in the correct functioning of IPCS. The ability of KEI1 to interact with IPCSs of different origins could therefore affect the activity observed, with poor interaction resulting in reduced activity and increased sensitivity. Alternatively, slight differences in the protein sequences could be responsible. As can be seen in Figure 2–8, whilst the *Tb*SLS protein sequences are highly conserved there are a couple of regions where the sequences differ. The first of these regions is a putative transmembrane domain, and therefore unlikely to be involved. The other is at the cytosolic C-terminus and is therefore more capable of interaction with other proteins or compounds.

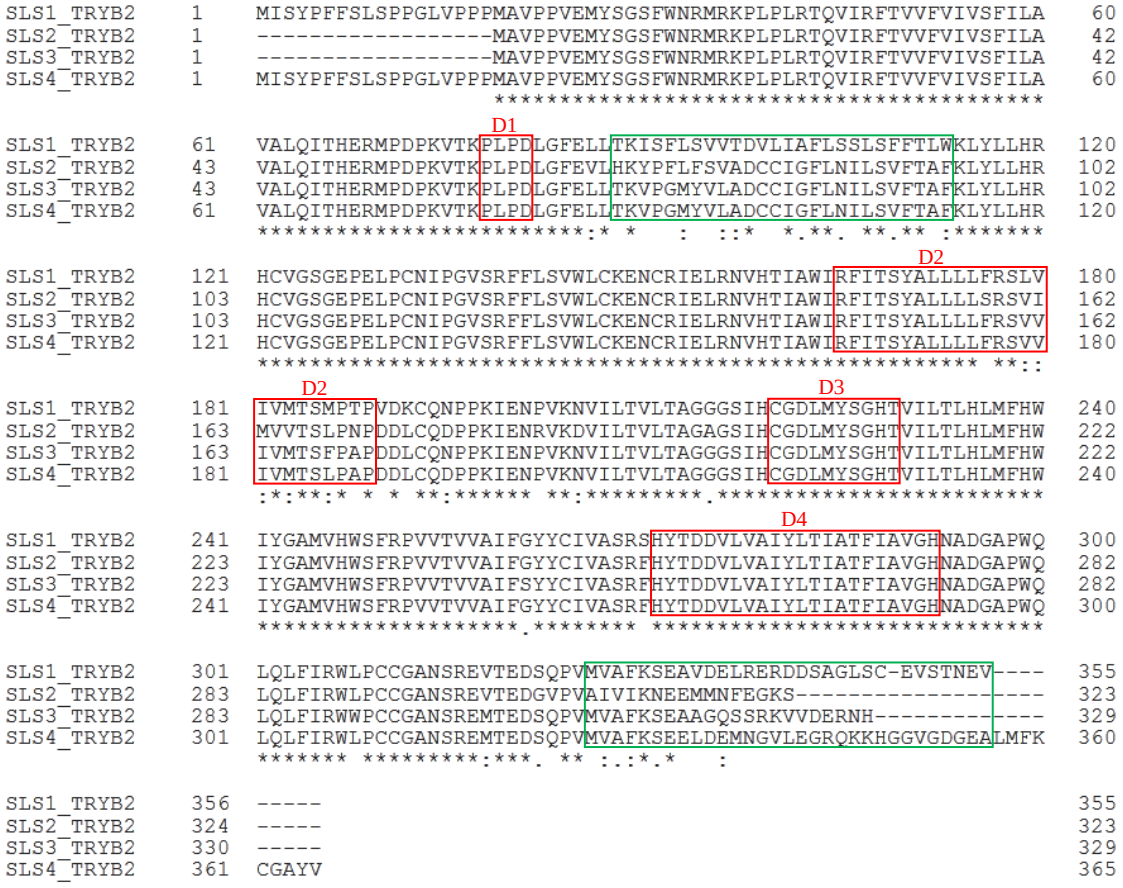

Figure 2–8: Alignment of the four *Tb*SLS coding sequences with the conserved domains proposed by Huitema et al.[209] for SMS shown in red and the variable regions shown in green

One additional possibility is that enzyme function is being affected by small variations in protein sequence. The alignment of the amino acid sequence for *Tb*SLS4 determined in-house with those from Goren *et al.*,[211] the TriTrypDB database (http://www.tritrypdb.org/tritrypdb/) and the UniProt archive (http://www.uniprot.org/) is shown in Figure 2–9 and demonstrates a lack of sequence consensus. Whilst this may be explained for UniProt sequence due to the source strain being different (*T. brucei* TREU927 rather than Lister 427) there are still eight positions where amino acid identity differs between the other three sequences. Notably, there is also a deletion in the Durham sequence compared to the other three, and this along with seven of the ten amino acid discrepancies are located in the C-terminal region beyond D4.

Figure 2–9: Alignment of the *Tb*SLS4 coding sequences with the conserved domains proposed by Huitema et al.[209] for SMS shown in red, amino acid variations shown in green and the deletion shown in blue

This could be significant given that there is still debate as to where AbA binds to the IPCS enzyme. In an investigation of the yeast AUR1 enzyme, Aeed *et al*. observed conflicting results; synthetic compounds based on fragments of AbA showed competitive inhibition, suggesting binding in the active site, whereas AbA showed non-competitive inhibition against an AbA-resistant AUR1 mutant.[328] This resistance was due to the mutation of a single amino acid (F158Y) that is considerably removed from the residues of the catalytic triad, and whilst it is possible that this mutation results in a conformation shift that prevents AbA binding in the active site, it is equally possible that this residue is involved in AbA binding. Interestingly, mutation of the neighbouring amino acid (H157Y) also generates a resistant enzyme,[200] which might support the theory that AbA binding is distant from the active site. The C-terminal region, which is a large cytosolic domain (and hence more accessible than the active site in the Golgi lumen), might therefore present a possible binding site in the kinetoplastid IPCS enzymes.

Furthermore, the C-terminus has been shown to be essential for IPCS function; Nagiec *et al*. demonstrated that a frame-shift mutation of AUR1 resulting in deletion of the C-terminus led to a loss of IPCS activity.[202] It is therefore possible that some residues in this region may be essential for activity and, given that the *Tb*SLS enzymes are multifunctional, it could be hypothesised that one or more of the mutations in the Durham sequence may be responsible for the apparent lack of sphingomyelin synthase activity demonstrated by *Tb*SLS4. Further investigation, such as site-directed mutagenesis to identify the key residues responsible for IPC and sphingomyelin synthase activity as well as AbA sensitivity, would be required to fully investigate this observation.

2.4 Conclusion

The work described in this chapter involved the construction of yeast strains complemented with kinetoplastid SLS enzymes. *Lmj*IPCS, *Tb*SLS1 and *Tb*SLS4 were all shown to be capable of synthesising IPC, and whilst *Lmj*IPCS and *Tb*SLS1 were insensitive to AbA, *Tb*SLS4 was found to be sensitive. This supports the previous work undertaken in the group and is evidence that selective inhibition of related kinetoplastid SLSs is achievable.

Having constructed and validated the complemented strains, attention turned to the second aim of the project, which was to develop and implement a HTS-compatible assay. Neither of the assays utilised thus far are suitable; both are low throughput and quantification of the results is possible but imprecise. The 96-well plate format biochemical assay is also unsuitable due to the numerous manual handling steps required.[320] A miniaturised cell-based assay using the constructed strains was therefore required, and the development of this will be described in the following chapter.

Chapter 3

Development of a HTS-Compatible Assay

3.1 Introduction

With the engineered yeast constructs in hand, the next step was to establish a HTS-compatible assay in order to screen the 1.8 million compound library held at the GSK facilities located in Tres Cantos, Spain. As discussed in section 1.4.2.2.3, a number of factors had to be considered when designing the assay, with cost and time being the major issues. As a result, the assay was required to be quick and easy to run, maximising the use of automation and minimising the number of reagents and components involved.

Of the three strains constructed, α-*Lmj* was selected to be used in the screen for two reasons. Firstly, whilst the number of HAT cases has decreased by 76% since 2000, the number of cases of leishmaniasis has increased exponentially and consequently is it considered by the WHO, and therefore also by GSK, to be a greater priority.[1] Secondly, *Leishmania* spp. possess only a single IPCS enzyme. *T. brucei* has four and, whilst RNA interference studies have shown that inhibiting gene expression of all four isoforms results in arrested division and some cell death,[217] it is not known whether the enzymes are redundant and therefore if the parasites could continue to divide and grow with up to three isoforms inhibited. HTS against *Tb*SLS would therefore have to be undertaken against all four isoforms in order to identify common inhibitors; this would be extremely time consuming, making α-*Lmj* the obvious choice.

3.2 Yeast Multiplexing Assay

3.2.1 Assay Rationale

The first assay format proposed was a novel multiplexing assay in which the growth of two different yeast strains in the same well could be compared by engineering the strains to produce different, complimentary fluorescent proteins. If, for example, α-*Lmj* produced green fluorescent protein (GFP) and α-AUR1 produced red fluorescent protein (RFP), the overall fluorescence readout from the wells containing test compounds would indicate which, if either, of the two strains was growing and hence which SLS had been inhibited (Figure 3–1). An assay of this type would also allow compounds that act via off-target effects to be identified.

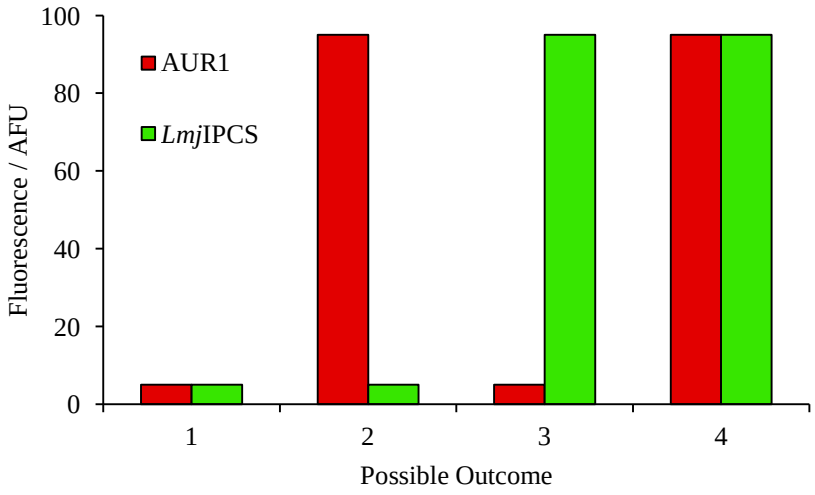

Figure 3–1: Graphical representation of the potential well readouts of the proposed multiplexing assay. If the test compound inhibits both AUR1 and *Lmj*IPCS or is a general antifungal (1), growth of both strains will be low and low fluorescence will be detected. If only *Lmj*IPCS is inhibited (2) the readout at red fluorescence wavelength (580−590 nm) would be much higher than at the green wavelength (505−510 nm), and vice versa if only AUR1 is inhibited (3). If the compound is inactive (4) both fluorescence readouts will be high

This strategy was possible due to the presence of two MCSs in the pEL plasmid vector, as shown in Figure 2–1. With the required SLS already present in MCS 2, the gene for the required fluorescent protein could be cloned into the vacant MCS 1 which would place it under the control of the GAL promoter. As a result, growing in medium containing galactose to induce SLS expression would also result in the same level of expression of the fluorescent protein, hence fluorescence levels should correlate with levels of growth.

3.2.2 Construction of Mutant Yeast Strains Expressing Fluorescent Proteins

The eGFP coding sequence was cloned into MCS 1 of the previously constructed pEL.*LmjIPCS*$^{+}$ and pEL.*ScAUR1*$^{+}$ plasmids. Further work on the construction of fluorescent strains was undertaken at Tres Cantos by Dr J. Mina, who successfully cloned the fluorescent proteins tRFP, mTurquoise and Venus into the pEL.*LmjIPCS*$^{+}$ and pEL.*ScAUR1*$^{+}$ plasmids. These plasmids were used to transform *S. cerevisiae* as discussed in the previous chapter, although a plasmid shuffle to remove the pRS316.*URA*$^{+}$.*ScAUR1*$^{+}$ plasmid was not undertaken.

3.2.3 Confocal Microscopy of Fluorescent Yeast Strains

The fluorescence profiles of the yeast strains were checked prior to further assay development by diluting the samples to produce a single cell layer on the bottom of the wells in a test plate, which was then analysed by confocal microscopy. Very low proportions of cell populations proved to be fluorescent, with tRFP being the only fluorescent protein that was detectably expressed in more than 10% of cells (Figure 3–2). This low and variable fluorescence output made accurate comparison of the growth of two different strains in the same well unfeasible. Consequently, although an assay of this type has since been reported,[287] it was concluded that this assay format was not robust enough for HTS and the reason for the low fluorescence was not determined due to time restrictions.

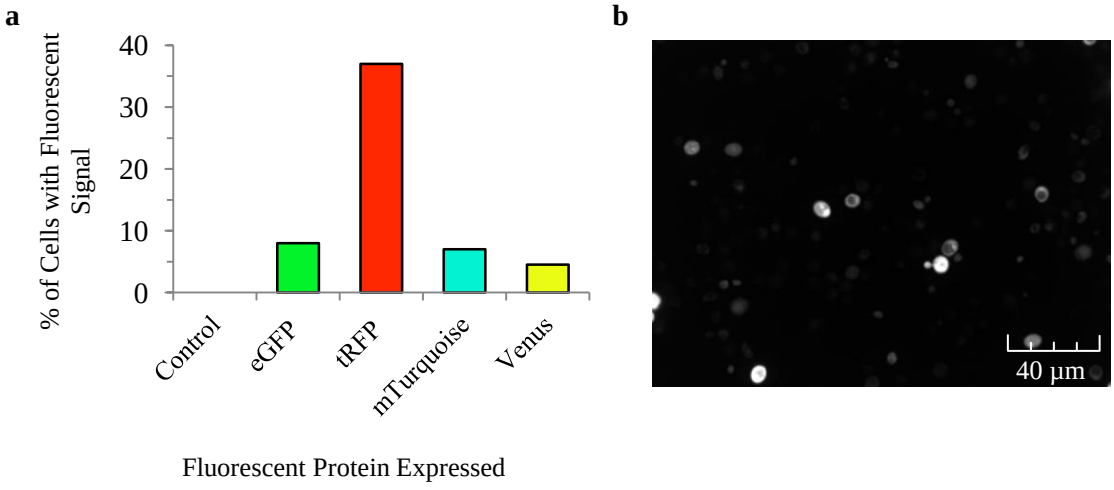

Figure 3–2: (a) The % of the cell population expressing the various fluorescent proteins and (b) the microscopic image of a monolayer of cells expressing eGFP. Low and uneven fluorescence readouts show that this was not a suitable option for HTS

3.3 Fluorescein Production Assay

3.3.1 Assay Rationale

Given that the multiplex assay format based on fluorescent protein expression was non-viable for HTS, an alternative format was required. It was subsequently proposed that the production of the extracellular enzyme exo-β-glucanase by *S. cerevisiae* could be exploited as a measure of growth. Whilst the intrinsic function of this enzyme is modification of the cell wall in preparation for budding, it is also capable of hydrolysing the commercially available, non-fluorescent substrate fluorescein di-(β-D-glucopyranoside) (FDGlu) to the fluorescent product molecule fluorescein, as shown in Figure 3–3.[329]

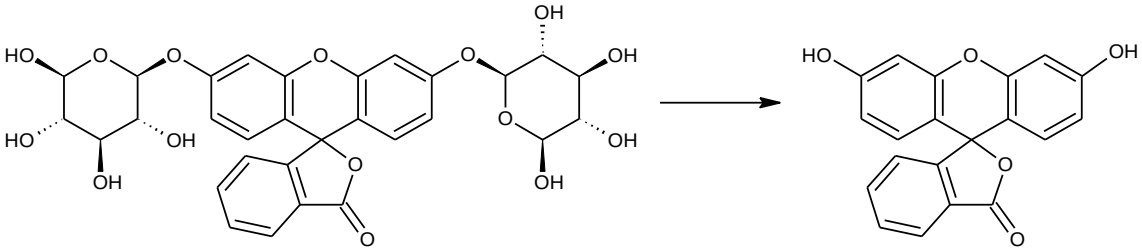

Figure 3–3: The hydrolysis of FDGlu to fluorescein by exo-β-glucanase

Although low levels of exo-β-glucanase are maintained throughout the cell cycle, it is thought that the enzyme is synthesised discontinuously with production limited to the G_2 phase in order to prepare for budding and cell division.[330] Therefore, in terms of a library screening assay, a compound which inhibits the SLS would prevent growth, resulting in little exo-β-glucanase production and hence low levels of fluorescence. On the contrary, an inactive compound would have no effect on growth and as a result exo-β-glucanase levels would increase as the yeast divides and grows, causing a subsequent increase in FDGlu hydrolysis.

3.3.2 Optimisation of Assay Parameters

FDGlu assays have been utilised in the past by GSK,[331, 332] so it was hoped that adaptation of the assay for screening the α-*Lmj* yeast would prove straightforward. This adaptation process comprised the optimisation of several parameters, the primary one being the constitution of the assay mixture. This included the composition of the

culture medium, the starting yeast culture concentration required to give sufficient growth and the concentration of FDGlu required to produce adequate fluorescence. The necessity for a buffer and identity of a suitable positive control compound were also investigated.

3.3.2.1 Galactose Concentration

As perhaps the simplest condition to study, the concentration of galactose in the culture medium was the first parameter to be investigated. Whilst galactose is required for the induction of expression of the SLS gene and hence is essential for the growth of the yeast, raffinose results in faster growth and hence is preferred as the primary carbon source.[333] The concentration of galactose therefore only needs to be high enough to induce expression.

In addition to investigating different galactose concentrations using glucose as a negative control, target validation was also permitted by the use of three test compounds. AbA (**17**, Figure 1–15), which has been shown to be inactive against *Lmj*IPCS, should inhibit growth of α-AUR1 but not α-*Lmj* whilst two general antifungals AmB (**4**, Figure 1–4) and cycloheximide (**20**) (Figure 3–4) should prevent the growth of either yeast strain.

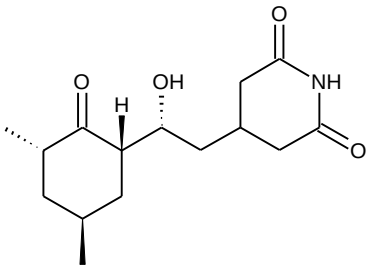

Cycloheximide (**20**)

Figure 3–4: The structure of the general antifungal cycloheximide, which inhibits protein biosynthesis

Various conditions were tested in a matrix assay in a 96-well plate (Appendix A.1) against both α-*Lmj* and α-AUR1. Compound concentration was decreased down rows A−F at a dilution factor of ¼; this resulted in a concentration range of 10 µM to 10 nM. Row G contained the DMSO vehicle control, and row H was a control row with no yeast cells. Galactose concentration was decreased across columns 1−8 at a dilution

factor of ½; this resulted in a concentration range of 10% to 0.08%. Column 9 was a control column containing no galactose, and columns 10−12 were control columns containing increasing concentrations of glucose. Monitoring of growth was achieved by measuring the optical density (OD) at 630 nm; whilst 600 nm is preferred, the imaging equipment utilised was only capable of reading ODs at set values, with 630 nm being the closest available option.

An initial experiment involved the setup of the assay using a starting yeast OD_{630} of 0.02. However, the readings after 24 hours (the maximum assay time permissible to achieve the required throughput rate) showed that growth of the yeast had been slow and no conclusions could be drawn. The experiment was subsequently repeated using an increased starting yeast OD_{630} of 0.05. Following this modification, 24 hours was sufficient to obtain adequate levels of growth for data interpretation and the results are shown in Figure 3–5.

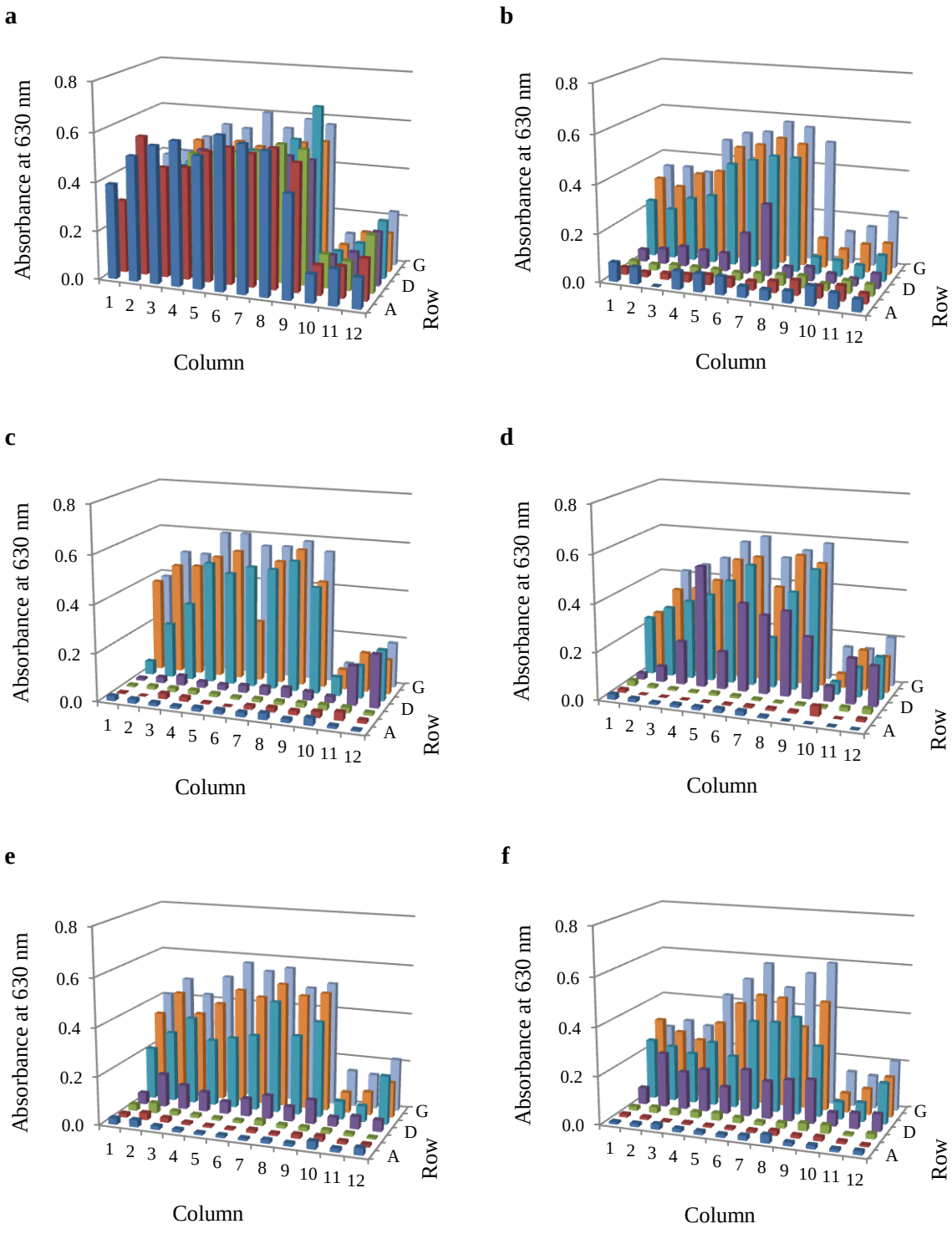

Figure 3–5: Growth of (a, c and e) α-*Lmj* and (b, d and f) α-AUR1 in the presence of (a and b) AbA, (c and d) AmB and (e and f) cycloheximide. As expected, AmB and cycloheximide inhibited the growth of both yeast strains whilst AbA only affected α-AUR1. Column and row labels refer to the plate design in Appendix A.1

AbA, as expected, displayed inhibition of growth of α-AUR1 but was ineffective against α-*Lmj*. In addition, glucose inhibited the growth of both yeast strains, a result that correlated with the previously performed complementation assay (section 2.2). These results confirm that a functioning IPCS is required for yeast growth and justify

the use of yeast as a vector for the screen. Cycloheximide, which is an inhibitor of protein biosynthesis,[334] displayed comparable activity against the two strains; AmB, however, appeared slightly more effective against α-*Lmj* than α-AUR1. As AmB functions by sequestering sterols, this result suggests a difference in membrane composition between the two strains. Therefore, whilst *Lmj*IPCS is functionally homologous to AUR1, the two enzymes may not operate at the same rate; possible reasons for differences in protein activity are discussed in section 2.3.2.

Somewhat surprisingly, growth for both strains was high in raffinose only medium (column 9). This highlights the leakiness of the GAL promoter when unrepressed. Another interesting observation was that for both α-*Lmj* and α-AUR1, growth began to decrease at concentrations of galactose greater than 0.31% (columns 1−5). This could possibly be attributed to adverse osmotic effects (the loss of water from the yeast cells due to the highly concentrated media). Alternatively, high galactose concentrations may result in the overexpression of IPCS. This could impact yeast growth in a number of ways; for example, the Golgi membrane composition could be significantly affected, which may in turn have a detrimental effect on the structure or folding of other proteins. Another possibility is that IPCS overexpression could adversely affect sphingolipid homeostasis. As discussed in section 1.3.3, ceramide is the central metabolic hub in sphingolipid metabolism;[189] overproduction of IPC would therefore reduce intracellular ceramide levels and impact on the levels of other complex sphingolipids. As a result, the galactose concentration of the culture medium was set at 0.1%.

3.3.2.2 FDGlu and Culture Concentrations

Having established a suitable medium composition attention then turned to maximising the fluorescence output of the assay. As was observed previously, starting culture concentration needed to be investigated in order to produce sufficient growth during the time period of the assay. In addition, the concentration of FDGlu required to give sufficient fluorescence output also needed to be determined, and it was predicted that a high starting culture concentration would require a low FDGlu concentration and vice versa. This, however, led to competing demands as FDGlu is expensive and its use would ideally be minimised. In contrast, large scale yeast culture is relatively cheap but is time consuming and requires equipment designed to deal with high volumes.

In order to account for these limitations, two potential methods of minimising the concentrations required were proposed. The first was the possibility that adding FDGlu post-incubation rather than pre-incubation may decrease the concentration required due to the fact that the quantity of the exo-β-glucanase enzyme could have built up to high levels in the culture medium during the 24 hour incubation period. Therefore, by adding the reagent when enzyme levels are high, less FDGlu may be required to produce a sufficient difference in fluorescence between positive and negatives samples.

The other consideration made was the fact that *S. cerevisiae* grows well under mildly acidic conditions and can produce small quantities of organic acids such as lactic acid, succinic acid and pyruvic acid in order to acidify the culture medium.[335] Fluorescein, however, fluoresces best at neutral pH and therefore addition of a buffer at pH 7.0 often results in an improved fluorescence readout.[336] As a result, the addition of a neutral buffer such as phosphate buffer post-incubation may reduce the concentration of FDGlu required to obtain a sufficiently strong fluorescent signal.

In order to investigate these possibilities, a matrix assay was designed (Appendix A.2) to test a range of concentration combinations in low volume 384-well plates. Starting culture concentration was decreased down rows A−L at a dilution factor of ⅘; this resulted in a concentration range of OD_{600} 0.125 to 0.011 (yeast OD was measured at 600 nm using a standard spectrophotometer). FDGlu concentration was decreased across columns 1−12 at a dilution factor of ⅘; this resulted in a concentration range of 20 µM to 1.7 µM. The matrix was repeated in A13−L24 to produce a duplicate set of results in a single plate.

Two test plates were prepared using α-*Lmj*, one with FDGlu added and one without. Monitoring of the plate to which FDGlu was added post-incubation showed that fluorescence increase over a 1 hour period was negligible, suggesting that either the enzyme has a very low turnover rate or that levels do not build up in the culture medium during growth and therefore little enzyme is present. The addition of a pH 7.0 phosphate buffer, however, proved successful and resulted in the fluorescence readout from both plates increasing approximately tenfold. The results following the addition of phosphate buffer (Figure 3–6) highlight the distinction between the differential additions of FDGlu.

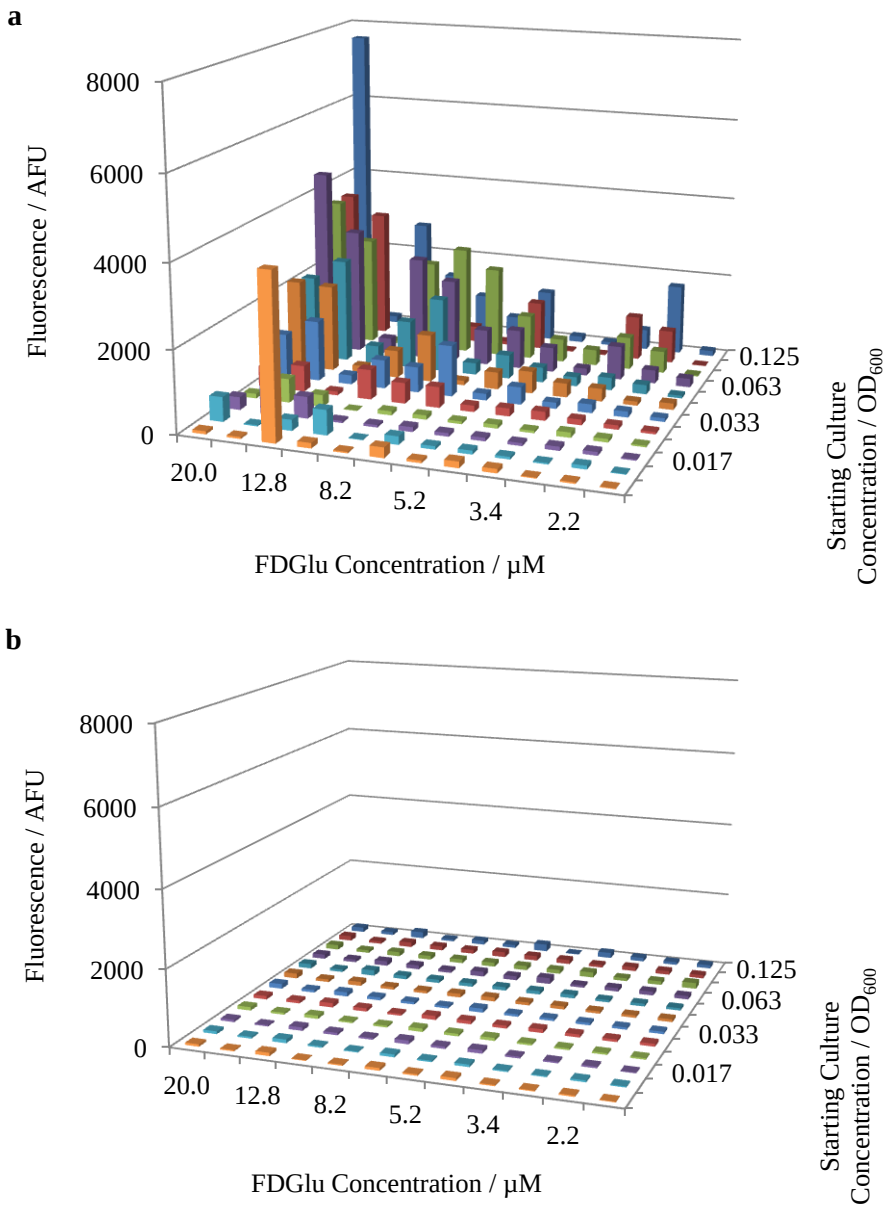

Figure 3–6: The fluorescence readouts following the addition of phosphate buffer in response to varying starting culture and FDGlu concentrations when FDGlu was added (a) pre-incubation and (b) post incubation, plotted on the same scale. Each column represents the average of the two fluorescence values that were obtained

From this experiment, it was clear that adding FDGlu post-incubation was not a valid option for HTS as, based on this evidence, a lengthy second incubation with FDGlu would be required which would add both time and complexity to running the assay. On the contrary, the addition of phosphate buffer post-incubation proved highly successful resulting in a much higher fluorescence readout from the two plates, so this step was added to the assay protocol. However, whilst the results show the basic overall pattern that would be expected (lower fluorescence at low starting culture and FDGlu concentrations than at high ones) when FDGlu was added pre-incubation, no definitive

conclusions in terms of optimal concentrations could be drawn given the general lack of trends down individual rows and columns and the high number of anomalous results. This was attributed to large errors due to the use of a manual multichannel pipette on such a small volume scale.

In order to improve upon the results obtained thus far, a repeat of the experiment was undertaken again in a low volume 384-well plate but using a higher volume to reduce the pipetting errors and a smaller range of conditions (Appendix A.3) to reduce the complexity of the assay. Starting culture concentration was decreased down rows A−D at a dilution factor of ½; this resulted in a concentration range of OD_{600} 0.125 to 0.016. Row E was a control row with no yeast cells. FDGlu concentration was decreased across columns 1−4 at a dilution factor of ½; this resulted in a concentration range of 20 µM to 2.5 µM. Column 5 was a control column with no FDGlu. The matrix was repeated in A11−E15 to produce a duplicate set of results in a single plate and, following incubation, phosphate buffer was added and the fluorescence of the plates read. The results are shown in Figure 3–7 and, unlike the previous experiment, they show excellent correlations between the concentrations of the two factors and the resulting fluorescence output.

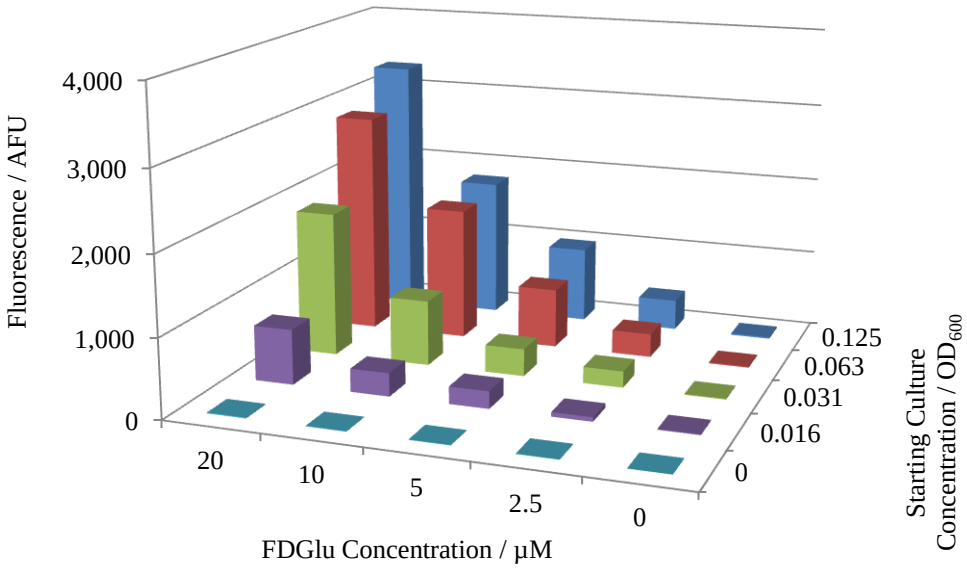

Figure 3–7: The fluorescence readouts following the addition of phosphate buffer in response to varying starting culture and FDGlu concentrations. Each column represents the average of the two fluorescence values that were obtained

As expected the highest readout was obtained from the highest FDGlu and culture concentrations tested, but sufficient fluorescence (> 1000 arbitrary fluorescence units

(AFU)) was also achieved using other combinations of concentrations. From this, it was decided that two sets of conditions would be tested further: an FDGlu concentration of 20 µM and a starting culture OD_{600} of 0.031; and an FDGlu concentration of 10 µM and a starting culture OD_{600} of 0.063.

3.3.2.3 Z′ Optimisation

Having identified two combinations to test further, finalisation of the assay setup was undertaken in 1,536-well plates in order to mimic the format in which the HTS assay was to be run. It was decided that the origin of the starting α-*Lmj* culture (either fresh or from frozen stocks) should be investigated. Whilst it was predicted that fresh culture would exhibit superior growth to culture of frozen origin, adjusting the OD_{600} of the fresh culture to the correct value at the start of every assay would be both time consuming and increase the potential for contamination; it would therefore be beneficial to utilise previously prepared frozen aliquots of culture if at all possible.

In addition, the compound most suitable for use as a positive control needed to be identified. AmB (**4**) and cycloheximide (**20**) both showed inhibition of growth during the experiments to determine the optimal galactose concentration, so were retested in this assay format. Two additional compounds were also tested; both clemastine (**21**) and suloctidil (**22**) (Figure 3–8) were identified in a previous small scale screen as having high activity both in the biochemical assay and against *L. major* promastigotes, so it was predicted that both would show inhibition of yeast growth in this assay.

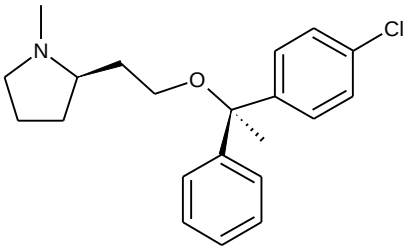

Clemastine (**21**)

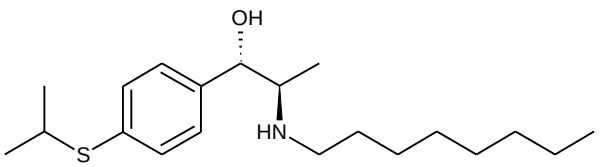

Suloctidil (**22**)

Figure 3–8: The structures of clemastine and suloctidil, which were both shown to be potent inhibitors of *Lmj*IPCS in a previous screen

The combinations of conditions were tested in 1,536-well plates (Appendix A.4) using both fresh and frozen yeast cultures. Each set of conditions was tested across four

full rows, resulting in 192 data points. A starting culture containing yeast at OD_{600} = 0.031 and 20 µM FDGlu was used to fill rows A–L, whilst a starting culture containing yeast at OD_{600} = 0.063 and 10 µM FDGlu was used to fill rows Q–BB. AmB or suloctidil was tested in rows E–H and U–X, whilst cycloheximide or clemastine was tested in rows I–L and Y–BB. AmB and cycloheximide were tested at 10 µM, as this was shown to be effective in the assay to determine optimal galactose concentration, whilst suloctidil and clemastine, which were previously untested against yeast, were tested at 100 µM. The DMSO vehicle was used a control for rows A–D and Q–T.

Upon plate reading, however, it was instantly obvious that there was a major issue with the assay setup. Rather than the fluorescence readout being constant for each condition, the data obtained revealed a significant doming effect with high fluorescence values being obtained in the centre of the plate and a substantial decrease in fluorescence around the edges (Figure 3–9).

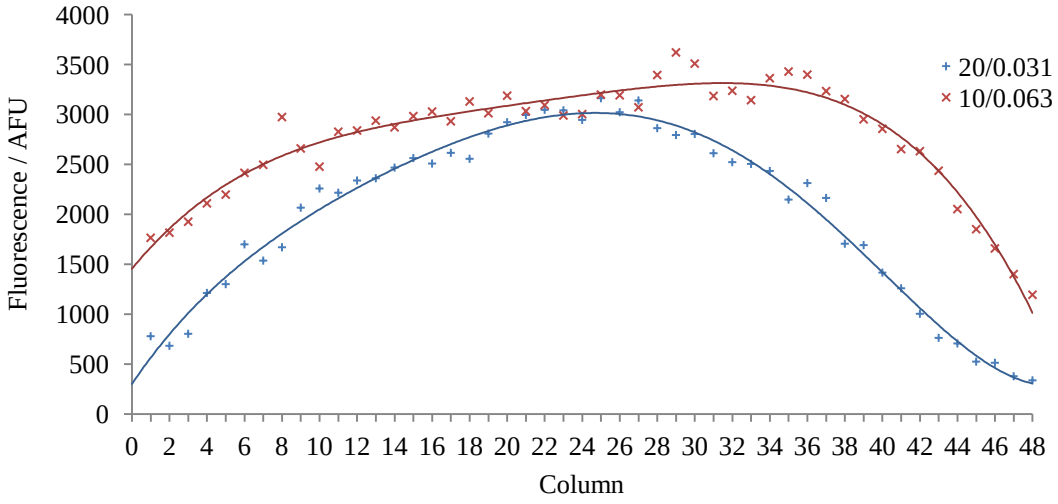

Figure 3–9: The variation in fluorescence across row A (20/0.031, no test compound) and row Q (10/0.063, no test compound) in a plate for fresh culture. 20/0.031 refers to an FDGlu concentration of 20 µM and a starting culture OD_{600} of 0.031, whilst 10/0.063 refers to an FDGlu concentration of 10 µM and a starting culture OD_{600} of 0.063

This doming effect was obviously a severe problem given that the very nature of the assay involved comparison of fluorescence values between different wells to determine the percentage inhibition of growth due to the effect of an added compound. Compounds are dispensed across the entire plate for a HTS assay and therefore an effect such as this would prevent the acquisition of any meaningful data; for example, compounds dispensed around the edges of the plate may appear active without possessing any inhibitory activity. In addition, for this particular experiment, the

observation that 10 µM FDGlu and starting OD_{600} = 0.063 produced a higher fluorescence output could simply be due to the fact that this set of conditions was tested in rows Q−T along the centre of the plate, whilst 20 µM FDGlu and starting OD_{600} = 0.031 was tested in rows A−D along the edge of the plate.

The explanation for this effect was increased evaporation during incubation from the wells around the edges of the plate in comparison to the wells in the centre. A subsequent investigation into ways of reducing this evaporation showed that utilising a spare plate to cover the test plate rather than the provided lid significantly reduced this evaporation and resulted in constant fluorescence across the rows. This was attributed to the fact that the lids used were generic and capable of covering any type of plate so did not produce an exact fit, whereas using a spare plate of the same type resulted in an improved fit hence reducing evaporation.

Having resolved the problem, the assay was subsequently repeated and comparison of sets of conditions at this stage was achieved by means of Z′ calculation with a value as close to 1.0 as possible being desirable (as discussed in section 1.4.2.3). The results are shown in Figure 3–10. Somewhat surprisingly, fresh and frozen cultures produced comparable fluorescence readouts suggesting that, providing numerous freeze-thaw cycles are avoided, there should be no problem with utilising frozen yeast stocks during HTS.

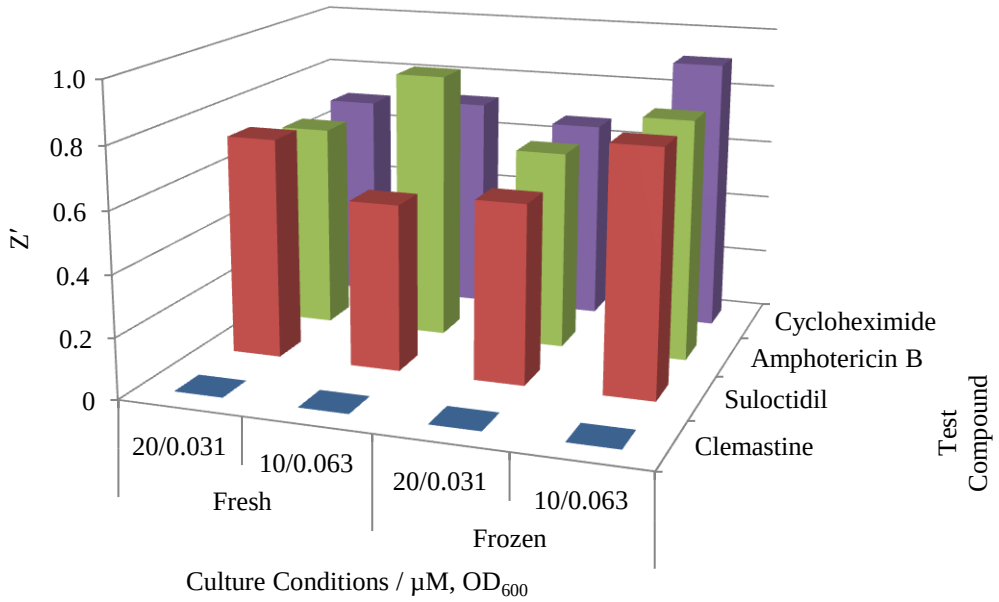

Figure 3–10: The calculated Z′ values using four test control compounds and different culture conditions. 20/0.031 refers to an FDGlu concentration of 20 µM and a starting culture OD_{600} of 0.031, whilst 10/0.063 refers to an FDGlu concentration of 10 µM and a starting culture OD_{600} of 0.063

The observation that clemastine appeared to be ineffective at inhibiting yeast growth was unanticipated. Given that this compound demonstrated a high potency against the parasite promastigotes, this lack of inhibition could only be attributed to the differences between parasite and yeast biochemistry, either in terms of membrane composition and transport or compound metabolism. This highlights one of the major drawbacks of the assay, as library compounds which may be highly active against the enzyme itself would not be identified if they were unable to cross the *S. cerevisiae* cell wall and plasma membrane.

The other three compounds tested all showed effective inhibition of yeast growth which translated into Z′ values sufficient for a high throughput screen. As a result, the conditions selected were those that gave the highest Z′ value of 0.91. These conditions were 10 µM FDGlu and a starting culture OD_{600} of 0.063 prepared from frozen yeast stocks using 10 µM cycloheximide as the positive control.

3.3.3 Assay Validation

With assay optimisation complete, the next stage was to validate the assay against the GSK standard set of 9,766 compounds. This was undertaken in triplicate against

both α-*Lmj* and α-AUR1 to provide an initial appraisal of the specificity of the compounds for the two enzymes. Given that the only difference between the two strains is the origin of the IPCS enzyme, compounds which inhibit the growth of the α-*Lmj* yeast but not the α-AUR1 yeast are highly likely to be specific for the *Lmj*IPCS enzyme. Having no effect on the α-AUR1 yeast also suggests that compounds do not result in any significant off-target effects, which is a highly desirable criterion for a pharmaceutical compound.

The resulting Z′ values for each of the validation plates are shown in Figure 3–11. As discussed in section 1.4.2.3, the minimum Z′ for an assay to be approved is 0.5; for a screen requiring multiple test plates, this is the minimum mean Z′. Some test plates may therefore be higher or lower than this value, but in order to ensure result reliability, the minimum Z′ threshold for an individual plate was set at 0.4.

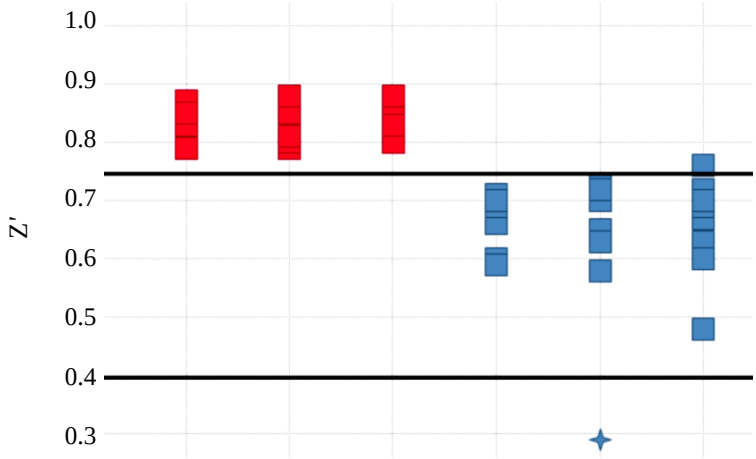

Figure 3–11: The Z′ values for each set of eight test plates for α-AUR1 (red) and α-*Lmj* (blue). Two columns (64 wells) of each control were tested per plate. Figure provided by Dr E. Alvarez

One plate into which α-*Lmj* had been dispensed displayed a strong evaporation effect resulting in a Z′ less than the threshold and so had to be failed. The Z′ values for the remaining plates were excellent with a mean of 0.82 for α-AUR1 and 0.68 for α-*Lmj*.

A numerical summary of the results is shown in Table 3–1. As a result of the plate failure, data analysis for the α-*Lmj* culture could only be carried out on the 8,373 compounds for which triplicate data was obtained. The standard deviation and statistical threshold (equation 1.1) were both calculated in terms of % inhibition, which

was calculated according to equation 3.1. The larger variation in the data for α-*Lmj* resulted in a higher threshold, indicating that a higher inhibition had to be exhibited in order for compounds to be considered as active. The F+ (compounds active in one of the three plates) rates were excellent in both cases, meaning few negative compounds would be incorrectly progressed to the next screening stage. The F– (compounds active in two of the three plates) rates were acceptable but slightly higher than ideal given that F– compounds cannot be recovered further down the line. No extreme false positives or negatives (inhibition values that differ in one plate compared to the other two by more than three times the standard deviation) were recorded.

Table 3−1: Validation results

Descriptor	*α*-AUR1	*α -Lmj*
Number of considered triplicates	9,766	8,373
Standard deviation / % inhibition	7.17	13.35
Statistical threshold / % inhibition	21.32	42.88
Hit rate / %	1.44	1.07
False positive rate / %	0.03	0.01
False negative rate / %	0.99	0.72
Extreme false positive rate / %	0.00	0.00
Extreme false negative rate / %	0.00	0.00

$$\% \text{ inhibition} = 100 \times [(D - C_1) / (C_2 - C_1)] \qquad (3.1)$$

where: D = data value
C_1 = mean negative control (DMSO)
C_2 = mean positive control (cycloheximide)

The measured hit rate was slightly higher for α-AUR1 than α-*Lmj*, a somewhat perturbing observation as it implies that more compounds were selective towards the yeast enzyme than *Lmj*IPCS and therefore that few selective compounds would be identified in the primary screen. However, further analysis showed that there were some compounds which were specific for *Lmj*IPCS as they did not show inhibition of α-AUR1 growth. Given that the validation collection is representative of the full 1.8 million compound library, a reasonable number of selective compounds were therefore expected to be identified from the primary screen.

Whilst validation was successful and sufficient evidence of an effective assay to commence the high throughput screen, it was noted that both of the control fluorescence means differed greatly to those observed during the optimisation stages. The DMSO control wells suffered a drop in fluorescence whilst an increase was observed in the cycloheximide control wells. Despite these differences in fluorescence output the Z′ values were still excellent (as shown in Figure 3–11). The reason for these variances, however, was unclear.

3.3.4 Primary Screen

Following validation, the next step of the HTS process was the primary screen against α-*Lmj*. Given the hit rate of 1.07% obtained against α-*Lmj* during validation, approximately 19,000 compounds were expected to be identified from the 1.8 million compound library. Further screening steps against both α-*Lmj* and α-AUR1 would subsequently be required to differentiate between compounds that act on *Lmj*IPCS and those that act via generic *S. cerevisiae* biochemical pathways.

The assay was commenced utilising the optimised conditions. Following the reading of the first test-set of 53 plates, however, it was immediately apparent that the cycloheximide control mean had risen further, implying a reduction in growth inhibition. This had a profound impact on the Z′ values and resulted in the majority of the plates in this test-set failing. A fresh cycloheximide solution was found to reverse this effect, suggesting that the numerous freeze-thaws that were undertaken during the optimisation and validation process contributed towards an elevated rate of breakdown of the compound in solution. The resulting action was to prepare a fresh solution on a weekly basis for the remainder of the screening process. In addition, the drop in fluorescence in the DMSO control wells was found to be due to the microplates used in the assay; during optimisation microplates were sterilised in house whereas for validation and screening they were purchased pre-sterilised. However, given that the Z′ values were still excellent, the decision was made to continue using the pre-sterilised plates in order to allow the throughput to remain as high as possible.

With these matters addressed, screening the remainder of the library was undertaken on an ultra-high throughput scale; on average, 120 plates (> 165,000

compounds) were tested per day. Following reading, plates were visualised using the GSK-developed statistical online data analysis (SODA) software providing an output as shown in Figure 3–12. The brighter the colour, the higher the inhibition of growth (the cycloheximide control mean was set to 100%).

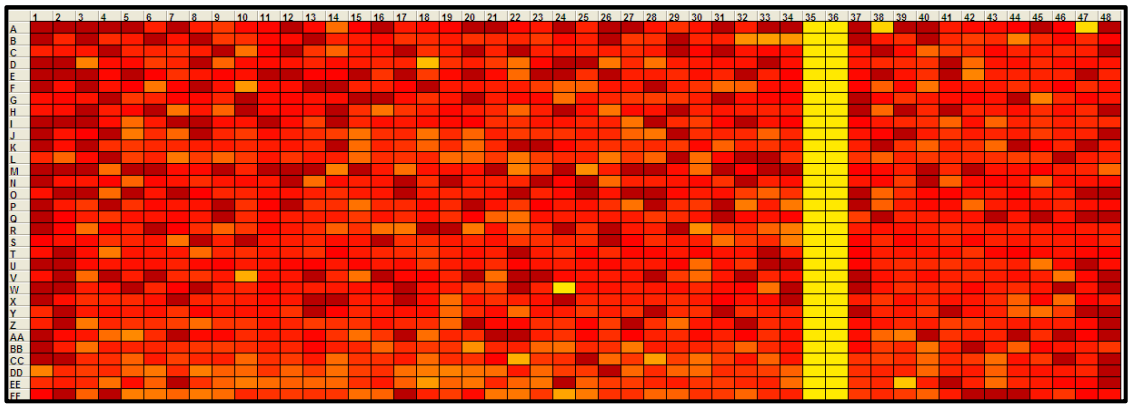

Figure 3–12: An example plate from the primary screen. The DMSO control is in columns 11 and 12 and the cycloheximide control is in columns 35 and 36. Wells with inhibited growth are coloured yellow, whilst wells showing no inhibition are red. Figure provided by Dr E. Alvarez

The SODA software was also used to calculate the Z′ for each test plate. Data from the plates that were above the Z′ threshold of 0.4 were uploaded to the ActivityBase software package (IDBS, Guildford, Surrey, UK) which is specifically designed for scientific data management.[337] A total of 1,312 plates were tested in the initial screen with 67 (5%) of these failing. The majority of these failed plates, which subsequently had to be retested, originated from the first test-set due to the problem with the cycloheximide solution, whilst very few plates failed during the remainder of the screen. The distribution of Z′ values for the primary screen is shown in Figure 3–13 with the overall mean being 0.70.

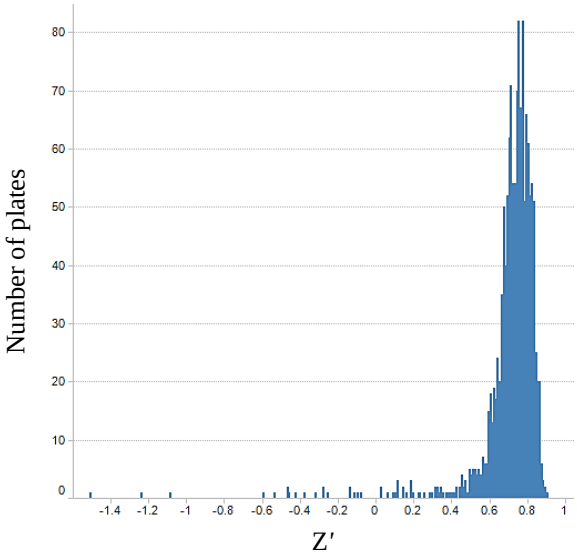

Figure 3–13: The distribution of Z' values for the primary screen

Before the data could be analysed, further processing was required to remove the patterns that were observed in a non-negligible number of plates. The majority of these were mild evaporation effects that were not significant enough to result in plate failure but still impacted on the numerical data obtained. Dispensation effects, where individual tips dispensed a lesser or greater amount than required into blocks of four rows, were also sporadically observed. In order to account for these effects the plate data were fed into a GSK-developed pattern recognition and fixing algorithm which subsequently corrected the affected data to diminish the effect of the pattern. Two examples of this are shown in Figure 3–14.

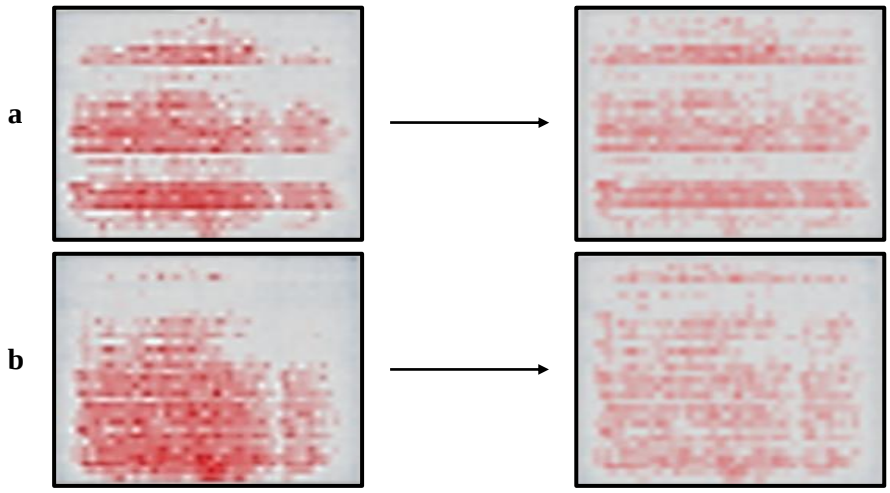

Figure 3–14: (a) The correction of a dispensation (positional) effect and (b) the correction of an evaporation effect in a 1,536-well test plate; the brighter the colour, the greater the effect. Figures provided by Dr G. Colmenarejo

Following this rectification, the % inhibition threshold was calculated for each test-set (to avoid day to day variation) using equation 1.1. This yielded 10,807 compounds that were statistical hits; however, this was far below the 19,000 compound estimate made following the screen of the validation set. Further analysis of the data revealed that there were many compounds with favourable drug-like properties (within the 'rule of 5' limits as discussed in section 1.4.2.5) that were just below the calculated threshold. To investigate this, the threshold was recalculated for all the compounds in each test-set with a calculated LogP (cLogP) less than or equal to 3 and a molecular weight less than or equal to 300. In every case the recalculated threshold was significantly lower than the original, in some cases by as much as 13% (Figure 3–15).

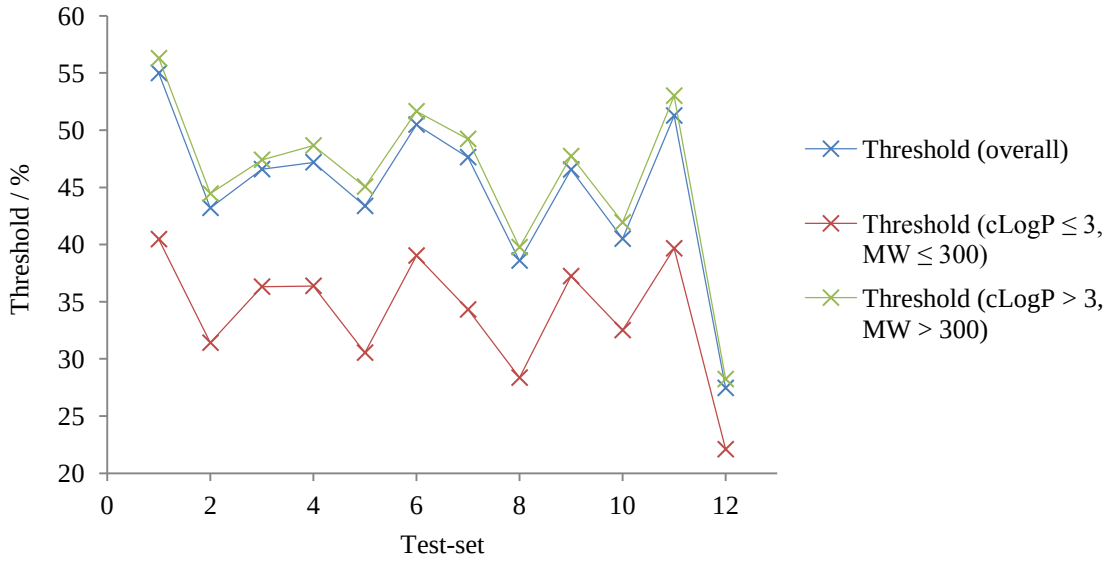

Figure 3–15: The difference between the calculated thresholds for small, polar compounds and large, non-polar compounds

These results mirrored a trend observed in the pharmaceutical industry in the early to mid 2000s whereby increasingly lipophilic compounds, rather than more polar ones, were being identified by screening and progressed to lead optimisation and clinical trials only to result in failure. This was observed in a study by Leeson and Springthorpe who noted that compounds in drug development programmes showed a mean cLogP value 1.5 log units greater than the mean for oral drugs launched between 1983 and 2007.[338] However, rising attrition rates indicated that this was not the best strategy to take and suggested that high polarity compounds were more promising as potential drugs due to factors such as increased solubility and biodistribution.

It was therefore necessary to rescue these small, polar compounds that would otherwise be lost from the screening process. In order to achieve this, the test-sets were separated into the two groups of compounds (cLogP ≤ 3, MW ≤ 300 and cLogP > 3, MW > 300) and reanalysed using the recalculated thresholds shown in Figure 3–15. This resulted in the inclusion of many drug-like compounds that were classed as inactive using the overall thresholds, and the total number of compounds that were classified as hits using this method was 19,382. However, larger compounds that were classed as hits using the overall threshold but were inactive using the slightly higher threshold for the cLogP > 3, MW > 300 group were also included so as not to discount potentially active compounds. As a result, the total number of hit compounds arising from the primary screen was 19,669.

3.3.5 Confirmation of Hits

With these compounds in hand, the next stage was to retest them in order to confirm their activity and discount the possibility that they were false positives. An extra consideration to take into account was the fact that the next stage of the HTS process, the production of dose-response curves, can only be undertaken on a maximum of ~5,000 compounds. As this assay format proved very robust and produced consistently high Z′ values, the probability that retesting alone would reduce the number of compounds from 19,669 to fewer than 5,000 was low. The decision was therefore made to run this assay against both the α-*Lmj* and α-AUR1 strains in order to allow the removal of compounds which inhibited the growth of both strains. This meant that compounds targeting both the *Lmj*IPCS and the yeast AUR1 would be lost, but this number was predicted to be small given that the majority of compounds that affect both strains would likely be acting via off-target effects.

The confirmation assay was undertaken in duplicate for each strain, and example plate images are shown in Figure 3–16. The majority of the tested compounds showed activity against α-*Lmj* (Figure 3–16 (a)), as would be expected given that they were all above the inhibition threshold in the primary screen. Gratifyingly, whilst many compounds were also active against α-AUR1, there were many that displayed lower activity than against α-*Lmj* or were inactive altogether (Figure 3–16 (b)).

a

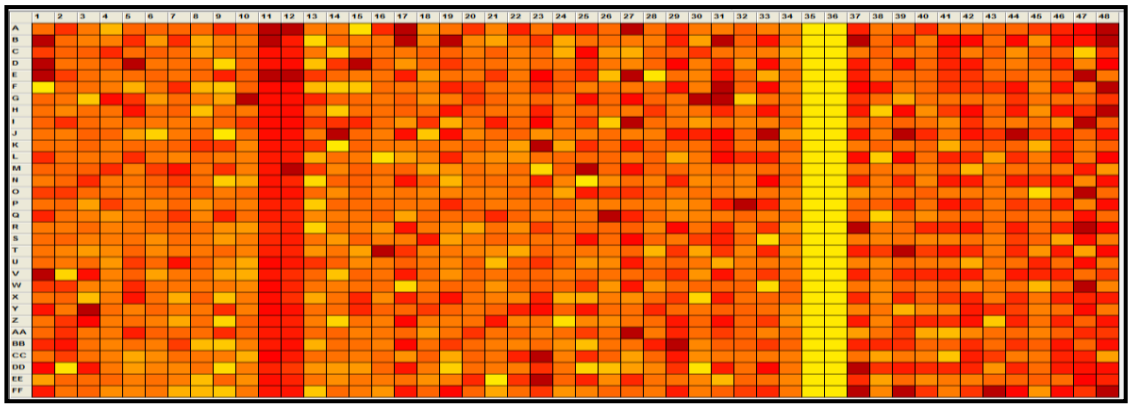

b

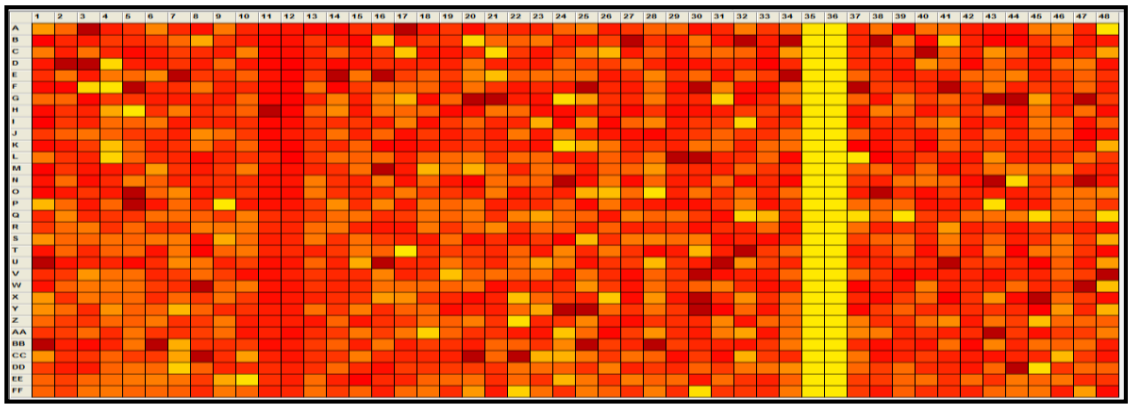

Figure 3–16: Example plates from the confirmation screen for (a) 10 μM against α-*Lmj* and (b) 10 μM against α-AUR1. The DMSO control is in columns 11 and 12 and the cycloheximide control is in columns 35 and 36. Wells with inhibited growth are coloured yellow, whilst wells showing no inhibition are red. Figures provided by Dr E. Alvarez

In order to select which compounds to progress to the dose-response stage, the separate inhibition thresholds for each strain were calculated and compounds that produced a response below the α-*Lmj* threshold were filtered out. Of the remaining compounds, those that showed activity above the α-AUR1 threshold were also removed, leaving 3,573 compounds which demonstrated specificity for the *Lmj*IPCS enzyme. To these were added all the compounds which showed a response greater than 80% inhibition against α-*Lmj* regardless of the response against α-AUR1. This step was performed to avoid highly potent compounds being lost due to the stringent filtering based on specificity. As a result, there were 4,166 compounds that were progressed to dose-response studies.

3.3.6 Dose-Response Studies

The final stage of the high-throughput screen undertaken was the dose-response study, which involved testing the remaining compounds against both the α-*Lmj* and α-AUR1 strains over a range of concentrations. This would allow the determination of IC_{50} values (the concentration of the compound required to give 50% inhibition) against both strains, hence providing a more comprehensive analysis of compound specificity. The dose-response assay was undertaken in duplicate for each strain utilising a dilution factor of ⅓ for each compound; this resulted in a concentration range of 100 µM to 1.7 nM with a total of 11 concentrations tested. An example plate is shown in Figure 3–17.

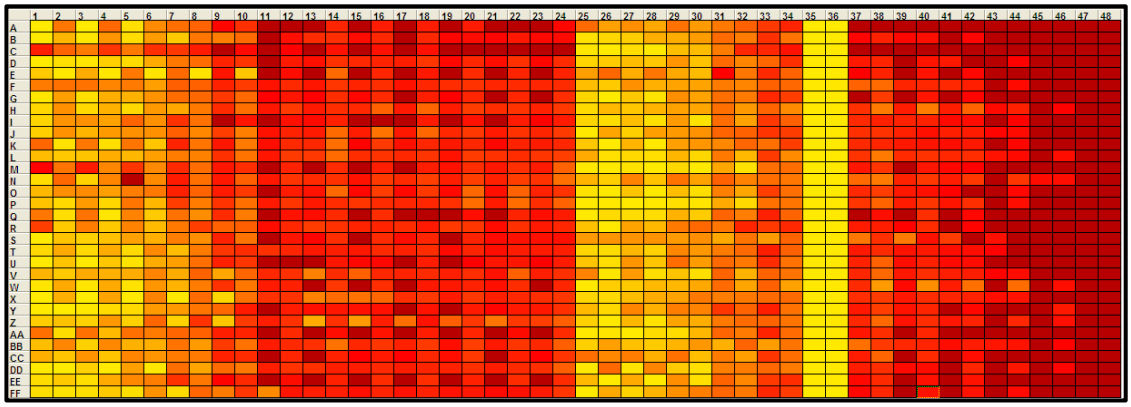

Figure 3–17: An example plate from the dose-response screen. Four compounds could be tested per row, two in the odd columns (1, 3, 5 ... 23 and 25, 27, 19 ... 47) and two in the even columns (2, 4, 6 ... 24 and 26, 28, 30 ... 48) with compound concentration decreasing from left to right. The DMSO control is in columns 11 and 12 and the cycloheximide control is in columns 35 and 36. Wells with inhibited growth are coloured yellow, whilst wells showing no inhibition are red. Figure provided by Dr E. Alvarez

The results from this experiment were analysed using the ActivityBase software package (IDBS, Guildford, Surrey, UK) which was used to fit curves to the data (examples shown in Figure 3–18). From these the pIC_{50} ($-\log_{10}(IC_{50})$) values for each compound were calculated against both α-*Lmj* and α-AUR1, and the resulting plot is shown in Figure 3–18 (c)). Given that this is a log scale, a pIC_{50} of 4 corresponds to 10^{-4} (100 µM), 5 corresponds to 10^{-5} (10 µM) and so on. Therefore, in terms of the selectivity indices used to group compounds on the plot (with the corresponding numerical data in Table 3–2) a selectivity index (SI) of 1 indicates that a compound is 10 times more potent against α-*Lmj* than α-AUR1. Similarly, a SI of 2 indicates a 100-fold difference in potency.

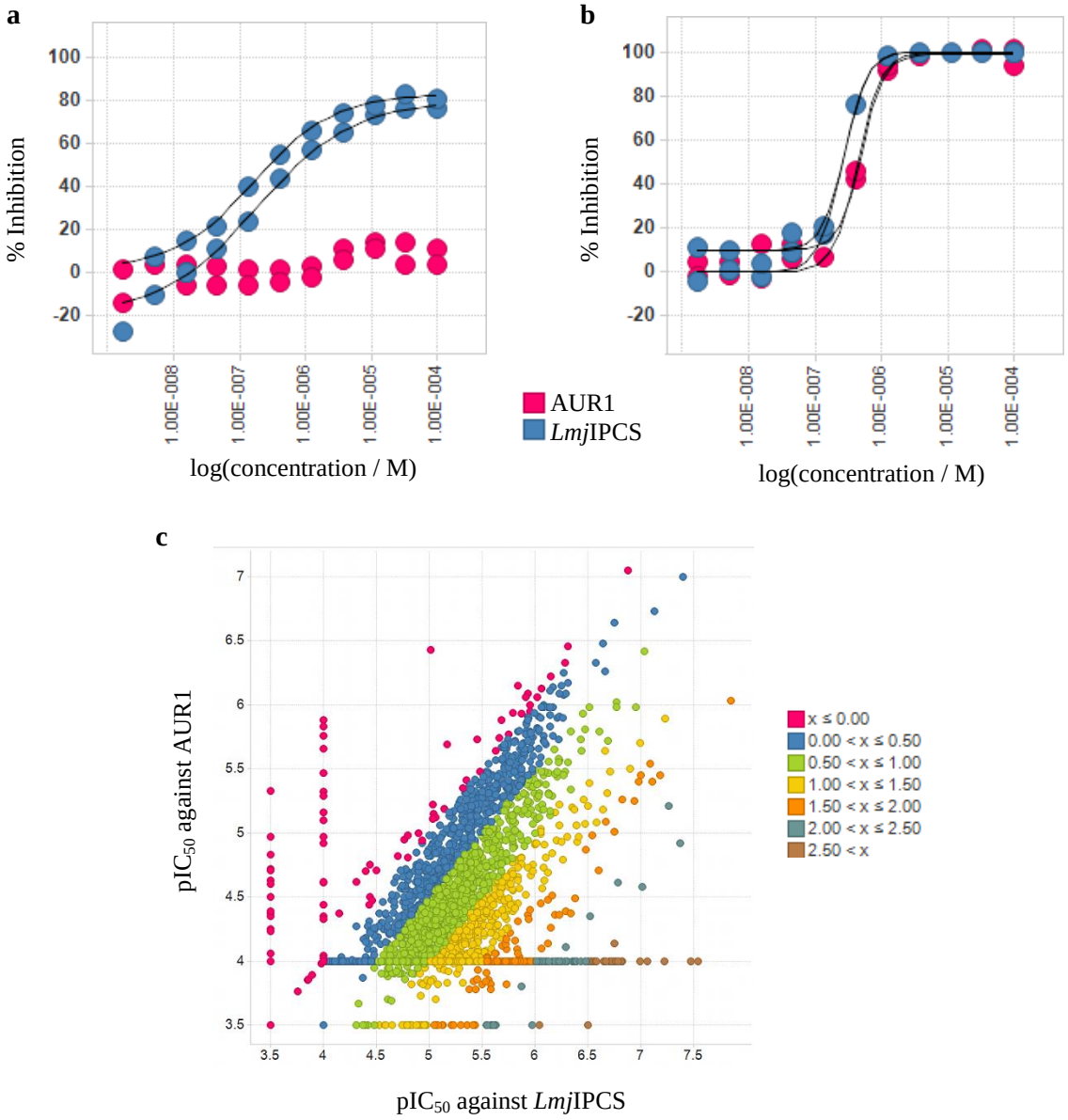

Figure 3–18: Example dose response curves for (a) a compound selective for *Lmj*IPCS over AUR1 and (b) an unselective compound. (c) A plot of the pIC_{50} for AUR1 against the pIC_{50} for *Lmj*IPCS for each compound, where x is the selectivity index for *Lmj*IPCS over AUR1. Figures provided by Dr E. Alvarez

Table 3–2: The number of compounds per selectivity index band in the dose-response assay

Selectivity Index (x)	Number of Compounds
$x \leq 0.0$	508
$0.0 < x \leq 0.5$	765
$0.5 < x \leq 1.0$	1,308
$1.0 < x \leq 1.5$	1,085
$1.5 < x \leq 2.0$	397
$2.0 < x \leq 2.5$	77
$2.5 < x$	26

These data showed that, of the 4,166 compounds tested, there were 500 with a SI greater than 1.5 and 103 with a SI greater than 2.0. These compounds were therefore highly active against the *Lmj*IPCS enzyme yet showed little activity against the *S. cerevisiae* AUR1 enzyme and resulted in few off-target effects. These numbers were unexpectedly high given the observations that were made during the validation screen of the HTS process (discussed in section 3.3.3), indicating that the screen was more fruitful than originally anticipated.

The compounds were subsequently clustered into structural families by Dr G. Colmenarejo (GSK Computational and Structural Chemistry group). This was achieved using an in-house sphere exclusion algorithm as described by Butina.[339] Briefly, the software first created a unique fingerprint for each compound by examining the location of each atom with respect to every other atom within 7 bonds. The fingerprint for each molecule in the set was then compared to the fingerprint for every other molecule, and the compound with the largest number of neighbours was used to lead the first cluster. Any compounds with a similarity greater than 0.85 (where similarity is on a scale from 0 to 1) were sorted into that cluster and removed from the list, excluding them from subsequent searches. The compound with the next highest number of neighbours was subsequently selected and the process repeated until only compounds with no similarity to any other, named singletons, were remaining. Two representatives from each cluster were selected at random for further testing along with all the singletons. A total of 216 compounds were ultimately selected for additional investigation.

3.4 Conclusion

The work described in this chapter involved the development and optimisation of an assay that was suitable for HTS. An assay format based on fluorescence output was selected over a multiplex assay and was subsequently used to screen GSK's 1.8 million compound library. A total of 216 compounds were ultimately selected for further investigation, which is described in the next chapter. To the best of the author's knowledge, this is the largest screening programme conducted by an academic group to date.

Chapter 4

Identification of a Lead Compound Series

4.1 Introduction

Having selected 216 compounds from the HTS campaign, the next stage of the project was to identify a small number of compounds or compound series to investigate further. This aim necessitated the use of a number of assays not previously utilised in the project. This ongoing screening project was undertaken with the support and assistance of GSK.

4.2 *L. major* Promastigote Screening

The continued screening commenced with the testing of the 216 compounds against the promastigote stage (found in the insect vector) of the wild type, Friedlin virulent strain (FV1) *L. major* parasites. All of the compounds selected for continued testing displayed a pIC_{50} of 5.0 or greater in the dose-response assay against *Lmj*IPCS, which is equivalent to 50% inhibition of growth at 10 μM. Testing against *L. major* promastigotes at 10 μM would therefore give an indication of how many compounds retain activity against parasites.

As with the HTS yeast assay, the parasite cytotoxicity assay was based on fluorescence and involved the incubation of *L. major* promastigote parasites with the test compounds prior to the addition of resazurin (trade name AlamarBlue®). This is a blue, weakly fluorescent dye that is reduced *in cellulo* to the pink, highly fluorescent compound resorufin (Figure 4–1).[340] The fluorescence output is therefore representative

of parasite viability, with a lower readout indicative of decreased growth and hence an effective antiparasitic compound.

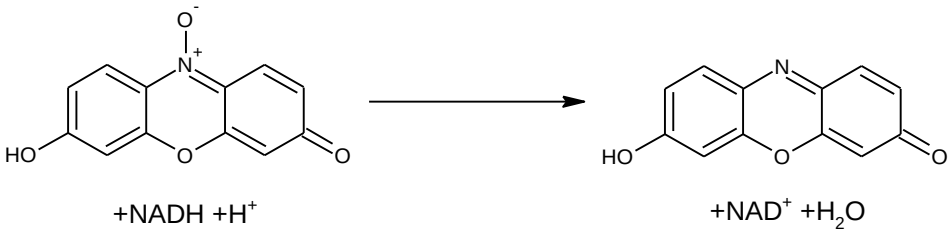

Figure 4–1: The reduction of resazurin to resorufin

The first iteration of the assay followed an established protocol,[320] whereby parasites at a concentration of 4.0×10^5 ml^{-1} were incubated with the compounds (with the antileishmanial drug AmB (**4**, Figure 1–4) used as the positive control) for 24 hours prior to AlamarBlue® addition. However, the results between replicates were inconsistent and only 17 compounds repeatedly demonstrated inhibition above 50%. One possible explanation is that the number of cells per well between this assay and the HTS assay is extremely different, with this assay using 4.0×10^4 well^{-1} and the HTS assay using approximately 3.9×10^3 well^{-1}. The 10 fold increase in cells effectively reduces the relative concentrations of the test compounds and could explain why lower levels of inhibition were observed.

In order to address this, a lower starting concentration of parasites was required; this would, however, have to be accompanied by an increase in incubation time in order to maintain sufficient fluorescence readout. The growth of various starting concentrations of parasites was subsequently examined over three different time periods (Appendix B) and, as predicted, reducing parasite concentration resulted in insufficient fluorescence output after 24 hours. Whilst 48 hours resulted in a significant improvement, a 72 hour incubation period was selected in order to accurately mirror the protocol used for testing *L. donovani* axenic amastigotes (discussed later).[341] On this curve, a linear relationship was achieved up to a starting concentration of 1.5×10^4 ml^{-1}, and a starting concentration of 5.0×10^3 ml^{-1} was selected for use in the assay.

Testing of the 216 compounds was repeated using the modified protocol and the results are shown in Figure 4–2. Of the 216 compounds, 99 retained inhibitory activity greater than 50%, with 43 of these demonstrating complete inhibition. 117 compounds therefore showed a reduction in activity compared to the yeast dose-response assay,

with many appearing to have a mitogenic effect. This could potentially be explained by differences in membrane composition between the two organisms, or by an increased rate of drug metabolism in *L. major* compared to yeast. Alternatively, there could be a difference in the rate at which the organisms transport compounds out of the cell using drug efflux pumps.

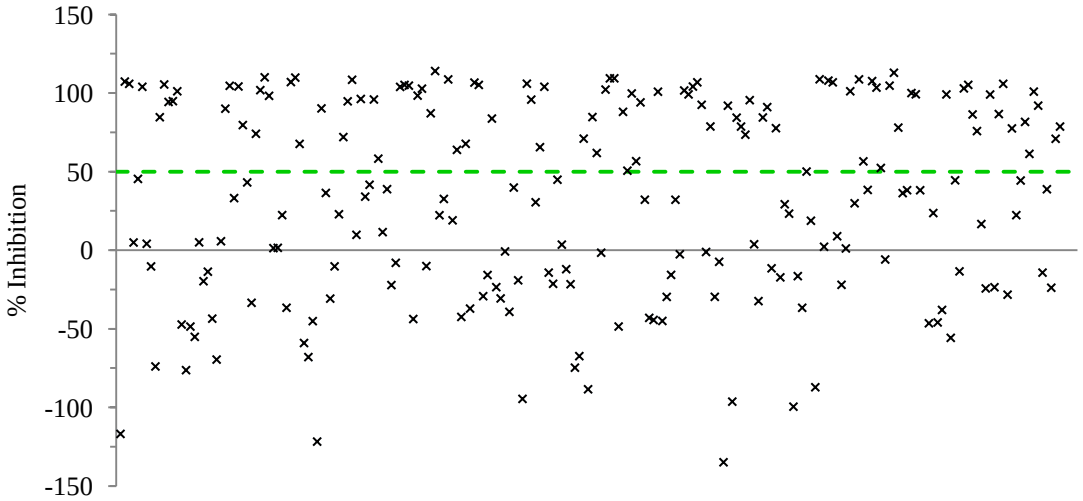

Figure 4–2: The inhibitory activities of the 216 compounds tested at 10 μM against 5.0×10^3 ml^{-1} *L. major* wild type promastigote parasites for 72 hours

These results were promising, with 99 compounds demonstrating significant antiparasitic activity. However, whilst CL, of which *L. major* is a causative species, is more prevalent than VL, its non-fatal clinical manifestation means that it is less of a priority for drug discovery for GSK. VL, on the other hand, has been targeted for control by 2020,[162] and therefore compounds that have inhibitory activity against the IPCS from a species that causes VL, such as *L. donovani*,[21] would be favoured for progression. The following cell-based screening assays described in section 4.3 were carried out with the support of GSK at Tres Cantos.

4.3 Compound Triage

4.3.1 Primary Compound Triage

4.3.1.1 *L. donovani* Axenic Amastigote Screening

Testing of the 216 compounds against *L. donovani* was initially undertaken in a dose-response assay against axenic amastigote parasites. As discussed in section

1.2.1.2, amastigotes are the life cycle stage observed intracellularly in the mammalian host and are therefore more clinically relevant than the insect stage promastigotes.[33] Axenic testing was preferred at this stage due to the ease of assay implementation and the higher throughput achievable.

The assay was executed according to an established protocol,[341] again relying on fluorescence resulting from resorufin production. As with the *L. major* promastigote screening, 5.0×10^3 ml^{-1} parasites were incubated with the compounds for 72 hours prior to resazurin addition. A dilution factor of ⅓ was used for each compound; this resulted in a concentration range of 50 µM to 0.85 nM with a total of 11 concentrations tested. This allowed the determination of the ED_{50} (the concentration required to produce 50% inhibition of growth) and subsequently the pED_{50} ($-\log_{10}(ED_{50})$) for each compound. The results (Figure 4–3) were promising; whilst 56 compounds were completely ineffective, 75 demonstrated a pED_{50} greater than or equal to 5.0 (equivalent to 50% inhibition at 10 µM).

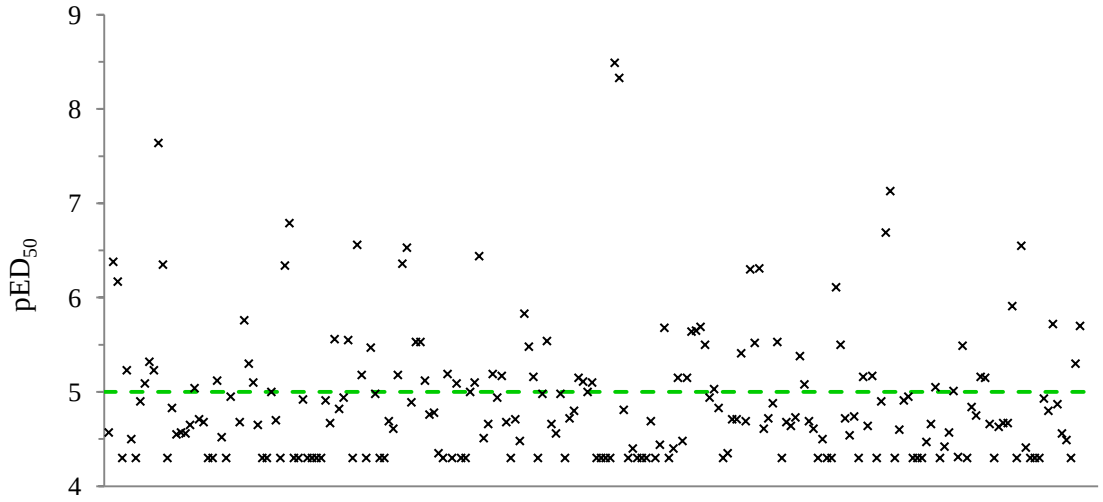

Figure 4–3: The pED_{50} values of the 216 compounds tested against 5.0×10^3 ml^{-1} axenic *L. donovani* amastigotes for 72 hours

Of these 75 compounds, 51 showed inhibition greater than 50% at 10 µM against *L. major*. This number was larger than expected as the difference in biochemistry between species,[342] as well as between promastigotes and amastigotes, is significant. For example, the different forms utilise different energy sources; *L. donovani* promastigotes predominantly metabolise glucose whilst amastigotes utilise fatty acid metabolism,[343] and one *L. donovani* glycolytic enzyme is only a pseudogene in *L. major*.[344] The *L. donovani* assay is also conducted at pH 5.5 in order to mimic the

intramacrophage environment, and compounds therefore have to remain stable in an acidic environment. However, the IPCS coding sequence from *L. donovani* is very similar to *L. major* (93% identity) so the fact that so many compounds retained activity against two different *Leishmania* species was reassuring as it suggests that the target is valid in at least these two species. In addition, it verifies that the assays used are effective at identifying inhibitors of highly related targets.

4.3.1.2 HepG2 Cytotoxicity Screening

With the ultimate aim of identifying a compound series suitable for entry into *in vivo* proof of concept studies, the next stage of compound testing was a cytotoxicity assay to identify compounds with significant host toxicity. As a preliminary way of investigating host toxicity, the 216 compounds were tested against cells from the HepG2 line, which is derived from a human hepatocellular carcinoma.[345] This cell line is commonly used as an indicator of cytotoxicity due to the fact that the majority of drug metabolism occurs in the liver and hence the effect of both the parent compound molecule and any modified metabolites can be observed and measured.[346]

The assay was executed according to an established protocol.[347] Briefly, 1.2×10^5 ml^{-1} HepG2 cells were incubated with the compounds for 48 hours. A dilution factor of ⅓ was used for each compound; this resulted in a concentration range of 100 µM to 1.7 nM with a total of 11 concentrations tested. Compound toxicity following incubation was measured by the addition of CellTiter-Glo® (Figure 4–4). This reagent allows the quantification of cell viability by producing a luminescent signal proportional to the quantity of adenosine triphosphate (ATP) present. The luminescence output is therefore representative of cell viability, with a lower readout indicative of decreased growth and hence a cytotoxic compound.

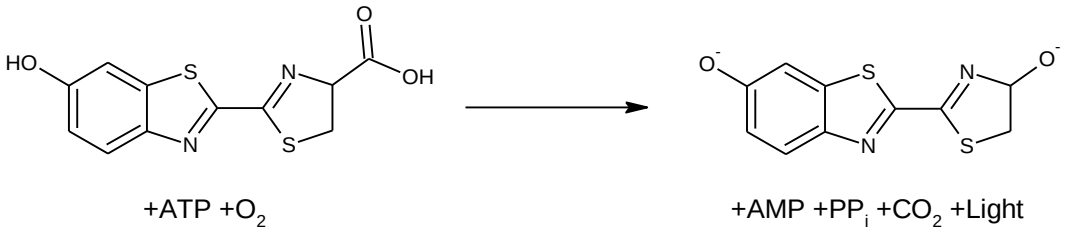

Figure 4–4: The conversion of luciferin to oxyluciferin by Ultra-Glo™ recombinant luciferase accompanied by the production of light

The results are shown in Figure 4–5. In total, 148 of the 216 compounds tested demonstrated a pED_{50} less than or equal to 4.0 and hence were classed as non-toxic against the HepG2 cells. However, comparison with the *L. donovani* axenic amastigote assay results was required in order to select compounds of interest.

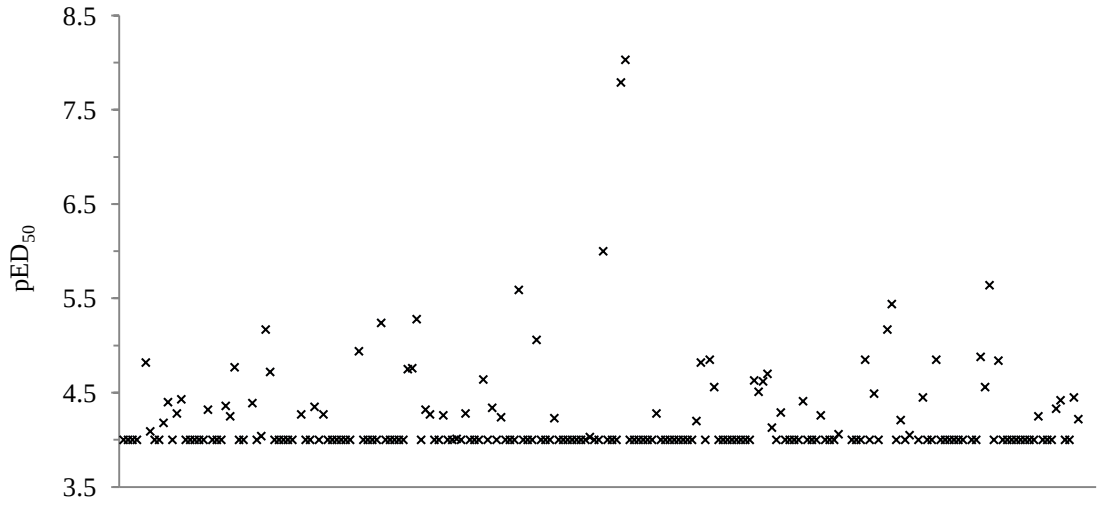

Figure 4–5: The pED_{50} values of the 216 compounds tested against 1.2×10^5 ml^{-1} HepG2 cells for 48 hours

4.3.1.3 Compound Selection

The primary compound selection was achieved using two factors (criteria set 1):

1. The pED_{50} against axenic *L. donovani* amastigotes was required to be greater than or equal to 5.0. This is equivalent to an ED_{50} of less than or equal to 10 µM.
2. The pSI (logarithm of the selectivity index, as discussed in section 3.3.6) over HepG2 cells was required to be greater than or equal to 1.0. This is equivalent to the compound demonstrating at least 10 fold greater potency against the *L. donovani* amastigotes than the HepG2 cells.

The application of this set of criteria is shown in Figure 4–6. Compounds which were inactive against *L. donovani* amastigotes, or which were active but also cytotoxic to HepG2 cells, were filtered out. Of the 216 compounds, 53 fulfilled both of the above criteria and were investigated further.

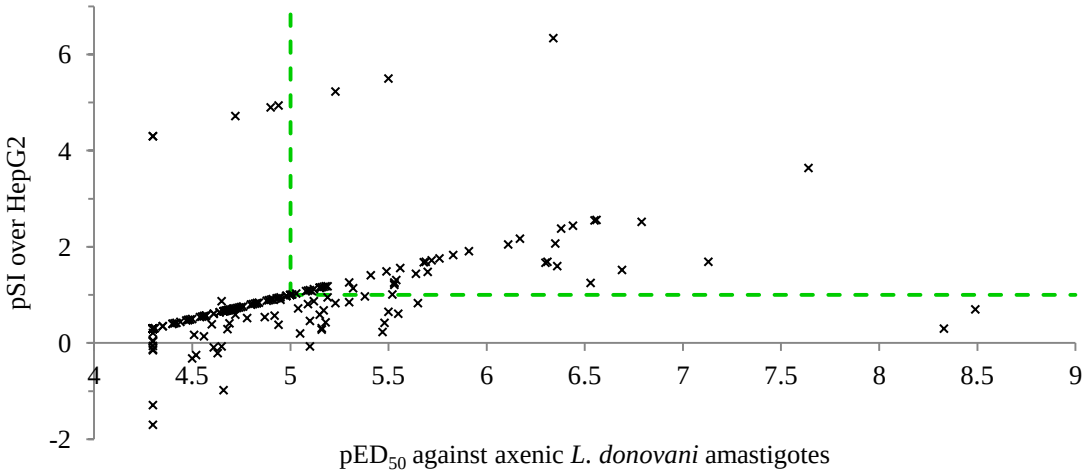

Figure 4–6: The pSI for axenic *L. donovani* amastigotes over HepG2 cells plotted against the pED_{50} against axenic *L. donovani* amastigotes for the 216 compounds, with the limits of criteria set 1 shown in green

4.3.2 Secondary Compound Triage

The secondary stage of compound selection was achieved based on physicochemical properties. As discussed in sections 1.4.2.5 and 3.3.4, smaller and more hydrophilic compounds are favoured for progression due to their tendency to result in more effective drugs. As a result, the secondary compound selection was achieved using two factors (criteria set 2):

1. The number of aromatic rings was required to be less than or equal to 4. Aromatic rings increase hydrophobicity, hence compounds with fewer rings are more likely to possess favourable overall drug-like properties.
2. The property forecast index (PFI), calculated as shown in equation 4.1, was required to be less than or equal to 8.0. This term is a measure of the intrinsic hydrophobicity of a compound; high PFI is indicative of high hydrophobicity and is often accompanied by low solubility and high compound promiscuity.[348]

$$PFI = LogD_{7.4} + \#Ar \qquad (4.1)$$

where: PFI = property forecast index
$LogD_{7.4}$ = logarithm of the 1-octanol−water distribution coefficient
#Ar = number of aromatic rings

Whilst PFI is sometimes calculated using the LogP value, this does not take into account the fact that ionisable compounds will be present in both the ionised and unionised forms dependent on the pH. It is therefore more accurate to utilise the

$LogD_{7.4}$, which is dependent upon the concentrations of both the ionised and unionised forms in octanol and water. LogD is often measured pharmaceutically at pH 7.4, as this is the physiological pH of blood serum. The $LogD_{7.4}$ values of the 216 compounds, however, had not been determined and therefore PFI was predicted using cLogP values.

The application of this set of criteria is shown in Figure 4–7. Of the 53 compounds studied, all possessed a maximum of 4 aromatic rings and therefore fulfilled the first criterion. The suitability of the compounds for selection was therefore dependent upon the PFI, and 30 of the 53 compounds possessed a PFI value lower than or equal to the threshold and were therefore advanced for additional testing.

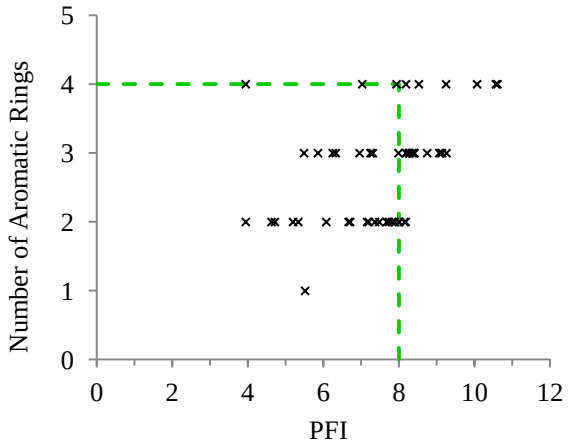

Figure 4–7: The number of aromatic rings plotted against the predicted PFI for the 53 compounds, with the limits of criteria set 2 shown in green

4.3.3 Tertiary Compound Triage

4.3.3.1 *L. donovani* Intramacrophage Screening

The 30 selected compounds were subsequently tested against intramacrophage *L. donovani* amastigotes. This assay more accurately mimics the disease state than the previously utilised axenic assay and is therefore a better representation of how effective the compounds might prove to be in *in vivo* studies.

The assay was executed according to an established protocol.[341] The human biological samples were sourced ethically and their research use was in accord with the terms of the informed consents. Briefly, 6.0×10^5 ml^{-1} THP-1 derived macrophages were infected with mutant *L. donovani* amastigotes expressing eGFP at an infection

multiplicity of 10 and incubated prior to the addition of the test compounds. A dilution factor of ⅓ was used for each compound resulting in a concentration range of 50 µM to 0.85 nM with a total of 11 concentrations tested. Following a 96 hour incubation the cells were fixed and stained. Wells were imaged by microscopy (an example is shown in Figure 4–8) and analysed using Acapella® High Content Imaging and Analysis software, and inhibitory activity was determined by parasite count.

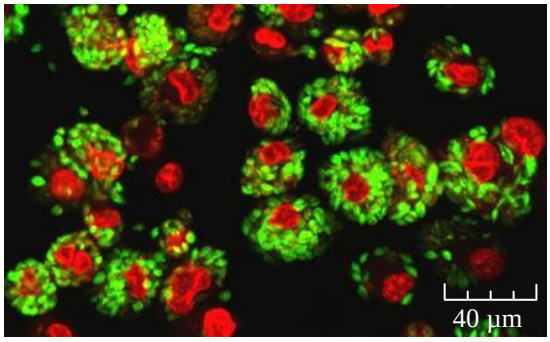

Figure 4–8: The infection of macrophages, the nuclei of which have been stained red, with *L. donovani* amastigotes expressing eGFP. Figure provided by Dr J. Martin

The results of this assay (Figure 4–9) were promising, with only 10 compounds being completely ineffective (pED_{50} less than or equal to 4.3) against the intramacrophage amastigotes. The loss of activity for some compounds was expected given that, as discussed in section 1.4.2.2.1, they have to be capable of crossing multiple membranes.[266] In addition, macrophages themselves express a range of drug transporters that control the uptake and efflux of the compounds being tested and hence will affect the concentration of the test compound that the parasites are exposed to.[349] Despite this, seven compounds displayed activity in the low µM range (pED_{50} greater than 5.5), with one compound displaying nM activity with a pED_{50} of 6.2.

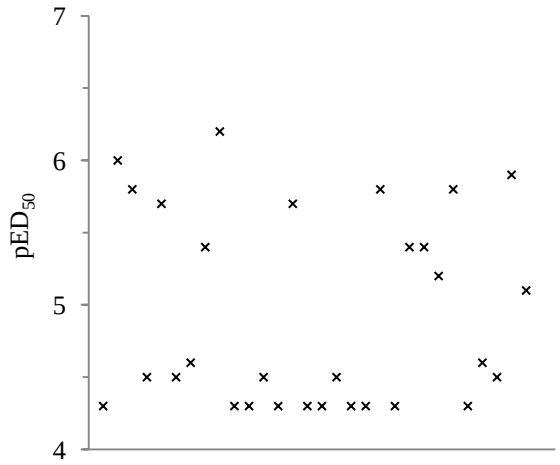

Figure 4–9: The pED_{50} values of the 30 compounds tested against intramacrophage *L. donovani* amastigotes for 96 hours

4.3.3.2 THP-1 Cytotoxicity Screening

In order to confirm the activities observed against intramacrophage *L. donovani* amastigotes, a second cytotoxicity assay was required against the macrophages themselves. These were obtained by the differentiation of THP-1 premonocytes, a cell line derived from the blood of a human patient with acute monocytic leukaemia.[350] Differentiation is achieved by exposure to phorbol myristate acetate, which is an activator of protein kinase enzymes and a promoter of tumour growth.[351] THP-1 derived macrophages exhibit multiple advantages compared to those derived from commercially available peripheral blood mononuclear cells, including a faster growth rate, increased stability and, as they are derived from a single source, greater consistency between batches.[352]

The assay was conducted as in section 4.3.3.1 with the modification that *L. donovani* amastigotes were not added; instead, compound inhibitory activity against the macrophages was determined using HCS CellMask™ Deep Red dye and the subsequent cell count. The results (Figure 4–10) show that 19 of the 30 compounds exhibited no cytotoxic activity on the macrophages (pED_{50} less than or equal to 4.3). However, as with the HepG2 cytotoxicity assay, comparison with the *L. donovani* intramacrophage assay results was subsequently required.

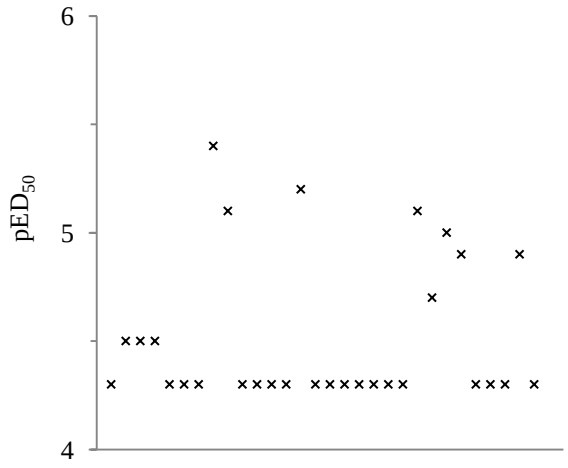

Figure 4–10: The pED_{50} values of the 30 compounds tested against THP-1 cells for 96 hours

4.3.3.3 Compound Selection

The tertiary compound selection was achieved using two factors (criteria set 3):

1. The pED_{50} against intramacrophage *L. donovani* amastigotes was required to be greater than or equal to 5.0. This is equivalent to an ED_{50} of less than or equal to 10 µM.
2. The pSI over THP-1 cells was required to be greater than or equal to 1.0. This is equivalent to the compound demonstrating at least 10 fold greater potency against the *L. donovani* intramacrophage amastigotes than the THP-1 cells.

The application of this set of criteria is shown in Figure 4–11. Compounds which were inactive against intramacrophage *L. donovani* amastigotes, or which were active but also cytotoxic, were filtered out. Of the 30 compounds tested at this stage, six fulfilled both of the above criteria. These compounds, which include two series and two singletons, are shown in Table 4–1.

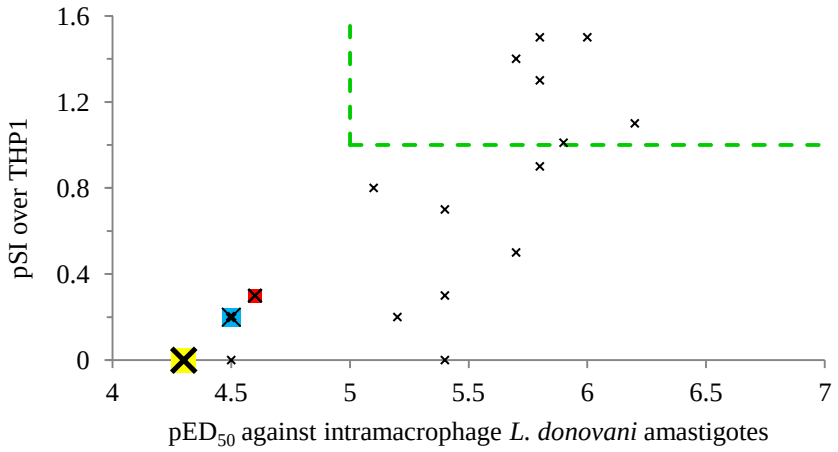

Figure 4–11: The pSI for intramacrophage *L. donovani* amastigotes over THP-1 cells plotted against the pED_{50} against intramacrophage *L. donovani* amastigotes for the 30 compounds, with the limits of criteria set 3 shown in green. 10 compounds are overlaid on the marker highlighted in yellow, 4 are overlaid on the marker highlighted in blue and 2 are overlaid on the marker highlighted in red

Table 4−1: The structures, properties and inhibition results of the 6 compounds which fulfil all the selection criteria

Compound	*L. mj* % Inh. at 10 µM	Axenic *L. don* pED_{50}	InMac *L. don* pED_{50}	HepG2 pED_{50}	THP-1 pED_{50}	PFI	#Ar
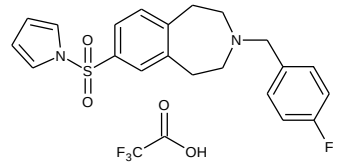 CS100462-069A11B16 (**23**)	94.4	7.6	6.0	4.0	4.5	6.3	3
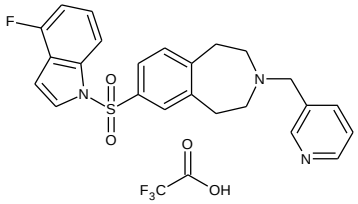 CS100462-069A14B4 (**24**)	94.9	6.4	5.8	4.3	4.5	7.0	4
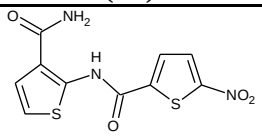 ST/918837 (**25**)	105.9	6.6	5.9	4.0	4.9	4.0	2
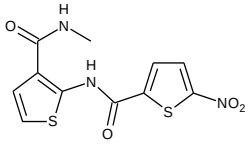 ST/492114 (**26**)	104.2	5.7	5.8	4.0	4.3	4.6	2
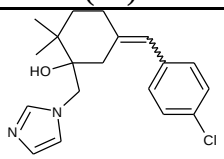 ST/1098001 (**27**)	98.4	5.5	6.2	4.3	5.1	7.5	2
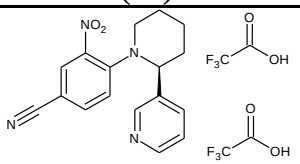 MA102475-064A1B46 (**28**)	74.1	5.3	5.7	4.0	4.3	4.7	2

From the data shown above, the two series appear to be the most promising options for further development. The benzazepane compounds (**23** and **24**) demonstrate the most potent antiparasitic activity, with both active in the nM range against axenic amastigotes and in the low μM range against intramacrophage parasites. However, their physicochemical properties are at the upper end of the limits set by the selection criteria, which could result in a reduced potency *in vivo*.

By contrast, the dithiophene compounds (**25** and **26**) possess comparable antiparasitic activities against intramacrophage parasites to the benzazepanes whilst their PFI values are far more favourable and well within the permitted limits. The basic chemical structure of the dithiophenes is also simpler than the benzazepanes, meaning they may lend themselves more favourably to a medicinal chemistry campaign. The presence of the nitro group, however, is a possible cause for alarm given that this functional group can undergo enzymatic reduction and has been linked to a range of toxic issues including hepatotoxicity, carcinogenicity and immunosuppression.[353] Whilst the presence of a nitro group does not necessarily preclude a compound making it to market (Nifurtimox (**10**, Figure 1–7) being one such example) it remains a cause for concern.

The singleton **28** is the least potent of the six compounds in both *L. donovani* assays. In addition, this compound also possesses a nitro group. Singleton **27**, on the other hand, was the only compound tested in the intramacrophage *L. donovani* assay that exhibited a potency in the nM range. This was, however, offset by significant activity against THP-1 cells, resulting in a pSI of only 1.1.

Overall, the continued screening campaign was successful in significantly reducing the number of compounds of interest. However, all of the screens described above were conducted at the cellular level and provide no information on the specific activities of the compounds against the IPCS enzyme; the only information regarding this so far were the dose-response results against yeast. Additional screens were therefore required in order to identify which, if any, of the six compounds were specific inhibitors of IPCS *in vitro*.

4.4 Lead Selection

In order to permit dose-response testing, additional quantities of compounds **25**, **26**, **27** and **28** were provided by GSK. The benzazepane compounds **23** and **24** were resynthesised as the free base compounds **29** and **30** respectively (Figure 4–12) by the pharmaceutical services company Aptuit (www.aptuit.com). Of the six compounds, these were the most attractive due to the fact that they are obviously part of a series rather than singletons, and they lack the concerning nitro group. In addition, there was no competing interest with regards to these compounds from other drug development campaigns within GSK.

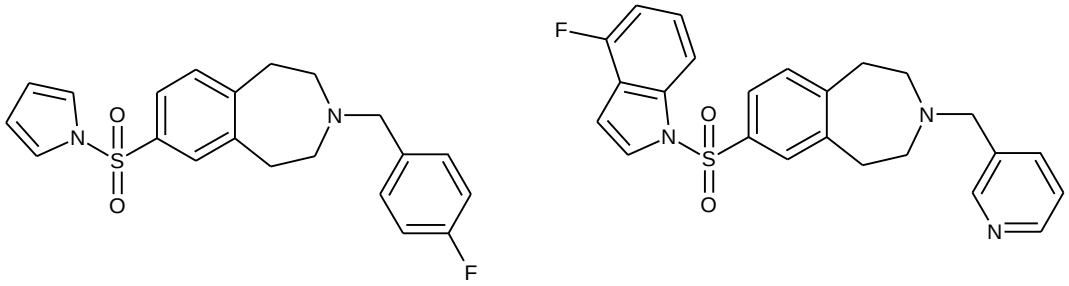

SB-762123-AAA (**29**) VAPT/8555/172/3 (**30**)

Figure 4–12: The structures of the resynthesised free bases

4.4.1 *L. major* pED_{50} Determination

The six selected compounds, which all showed greater than 50% inhibition against *L. major* promastigotes at 10 µM (Figure 4–2), were subsequently tested in a dose-response assay. In order to allow comparison, it was decided to conduct experiments against both wild type *L. major* FV1 parasites and *L. major lcb2Δ* mutants, which lack subunit 2 of the serine palmitoyltransferase enzyme.[354, 355] These mutants still produce the IPCS but the enzyme is redundant due to the lack of available *in situ* substrate. This strain should therefore be resistant to inhibitors specific for IPCS.

Before screening could commence, the starting concentration of parasites in the assay needed to be checked as slower growth is observed with the sphingolipid-deficient mutants. The resulting growth curve for an incubation period of 72 hours (Appendix B.4) showed that a concentration of 5.0×10^3 ml^{-1}, which was used previously against wild type *L. major* promastigotes, produced an insufficient

fluorescence output even after 8 hours incubation with AlamarBlue®. The decision was therefore made to increase the starting concentration for both wild type and mutant *L. major* dose-response assays to 1.0×10^4 ml^{-1}. This resulted in the doubling of the fluorescence readout for the mutants in a consistent, reproducible manner, whilst remaining as close to the original assay parameters as possible.

The dose-response assay was conducted with a dilution factor of ½ for each compound; this resulted in a test concentration range of 10 µM to 78 nM with a total of 8 concentrations tested. The results are shown in Figure 4–13. Compounds **26** and **28**, despite demonstrating significant inhibition of growth of *L. major* FV1 parasites at 10 µM, were weakly inhibitory at lower concentrations and the pED_{50} values were calculated at less than or equal to 5.0. Of the remaining four compounds, only **25** showed a significant difference in inhibition between the wild type and mutant parasites, with a *t*-test producing a P value of 0.033 (meaning that, if there was no significant difference between the results, there would be only a 3.3% probability of this observation occurring). However, the fact that the compound was more effective against the *L. major lcb2Δ* mutants than the wild type, and that no significant difference was observed for any of the other compounds, suggests that either IPCS is not being inhibited or that the compounds have additional effects on targets other than IPCS. In order to clarify this, additional testing of the compounds in a biochemical format was required.

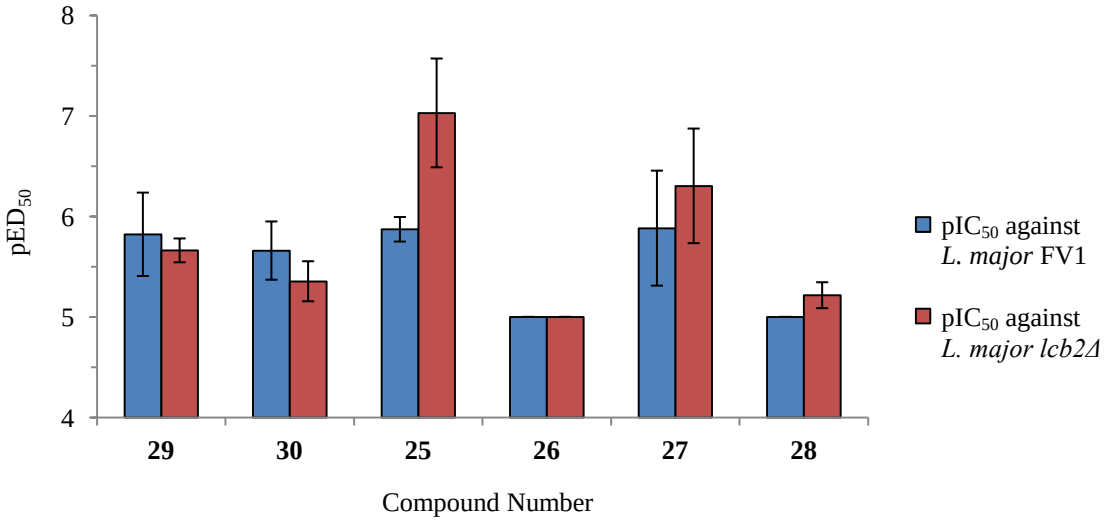

Figure 4–13: The pED_{50} values of the 6 selected compounds tested against wild type *L. major* FV1 and sphingolipid-deficient mutant *L. major lcb2Δ* for 72 hours. Error bars show the standard error of the mean for a triplicate set of data

4.4.2 Biochemical Screening

4.4.2.1 Primary Screening

The biochemical assay, as described in section 2.4.2, involved incubating *Lmj*IPCS-enriched microsomal membranes with NBD-C_6-ceramide, a fluorescent ceramide analogue, to produce the fluorescent product NBD-C_6-IPC (Figure 2–6). However, due to the low throughput possible with the HPTLC assay, screening was instead conducted in 96-well plate format.[320] The separation of the product from the starting material was possible using an ion exchange resin.

The assay was initially conducted according to the protocol previously developed in the group.[320] However, further optimisation proved to be necessary as the preliminary trial results were extremely inconsistent. This was postulated to be predominantly due to the use of the vacuum manifold during the separation steps, which appeared to apply an uneven vacuum across the plates. This issue was resolved by using a centrifuge for these steps, although the spin time had to be carefully controlled to prevent the ion exchange resin drying out. In addition, the duration of the incubation steps was modified; the pre-incubation step was reduced to 15 minutes and the assay time shortened to 25 minutes as this was also found to improve consistency.

Prior to commencing the screening, a suitable positive control compound had to be identified. Clemastine (**21**, Figure 3–8), which had previously displayed a pIC_{50} of 6.4 in the biochemical assay, was tested alongside the three ceramide analogues (Figure 4–14 (a)) with the highest inhibitory activity from a library synthesised and tested by Dr J. Mina.[212] The results (Figure 4–14 (b)) were unexpected, with clemastine showing the least inhibition compared to the DMSO control; this resulted in a Z′ of 0.28 when tested at 25 μM. This was postulated to be due to compound instability in solution, although this was not explored further. The best of the compounds tested was JM222 (**32**) which reduced the mean fluorescence output from 11,900 to 595. This was equivalent to a Z′ of 0.75, and this compound was consequently selected for use as the control.

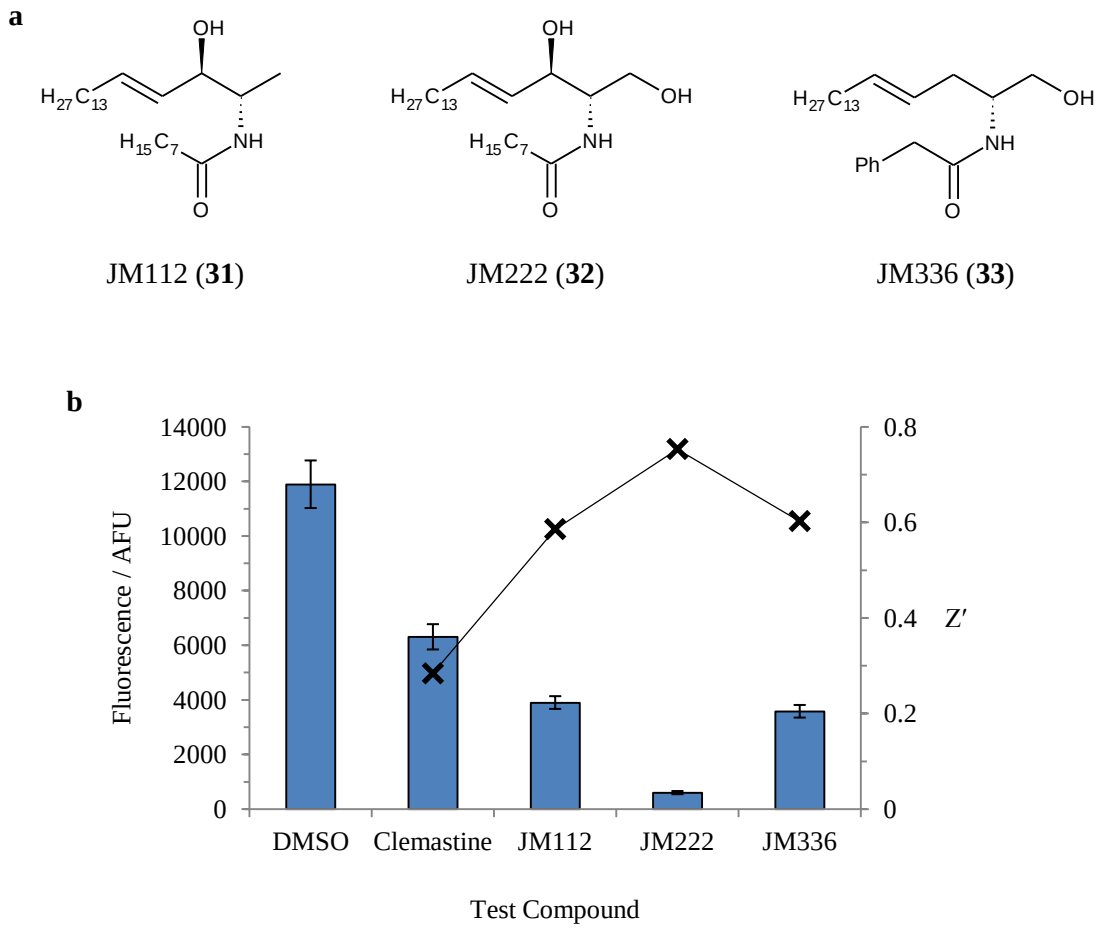

Figure 4–14: (a) The structures of the inhibitors tested in the biochemical assay and (b) the results of the inhibition testing at 25 µM. Error bars show the standard error of the mean for a quadruplicate set of data

Whilst only six compounds fulfilled the selection criteria as described previously, the decision was made to run the assay against all 216. This was in order to validate the compounds which, due to the nature of the HTS screening process described in the previous chapter, should all be inhibitors of *Lmj*IPCS. This assay, being the only one performed *in vitro*, was also orthogonal to all the assays utilised thus far and therefore may identify potent inhibitors of *Lmj*IPCS which were not active *in cellulo*.

The 216 compounds, plus the two resynthesised benzazepanes, were tested at 10 µM and the results are shown in Figure 4–15. Whilst 12 of the 216 showed good activity (inhibition greater than 50%), the inhibition values obtained were, in general, significantly lower than in any of the parasite assays, or the original HTS assay, thus far. One possible explanation for this is that the amount of biological material in this assay (0.6 enzyme units (U) per well, where 1 U = 1 pmol(product) min^{-1}) is significantly greater than that used in the HTS assay (approximately 4.0×10^{-5} U per

well); as discussed in section 4.2, this effectively reduces the relative concentration of the test compounds. Whilst this variation is obviously not ideal, this is the minimum amount of microsomal material required in the biochemical assay to produce a measurable signal with sufficient signal to noise; the use of less also decreased result consistency.

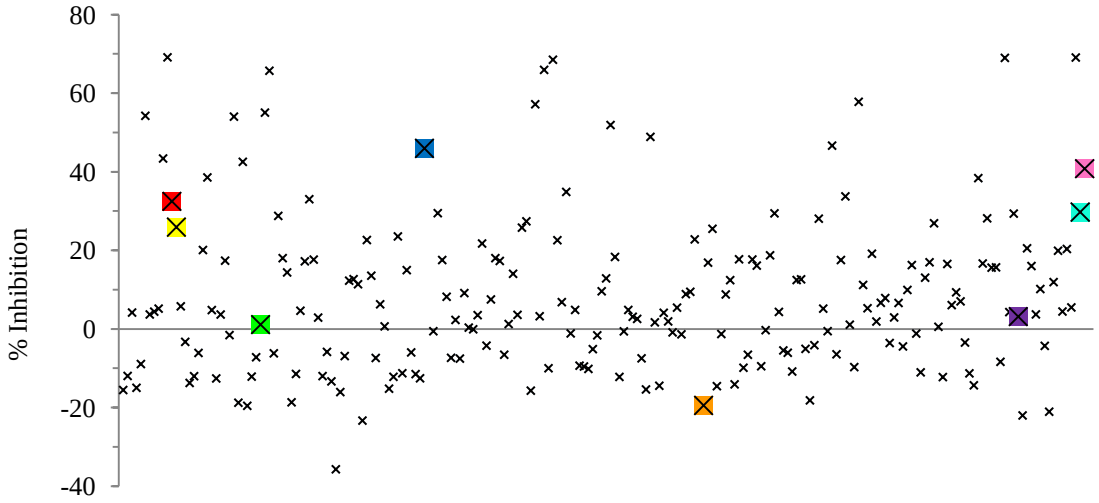

Figure 4–15: The inhibitory activities of the 216 compounds and the resynthesised benzazepanes tested at 10 µM against *Lmj*IPCS microsomes. From left to right, compound **23** is highlighted in red, compound **24** in yellow, compound **28** in green, compound **27** in blue, compound **26** in orange, compound **25** in purple, compound **29** in turquoise and compound **30** in pink

One other factor that has to be considered is that the IPCS enzyme is membrane-bound, and hence cannot be readily expressed in and purified from bacteria such as *E. coli*. As a result, it is not pure enzyme that is being tested in the biochemical assay but microsomes which, whilst enriched in *Lmj*IPCS, contain a variety of other proteins possibly including cytochrome P450s.[356] These enzymes account for roughly 75% of drug metabolism,[357] and it is possible that compound degradation could be occurring during the course of the assay despite the overall incubation time being reduced from the published protocol. This hypothesis could be checked using a known cytochrome P450 inhibitor, such as quinidine,[358] which would be incubated along with the test compounds in order to see if apparent inhibitory activity was improved.

Despite the inhibition values being lower than ideal, compound **27** along with both the original benzazepanes (**23** and **24**) and the free bases (**29** and **20**) showed greater than 25% inhibition, putting them in the top 15% of the compounds tested. These compounds therefore warranted further investigation at the biochemical level.

4.4.2.2 pIC_{50} Determination

The three selected compounds were subsequently subjected to IC_{50} determination in a dose-response assay, which was conducted with a dilution factor of ⅓ for each compound. This resulted in a test concentration range of 100 µM to 46 nM with a total of 8 concentrations tested. Examples of the curves produced are shown in Figure 4–16.

Compound **27**, which displayed the highest inhibition of the three compounds in the primary assay, was the least active at 100 µM and was calculated to have a pIC_{50} of 4.5. This level of activity was not sufficient to warrant further exploration as a potential IPCS inhibitor. On the other hand, the two benzazepane compounds yielded excellent results, with **29** exhibiting a pIC_{50} of 6.1 and **30** exhibiting a pIC_{50} of 5.7. These two compounds have therefore proven themselves to be potent inhibitors of *Lmj*IPCS, with this translating into good antileishmanial activity against both *L. major* and *L. donovani*. As a result, it was decided to utilise the benzazepanes as starting points for a hit-to-lead optimisation, which would hopefully result in a suitable candidate for clinical trials.

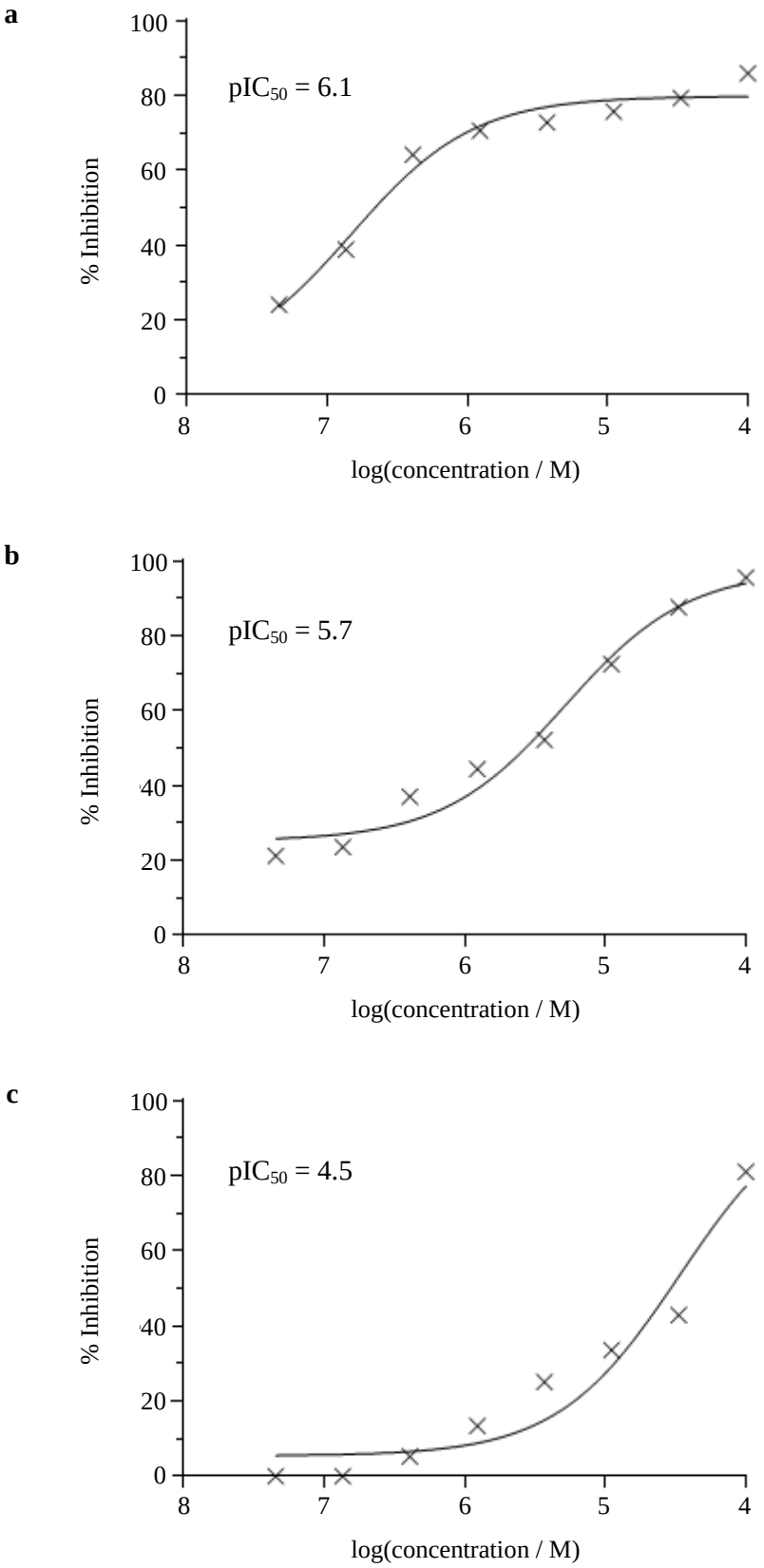

Figure 4–16: Example IC_{50} curves from a single experiment for (a) compound **29**, (b) compound **30** and (c) compound **27**. The mean pIC_{50} values, calculated from a quadruplicate set of data, are shown

4.5 Conclusion

The work described in this chapter involved the further screening of 216 compounds identified by HTS. Six compounds with high antileishmanial activity, low mammalian cytotoxicity and favourable physicochemical properties were identified, and further biochemical testing identified two compounds from the same structural family as potent inhibitors of *Lmj*IPCS. Additional testing in order to determine whether this series was suitable for lead optimisation and subsequent progression to clinical trials was therefore required and is described in the next chapter.

Chapter 5

Exploration of the Benzazepane Series

5.1 Introduction

Having identified a compound series worthy of further investigation, attention turned to the exploration of SARs in order to determine whether the antiparasitic and biochemical properties of the two compounds studied thus far could be improved upon. With the core benzazepane structure identical between the two compounds, the primary variations explored were the left and right hand sides of the compounds. The simplest examples, the mix and match compounds with the right hand sides of compounds **29** and **30** exchanged (Figure 5–1), were prioritised for analysis.

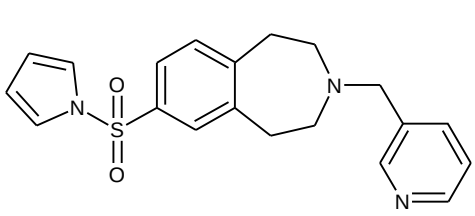

VAPT/8576/13/3 (**34**)

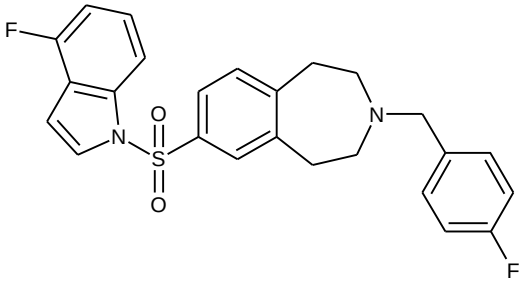

VAPT/8555/173/1 (**35**)

Figure 5–1: The structures of the mix and match benzazepane compounds

5.2 Pyrrole-Pyridine Benzazepane

5.2.1 Antileishmanial and Biochemical Activity

Compound **34** was initially subjected to a range of assays as previously described in chapter 4. As can be seen from Figure 5–2, the biochemical activity (pIC_{50} = 4.2) was reduced more than tenfold from either of the parent compounds; this suggests that

biochemical activity is to a certain extent dependent on either the substituted indole ring on the left hand side of the molecule or the substituted benzene ring on the right hand side. With little known about the structure of the IPCS protein, it is not clear why particular rings would be important, although they could either fit better into a pocket in the protein structure or be involved with π-stacking interactions with aromatic amino acids.[359] This decrease in biochemical activity did not, however, result in a decrease in antileishmanial activity; on the contrary, pED_{50}s of 5.6 and 6.3 were observed against *L. major* wild type promastigotes and intramacrophage *L. donovani* amastigotes respectively. The high potency against intramacrophage *L. donovani* was particularly exciting given that the pED_{50} against THP-1 macrophages was only 5.0. Whilst the physicochemical properties were not ideal – the PFI was 8.4, which would not have passed the selection criteria described in chapter 4 – the high potency against *L. donovani* intramacrophage amastigotes led to the decision to test the compound *in vivo*, which was carried out with the support of the London School of Hygiene and Tropical Medicine (LSHTM).

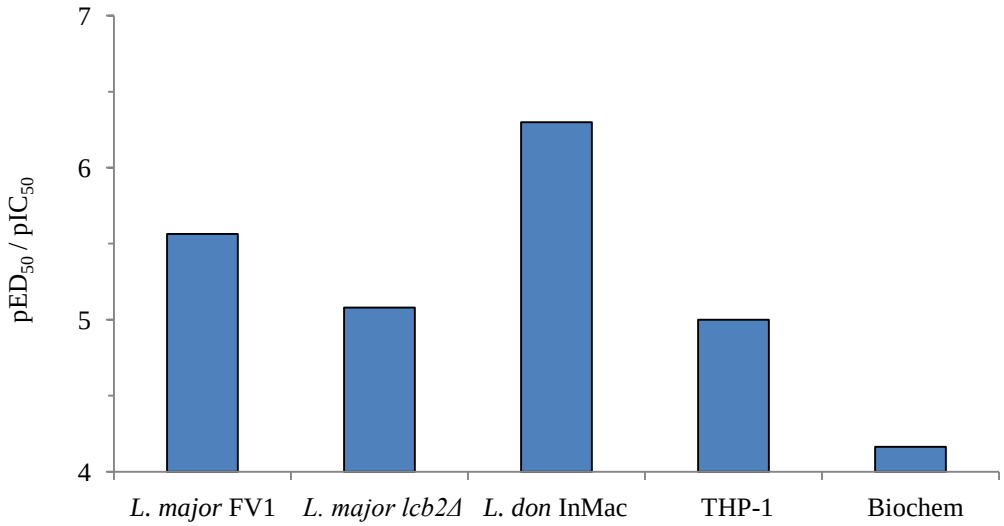

Figure 5–2: The assay results for compound **34**. Note that due to assay restrictions, the lowest possible pED_{50} / pIC_{50} measurements are 5.0 for the *L. major* assays, 4.3 for the *L. donovani* and THP-1 assays and 4.0 for the biochemical assay

5.2.2 *In vivo* Activity

The use of animal models is crucial in drug discovery as it is the only way, save for human clinical trials, to determine factors such as distribution, metabolism and bioavailability. The most commonly used animal species that serve as experimental

hosts for VL are Syrian hamsters (*Mesocricetus auratus*) and mice (*Mus musculus*), although dogs and non-human primates are also occasionally used for testing.[360] Whilst infected hamsters often exhibit clinical symptoms that closely mimic the human disease, their use in immunisation trials is precluded by a lack of reagents for immunological analysis.[361] As a result, murine models are the most extensively used, although not all strains are equally susceptible to *L. donovani* infection.[362] One of the most commonly used strains, due to the fact that it produces highly consistent levels of infection, is the BALB/c strain,[360] and this was selected for the testing of compound **34**.

Prior to *in vivo* activity determination, the compound was tested in a metabolic stability assay. This involved incubating human and mouse liver microsomes with the compound and measuring the intrinsic clearance (CL_{int}), with a higher value indicating a faster rate of clearance and hence greater metabolic instability. The human biological samples were sourced ethically and their research use was in accordance with the terms of the informed consents. Compound **34** was observed to have a CL_{int} of 2.3 ml min^{-1} g^{-1} against human microsomes, implying a favourable low rate of clearance. However, against mouse microsomes it produced a CL_{int} of 29 ml min^{-1} g^{-1}, which was outside of the desired range (above 15).[363] Whilst a difference between microsomes from two different species is not unexpected and frequently observed,[364] a high clearance in mouse microsomes prior to *in vivo* testing in mice was not ideal.

It was postulated that this high clearance level in mouse microsomes was due to the metabolically labile benzylic carbon; this atomic position is known to be readily oxidised to a benzylic alcohol by cytochrome P450 enzymes.[365] This theory would support the speculation discussed in section 4.4.2.1 that drug metabolism, potentially due to cytochrome P450 activity, was responsible for the general low levels of activity observed. In order to investigate this, the fact that cytochrome P450 oxidation of benzylic carbon atoms is known to exhibit a kinetic isotope effect, with the rate of oxidation for a carbon-hydrogen bond being 11 times greater than that for a carbon-deuterium bond,[366] was exploited. The deuterated compound **36** (Figure 5–3) was therefore synthesised by Aptuit and provided for testing. This compound did not, however, display increased metabolic stability; the CL_{int} values against human and mouse microsomes were 5.0 ml min^{-1} g^{-1} and > 30 ml min^{-1} g^{-1} respectively. This indicates that the benzyl position is not labile to cytochrome P450 oxidation, meaning

the reason for the instability in mouse microsomes remained unclear. Despite this result, both compound **34** and compound **36** were progressed to *in vivo* testing.

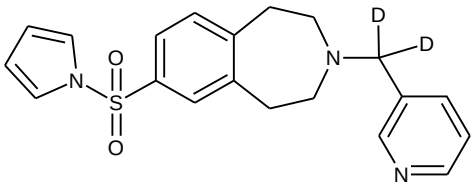

VAPT/8559/99/2 (**36**)

Figure 5–3: The structure of the deuterated analogue of compound **34**

The *in vivo* testing was executed according to an established protocol.[367] All animal studies were ethically reviewed and carried out in accordance with the Animals (Scientific Procedures) Act 1986 and the GSK policy on the Care, Welfare and Treatment of Animals. Briefly, BALB/c mice were infected with *L. donovani* amastigotes and the infection was allowed to develop over 7 days. Half the mice were subsequently dosed orally at 50 mg kg^{-1} twice a day for 5 days, before all the mice were sacrificed 14 days post infection. Counting the number of amastigotes per liver cell allowed any effect on parasite burden to be determined.

Whilst compound **34** disappointingly demonstrated a 0% reduction on liver parasitaemia, treatment with compound **36** resulted in a 32% reduction in parasite burden. This was unexpected given the microsomal stability results discussed above, but could possibly be explained by the different pharmacokinetic profiles exhibited by the two compounds (Figure 5–4). Compound **36** achieved a maximum concentration three times larger than compound **34** and reached that level in less than half the time. In addition, the dose normalised area under the curve (DNAUC) measurement, which is an indication of total dug exposure, for compound **36** was more than twice as large as for compound **34**. All of these measurements suggest that the oral uptake and biodistribution of compound **36** is greater; this is possibly due to the fact that some deuterated drugs, such as amphetamines, have been shown to exhibit different transport processes than their non-deuterated counterparts, although the reasons for this phenomenon are unclear.[368, 369] In addition, in some drugs deuteration leads to metabolic switching, whereby the site of metabolism is altered and the process occurs via a different pathway. Therefore, whilst compound **36** may not be more active than **34**, the parasites were exposed to a greater amount of it for a longer period of time.

a

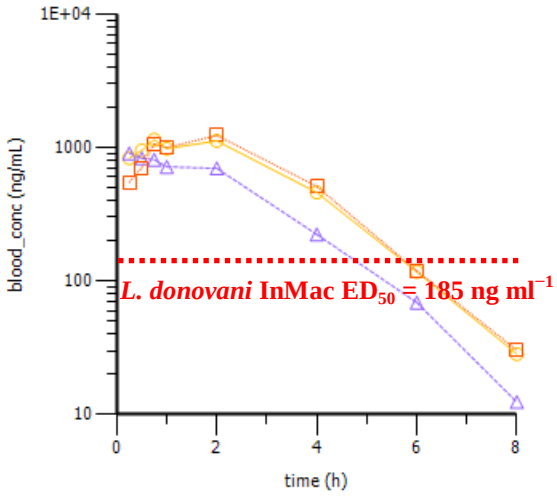

C_{max} / ng ml^{-1}	t_{max} / min	DNAUC / ng h ml^{-1} per mg kg^{-1}
1091	60	71

b

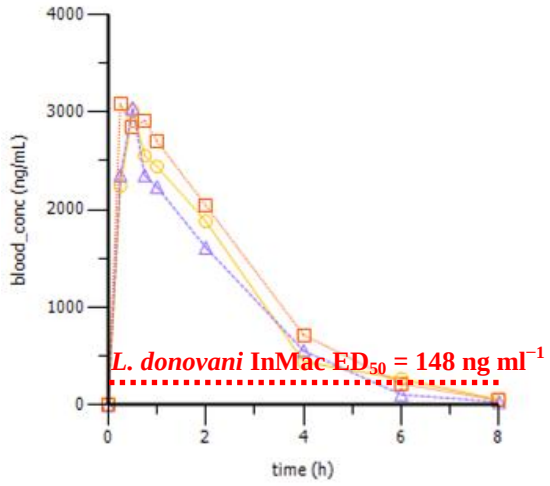

C_{max} / ng ml^{-1}	t_{max} / min	DNAUC / ng h ml^{-1} per mg kg^{-1}
3043	25	150.7

Figure 5–4: The pharmacokinetic profile of (a) compound **34** and (b) compound **36**, where C_{max} is the maximum blood concentration attained, t_{max} is the time after which the maximal concentration is reached, and DNAUC is a measure of total drug exposure over time. The concentrations required to show 50% inhibition in the *L. donovani* intramacrophage assay are indicated. Figure provided by DDW, GSK, Tres Cantos

Despite these differences, the compounds were less active than hoped for; as can be seen from the graphs, both were present at a concentration greater than the pED_{50} against intramacrophage *L. donovani* amastigotes for several hours following dosing. One possible explanation for this was that the *L. donovani* strains used for the two assays were different; the intramacrophage testing utilised *L. donovani* MHOM/SD/62/1S-CL2D (LdBOB), whilst the *in vivo* testing utilised *L. donovani* MHOM/ET/67/L82. These strains have different geographic origins (Sudan and Ethiopia respectively) and therefore may demonstrate slight variations in biochemistry. It is possible, for example, that MHOM/ET/67/L82 may possess more drug efflux

transporters or they may act at an increased rate, which would therefore decrease the susceptibility to drug compounds compared to LdBOB.

One other consideration is that whilst intramacrophage testing is the most biologically relevant assay possible *in cellulo*, it is still a very simplified model in comparison to *in vivo* testing. The latter introduces a new range of factors to take into consideration, such as oral uptake, biodistribution, correct localisation and excretion. All of these affect the relative compound concentration the parasites are exposed to compared to *in cellulo* studies. For example, if a compound acts as a prodrug and is metabolised into an active drug, this would remain present in the wells in an *in cellulo* assay but would face excretion in an *in vivo* model. Irrespective of the reason for the results obtained, however, the potencies demonstrated by both compounds were insufficient to justify progressing them further towards clinical trials.

5.3 Indole-Benzene Benzazepane

With compound **34** proving disappointing in the *in vivo* tests, attention turned to the other mix and match compound, **35**. This was subjected to the same range of assays as discussed in section 5.2.1, with the results being shown in Figure 5–5. Whilst demonstrating a pED_{50} of only 4.7 against intramacrophage *L. donovani* amastigotes (and a pSI against THP-1 macrophages of 0.4), compound **35** produced a pIC_{50} of just above 6.0 in the biochemical assay. This is comparable to the two parent compounds.

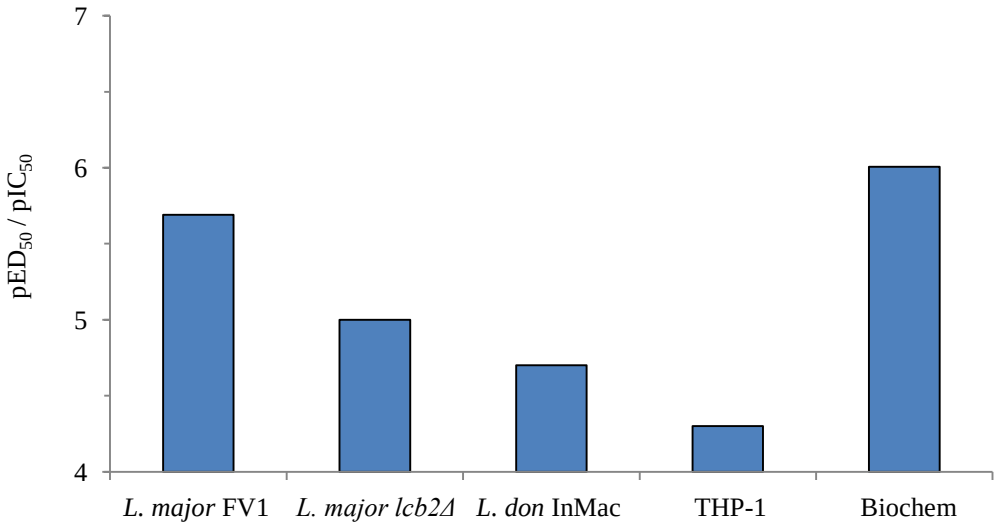

Figure 5–5: The assay results for compound **35**. Note that due to assay restrictions, the lowest possible pED_{50} / pIC_{50} measurements are 5.0 for the *L. major* assays, 4.3 for the *L. donovani* and THP-1 assays and 4.0 for the biochemical assay

Compound **35** did, however, produce a unique result in that it demonstrated a pED_{50} of 5.7 against *L. major* wild type promastigotes whilst being completely ineffective at 10 µM against *L. major lcb2Δ* promastigotes. This is more clearly visible from the IC_{50} curves produced (Figure 5–6). This therefore suggests that compound **35** is a specific IPCS inhibitor with few, if any, off-target effects.

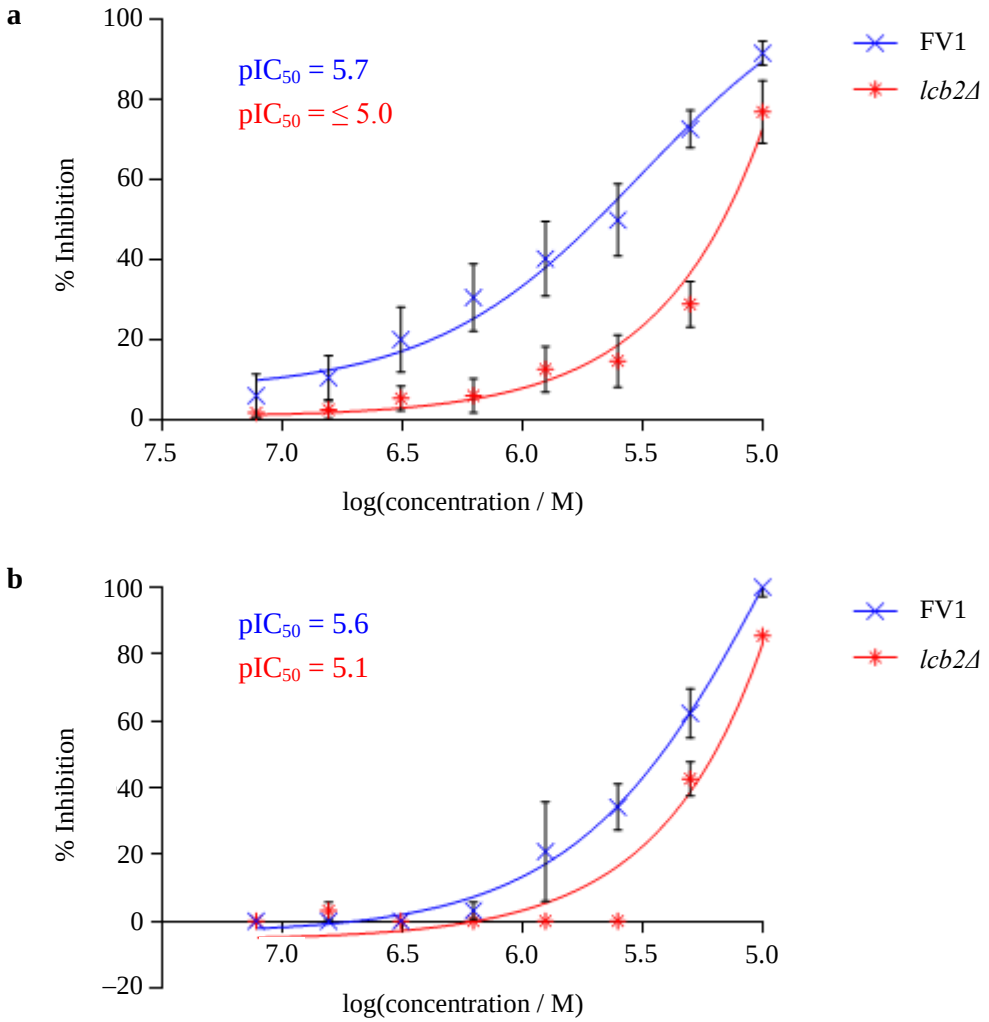

Figure 5–6: The IC_{50} curves and mean pIC_{50} values against *L. major* FV1 and *lcb2Δ* promastigotes for (a) compound **35** and (b) compound **34**. Error bars show the standard error of the mean for a sextuplet set of data for **35** and a triplicate set of data for **34**

In order to investigate this result further, compound **35** was tested alongside its two parent compounds, **29** and **30**, in a metabolic labelling assay, which was undertaken using the *L. major lcb2Δ* mutants. As discussed in section 4.4.1, these parasites are lacking subunit 2 of serine palmitoyltransferase, the first enzyme in the sphingolipid synthesis pathway. Whilst this renders the rest of the enzymes in the pathway, including IPCS, redundant, they remain capable of performing their usual roles. As a result, IPCS function can be measured by introducing a fluorescently-labelled ceramide

analogue, such as BODIPY FL C_5-ceramide, and monitoring the conversion to fluorescently-labelled IPC (Figure 5–7) in the presence or absence of test compounds. Given the absence of *in situ* ceramide to act upon, there is no substrate competition for IPCS and therefore fluorescence output is proportional to the amount of fluorescent product produced, and hence IPCS activity.

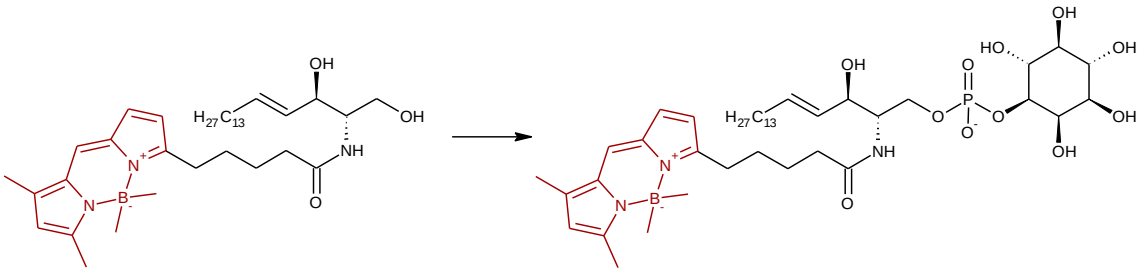

Figure 5–7: The conversion of BODIPY FL C_5-ceramide to BODIPY FL C_5-IPC by IPCS

Initial experiments were conducted according to an established protocol.[370] Briefly, the parasites were incubated with the test compound for 1 hour in serum-free media to ensure the absence of competing ceramide. The cells were subsequently incubated with BODIPY FL C_5-ceramide for 1 hour prior to the extraction and analysis of the cellular contents. However, the samples all produced comparable fluorescence, and this was postulated to be due to the short incubation time with the test compounds. The incubation time was subsequently increased from 1 hour to 18 hours and this adjustment resulted in more promising results (Figure 5–8).

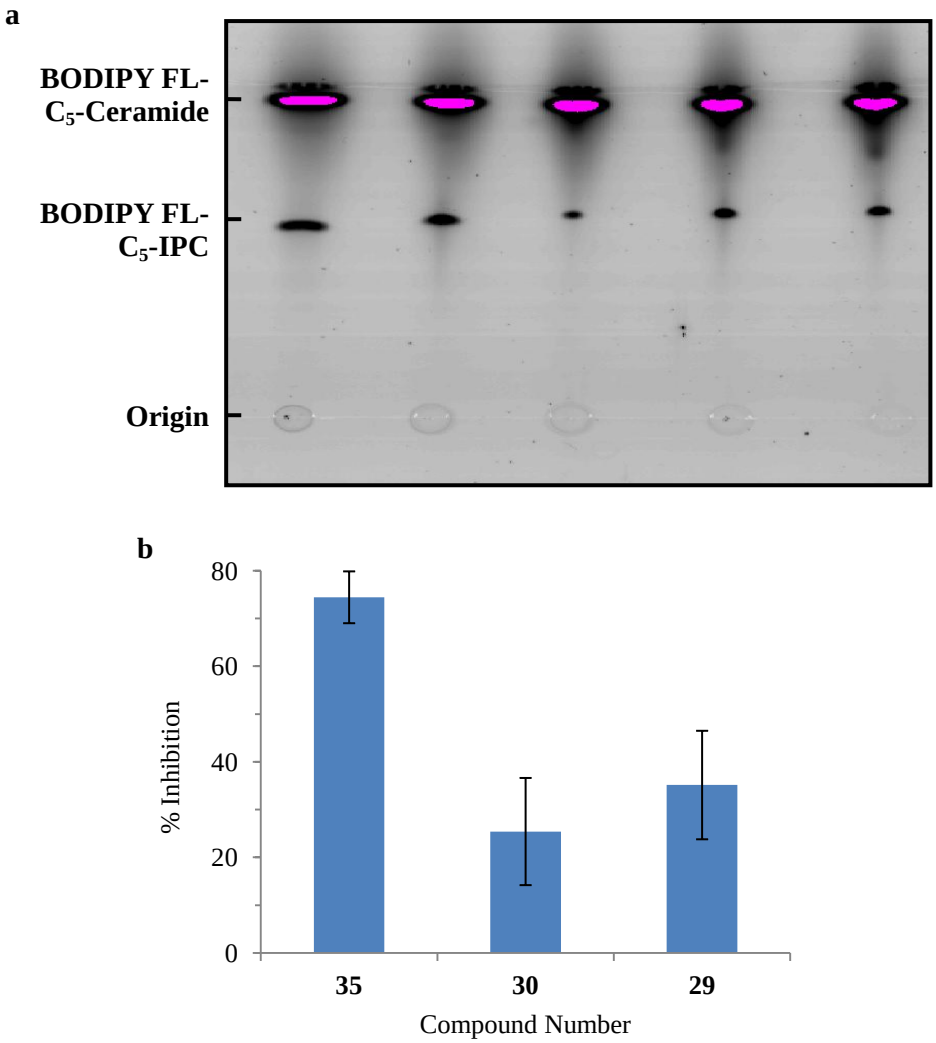

Figure 5–8: (a) HPTLC of the metabolic labelling assay. Lane allocation from left to right: media, DMSO control, compound **35**, compound **30** and compound **29**. (b) The inhibition of *L. major lcb2Δ* promastigote growth in response to the test compounds at 10 µM. Error bars show the standard error of the mean for a triplicate set of data

Whilst compounds **29** and **30** both demonstrated approximately 30% inhibition compared to the media and DMSO controls, compound **35** inhibited BODIPY FL C_5-IPC production by 80%. This assay therefore verifies the results obtained in the *in vitro* biochemical assay and confirms compound **35** as a potent inhibitor of *L. major* IPCS in a cellular environment.

The low potency of compound **35** against intramacrophage *L. donovani* amastigotes coupled with a PFI of 12.8 suggests that the probability of developing this compound as an oral antileishmanial is low. *L. major*, however, causes the cutaneous form of the disease, and it is therefore possible that this compound could be further developed as a topical therapy for localised CL. Alternatively, it has a potential future as a chemical

probe with the possibility of being utilised to further our understanding of *Leishmania* IPCS enzyme function and role.

5.4 SARs of the Benzazepane Series

Having identified a potent and selective IPCS inhibitor but not an antileishmanial lead with *in vivo* activity, attention turned to the exploration of SARs in order to determine whether the IPCS inhibitory and, in particular, the antileishmanial properties of the benzazepanes studied thus far could be improved upon. The compounds exhibit the same three structural features (Figure 5–9); the left hand side (LHS) of the molecule is a heteroaromatic ring attached via a sulphonyl linkage to the benzene ring of a benzazepane core group, whilst the right hand side (RHS) is an aromatic ring attached by a single carbon linker to the nitrogen of the benzazepane core group. With only the two parents and the two mix and match compounds, however, it is impossible to draw any conclusions; the left and right hand side rings may not need to be aromatic, or they may not need to be rings at all. Similarly, is the benzazepane core necessary or is this simply a means of connecting the LHS and RHS functional groups of the molecule?

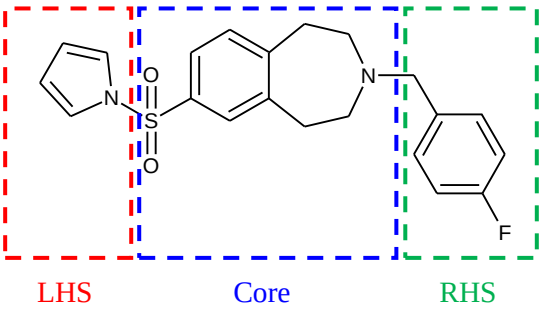

Figure 5–9: The three separate structural features of the benzazepane compounds, indicated on compound **29**

In order to investigate this, the 1.8 million compound library previously screened was searched for molecules with structural similarity to the two known benzazepanes, and 63 compounds were identified for further investigation. A number of additional compounds were synthesised by Aptuit (www.aptuit.com) with the majority containing a pyrrole ring on the LHS to allow comparison with compound **34**, which demonstrated the better antileishmanial properties of the two mix and match compounds. This resulted in a range of compound structures for further study; these compounds were subjected to a range of assays as previously described in chapter 4 (full data are

presented in Appendix C), although due to the overall aims of the project, the biochemical and intramacrophage *L. donovani* amastigote assays were prioritised.

5.4.1 Right Hand Side SARs

Whilst many of the compounds identified from the GSK library possessed an indole ring on the LHS, like compound **30**, a wide variety of substitution patterns were present which would render it difficult to draw accurate conclusions. There were, however, 14 compounds with unsubstituted pyrrole rings as seen in compound **29**, so these were used alongside the Aptuit compounds as a starting point for SAR investigation.

5.4.1.1 Steric Bulk

Whilst a degree of intramacrophage activity was retained when the RHS functional group was removed completely (compound **37**), biochemical activity and activity against *L. major* was completely abolished (Figure 5–10). This suggests that the RHS functional group is necessary for interaction with the IPCS enzyme; alternatively, the resulting N–H bond could result in novel hydrogen bonding with the protein leading to an alteration in binding and a loss of activity. The addition of a small, single methyl group (compound **38**) restored limited biochemical activity (pIC_{50} = 4.6), supporting the theory that H-bonding could be the reason for activity loss, although activity subsequently decreased with the 2,2-dimethylpentane RHS (compound **39**). This functional group is more sterically bulky (A-Value = 4.9) than either the benzene or pyridine rings (A-Values ~ 3.0) present in the parent compounds **29** and **30**, meaning it may not fit into the same physical space as the parents and hence not be as active. Compound **39** does, on the other hand, display potent intramacrophage amastigote activity (pED_{50} = 6.1) whilst being non-toxic against THP-1 cells, suggesting it hits multiple parasitic targets.

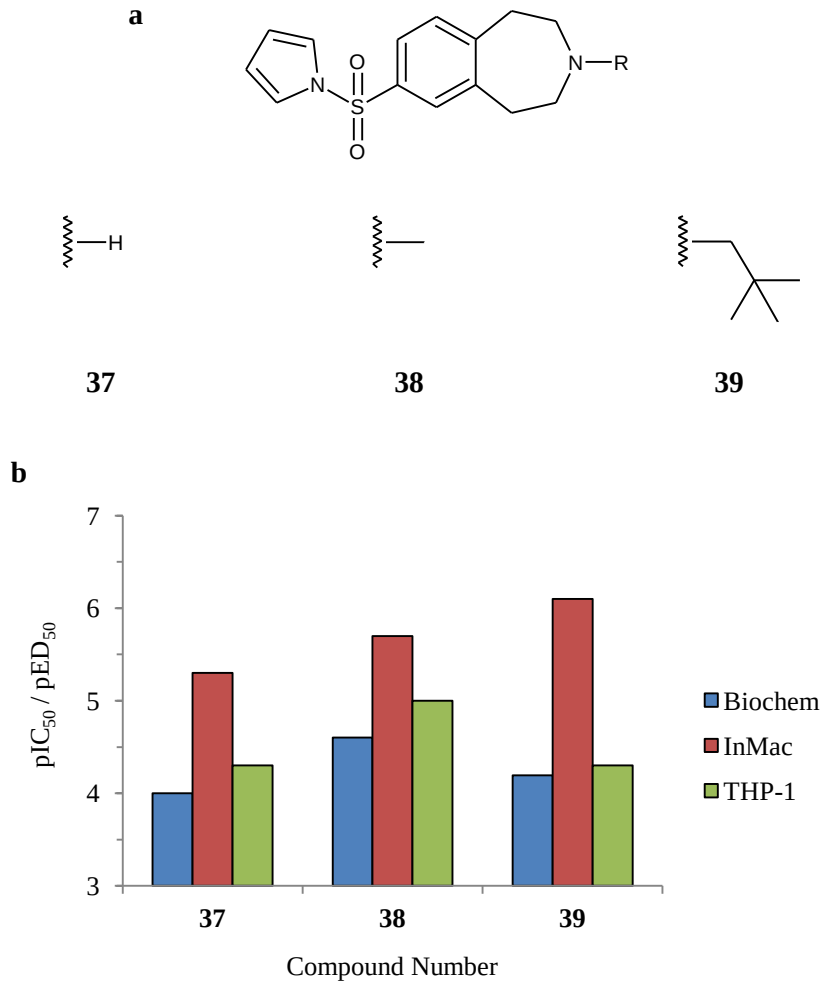

Figure 5–10: (a) The structures of the analogues tested and (b) the effect of steric bulk on benzazepane activity

5.4.1.2 Non-Aromatic Rings

The results for the three non-aromatic rings tested were somewhat surprising; whilst the cyclohexane (compound **40**) and the piperidine (compound **42**) demonstrated significant IPCS inhibition (pIC_{50}s of 5.5 and 4.9 respectively), the tetrahydropyran (compound **41**) was completely ineffective (Figure 5–11). The reason for this striking difference is not clear, and this pattern was not observed with the antiparasitic activities. Whilst compounds **40** and **41** displayed modest activity against intramacrophage amastigotes (pED_{50} = 5.7), compound **42** displayed a pED_{50} of 6.9. These results therefore suggest that H-bonding donor capability in the *para* ring position is critical for antiparasitic activity, at least in non-aromatic rings. Future experiments on non-aromatic rings of different sizes, and with the heteroatom in different positions, would help to elucidate this observation further.

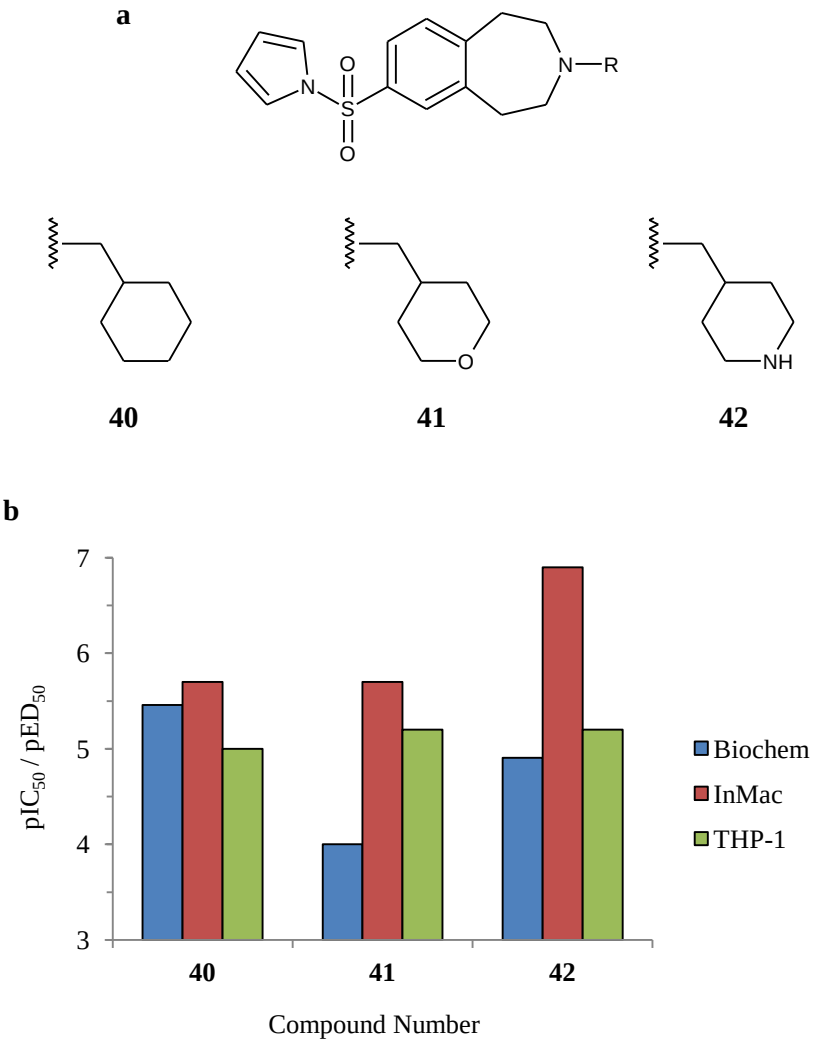

Figure 5–11: (a) The structures of the analogues tested and (b) the effect of non-aromatic rings on benzazepane activity

5.4.1.3 Aromatic Rings

5.4.1.3.1 Benzene Rings

None of the three compounds with an oxy substituent (compounds **43**, **44** and **45**) demonstrated IPCS inhibitory activity or activity against *L. major* promastigotes. In the *L. donovani* intramacrophage assay, however, a methoxy group in the *ortho* position resulted in a pED_{50} of 6.2 whilst activity in the *meta* position was significantly lower (Figure 5–12). Exchanging the methoxy group for a hydroxyl group in the *meta* position subsequently restored activity against intramacrophage amastigotes; this could potentially be due to the H-bond donor capabilities of the hydroxyl group or its capability to act as a nucleophile. Whilst it would be interesting to determine the effect

of an *ortho* hydroxyl group and both hydroxyl and methoxy substituents in the *para* position, the lack of *in vitro* and *L. major* promastigote activity suggests that these compounds are acting off-target in *L. donovani* and they are therefore not a priority for further investigation.

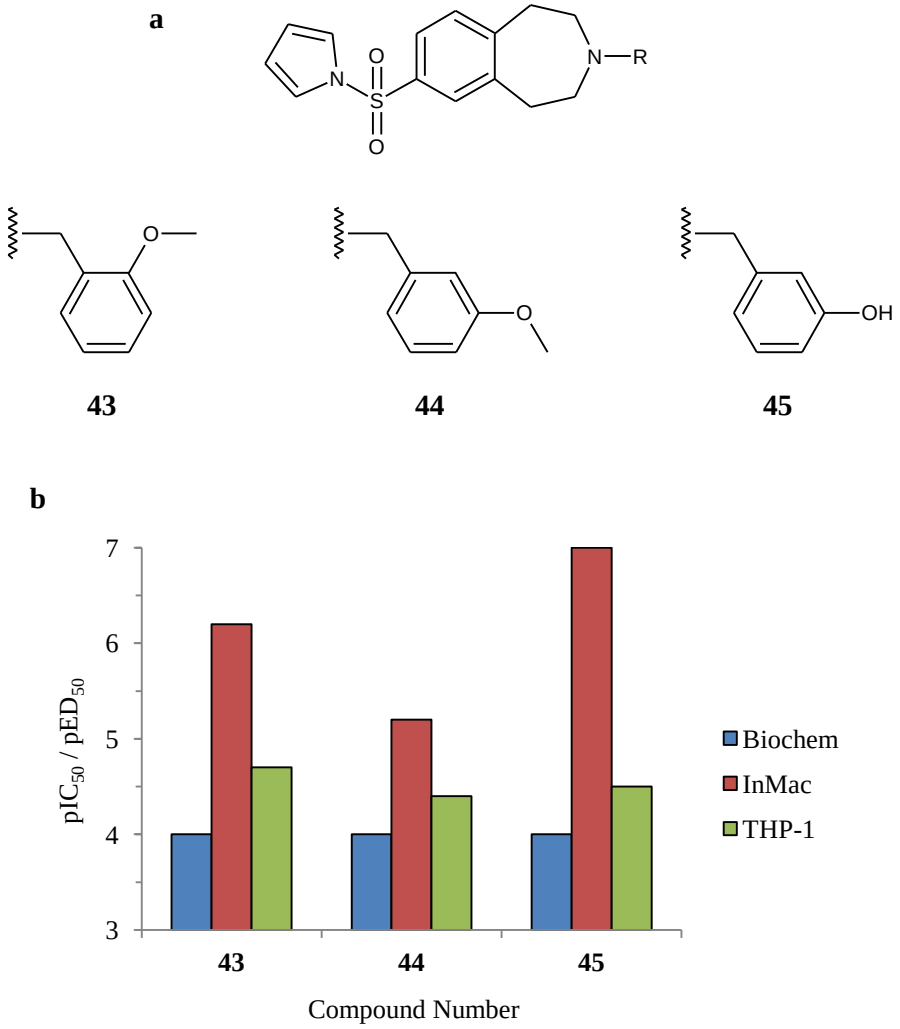

Figure 5–12: (a) The structures of the analogues tested and (b) the effect of oxy-substituted benzene rings on benzazepane activity

The other substituted benzene RHS groups tested are shown in Figure 5–13. A *meta* nitro group (compound **46**), whilst showing limited activity against *Lmj*IPCS *in vitro*, only demonstrated a pED_{50} of 5.2 in the intramacrophage assay; this activity was the same as that obtained for the *meta* methoxy group (Figure 5–12). A nitrile group, however, demonstrated potent antiparasitic activity against both *L. major* and *L. donovani* whether in the *meta* (compound **48**) or *para* (compound **47**) position. Nitriles are prevalent in pharmaceuticals due to their stability and biocompatibility; they also typically lower lipophilicity when used to replace groups such a hydrogen, methyl or halogen and hence result in more favourable pharmacokinetic properties.[371] A

potential future strategy could therefore be based around the incorporation of the nitrile functionality into the parent and mix and match benzazepanes. Finally, following continued speculation about the benzyl position, compound **49** demonstrated that introducing a carbonyl group into this position resulted in the loss of *in vitro* activity compared to the parent compound **29** (pIC_{50} = 6.1). This therefore confirms that the benzyl position holds critical significance for compound function, although the nature of this effect remains unclear.

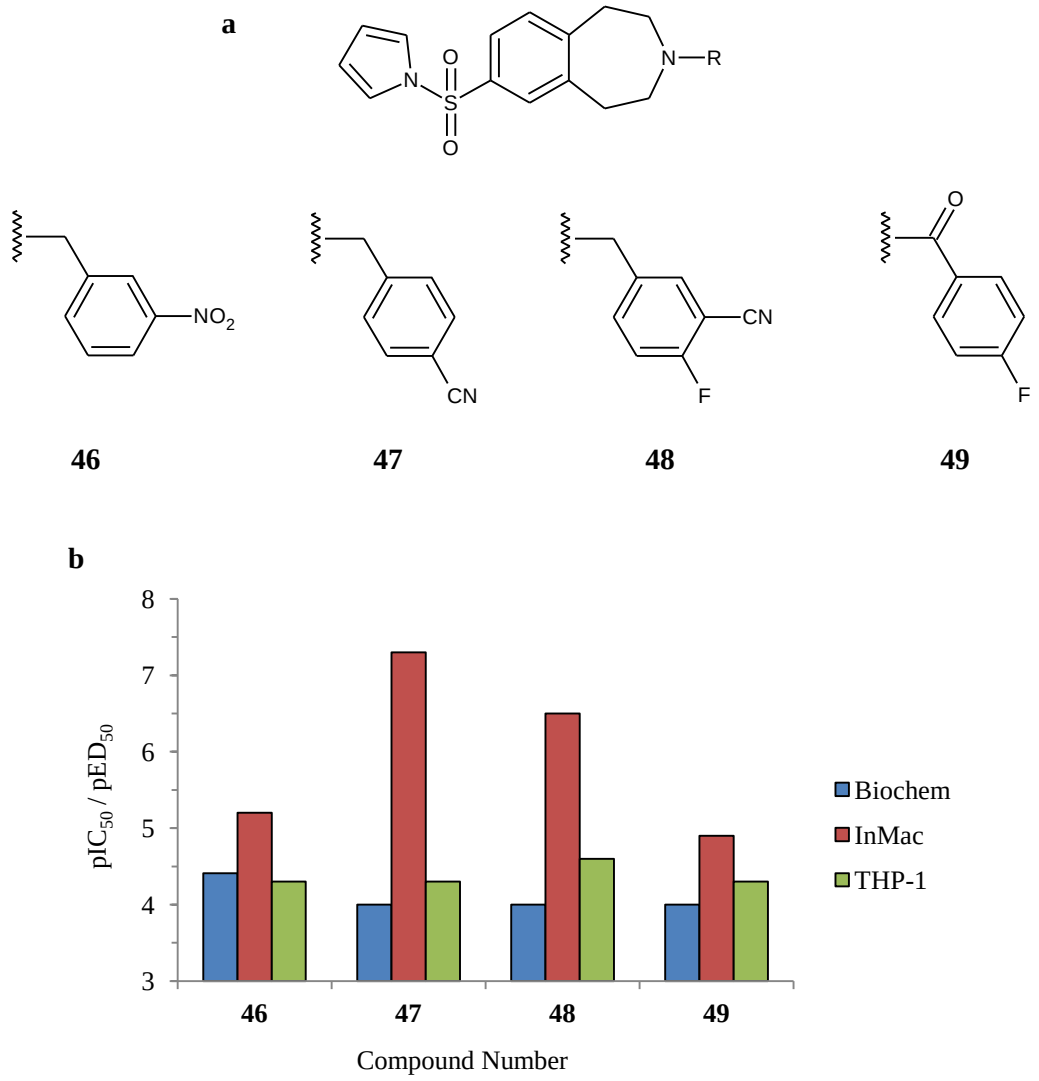

Figure 5–13: (a) The structures of the analogues tested and (b) the effect of substituted benzene rings on benzazepane activity

5.4.1.3.2 Pyridine Rings

The observation made above regarding the benzyl position was further verified by the results from compounds **50** and **51**, which both differ from the mix and match compound **34** by a substituent on the benzyl carbon (Figure 5–14). These results

showed that substitution in this position also resulted in a loss of activity against intramacrophage *L. donovani* amastigotes; whilst compound **34** demonstrated a pED_{50} of 6.3, compounds **50** and **51** displayed pED_{50}s of 5.4 and 5.0 respectively.

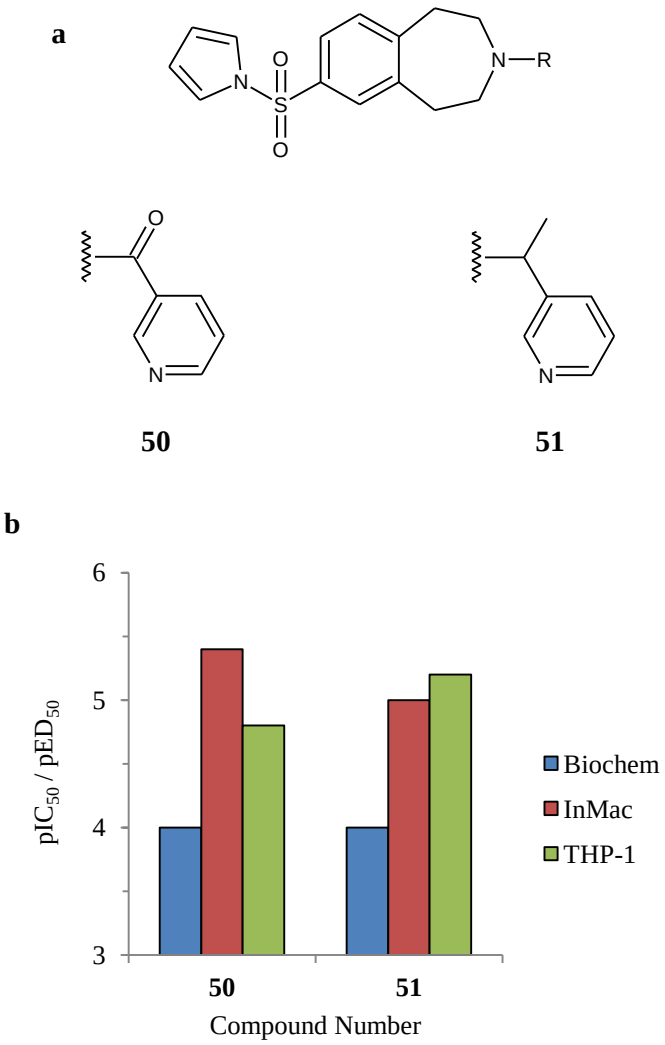

Figure 5–14: (a) The structures of the analogues tested and (b) the effect of benzyl-substituted pyridine rings on benzazepane activity

The additional pyridine compounds investigated are shown in Figure 5–15 (along with the mix and match compound **34** for comparison). Compound **52**, which contains a pyridine ring with a fluorine in the *para* position (relative to the benzazepane core), is a fusion of the RHS groups of the parent compounds. This is reflected in the results; whilst lacking *in vitro* activity, its effectiveness against intramacrophage amastigotes was greater than compound **29** (benzene with fluorine substituent) but lower than compound **34** (unsubstituted pyridine). This therefore suggests that the fluorine in the *para* position has a detrimental effect on compound efficacy; one possible explanation is that the electrostatic interactions between the fluorine substituent and the π-faces of

aromatic amino acids could result in an offset in stacking geometry and hence hinder the ability of the compound to bind to that target.[372] On the other hand, when the fluorine substituent was exchanged for a nitrile group (compound **53**), intramacrophage activity was greatly improved. This further solidifies the theory suggested in section 5.4.1.3.1 that nitrile substituents could be an important route for further compound optimisation studies. Finally, compound **54**, in which the benzazepane core is *ortho* to the pyridine nitrogen rather than *meta*, demonstrated reduced antiparasitic activity compared to the other pyridine analogues. It would not be possible to draw a definitive conclusion from this, however, given that the effect of the methyl substituent that has also been introduced is unknown.

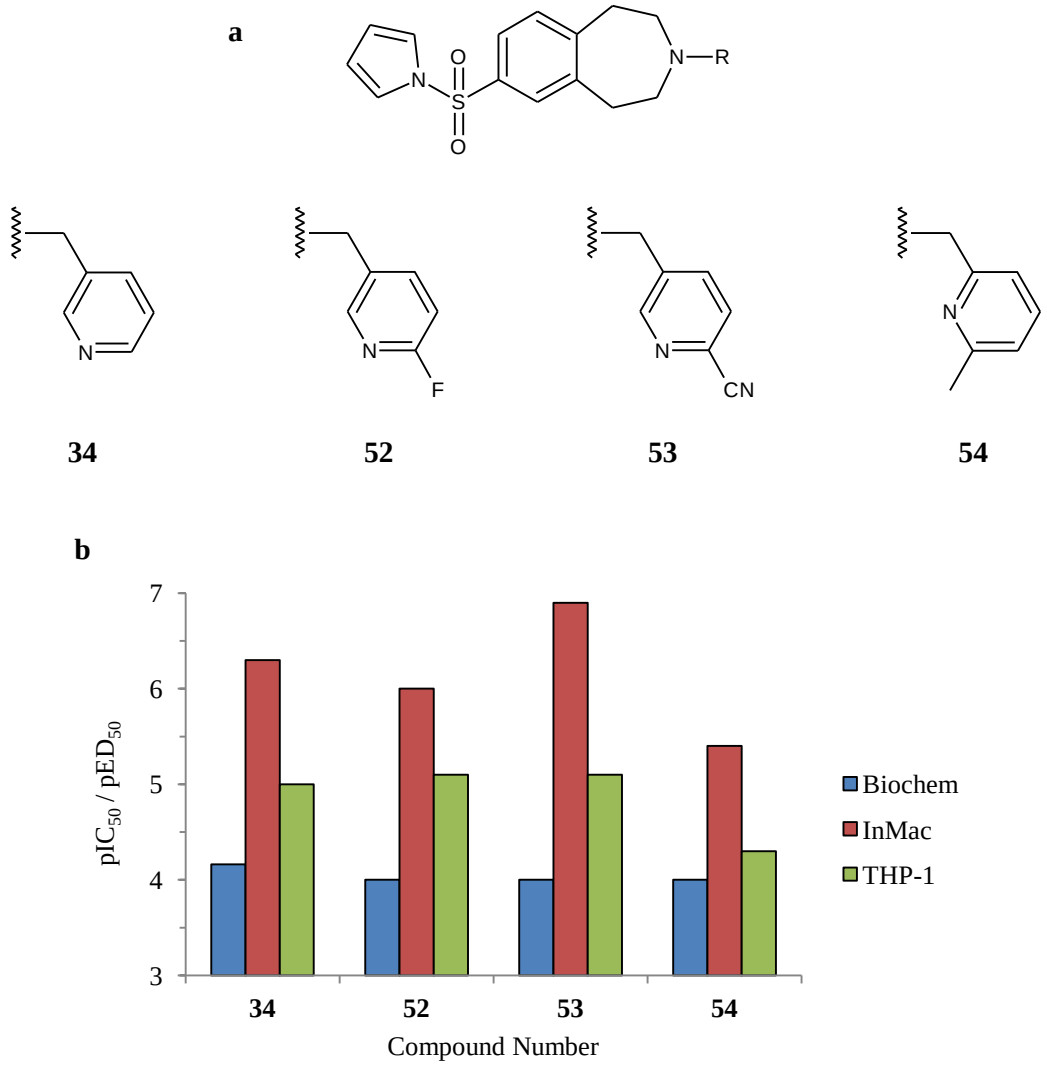

Figure 5–15: (a) The structures of the analogues tested and (b) the effect of substituted pyridine rings on benzazepane activity

5.4.1.3.3 Imidazole Rings

In order to investigate whether a 6-membered ring was necessary, a small group of compounds containing imidazole rings were also investigated. Those with a pyrrole LHS are shown in Figure 5–16; whilst neither demonstrated any activity against *Lmj*IPCS, both compounds **55** and **56** proved to be potent in the intramacrophage assay with pED_{50}s of 6.4 and 6.8 respectively. This effectiveness was offset slightly in compound **56** by an increase in pED_{50} against THP-1 macrophages, but the difference in potency remained significant.

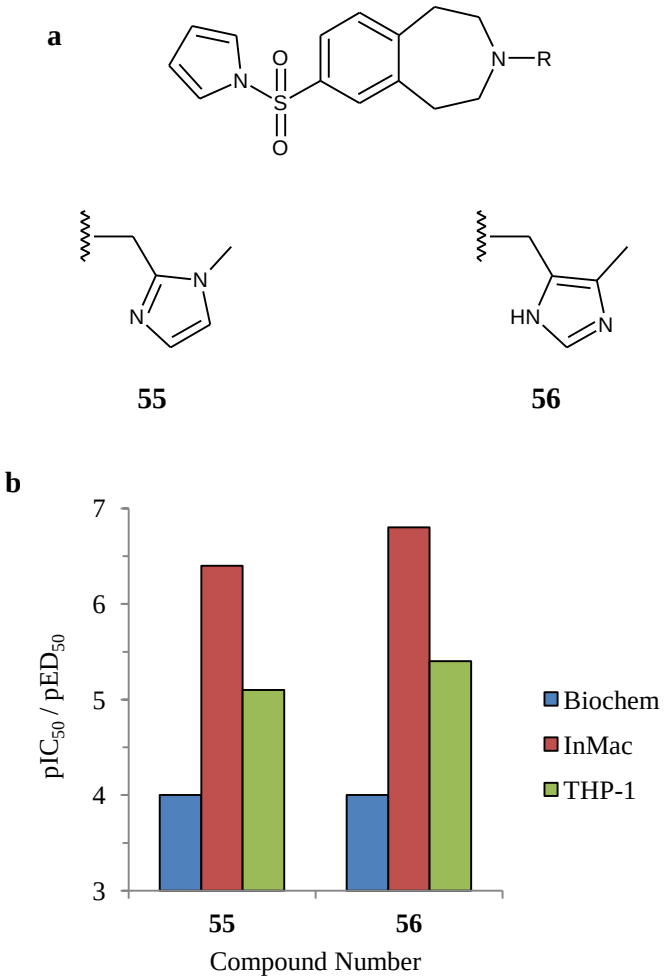

Figure 5–16: (a) The structures of the analogues tested and (b) the effect of imidazole rings on benzazepane activity

Four imidazole compounds with indole-based LHSs were also available for testing. Whilst high potency against intramacrophage amastigotes was maintained in compound **57**, substitution of the indole ring led to reductions in activity in the three other analogues tested (Figure 5–17). As discussed above, this is possibly due to the effects of the substituents on π-stacking interactions. These results do, however, suggest that

the use of imidazole substituents on the RHS would definitely be worth further investigation, although this would have to be accompanied by the determination of suitable LHS groups to pair them with.

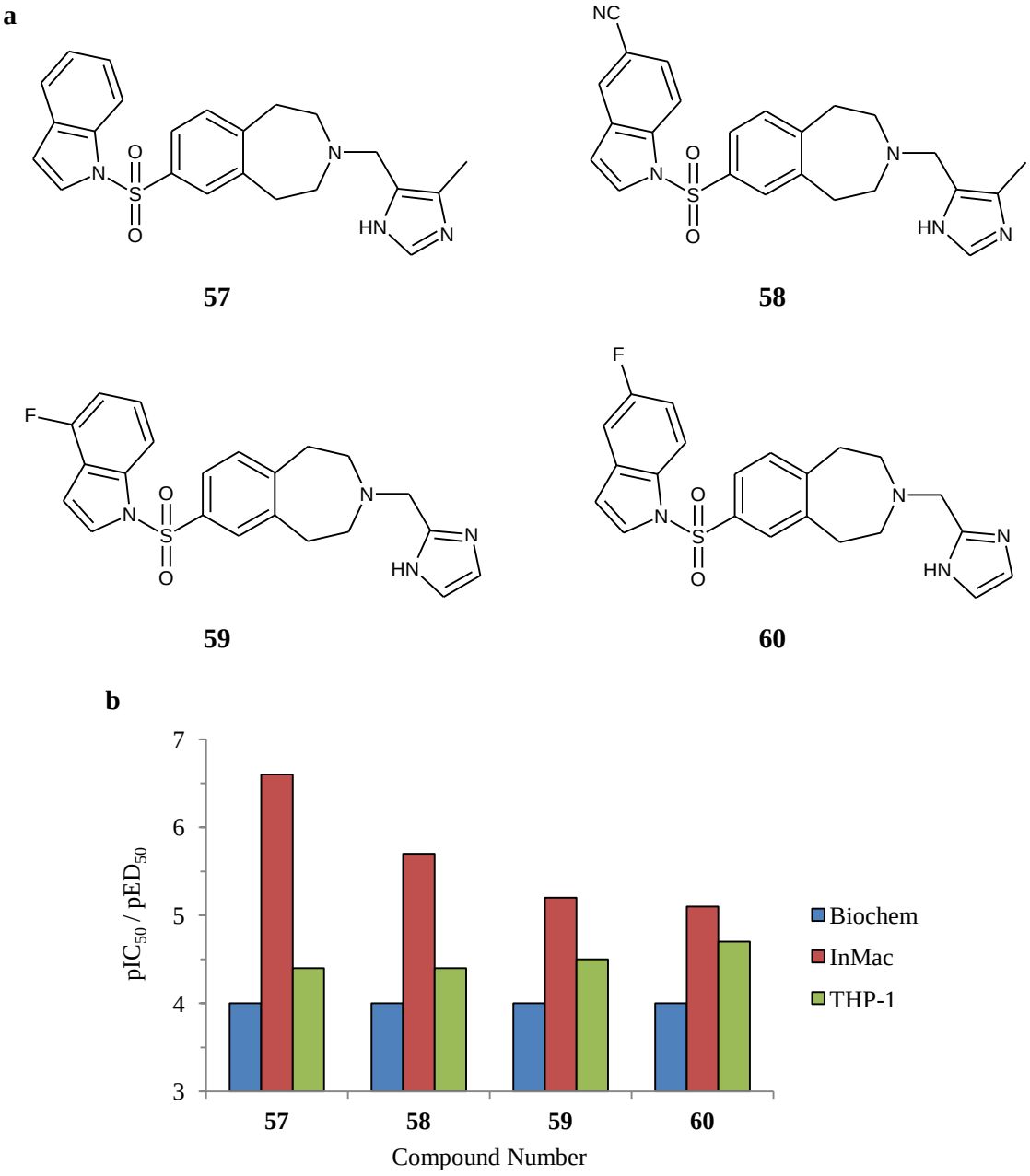

Figure 5–17: (a) The structures of the analogues tested and (b) the effect of imidazole rings and indole substituents on benzazepane activity

5.4.2 Left Hand Side SARs

The investigation of SARs of the LHS of the benzazepane core was limited due to the fact that RHS functionality was incredibly diverse and hence comparisons, in many cases, were not possible. The LHS functional group was, however, shown to be

necessary; compound **61**, which lacks any LHS functionality, was ineffective *in vitro* and non-toxic to both *L. major* promastigotes and intramacrophage *L. donovani* amastigotes (Figure 5–18). Combined with the observations for compound **37**, this suggests that both the LHS and RHS functional groups are integral to compound efficacy. Furthermore, the low potency of compound **61** suggests that the role of the benzazepane core is likely to be structural – keeping the LHS and RHS in fixed positions relative to each other – rather than interaction with the enzyme, although further investigation would be needed to confirm this.

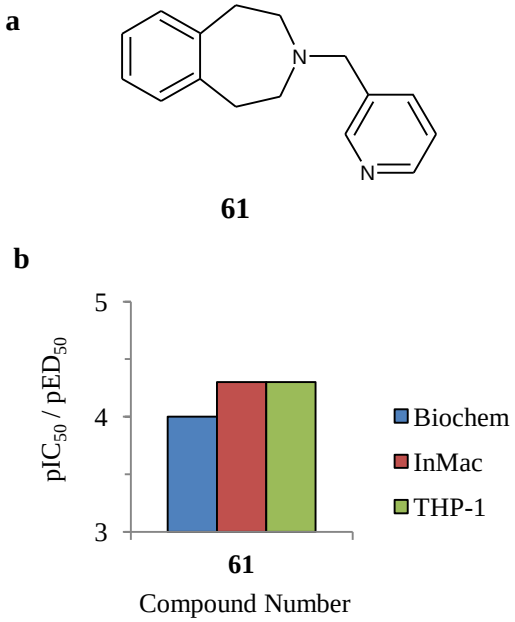

Figure 5–18: (a) The structure of the analogue tested and (b) the effect of no LHS functional group on benzazepane activity

One analysis that was possible was the investigation of the effect of methyl substituents in every position of the indole ring (Figure 5–19). The RHS for this analysis was a single methyl group, permitting comparison with compound **38** (methyl RHS with a pyrrole LHS). The unsubstituted compound **62** was a full order of magnitude less active against intramacrophage *L. donovani* amastigotes than compound **38** (pED_{50}s of 4.7 and 5.7 respectively), which might suggest that the bicyclic ring system was unfavourable due to the increased steric bulk. However, any substituent position resulted in an increase in activity against intramacrophage amastigotes compared to the unsubstituted compound **62**; this was in contrast to the results shown in Figure 5–16 where the unsubstituted compound **57** demonstrated increased activity over the substituted compounds. It is important to note, though, that the RHS functionalities of the molecules in these cases are very different, and the methyl substituent, in

comparison to those studied in Figure 5–17, is non-polar and so would interact differently to the polar groups previously studied. Strikingly, compound **67** was the only one to show any activity against *Lmj*IPCS, and compound **68** was unique in demonstrating activity against *L. major* promastigotes. These results therefore indicate extremely specific mechanisms of action, such as fitting into a tight binding pocket, or being more resistant to metabolism than the compounds with substituents in other positions. These observations would require further investigation to elucidate fully.

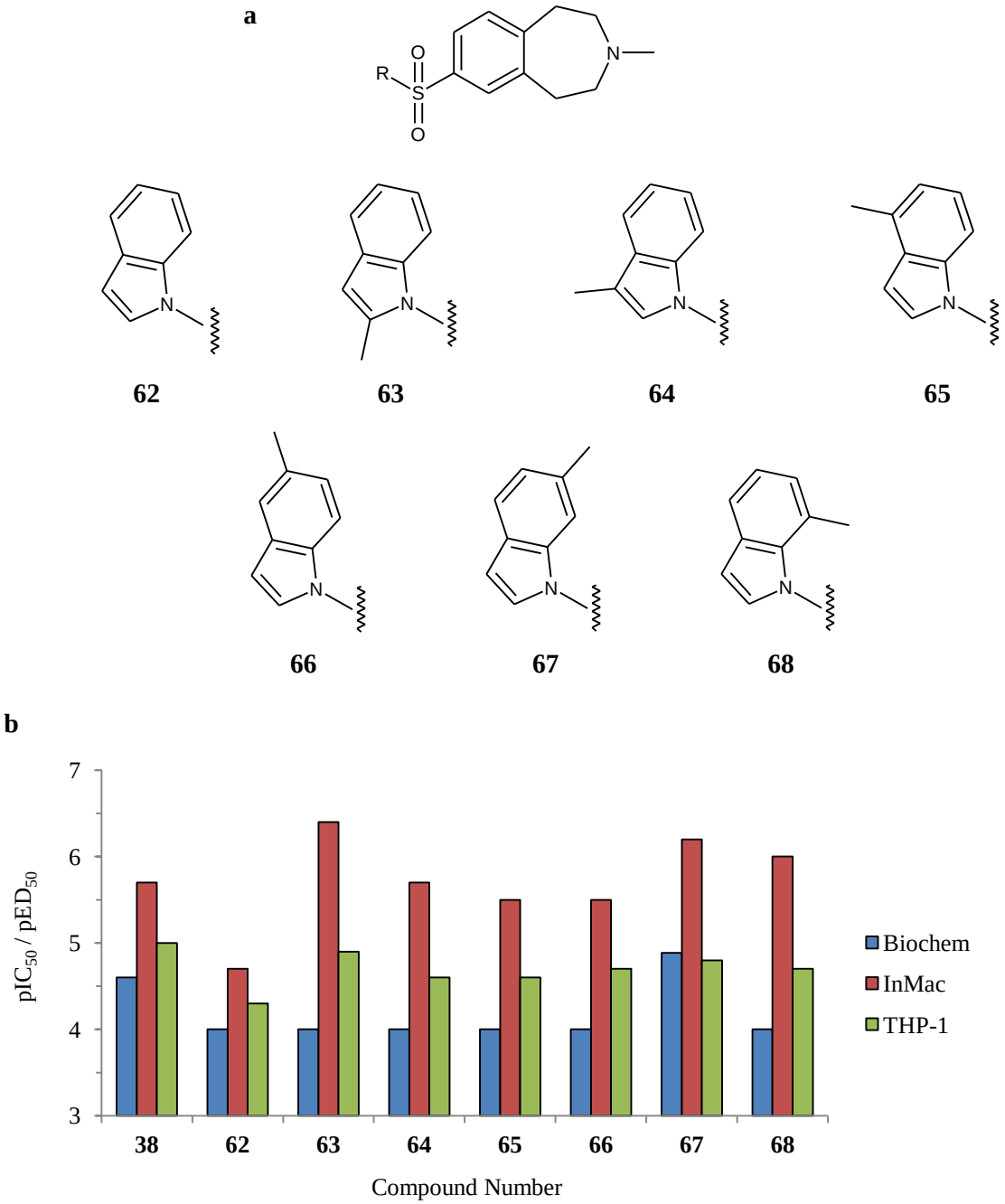

Figure 5–19: (a) The structures of the analogues tested and (b) the effect of the substitution position of indole on benzazepane activity

The results discussed above must, however, be viewed cautiously. As was observed in section 5.4.1.1, the methyl group was far from the best RHS functionality when combined with a pyrrole LHS (compound **38**) and exchanging for an alternative has drastic effects, as shown in Figure 5–20. Compound **69** demonstrated no efficacy against *Lmj*IPCS at 100 μM whereas compound **38** demonstrated a pIC_{50} of 4.6; this single result implies that the substituted indole LHS is detrimental to activity against the enzyme. However, the mix and match compound **35** demonstrated a high *in vitro* potency, which would suggest that this is not the case. It is therefore possible that compound activity is not simply dependent upon the individual LHS and RHS functional groups, but on the combination of the two groups acting in tandem. Testing of molecular fragments, both individually and in combination, could help confirm or deny this hypothesis.

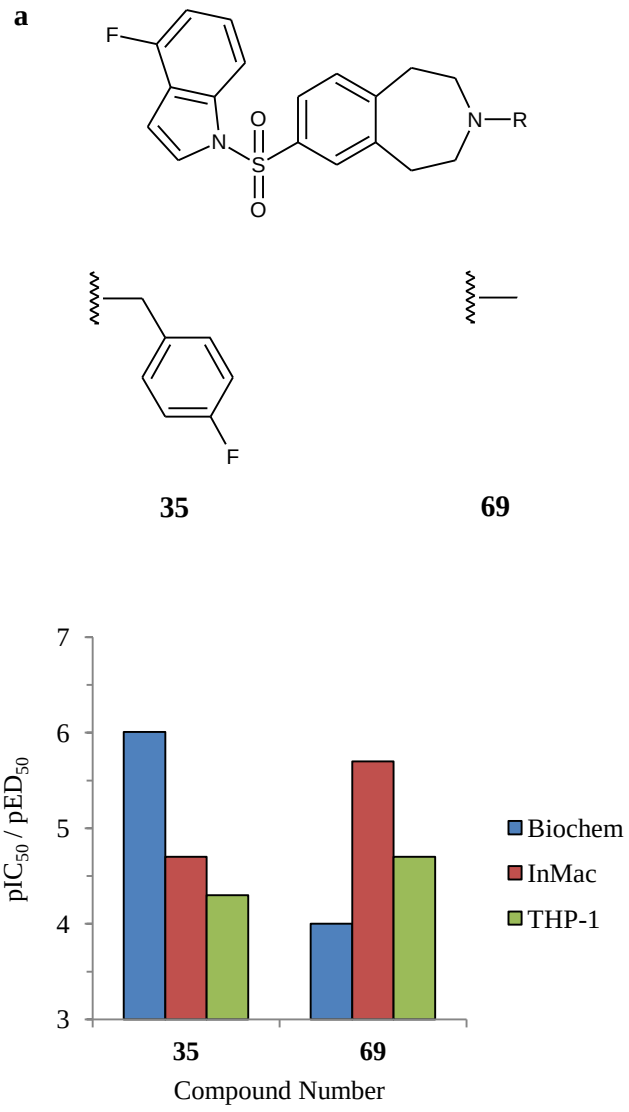

Figure 5–20: (a) The structures of the analogues tested and (b) the effect of RHS functionality on benzazepane activity

5.4.3 Benzazepane Core SARs

The final feature to consider was the benzazepane core. Two possible alterations were considered: removing the azepane ring, and removing the benzene ring, to determine if either was necessary for function. The results (Figure 5–21) were conclusive; in comparison to the mix and match compound **34**, compound **70** lost all efficacy against both *L. major* promastigotes and *L. donovani* intramacrophage amastigotes at the concentrations tested. On the other hand, the azepane compound **71** maintained intramacrophage activity whilst displaying a slightly improved selectivity over THP-1 macrophages. Therefore, the azepane ring appears to be necessary for antiparasitic activity but the benzene ring is not. Compound **71** also has the additional benefit of having one less aromatic ring resulting in a much more favourable PFI than compound **34** (6.0 compared to 8.4). It can therefore be predicted that compounds based on azepane cores would exhibit more favourable pharmacokinetic properties than their benzazepane counterparts, and this could potentially lead to compounds with more success *in vivo* than has so far been achieved.

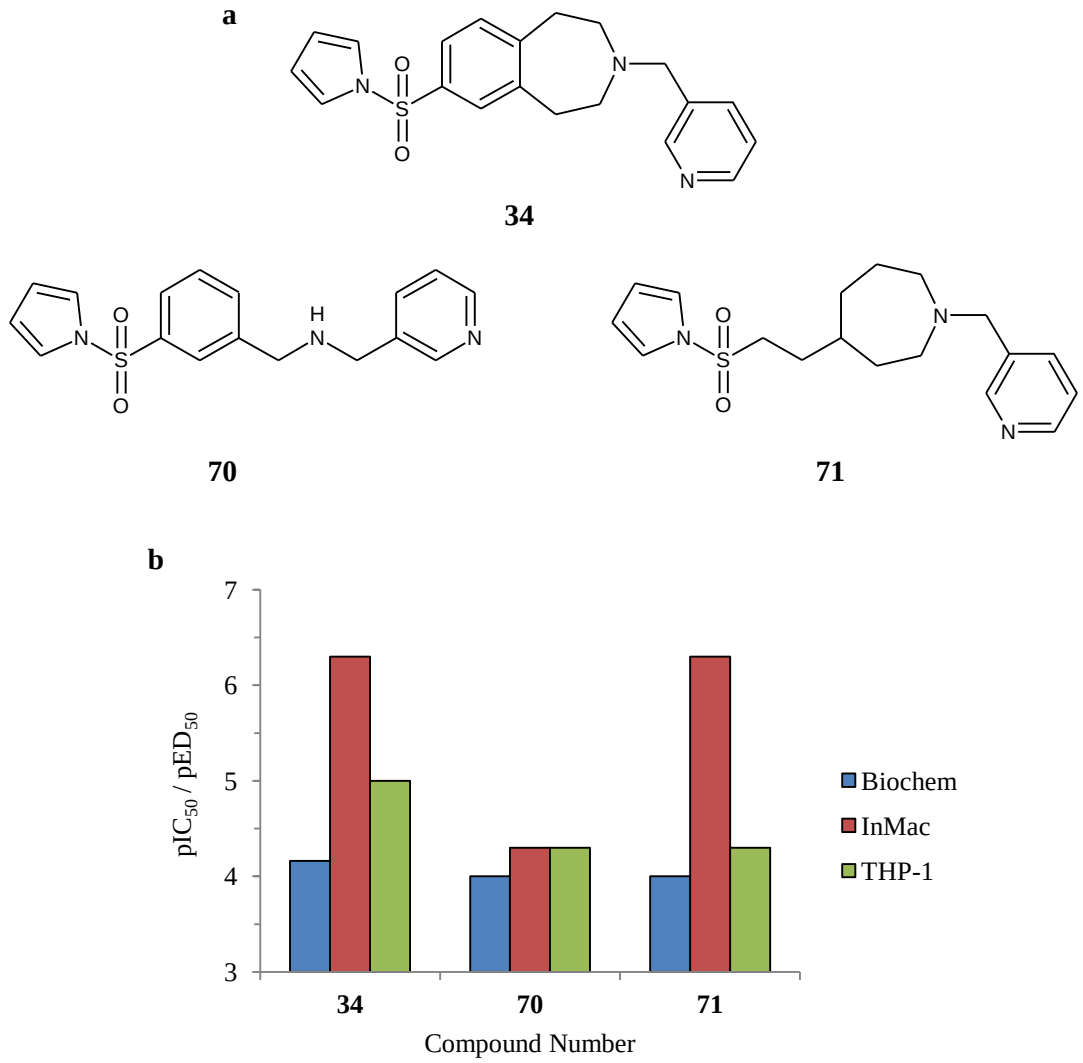

Figure 5–21: (a) The structures of the analogues tested and (b) the effect of altering the benzazepane core on compound activity

5.4.4 SAR Summary

Overall, it is difficult to draw definitive conclusions due to the fact that, as demonstrated above, both *in vitro* and *in cellulo* activity is dependent upon the LHS and RHS combination rather than being dependent upon the presence of a specific functional group. The mix and match compounds originally tested at the beginning of this chapter remain two of the best; compound **35**, along with the parent compounds **29** and **30**, remains the best *Lmj*IPCS inhibitor with high potency being demonstrated both *in vitro* and *in cellulo*, with no compound studied in the SAR analysis being able to improve upon this. Compound **34**, on the other hand, has had its antileishmanial activity matched and even bettered, with two obvious trends being the high activities observed with nitrile substituents and imidazole rings on the RHS. Further investigation

with these two functionalities, and possibly combining them with the azepane core, could therefore potentially lead to antileishmanial compounds with greater potency than has been observed to date.

5.5 Conclusion

The work described in this chapter initially involved the screening of the two mix and match benzazepane compounds. Compound **35** proved to be a potent and selective inhibitor of the *L. major* IPCS enzyme. Compound **34** demonstrated increased antileishmanial activity but lower biochemical activity compared to the parents and ultimately proved to be ineffective *in vivo*. The determination of SARs for the benzazepanes show overall disconnection between the cell-based and biochemical activity, suggesting that compounds in this chemical family are promiscuous and are capable of hitting multiple cellular targets. Despite this, selectivity for the intramacrophage *L. donovani* amastigotes over the THP-1 cells was frequently observed, meaning that this compound class still shows the potential to produce a lead compound in the future. Several possible solutions for improving antileishmanial activity, most notably shifting to an azepane core, have been proposed.

Chapter 6

Conclusions and Future Work

6.1 Conclusion

The changing landscape of drug discovery for NTDs brought about by the London Declaration in 2012[162] means that the ideal of effective, affordable treatments for a wide range of diseases is closer now than ever before. The work presented in this thesis has contributed towards the overall goal of finding new therapeutic agents for the widespread, potentially fatal NTD leishmaniasis and the related disease HAT.

In order to characterise the SLS enzymes from *L. major* and *T. brucei*, existing methodology was adapted to engineer novel mutant *S. cerevisiae* strains dependent on the expression of a kinetoplastid SLS for viability. The fact that all the complemented strains prepared were viable showed that all the kinetoplastid SLSs investigated thus far are functional orthologues of the yeast AUR1. This supports previous work in the group[217] and contradicts claims that *Tb*SLS4 does not synthesise IPC.[322] Furthermore, differential sensitivity to AbA was observed between isoforms 1 and 4 of *Tb*SLS. Whilst this observation is unprecedented in the literature (to the best of the author's knowledge), it is known that a single F158Y mutation in AUR1 confers resistance of *S. cerevisiae* to AbA.[201] It can therefore be hypothesised that AbA has an extremely specific mechanism of action, resulting in differential sensitivity between the two highly similar *Tb*SLS enzymes. Additional investigation will be required to identify the source of this variation and determine the binding site of AbA.

The complemented yeast strains were subsequently utilised to develop and optimise a HTS-compatible assay to screen the 1.8 million compound library. Whilst the initially-proposed multiplex assay was not robust enough to pursue, an alternative assay

based on conversion of FDGlu to fluorescein proved successful. The primary assay progressed smoothly with a mean Z′ of 0.7 and, following confirmation and dose-response testing, a total of 500 compounds demonstrated a selectivity ratio greater than 1.5 log units.

Whilst yeast-based assays are not common place, they are increasing in popularity with many screens being undertaken in recent years. However, the majority of these are on the order of magnitude of tens of thousands of compounds[373, 374] to a few hundred thousand compounds.[375] To the best of the author's knowledge this is the largest screen utilising a yeast-based assay recorded in the literature, and is quite possible the largest scale screen undertaken to date by an academic research group. Additionally, the genetic tractability of yeast has allowed an otherwise difficult target – a parasitic membrane protein – to be readily and extensively tested in a fashion that would have been difficult in the more commonly-utilised bacterial vector. This assay therefore verifies the use of eukaryotic organisms, and yeast in particular, as suitable vectors for HTS.

Following the successful HTS assay, the screening programme was continued against *Leishmania* promastigote and amastigote parasites. Testing against mammalian cells was also achieved and allowed the identification of six compounds with high antileishmanial activity, low mammalian toxicity and favourable physicochemical properties. Further biochemical testing narrowed this down to two compounds with a common benzazepane core that acted as potent inhibitors of the *L. major* IPCS enzyme *in vitro*.

Additional investigation of benzazepane analogues identified one compound which was a highly potent enzyme inhibitor in both *in vitro* and *in cellulo* assay formats. This compound could therefore be utilised in the future as a chemical probe to further investigate *Lmj*IPCS; there is also the possibility of further development as a topically-applied treatment for localised CL. The majority of the additional analogues demonstrated low inhibitory activity against the *L. major* IPCS enzyme; however, many of these retained antileishmanial activity. This disconnection between biochemical and antiparasitic activity suggests that the compounds are promiscuous and hit more than a single target. Despite this fact, 21 of the 40 benzazepane compounds tested (53%)

demonstrated greater potency against intramacrophage *L. donovani* parasites than macrophages (as defined by a SI greater than or equal to 1.0), suggesting that further lead optimisation could eventually result in a suitable candidate for clinical trials.

In summary, the work accomplished has fulfilled the original aims of the project and identified, from a library of 1.8 million compounds, a novel family of structurally-related compounds which display high potency both *in vitro* and *in cellulo*. This compound class forms the starting point for a future medicinal chemistry campaign, with the ultimate aim being the development of new treatments for leishmaniasis.

6.2 Proposed Future Work

Building on the work achieved thus far, future work can be divided into two separate categories.

6.2.1 Further Lead Optimisation

Perhaps the primary focus for future work would be the continuation of the SAR study described previously (Chapter 5). Whilst a highly potent enzyme inhibitor was identified from this study, an active *in vivo* antileishmanial was not. Given that this is the final stage before clinical trials, high *in vivo* potency is a necessity for compound progression. Therefore, new benzazepane analogues with high potency against intramacrophage *L. donovani* amastigotes, low cytotoxicity against THP-1 cells and improved metabolic stability need to be identified. From the SAR study, imidazole rings and aromatic rings with nitrile groups were both identified as resulting in high antileishmanial activity against intramacrophage *L. donovani* amastigotes, suggesting that a more focussed SAR study centred on these substituents could improve potency beyond what has been observed to date. In addition, pairing these with the more physicochemically favourable azepane core could go some way towards improving oral absorption and biodistribution, and hence *in vivo* antileishmanial efficacy.

Also important is the determination of the mechanism of action by which the benzazepane compounds inhibit IPCS. The ideal scenario would be to obtain a crystal structure of the IPCS protein which would then allow computational docking studies to

be undertaken. This would provide information as to where the compounds bind to the enzyme and may allow further compound modification to be directed towards functional groups which would improve these interactions. Unfortunately, membrane proteins remain one of the greatest challenges facing crystallographers; the number of entries in the Protein Data Bank (PDB, www.rcsb.org/pdb), an online repository for information about protein structures, topped 100,000 in 2014. Of these, only 499 (0.5%) were membrane proteins.[376]

One possibility, should crystallisation and structure determination prove unsuccessful, would be to attempt computational studies using LPP structures. As discussed in section 1.3.4, this family of enzymes possess two domains similar to the fungal and *Leishmania* IPCS, with the residues of the catalytic triad located in these domains. Whilst LPPs are also integral membrane proteins,[377] the soluble enzyme epoxide hydrolase has been observed to possess LPP activity[378] and structures for this enzyme have recently been published.[379] It is therefore possible that computational docking experiments using these crystal structures could confirm or deny the binding of benzazepane compounds in the active site.

6.2.2 Extension to Human African Trypanosomiasis and Chagas Disease

Much of the work discussed in this thesis has focussed on drug discovery for leishmaniasis, with only a limited analysis of the *T. brucei* SLS isoforms 1 and 4 conducted as described in Chapter 2. These basic experiments, however, generated interesting results with differential sensitivity to the fungal AUR1 inhibitor AbA being observed. As discussed previously, the reason for this difference is not currently known; site-directed mutagenesis of the amino acid sequences of the two isoforms could therefore help to identify key residues involved in enzyme function and AbA sensitivity. Furthermore, only two of the four *T. brucei* SLS isoforms have thus far been investigated. The expansion of the analysis to include isoforms 2 and 3 could therefore aid the investigation into which amino acids are essential for function.

The project could also be extended further to include Chagas disease, the third disease caused by a trypanosomatid parasite. Like *Leishmania* spp. and *T. brucei*, *T. cruzi* also synthesises IPC; the *T. cruzi* IPCS enzyme was first observed by

Figueiredo *et al*. in 2005,[380] and the following year Denny *et al*. noted that two isoforms of the enzyme were present.[196] The inclusion of these enzymes in the analysis, along with those from additional *Leishmania* species such as *L. donovani*, would result in a greater breadth of data that should facilitate the observation of trends between the enzymes from different species and allow more accurate, detailed conclusions to be drawn.

Finally, testing of any highly potent compounds from the further lead optimisation process against the variety of enzymes described above would allow the identification of any chemical entities with activity against a range of species. If this is successful and a potential drug candidate is obtained, the future of the project lies with the pharmaceutical companies, or an organisation such as the DNDi, to ensure that the lead compound receives the best possible chance of succeeding in clinical trials and eventually progressing to market as a novel antikinetoplastid therapeutic agent.

Chapter 7

Biological Materials and Methods

7.1 Materials

In-Fusion® HD Cloning Kit with Cloning Enhancer and Herring Testes Carrier DNA were obtained from Clontech. Phusion Flash PCR Master Mix, SmaI restriction enzyme, 10× Buffer Tango, T4 DNA Ligase, 100 bp DNA ladder, 1 kb DNA ladder, 6× DNA Loading Dye, ethidium bromide, HCS CellMask™ Deep Red stain, RPMI media 1640, pyruvate, glutamine and HEPES were obtained from Thermo Scientific™. QIAquick PCR Purification kit and QIAprep Spin Miniprep kit were from Qiagen. Protein LoBind tubes were obtained from Eppendorf. Miller's LB broth powder was obtained from Melford. Raffinose pentahydrate, galactose, yeast nitrogen base, 5-Fluoroorotic acid monohydrate, amino acids and amino acid dropout packages were obtained from ForMedium™. Acid-washed glass beads (425−600 µm), glycerol, sucrose, glucose, agarose, agar, glacial acetic acid, phenol red, adenosine, folic acid, resazurin, Hemin, MES hydrate, PEG3350, IGEPAL® CA-630, $MgCl_2$, LiAc, KCl, $CaCl_2$, HCl, NaOH, DMSO, BSA, PBS, EDTA, CHAPS, PMA, Trizma® base, KH_2PO_4, K_2HPO_4, $(NH_4)_2SO_4$, $NaHCO_3$, HCO_2H, HCO_2K, Giemsa stain, ampicillin, amphotericin B, cycloheximide, suloctidil, trypsin, 100× RPMI vitamin solution, 50× RPMI amino acid solution, Eagle's Minimum Essential Medium and Schneider's Insect Medium were obtained from Sigma Aldrich. $MgSO_4$ was obtained from Panreac. Aureobasidin A was a generous gift from AureoGen. AlamarBlue®, Na_2CO_3, Penicillin/Streptomycin, NBD-C_6-ceramide and BODIPY® FL C_5-ceramide complexed to BSA were obtained from Invitrogen. CellTiter-Glo® reagent was from Promega. Complete® EDTA-free Protease Inhibitor Cocktail Tablets were from Roche Applied Science. HBSS buffer was obtained from Gibco. FDGlu was obtained from Marker Gene Technologies Inc. or Invitrogen. Clemastine was obtained from Tocris

Bioscience. Bradford Reagent and AG 4-X4 ion exchange resin was obtained from Bio-Rad. Heat-inactivated FCS was obtained from Labtech. *L*-α-phosphatidyl inositol (sodium salt, bovine liver) was obtained from Avanti Polar Lipids. Reactions and media were prepared using distilled, high purity water. All other solvents used were of the highest purity available commercially.

7.2 Instruments and Equipment

Centrifugation steps were carried out using Beckman Coulter centrifuges or ultracentrifuges. Eppendorf tubes were centrifuged using a Sigma 1-14 microfuge. Eppendorf contents were dried using an Eppendorf Vacuum Concentrator 5301 from Brinkmann. Disruption of cells was performed using an IKA® Vortex Genius 3. Agarose gels were imaged using a Bio-Rad Gel Doc™ XR+ System and Quantity One 1-D Analysis software (version 4.6.6). HPTLC silica plates were from Merck Millipore and were imaged using a Fuji FLA−3000 plate reader and AIDA Image Analyser® software (version 3.52). Media were filtered using a Corning® 1000 ml Vacuum Filter/Storage Bottle System, 0.22 µm pore CA membrane. Multiwell plates were read using a PerkinElmer Opera® High Content Screening System, an Ultramark Microplate Imaging System, a PerkinElmer ViewLux ultraHTS Microplate Imager or a BioTek FLx800 Fluorescence Microplate Reader. Multiwell plate readouts were analysed using GSK-developed Statistical Online Data Analysis Software (SODA) or Gen5™ 1.08 Data Analysis Software from BioTek. Macrophage screening assays were imaged using an Opera QEHS high-content microscope and the readouts analysed using the automated Acapella® High Content Imaging and Analysis Software (PerkinElmer). 96-well plates used were Corning® Costar® cell culture plates 3596 (clear), Corning® Costar® cell culture plates 3595 (clear), Corning® V-bottom 3897 (clear), MultiScreen® Solvinert filter plates from Merck Millipore or PerkinElmer OptiPlate-96 Black. 384-well plates used were Greiner Bio-One FLUOTRAC™ 200 784076 (low volume, black base). 1,536-well plates used were either Greiner Bio-One FLUOTRAC™ 200 782076 (non-sterile) or Greiner Bio-One FLUOTRAC™ 600 782077 (sterile). Low volumes were dispensed using a Thermo Scientific™ Multidrop Combi Reagent Dispenser, a Thermo Scientific™ Multidrop Combi nL or a Labcyte Echo® liquid handler.

7.3 Buffers, Solutions and Media Compositions

Details of the buffers and solutions used are given in Table 7–1. Media compositions are given in Table 7–2. Solutions that are not sterilised prior to use, either by autoclaving or filtration, are indicated by an asterisk (*). Components that must be sterilised by filtration and added after autoclaving are indicated by a hash (#).

Table 7−1: Buffer and solution compositions

Buffer/Solution	Vol. / Mass	Stock
TAE Buffer	48.4 g	Trizma® Base
(1 L, 10×)	11.4 ml	Glacial Acetic Acid
	20 ml	EDTA (0.5 M, pH 8.0)
	968.6 ml	Water
TE Buffer	100 ml	Tris−HCl (1 M, pH 7.4)
(1 L, 10×)	20 ml	EDTA (0.5 M, pH 8.0)
	880 ml	Water
TE/LiAc Buffer	5 ml	LiAc (1 M)
(50 ml, 10×)	5 ml	TE Buffer (10×)
	40 ml	Water
PEG/LiAc	5 ml	LiAc (1 M)
(50 ml, 10×)	5 ml	TE Buffer (10×)
	40 ml	PEG 3350 (50%)
STE Buffer	12.5 ml	Sucrose (1 M)
(50 ml)*	1.25 ml	Tris−HCl (1 M, pH 7.4)
	0.1 ml	EDTA (0.5 M, pH 8.0)
	1 tablet	Complete® Protease Inhibitor Cocktail
	36.15 ml	Water
Storage Buffer	2.5 ml	Tris−HCl (1 M, pH 7.4)
(50 ml)*	6.25 ml	Glycerol (80% w/v)
	0.25 ml	$MgCl_2$ (1 M)
	1 tablet	Complete® Protease Inhibitor Cocktail
	41 ml	Water
Tris/EDTA/BSA Buffer	12.5 ml	Tris−HCl (1 M, pH 7.4)
(50 ml)*	2.5 ml	EDTA (0.5 M)
	750 mg	BSA (Fatty Acid Free)
	35 ml	Water
		HCl (to pH 6.0)

Phosphate Buffer	13.1 g	KH_2PO_4
(1 L, 0.25 M, pH 7.0)*	26.8 g	K_2HPO_4
	1 L	Water
Phosphate Buffer	3.77 g	KH_2PO_4
(1 L, 71.4 mM, pH 7.0)*	7.71 g	K_2HPO_4
	1 L	Water
Resazurin Solution	25 mg	Resazurin
	0.1 g	IGEPAL® CA-630
	1 tablet	PBS
	200 ml	Water

Table 7−2: Media compositions

Growth Media	Vol. / Mass	Stock
LB Broth	25 g	LB broth
(1 L)	20 g	±Agar (for solid media)
	1.5 ml	±Ampicillin (100 mg ml^{-1}) (#)
	1 L	Water
SD –W –URA	20 g	Glucose
(1 L)	1.93 g	Yeast Nitrogen Base −Amino Acids −Ammonium Sulphate
	5 g	$(NH_4)_2SO_4$
	15 g	±Agar (for solid media)
	634 mg	Amino Acids Dropout Supplement −W −L −URA (#)
	60 mg	Leucine (#)
	1 L	Water
SGR −W −L	1 g	Galactose
(1 L)	10 g	Raffinose Pentahydrate
	1.93 g	Yeast Nitrogen Base −Amino Acids −Ammonium Sulphate LoFlo
	5 g	$(NH_4)_2SO_4$
	15 g	±Agar (for solid media)
	1 g	±5-Fluoroorotic Acid Monohydrate (#)
	640 mg	Amino Acids Dropout Supplement −W −L (#)
	1 L	Water

Schneider's Insect Medium (stock) (1 L, pH 7.0) #	24.5 g	Schneider's Insect Medium
	0.4 g	$NaHCO_3$
	0.6 g	$CaCl_2$
		HCl (for pH adjustment)
		NaOH (for pH adjustment)
	1 L	Water
Schneider's Insect Medium (50 ml, pH 7.0, 15% FCS) #	42.5 ml	Schneider's Insect Medium (stock)
	7.5 ml	Heat-inactivated FCS
Amastigote Growth Medium (1 L) #	1.1 g	KCl
	19.5 g	KH_2PO_4
	60 mg	$MgSO_4$
	2.5 g	Na_2CO_3
	4.5 g	Glucose
	146 mg	Glutamine
	5 mg	Hemin
	4.4 mg	Folic acid
	27 mg	Adenosine
	4.9 g	MES hydrate
	4 mg	Phenol Red
	10 ml	100× RPMI Vitamin Solution
	20 ml	50× RPMI Amino Acid Solution
	500 U ml^{-1}	Penicillin/Streptomycin
	200 ml	Heat-inactivated FCS
	770 ml	Water
THP-1 Growth Medium (1 L, pre-differentiation) #	110 mg	Pyruvate
	365 mg	Glutamine
	6 g	HEPES
	18.5 µg	±PMA
	100 ml	Heat-inactivated FCS
	900 ml	RPMI Media 1640
THP-1 Growth Medium (1 L, post-differentiation) #	2.6 g	Na_2CO_3
	18.5 µg	PMA
	20 ml	Heat-inactivated FCS
	980 ml	RPMI Media 1640
HepG2 Growth Medium (1 L) #	9.6 g	Eagle's Minimum Essential Medium (with Earle's salts, glutamine and non-essential amino acids)
	100 ml	Heat-inactivated FCS
	900 ml	Water

7.4 Protocols

All of the following biological procedures were carried out under sterile conditions unless otherwise stated.

7.4.1 Molecular Biology Protocols

7.4.1.1 PCR

PCR reactions were carried out using Phusion Flash PCR Master Mix according to the manufacturer's protocol. Each reaction typically contained 2× Phusion Flash PCR Master Mix (10 µl), sterile water (6 µl), forwards primer (10 µM, 1 µl), reverse primer (10 µM, 1 µl) and template DNA (5 ng μl^{-1}, 2 µl). The PCR reactions were cycled as shown in Table 7–3 before being purified using the QIAquick PCR Purification kit according to the manufacturer's protocol and analysed by agarose gel electrophoresis.

Table 7−3: Cycling conditions for PCR using Phusion Flash PCR Master Mix

Stage	Time / s	Temperature / °C	Cycles
Initial denaturation	10	98	1
Denaturation	1	98	30
Annealing	5	Tm of lower Tm primer	
Extension	15 kb^{-1}	72	
Final extension	60	72	1
	hold	4	

7.4.1.2 Agarose Gel Electrophoresis

The following protocol was carried out under non-sterile conditions. 0.8% w/v agarose in 1× TAE buffer was autoclaved prior to use. Ethidium bromide (5 mg ml^{-1}, 3 µl) was added to the agarose solution (30 ml) and the gel allowed to set. The DNA samples (5 µl) were mixed with 6× DNA Loading Dye (1 µl) prior to loading. An appropriate DNA ladder (5 µl) was used as a reference. Gels were run for 60 minutes at 100 V using 1× TAE buffer as the running buffer.

7.4.1.3 Enzymatic Digestion (SmaI)

SmaI restriction enzyme (10 U μl^{-1}, 1 µl) (where 1U = 1 µmol(substrate) min^{-1}) was mixed with water (16 µl), 10× Buffer Tango (3 µl) and DNA (10 µl). Following incubation at 30 °C for 16 hours the mixture was either stored at 4 °C or used immediately for ligation.

7.4.1.4 Ligation (In-Fusion Cloning)

The insert and plasmid DNA were quantified using agarose gel electrophoresis with an appropriate DNA ladder. The linearised vector was mixed with the insert DNA (200 ng total, insert:vector mass ratio at 3:1) and 5× In-Fusion HD enzyme premix (2 µl) and the volume adjusted to 10 µl with water. Following incubation at 50 °C for 15 minutes the mixture was either stored at −20 °C or used immediately for transformation.

7.4.1.5 Ligation (T4 Ligation)

The insert and plasmid DNA were quantified using agarose gel electrophoresis with an appropriate DNA ladder. The linearised vector (30 ng) was mixed with the insert DNA (insert:vector molar ratios at both 1:1 and 3:1), T4 ligase enzyme (0.5 µl), T4 ligase buffer (1.5 µl) and the volume adjusted to 15 µl with water. Following incubation at room temperature overnight the mixture was either stored at −20 °C or used immediately for transformation.

7.4.1.6 Preparation of Competent *E. coli*

The *E. coli* strain DH5α (stored at −80 °C) was inoculated onto LB agar medium and incubated at 37 °C for 16 hours. This was used to inoculate LB broth (10 ml) which was then incubated with shaking at 37 °C until OD_{600} = 0.5. The culture was incubated on ice for 15 minutes prior to centrifugation (3,000 × g for 10 minutes at 4 °C). The supernatant was discarded and the pellet resuspended in $CaCl_2$ (0.1 M, 30 ml). The suspension was incubated on ice for 30 minutes prior to centrifugation (3,000 × g for 10 minutes at 4 °C). The supernatant was discarded and the pellet resuspended in $CaCl_2$

(0.1 M, 6 ml) containing 15% v/v glycerol. Aliquots were frozen on dry ice and stored at −80 °C.

7.4.1.7 Transformation of Competent *E. coli*

DH5α competent cells (50 µl, stored at −80 °C) were thawed slowly on ice and gently mixed with the transforming DNA (4 µl, 7 µl and 9 µl for In-Fusion ligation mix, T4 ligation mix and purified plasmid respectively). The mixture was incubated on ice for 60 minutes before being heat shocked at 42 °C for 60 seconds. The mixture was chilled on ice for 2 minutes. LB broth (1 ml) was added and the mixture incubated with shaking at 37 °C for 1 hour. 200 µl was plated onto LB-Amp agar medium and incubated at 37 °C for 20 hours prior to storage at 4 °C.

7.4.1.8 Preparation of Purified Plasmid

LB-Amp broth (5 ml) was inoculated with a single colony and incubated with shaking at 37 °C for 16 hours. Frozen stocks were prepared by adding the culture (800 µl) to 80% glycerol (400 µl) and storing at −80 °C. The remaining culture was treated with the QIAprep Spin Miniprep kit according to the manufacturer's protocol and the product analysed by agarose gel electrophoresis.

7.4.1.9 Yeast Culture

The *S. cerevisiae* strain *α ade*$^{-}$*.lys*$^{-}$*.leu*$^{-}$*.Δaur1*$^{-}$.pRS316.*URA*$^{+}$*.ScAUR1*$^{+}$ (stored at −80 °C) was inoculated onto SD –W –URA agar medium and incubated at 30 °C for 48 hours prior to storage at 4 °C. This was used to inoculate SD –W –URA medium (5 ml) which was then incubated with shaking at 30 °C until OD_{600} = 0.5−0.6.

7.4.1.10 Yeast Transformation

5 ml of cells at OD_{600} = 0.5−0.6 were centrifuged (1,000 × g for 5 minutes at room temperature). The supernatant was discarded and the cells were resuspended in sterile TE buffer (5 ml). The cells were recentrifuged (1,000 × g for 5 minutes at room

temperature) and the supernatant was discarded. The cell pellet was resuspended in freshly prepared, sterile 1 × TE/LiAc buffer (1 ml) to form the competent yeast cells.

Herring testes carrier DNA (10 µl) was boiled at 95 °C for 10 minutes. To this were added purified plasmid (30 µl) and competent yeast cells (100 µl), with mixing achieved by vortexing. Freshly prepared, sterile PEG/LiAc (600 µl) was added and the mixture vortexed followed by incubation with shaking at 30 °C for 30 minutes. DMSO (70 µl) was added followed by mixing by gentle inversion. The mixture was heat shocked at 42 °C for 15 minutes before being chilled on ice for 2 minutes. The cells were centrifuged (14,400 × g for 5 seconds at room temperature), the supernatant was discarded and the cell pellet was resuspended in 1× TE buffer (200 µl). The cells were plated onto agar plates of permissive medium (SGR –W –L) and incubated at 30 °C until sufficient growth was observed, followed by storage at 4 °C.

7.4.1.11 Plasmid Shuffle

SGR –W –L medium (5 ml) was inoculated with transformed yeast and incubated with shaking at 30 °C until OD_{600} = 0.5−0.6. 200 µl was plated onto SGR –W –L +5FOA agar medium and incubated at 30 °C for 4 days prior to storage at 4 °C.

7.4.1.12 Colony PCR

Water (4 µl) was inoculated with a single colony. DMSO (1 µl) was added and the mixture vortexed. PCR was subsequently undertaken following the standard protocol (section 7.4.1.1) using the prepared mixture (2 µl) in the place of the template DNA. The PCR reactions were analysed by agarose gel electrophoresis.

7.4.1.13 Yeast Culture Scale-Up

Plasmid-shuffled yeast cultures were propagated in SGR –W –L medium. Liquid medium (5 ml) was inoculated and incubated with shaking at 30 °C until $OD_{600} \geq 0.8$. Fresh medium (600 ml) was added and the culture incubated with shaking at 30 °C until $OD_{600} \geq 0.8$. The culture was diluted into fresh medium (12 L) and incubated with

shaking at 30 °C until OD_{600} = 0.5−0.6. Frozen stocks were prepared by adding the culture (800 µl) to 80% glycerol (400 µl) and storing at −80 °C.

7.4.1.14 Preparation of Crude Microsomal Membranes

The following protocol was adapted from a literature procedure[320] and carried out under non-sterile conditions. The cells grown in large scale culture were harvested by centrifugation (4,000 × g for 10 minutes at 4 °C) and washed with cold PBS (3 × 20 ml). The cell pellet was weighed and resuspended in STE buffer (volume in ml 1.5 times the mass of the pellet in g). The cells were disrupted using pre-chilled, acid-washed glass beads (mass 1.5 times the mass of the pellet) by vortexing. Disruption involved 30 cycles of 1 minute vortexing followed by 1 minute resting on ice. The mixture was centrifuged (1,500 × g for 15 minutes at 4 °C) and the cell extract (supernatant) removed and stored. To the pellet was added a further measure of STE buffer (0.5 times the mass of the pellet) and disruption repeated, followed by further centrifugation (1,500 × g for 15 minutes at 4 °C).

The cell extracts were combined and centrifuged (23,000 × g for 30 minutes at 4 °C) to initially remove large organelles and any remaining cell debris. The supernatant was recentrifuged (150,000 × g for 90 minutes at 4 °C) to obtain a pellet enriched with microsomal membranes. The supernatant was discarded and the pellet resuspended in the minimal amount of storage buffer. The protein content was determined using the Bradford assay and the membranes stored at −80 °C.

7.4.1.15 Determination of Protein Concentration (Bradford Assay)

The following protocol was adapted from a literature procedure[381] and carried out under non-sterile conditions. A stock solution of BSA at a concentration of 100 µg ml^{-1} in water was prepared and used to create a standard curve ranging from 0.625 µg to 20 µg. The volumes were adjusted to 800 µl with water prior to the addition of Bradford reagent (200 µl). Following mixing the absorbance at 595 nm was measured and a standard curve produced. Samples of the microsomal membranes (from 1 µl to 20 µl) were diluted with water to give a final volume of 800 µl prior to the addition of Bradford reagent (200 µl). Following mixing the absorbance at 595 nm was measured.

Correlation with the standard curve allowed the protein content of the microsomal membranes to be determined in mg ml^{-1}.

7.4.1.16 Preparation of Washed Microsomal Membranes

The following protocol was performed according to a literature procedure[320] and carried out under non-sterile conditions. The crude microsomal membranes were adjusted to a concentration of 10 mg ml^{-1} using STE buffer and a 5% CHAPS stock solution was diluted to 2.5% with STE buffer. Equal volumes of the membranes and 2.5% CHAPS solution were mixed and chilled on ice for 1 hour. The mixture was centrifuged (150,000 × g for 90 minutes at 4 °C) and the pellet was resuspended in storage buffer. The protein content was determined using the Bradford assay and the membranes stored at −80 °C.

7.4.1.17 Determination of Protein Content in Enzyme Units

The following protocol was carried out under non-sterile conditions. A stock solution of NBD-C_6-ceramide at a concentration of 10 pmol μl^{-1} in DMSO was prepared and used to create a standard curve ranging from 0.2 pmol to 80 pmol. The volumes were adjusted to 200 µl with 1 M potassium formate in methanol. The fluorescence was read at Ex460/Em540 and a standard curve produced. Samples of the washed microsomal membranes were incubated with NBD-C_6-ceramide under assay conditions (section 7.4.2.1.2) and the product fluorescence read at Ex460/Em540. Correlation with the standard curve allowed the activity of the microsome preparation to be calculated in U μl^{-1} (where 1U = 1 pmol(product) min^{-1}). The membranes were adjusted to 1.5 U μl^{-1} and stored at −80 °C.

7.4.1.18 Preparation of Samples for Confocal Microscopy

The following protocol was carried out under non-sterile conditions. The frozen samples of transformed yeast (100 µl) were defrosted on ice and washed with HBSS buffer (900 µl). Following centrifugation (660 × g for 3 minutes at room temperature) the pellets were resuspended in HBSS buffer (1 ml). 100 µl, 75 µl, 50 µl, 25 µl, 10 µl and 5 µl of each sample were loaded into separate wells in a 96-well plate and all the

volumes adjusted to 100 µl with HBSS buffer. The plate was centrifuged (1,900 × g for 5 minutes at 4 °C) and imaged using the confocal microscope.

7.4.1.19 *L. major* Promastigote Culture

The frozen samples of *L. major* MHOM/IL/81/Friedlin promastigotes (1 ml) or *L. major* MHOM/IL/81/Friedlin/−/−*lcb2* promastigotes (1 ml) were rapidly defrosted and added to Schneider's Insect Medium (pH 7, 15% FCS, 5 ml). Incubation was carried out at 26 °C and promastigotes maintained in Schneider's Insect Medium (pH 7, 15% FCS). Frozen stocks were prepared by adding the culture (900 µl) to DMSO (100 µl) and cooling slowly to −140 °C.

7.4.1.20 Differentiation of THP-1 Cells

This protocol was conducted by personnel at GSK, Tres Cantos. THP-1 cells were added to THP-1 pre-differentiation growth medium (−PMA, 50 ml) to a concentration of 9.0×10^5 ml^{-1} and incubated at 37 °C for 72 hours. This was used to seed a culture (50 ml) of THP-1 cells at 6.0×10^5 ml^{-1} in pre-differentiation growth medium (+PMA) which was incubated at 37 °C for 24 hours under 5% CO_2. Differentiation was confirmed by microscopy and the cells were washed with 2 × 50 ml pre-differentiation growth medium (+PMA).

7.4.2 Biological Assay Protocols

7.4.2.1 *In vitro* Assay Protocols

7.4.2.1.1 HPTLC Assay

The following protocol was adapted from a literature procedure[320] and carried out under non-sterile conditions. PI (10 mM, 1 µl) was dried into each LoBind Eppendorf tube using the Eppendorf Concentrator. To each tube was added Tris/EDTA/BSA buffer (20 µl) and the contents mixed by vortexing. The tubes were centrifuged briefly to collect the material and the volume adjusted to 48 µl with water. The test compounds (0.5 µl) were added followed by washed microsomal membranes (1.5 U $µl^{-1}$, 0.5 µl)

and the tubes pre-incubated with shaking at 30 °C for 30 minutes. The reaction was initiated by the addition of NBD-C_6-ceramide (100 µM, 1 µl) and incubated with shaking at 30 °C for a further 25 minutes before being quenched with chloroform:methanol:water (10:10:3, 150 µl). Following centrifugation (14,400 × g for 5 minutes at room temperature), 20 µl of the organic layer were removed and loaded onto a HTPLC plate. This was run using the solvent system chloroform:methanol:0.25% aqueous KCl (55:45:10) and the fluorescence was read at Ex475/Em520.

7.4.2.1.2 96-Well Plate Assay

The following protocol was adapted from a literature procedure[320] and carried out under non-sterile conditions. All quantities are calculated for 96 reactions.

The test compounds and controls (1 µl) were dispensed into a 96 V-well plate. PI (10 mM, 40 µl) was dried into a LoBind Eppendorf tube using the Eppendorf Concentrator. To the tube was added phosphate buffer (71.4 mM, pH 7.0, 1.4 ml) and the contents mixed by vortexing. The contents were transferred to a glass vial and to this were added CHAPS (3 mM, 400 µl), storage buffer (160 µl) and CHAPS-washed microsomal membranes (1.5 U μl^{-1}, 40 µl). The solution (20 µl) was added to each well and the plate pre-incubated at 30 °C for 15 minutes. CHAPS (3 mM, 450 µl), phosphate buffer (71.4 mM, 1575 µl) and NBD-C_6-ceramide (200 µM, 112.5 µl) were mixed together by vortexing and the solution (19 µl) was added to each well. The plate was incubated at 30 °C for 25 minutes before the reaction was quenched by the addition of methanol (200 µl).

Separation of the product and starting material was achieved using ion exchange resin in 96-well filter plates. 20% w/v AG 4-X4 resin in ethanol (100 µl) was added per well and sedimented by centrifugation (2,450 × g for 27 seconds at room temperature). The resin was incubated with formic acid (50 µl) for 5 minutes before being centrifuged (2,450 × g for 27 seconds at room temperature). The resin was then washed with water (100 µl) and dried by centrifugation (2,450 × g for 27 seconds at room temperature).

The reaction mixture (200 µl) was loaded onto the resin and the starting material removed by centrifugation (2,450 × g for 1 minute at room temperature). The resin was washed with 5 × 200 µl methanol before the product was eluted into black plates using 4 × 50 µl of potassium formate in methanol (1 M) (all centrifugations at 2,450 × g for 1 minute at room temperature). The fluorescence was read at Ex460/Em540.

7.4.2.2 *In cellulo* Assay Protocols

7.4.2.2.1 Diffusion Assay

Agarose (280 mg) was added to SGR –W –L medium (14 ml) and autoclaved. To this was added liquid yeast culture to produce a solution of OD_{600} = 0.14, which was mixed by gentle inversion. This was poured into a square plate and left to set. A test compound and a control (DMSO) were spotted onto the surface of the agarose (1 µl, 2 µl and 3 µl of each) and the plate incubated at 30 °C for 96 hours.

7.4.2.2.2 HTS Assay

Cycloheximide (1 mM, 50 nl) was dispensed into the control wells of 1,536-well plates. The frozen stock of the required strain(s) (OD_{600} = 10) was thawed on ice. The required volume of assay mixture (10 µM FDGlu and *α-Lmj* or α-AUR1 of OD_{600} = 0.0625 in SGR –W –L) was subsequently prepared and dispensed (5 µl per well). Plates were incubated at 30 °C for 25 hours prior to the addition of phosphate buffer (0.25 M, pH 7.0, 5 µl per well). The fluorescence was read at Ex480/Em540.

7.4.2.2.3 *L. major* Cytotoxicity Assay

The following protocol was adapted from a literature procedure.[320] The test compounds and controls (1 µl) were dispensed into a sterile 96-well plate. *L. major* promastigotes (99 µl) were added to a final concentration of 5.0×10^3 ml^{-1} for the single shot assay or 1.0×10^4 ml^{-1} for the dose-response assay and the plate incubated at 26 °C for 72 hours. AlamarBlue® (10 µl) was added and the plate incubated at 26 °C for 4 hours for *L. major* FV1 promastigotes or 8 hours for *L. major lcb2Δ* mutant promastigotes. The fluorescence was read at Ex540/Em600.

7.4.2.2.4 Metabolic Labelling Assay

L. major lcb2Δ mutant promastigotes were centrifuged (1,500 × g for 10 minutes at room temperature) and the pellet washed three times with stock Schneider's Insect Medium (pH 7, no FCS). The pellet was subsequently resuspended in Schneider's Insect Medium (pH 7, no FCS) to a parasite concentration of 1.0×10^7 ml^{-1} and dispensed into Eppendorf tubes (250 µl per tube). Following a pre-incubation at 26 °C for 1 hour, the test compounds were added (1 µl) and the tubes incubated at 26 °C for 18 hours.

The reaction was initiated by the addition of BODIPY® FL C_5-ceramide complexed to BSA (0.5 mM, 1.25 µl). Following further incubation at 26 °C for 1 hour, the tubes were centrifuged (12,500 × g for 5 minutes at room temperature) and the pellets washed twice with PBS (250 µl). The pellets were resuspended in chloroform:methanol:water (10:10:3, 200 µl) followed by sonication in a water bath for 15 minutes. Water (25 µl) was added before centrifugation (14,400 × g for 10 seconds at room temperature). 20 µl of the organic layer were removed and loaded onto a HTPLC plate. This was run using the solvent system chloroform:methanol:0.25% aqueous KCl (55:45:10) and the fluorescence was read at Ex475/Em520.

7.4.2.2.5 Axenic *L. donovani* Cytotoxicity Assay

This protocol was conducted by personnel at GSK, Tres Cantos and was performed according to a literature procedure.[341] The test compounds and controls (30 nl) were dispensed into a sterile 1,536-well plate. *L. donovani* LdBOB amastigotes in amastigote growth medium (6 µl) were added to a final concentration of 5.0×10^3 ml^{-1} and the plate incubated at 37 °C for 72 hours under 5% CO_2. Resazurin solution (2 µl) was added and the plate incubated at room temperature for 4 hours. The fluorescence was read at Ex528/Em590.

7.4.2.2.6 HepG2 Cytotoxicity Assay

This protocol was conducted by personnel at GSK, Tres Cantos and was performed according to a literature procedure.[341] The test compounds and controls (250 nl) were

dispensed into a sterile 384-well plate. HepG2 cells in HepG2 growth medium (25 µl) were added to a final concentration of 1.2×10^5 ml^{-1} and the plate incubated at 37 °C for 48 hours under 5% CO_2 and at 80% relative humidity. The plate was incubated at room temperature for 30 minutes prior to the addition of CellTiter-Glo® (25 µl). The plate was incubated at room temperature for 10 minutes and the luminescent output measured.

7.4.2.2.7 Intramacrophage *L. donovani* Cytotoxicity Assay

This protocol was conducted by personnel at GSK, Tres Cantos and was performed according to a literature procedure.[341] Washed THP-1 cells at a concentration of 6.0×10^5 ml^{-1} (prepared using protocol 7.4.1.20, 50 ml) were infected with *L. donovani* LdBOB amastigotes to a final concentration of 6.0×10^6 ml^{-1} and the flask incubated overnight at 37 °C. Remaining extracellular parasites were removed by washing with 3 × 50 ml PBS before the cells were harvested with trypsin.

The test compounds and controls (250 nl) were dispensed into a sterile 384-well plate. Infected macrophages in post-differentiation growth medium (50 µl) were added to a final concentration of 6.0×10^4 ml^{-1} and the plate incubated at 37 °C for 96 hours under 5% CO_2. Wells were fixed with 4% (v/v) formaldehyde in PBS at room temperature for 30 minutes before washing with 2 × 100 µl PBS. Cells were stained with HCS CellMask™ Deep Red at room temperature for 30 minutes before washing with 2 × 50 µl PBS. PBS (50 µl) was added to each well and the wells imaged at Ex405/Em460 and Ex488/Em509. Images were analysed using the automated Acapella® High Content Imaging and Analysis Software from PerkinElmer.

7.4.2.3 *In vivo* Assay Protocol

This protocol was conducted by personnel at the London School of Hygiene and Tropical Medicine and was performed according to a literature procedure.[367] *L. donovani* amastigotes were isolated from the spleen of an infected hamster and 1.0×10^7 parasites were intravenously injected into female BALB/c mice, which were randomly sorted into groups of 5. The infection was allowed to develop over 7 days before the mice were dosed orally at 50 mg kg^{-1} twice a day for 5 days. The mice were

sacrificed 14 days post infection and the livers and spleens were removed and weighed prior to the preparation of smears, which were fixed with methanol and stained with Giemsa. The number of amastigotes per 500 liver or spleen cells × organ weight was calculated for treated and untreated mice and use as a measure of drug efficacy.

Chapter 8

References

1. WHO, *Investing to overcome the global impact of neglected tropical diseases - Third WHO report on neglected tropical diseases*, http://apps.who.int/iris/bitstream/10665/152781/1/9789241564861_eng.pdf?ua=1, (accessed 22nd May, 2015).
2. L. Manderson, J. Aagaard-Hansen, P. Allotey, M. Gyapong and J. Sommerfeld, *PLoS Negl. Trop. Dis.*, 2009, **3**, e332.
3. K. Nussbaum, J. Honek, C. Cadmus and T. Efferth, *Curr. Med. Chem.*, 2010, **17**, 1594-1617.
4. H. C. Turner, M. Walker, M. D. French, I. M. Blake, T. S. Churcher and M. G. Basanez, *Trends Parasitol.*, 2014, **30**, 562-570.
5. P. J. Hotez, M. Alvarado, M. G. Basanez, I. Bolliger, R. Bourne, M. Boussinesq, S. J. Brooker, A. S. Brown, G. Buckle, C. M. Budke, H. Carabin, L. E. Coffeng, E. M. Fevre, T. Furst, Y. A. Halasa, R. Jasrasaria, N. E. Johns, J. Keiser, C. H. King, R. Lozano, M. E. Murdoch, S. O'Hanlon, S. D. S. Pion, R. L. Pullan, K. D. Ramaiah, T. Roberts, D. S. Shepard, J. L. Smith, W. A. Stolk, E. A. Undurraga, J. Utzinger, M. R. Wang, C. J. L. Murray and M. Naghavi, *PLoS Negl. Trop. Dis.*, 2014, **8**, e2865.
6. J. Noblick, R. Skolnik and P. J. Hotez, *PLoS Negl. Trop. Dis.*, 2011, **5**, e1022.
7. K. Stuart, R. Brun, S. Croft, A. Fairlamb, R. E. Gurtler, J. McKerrow, S. Reed and R. Tarleton, *J. Clin. Invest.*, 2008, **118**, 1301-1310.
8. D. A. Maslov, S. A. Podtipaev and J. Lukes, *Mem. I. Oswaldo Cruz*, 2001, **96**, 397-402.
9. A. G. B. Simpson, J. R. Stevens and J. Lukes, *Trends Parasitol.*, 2006, **22**, 168-174.
10. P. A. Bates, *Int. J. Parasitol.*, 2007, **37**, 1097-1106.
11. WHO, *Status of endemicity of cutaneous leishmaniasis, worldwide, 2013*, http://gamapserver.who.int/mapLibrary/Files/Maps/Leishmaniasis_2013_CL.png, (accessed 23rd May, 2015).
12. WHO, *Status of endemicity of visceral leishmaniasis, worldwide, 2013*, http://gamapserver.who.int/mapLibrary/Files/Maps/Leishmaniasis_2013_VL.png, (accessed 23rd May, 2015).
13. J. Alvar, I. D. Velez, C. Bern, M. Herrero, P. Desjeux, J. Cano, J. Jannin and M. den Boer, *PLoS One*, 2012, **7**, e35671.
14. H. W. Murray, J. D. Berman, C. R. Davies and N. G. Saravia, *Lancet*, 2005, **366**, 1561-1577.
15. W. H. Markle and K. Makhoul, *Am. Fam. Physician*, 2004, **69**, 1455-1460.
16. R. Kubba, Y. Algindan, A. M. Elhassan, A. H. S. Omer, M. K. Kutty and M. B. M. Saeed, *Int. J. Dermatol.*, 1988, **27**, 702-706.

17. P. Desjeux, *Comp. Immunol. Microbiol. Infect. Dis.*, 2004, **27**, 305-318.
18. E. D. Franke, A. Llanoscuentas, J. Echevarria, M. E. Cruz, P. Campos, A. A. Tovar, C. M. Lucas and J. D. Berman, *Am. J. Trop. Med. Hyg.*, 1994, **51**, 77-82.
19. P. M. Woster, *Comp. Med. Chem. II*, 2007, **7**, 815-843.
20. WHO, *Working to overcome the global impact of neglected tropical diseases - First WHO report on neglected tropical diseases*, http://whqlibdoc.who.int/publications/2010/9789241564090_eng.pdf, (accessed 22nd May, 2015).
21. J. D. Berman, *Clin. Infect. Dis.*, 1997, **24**, 684-703.
22. I. L. Mauricio, J. R. Stothard and M. A. Miles, *Parasitol. Today*, 2000, **16**, 188-189.
23. V. E. Miranda de Araujo, M. H. Franco Morais, I. A. Reis, A. Rabello and M. Carneiro, *PLoS Negl. Trop. Dis.*, 2012, **6**, e1511.
24. F. R. Martins-Melo, M. D. Lima, A. N. Ramos, C. H. Alencar and J. Heukelbach, *PLoS One*, 2014, **9**, e93770.
25. E. E. Zijlstra, A. M. Musa, E. A. G. Khalil, I. M. el-Hassan and A. M. el-Hassan, *Lancet Infect. Dis.*, 2003, **3**, 87-98.
26. P. Desjeux and J. Alvar, *Ann. Trop. Med. Parasitol.*, 2003, **97**, 3-15.
27. CDC, *Life Cycle of Leishmania spp*, http://www.cdc.gov/dpdx/leishmaniasis/index.html, (accessed 24th May, 2015).
28. K. Leifso, G. Cohen-Freue, N. Dogra, A. Murray and W. R. McMaster, *Mol. Biochem. Parasitol.*, 2007, **152**, 35-46.
29. A. T. Peterson and J. Shaw, *Int. J. Parasitol.*, 2003, **33**, 919-931.
30. M. Rogers, P. Kropf, B. S. Choi, R. Dillon, M. Podinovskaia, P. Bates and I. Muller, *PLoS Pathog.*, 2009, **5**, e1000555.
31. O. Brandonisio, R. Spinelli and M. Pepe, *Microbes Infect.*, 2004, **6**, 1402-1409.
32. P. E. Kima, *Int. J. Parasitol.*, 2007, **37**, 1087-1096.
33. M. J. McConville and E. Handman, *Int. J. Parasitol.*, 2007, **37**, 1047-1051.
34. E. Gluenz, M. L. Ginger and P. G. McKean, *Curr. Opin. Microbiol.*, 2010, **13**, 473-479.
35. P. F. P. Pimenta, S. J. Turco, M. J. McConville, P. G. Lawyer, P. V. Perkins and D. L. Sacks, *Science*, 1992, **256**, 1812-1815.
36. J. Blum, P. Buffet, L. Visser, G. Harms, M. S. Bailey, E. Caumes, J. Clerinx, P. P. A. M. van Thiel, G. Morizot, C. Hatz, T. P. C. Dorlo and D. N. J. Lockwood, *J. Travel Med.*, 2014, **21**, 116-129.
37. G. O. Vianna, *Anais do VII Congresso Brasileiro de Medicina e Cirurgia*, 1912, **4**, 426-428.
38. G. Di Cristina and G. Caronia, *Pathologica*, 1915, **7**, 82-83.
39. U. N. Brahmachari, *Ind. J. Med. Res.*, 1922, **10**, 492-522.
40. A. K. Haldar, P. Sen and S. Roy, *Mol. Biol. Int.*, 2011, **2011**, e571242.
41. R. A. Gasser, A. J. Magill, C. N. Oster, E. D. Franke, M. Grogl and J. D. Berman, *Clin. Infect. Dis.*, 1994, **18**, 83-90.
42. S. Sundar and J. Chakravarty, *Int. J. Environ. Res. Publ. Health*, 2010, **7**, 4267-4277.
43. E. M. Andersen, M. Cruz-Saldarriaga, A. Llanos-Cuentas, M. Luz-Cjuno, J. Echevarria, C. Miranda-Verastegui, O. Colina and J. D. Berman, *Am. J. Trop. Med. Hyg.*, 2005, **72**, 133-137.
44. P. Shaked-Mishan, N. Ulrich, M. Ephros and D. Zilberstein, *J. Biol. Chem.*, 2001, **276**, 3971-3976.
45. A. K. Chakraborty and H. K. Majumder, *Biochem. Biophys. Res. Commun.*, 1988, **152**, 605-611.

46. S. Sundar, D. K. More, M. K. Singh, V. P. Singh, S. Sharma, A. Makharia, P. C. K. Kumar and H. W. Murray, *Clin. Infect. Dis.*, 2000, **31**, 1104-1107.
47. G. Mandal, S. Mandal, M. Sharma, K. S. Charret, B. Papadopoulou, H. Bhattacharjee and R. Mukhopadhyay, *PLoS Negl. Trop. Dis.*, 2015, **9**, e0003500.
48. A. N. Hazarika, *Ind. Med. Gaz.*, 1949, **84**, 140-145.
49. T. P. C. Dorlo and P. A. Kager, *PLoS Negl. Trop. Dis.*, 2008, **2**, e225.
50. A. Belehu and B. Naafs, *Lancet*, 1982, **1**, 1463-1464.
51. M. Sands, M. A. Kron and R. B. Brown, *Rev. Infect. Dis.*, 1985, **7**, 625-634.
52. M. Basselin, H. Denise, G. H. Coombs and M. P. Barrett, *Antimicrob. Agents Chemother.*, 2002, **46**, 3731-3738.
53. S. Sundar, *Med. Microbiol. Immunol.*, 2001, **190**, 89-92.
54. A. S. Nagle, S. Khare, A. B. Kumar, F. Supek, A. Buchynskyy, C. J. N. Mathison, N. K. Chennamaneni, N. Pendem, F. S. Buckner, M. H. Gelb and V. Molteni, *Chem. Rev.*, 2014, **114**, 11305-11347.
55. M. Roussel, M. Nacher, G. Fremont, B. Rotureau, E. Clyti, D. Sainte-Marie, B. Carme, R. Pradinaud and P. Couppie, *Ann. Trop. Med. Parasitol.*, 2006, **100**, 307-314.
56. R. Donovick, W. Gold, J. F. Pagano and H. A. Stout, *Antibiot. Ann.*, 1955, **3**, 579-586.
57. W. H. Trejo and R. E. Bennett, *J. Bacteriol.*, 1963, **85**, 436-439.
58. A. Prata, *Trans. R. Soc. Trop. Med. Hyg.*, 1963, **57**, 266-268.
59. J. Berman, *Am. J. Trop. Med. Hyg.*, 2015, **92**, 471-473.
60. S. Sundar, H. Mehta, A. V. Suresh, S. P. Singh, M. Rai and H. W. Murray, *Clin. Infect. Dis.*, 2004, **38**, 377-383.
61. C. P. Thakur, R. K. Singh, S. M. Hassan, R. Kumar, S. Narain and A. Kumar, *Trans. R. Soc. Trop. Med. Hyg.*, 1999, **93**, 319-323.
62. B. E. Cohen, *Int. J. Pharm.*, 1998, **162**, 95-106.
63. E. Castillo, M. A. Dea-Ayuela, F. Bolas-Fernandez, M. Rangel and M. E. Gonzalez-Rosende, *Curr. Med. Chem.*, 2010, **17**, 4027-4051.
64. WHO, *Report of a WHO informal consultation on liposomal amphotericin B in the treatment of visceral leishmaniasis*, www.who.int/neglected_diseases/resources/AmBisomeReport.pdf, (accessed 2nd July, 2015).
65. Y. D. Paila, B. Saha and A. Chattopadhyay, *Biochem. Biophys. Res. Commun.*, 2010, **399**, 429-433.
66. S. L. Croft, S. Sundar and A. H. Fairlamb, *Clin. Microbiol. Rev.*, 2006, **19**, 111-126.
67. M. Baginski, H. Resat and J. A. McCammon, *Mol. Pharmacol.*, 1997, **52**, 560-570.
68. A. Chattopadhyay and M. Jafurulla, *Biochem. Biophys. Res. Commun.*, 2011, **416**, 7-12.
69. B. Purkait, A. Kumar, N. Nandi, A. H. Sardar, S. Das, S. Kumar, K. Pandey, V. Ravidas, M. Kumar, T. De, D. Singh and P. Das, *Antimicrob. Agents Chemother.*, 2012, **56**, 1031-1041.
70. R. N. Davidson, M. den Boer and K. Ritmeijer, *Trans. R. Soc. Trop. Med. Hyg.*, 2009, **103**, 653-660.
71. R. A. Neal, S. Allen, N. McCoy, P. Olliaro and S. L. Croft, *J. Antimicrob. Chemother.*, 1995, **35**, 577-584.
72. C. N. Chunge, J. Owate, H. O. Pamba and L. Donno, *Trans. R. Soc. Trop. Med. Hyg.*, 1990, **84**, 221-225.

73. A. Ben Salah, N. Ben Messaoud, E. Guedri, A. Zaatour, N. Ben Alaya, J. Bettaieb, A. Gharbi, N. B. Hamida, A. Boukthir, S. Chlif, K. Abdelhamid, Z. El Ahmadi, H. Louzir, M. Mokni, G. Morizot, P. Buffet, P. L. Smith, K. M. Kopydlowski, M. Kreishman-Deitrick, K. S. Smith, C. J. Nielsen, D. R. Ullman, J. A. Norwood, G. D. Thorne, W. F. McCarthy, R. C. Adams, R. M. Rice, D. Tang, J. Berman, J. Ransom, A. J. Magill and M. Grogl, *New Engl. J. Med.*, 2013, **368**, 524-532.
74. S. Sundar, T. K. Jha, C. P. Thakur, P. K. Sinha, S. K. Bhattacharya, B. Nguyen, E. Kwan, A. Oudin, K. Valcke, S. Mathie, C. Ley, M. Rosenberg, E. L. Gaithersburg, L. Muenz, D. He, L. J. Wei, B. Ballanchanda, E. Wrone, E. Mahmoud, R. Davidson, R. Sweetow, M. Valente, L. Sheiner, S. Beal, E. Lin, W. Gee, Y. Huang, H. Chang and X. Li, *New Engl. J. Med.*, 2007, **356**, 2571-2581.
75. M. M. Fernandez, E. L. Malchiodi and I. D. Algranati, *Antimicrob. Agents Chemother.*, 2011, **55**, 86-93.
76. B. Chawla, A. Jhingran, A. Panigrahi, K. D. Stuart and R. Madhubala, *PLoS One*, 2011, **6**, e26660.
77. M. Maarouf, F. Lawrence, S. Brown and M. RobertGero, *Parasitol. Res.*, 1997, **83**, 198-202.
78. S. Teklemariam, A. G. Hiwot, D. Frommel, T. L. Miko, G. Ganlov and A. Bryceson, *Trans. R. Soc. Trop. Med. Hyg.*, 1994, **88**, 334-339.
79. M. Maarouf, M. T. Adeline, M. Solignac, D. Vautrin and M. Robert-Gero, *Parasite*, 1998, **5**, 167-173.
80. P. Hilgard, T. Klenner, J. Stekar and C. Unger, *Cancer Chemother. Pharmacol.*, 1993, **32**, 90-95.
81. S. L. Croft, D. Snowdon and V. Yardley, *J. Antimicrob. Chemother.*, 1996, **38**, 1041-1047.
82. K. Ritmeijer, A. Dejenie, Y. Assefa, T. B. Hundie, J. Mesure, G. Boots, M. den Boer and R. N. Davidson, *Clin. Infect. Dis.*, 2006, **43**, 357-364.
83. P. R. Machado, J. Ampuero, L. H. Guimaraes, L. Villasboas, A. T. Rocha, A. Schriefer, R. S. Sousa, A. Talhari, G. Penna and E. M. Carvalho, *PLoS Negl. Trop. Dis.*, 2010, **4**, e912.
84. S. Sundar and P. L. Olliaro, *Ther. Clin. Risk Manag.*, 2007, **3**, 733-740.
85. T. P. C. Dorlo, P. van Thiel, A. D. R. Huitema, R. J. Keizer, H. J. C. de Vries, J. H. Beijnen and P. J. de Vries, *Antimicrob. Agents Chemother.*, 2008, **52**, 2855-2860.
86. N. K. Verma and C. S. Dey, *Antimicrob. Agents Chemother.*, 2004, **48**, 3010-3015.
87. T. P. C. Dorlo, M. Balasegaram, J. H. Beijnen and P. J. de Vries, *J. Antimicrob. Chemother.*, 2012, **67**, 2576-2597.
88. K. Seifert, S. Matu, F. J. Perez-Victoria, S. Castanys, F. Gamarro and S. L. Croft, *Int. J. Antimicrob. Agents*, 2003, **22**, 380-387.
89. S. Cojean, S. Houze, D. Haouchine, F. Huteau, S. Lariven, V. Hubert, F. Michard, C. Bories, F. Pratlong, J. Le Bras, P. M. Loiseau and S. Matheron, *Emerg. Infect. Dis.*, 2012, **18**, 704-706.
90. K. Seifert and S. L. Croft, *Antimicrob. Agents Chemother.*, 2006, **50**, 73-79.
91. R. E. Saenz, H. Paz and J. D. Berman, *Am. J. Med.*, 1990, **89**, 147-155.
92. S. Sundar, P. K. Sinha, S. A. Dixon, R. Buckley, A. K. Miller, K. Mohamed and M. Al-Banna, *Am. J. Trop. Med. Hyg.*, 2011, **84**, 892-900.
93. J. Dogra, B. B. Lal and S. N. Misra, *Int. J. Dermatol.*, 1986, **25**, 398-400.

94. I. Arevalo, B. Ward, R. Miller, T. C. Meng, E. Najar, E. Alvarez, G. Matlashewski and A. Llanos-Cuentas, *Clin. Infect. Dis.*, 2001, **33**, 1847-1851.
95. DNDi, *DNDi R&D Project Portfolio*, http://www.dndi.org/diseases-projects/portfolio.html, (accessed 29th May 2015).
96. DNDi, *Target Product Profile for CL*, http://www.dndi.org/diseases-projects/diseases/vl/tpp/tpp-cl.html, (accessed 17th July, 2015).
97. DNDi, *Target Product Profile for VL*, http://www.dndi.org/diseases-projects/diseases/vl/tpp/tpp-vl.html, (accessed 17th July, 2015).
98. C. I. de Oliveira, I. P. Nascimento, A. Barral, M. Soto and M. Barral-Netto, *Parasitol. Int.*, 2009, **58**, 319-324.
99. J. R. Baker, *Parasite*, 1995, **2**, 3-12.
100. WHO, *Distribution of human African trypanosomiasis (T.b.gambiense), worldwide, 2013*, http://gamapserver.who.int/mapLibrary/Files/Maps/HAT_ga_2013.png, (accessed 4th June, 2015).
101. WHO, *Distribution of human African trypanosomiasis (T.b.rhodesiense), worldwide, 2013*, http://gamapserver.who.int/mapLibrary/Files/Maps/HAT_rh_2013.png, (accessed 4th June, 2015).
102. P. G. E. Kennedy, *J. Clin. Invest.*, 2004, **113**, 496-504.
103. WHO, *Human African trypanosomiasis (sleeping sickness), Fact sheet N°259*, http://www.who.int/mediacentre/factsheets/fs259/en/, (accessed 4th June, 2015).
104. S. C. Welburn, E. M. Fevre, P. G. Coleman, M. Odiit and I. Maudlin, *Trends Parasitol.*, 2001, **17**, 19-24.
105. J. R. Franco, P. P. Simarro, A. Diarra and J. G. Jannin, *Clin. Epidemiol.*, 2014, **6**, 257-275.
106. P. G. E. Kennedy, *Pract. Neurol.*, 2005, **5**, 260-267.
107. J. Rodgers, A. Jones, S. Gibaud, B. Bradley, C. McCabe, M. P. Barrett, G. Gettinby and P. G. E. Kennedy, *PLoS Negl. Trop. Dis.*, 2011, **5**, e1308.
108. A. J. Duggan and M. P. Hutchinson, *J. Trop. Med. Hyg.*, 1966, **69**, 124-131.
109. CDC, *Life cycle of T. b. gambiense and T. b. rhodesiense*, http://www.cdc.gov/dpdx/trypanosomiasisAfrican/index.html, (accessed 4th June, 2015).
110. E. M. Fevre, K. Picozzi, J. Jannin, S. C. Welburn and I. Maudlin, in *Advances in Parasitology, Vol 61: Control of Human Parasitic Diseases*, ed. D. H. Molyneux, Elsevier Academic Press Inc., San Diego, 2006, vol. 61, pp. 167-221.
111. H. Belete, G. Tikubet, B. Petros, W. A. Oyibo and I. N. Otigbuo, *Trop. Med. Int. Health*, 2004, **9**, 710-714.
112. M. Becker, N. Aitcheson, E. Byles, B. Wickstead, E. Louis and G. Rudenko, *Genome Res.*, 2004, **14**, 2319-2329.
113. J. R. Seed and S. J. Black, *J. Parasitol.*, 1997, **83**, 656-662.
114. B. Reuner, E. Vassella, B. Yutzy and M. Boshart, *Mol. Biochem. Parasitol.*, 1997, **90**, 269-280.
115. J. R. Seed and M. A. Wenck, *Kinetoplastid Biol. Dis.*, 2003, **2**, 3.
116. J. Van den Abbeele, Y. Claes, D. van Bockstaele, D. Le Ray and M. Coosemans, *Parasitology*, 1999, **118**, 469-478.
117. M. D. Urbaniak, M. L. S. Guther and M. A. J. Ferguson, *PLoS One*, 2012, **7**, e36619.
118. D. Steverding, *Parasite. Vector.*, 2008, **1**, 3.
119. N. Baker, H. P. de Koning, P. Maser and D. Horn, *Trends Parasitol.*, 2013, **29**, 110-118.

120. P. Babokhov, A. O. Sanyaolu, W. A. Oyibo, A. F. Fagbenro-Beyioku and N. C. Iriemenam, *Pathog. Glob. Health*, 2013, **107**, 242-252.
121. F. Doua, T. W. Miezan, J. R. S. Singaro, F. B. Yapo and T. Baltz, *Am. J. Trop. Med. Hyg.*, 1996, **55**, 586-588.
122. B. Bouteille, O. Oukem, S. Bisser and M. Dumas, *Fundam. Clin. Pharmacol.*, 2003, **17**, 171-181.
123. H. P. de Koning, *Mol. Pharmacol.*, 2001, **59**, 586-592.
124. D. Kayembe and M. Wery, *Ann. Soc. Belg. Med. Trop.*, 1972, **52**, 1-8.
125. E. L. M. Vansterkenburg, I. Coppens, J. Wilting, O. J. M. Bos, M. J. E. Fischer, L. H. M. Janssen and F. R. Opperdoes, *Acta Trop.*, 1993, **54**, 237-250.
126. M. P. Barrett, D. W. Boykin, R. Brun and R. R. Tidwell, *Br. J. Pharmacol.*, 2007, **152**, 1155-1171.
127. R. Brun, J. Blum, F. Chappuis and C. Burri, *Lancet*, 2010, **375**, 148-159.
128. A. J. Nok, *Parasitol. Res.*, 2003, **90**, 71-79.
129. M. Willson, M. Callens, D. A. Kuntz, J. Perie and F. R. Opperdoes, *Mol. Biochem. Parasitol.*, 1993, **59**, 201-210.
130. H. Dixon, C. D. Ginger and Williams.J, *Comp. Biochem. Physiol.*, 1971, **39**, 247-266.
131. S. N. Kibona, L. Matemba, J. S. Kaboya and G. W. Lubega, *Trop. Med. Int. Health*, 2006, **11**, 144-155.
132. A. G. Scott, A. Tait and C. M. R. Turner, *Acta Trop.*, 1996, **60**, 251-262.
133. E. A. H. Friedheim, *Am. J. Trop. Med. Hyg.*, 1949, **29**, 173-180.
134. D. Steverding, *Parasite. Vector.*, 2010, **3**, 15.
135. C. Burri, S. Nkunhu, A. Merolle, T. Smith, J. Blum and R. Brun, *Lancet*, 2000, **355**, 1419-1425.
136. I. Kuepfer, C. Schmid, M. Allan, A. Edielu, E. P. Haary, A. Kakembo, S. Kibona, J. Blum and C. Burri, *PLoS Negl. Trop. Dis.*, 2012, **6**, e1695.
137. S. Kappagoda, U. Singh and B. G. Blackburn, *Mayo Clin. Proc.*, 2011, **86**, 561-583.
138. J. Blum, S. Nkunku and C. Burri, *Trop. Med. Int. Health*, 2001, **6**, 390-400.
139. J. Keiser, O. Ericsson and C. Burri, *Clin. Pharmacol. Ther.*, 2000, **67**, 478-488.
140. M. L. Cunningham, M. Zvelebil and A. H. Fairlamb, *Eur. J. Biochem.*, 1994, **221**, 285-295.
141. A. H. Fairlamb, G. B. Henderson and A. Cerami, *Proc. Natl. Acad. Sci. USA*, 1989, **86**, 2607-2611.
142. R. Brun, R. Schumacher, C. Schmid, C. Kunz and C. Burri, *Trop. Med. Int. Health*, 2001, **6**, 906-914.
143. J. Robays, G. Nyamowala, C. Sese, V. Kande, P. Lutumba, W. Van der Veken and M. Boelaert, *Emerg. Infect. Dis.*, 2008, **14**, 966-967.
144. P. Pyana Pati, N. Van Reet, D. Mumba Ngoyi, I. Ngay Lukusa, S. Karhemere Bin Shamamba and P. Buscher, *PLoS Negl. Trop. Dis.*, 2014, **8**, e3212.
145. C. J. Bacchi, H. C. Nathan and S. H. Hutner, *Science*, 1980, **210**, 332-334.
146. B. F. Giffin, P. P. McCann, A. J. Bitonti and C. J. Bacchi, *J. Protozool.*, 1986, **33**, 238-243.
147. M. Iten, H. Mett, A. Evans, J. C. K. Enyaru, R. Brun and R. Kaminsky, *Antimicrob. Agents Chemother.*, 1997, **41**, 1922-1925.
148. G. Priotto, L. Pinoges, I. B. Fursa, B. Burke, N. Nicolay, G. Grillet, C. Hewison and M. Balasegaram, *BMJ*, 2008, **336**, 705-708.
149. C. Burri and R. Brun, *Parasitol. Res.*, 2003, **90**, S49-S52.
150. J. Pepin, F. Milord, B. Mpia, F. Meurice, L. Ethier, D. Degroof and H. Bruneel, *Trans. R. Soc. Trop. Med. Hygiene*, 1989, **83**, 514-517.

151. S. M. Townson, P. F. L. Boreham, P. Upcroft and J. A. Upcroft, *Acta Trop.*, 1994, **56**, 173-194.
152. S. Bisser, F. X. N'Siesi, V. Lejon, P. M. Preux, S. Van Nieuwenhove, C. M. M. Bilenge and P. Buscher, *J. Infect. Dis.*, 2007, **195**, 322-329.
153. G. Priotto, S. Kasparian, D. Ngouama, S. Ghorashian, U. Arnold, S. Ghabri and U. Karunakara, *Clin. Infect. Dis.*, 2007, **45**, 1435-1442.
154. P. P. Simarro, A. Diarra, J. A. R. Postigo, J. R. Franco and J. G. Jannin, *PLoS Negl. Trop. Dis.*, 2011, **5**, e1007.
155. F. Checchi, P. Piola, H. Ayikoru, F. Thomas, D. Legros and G. Priotto, *PLoS Negl. Trop. Dis.*, 2007, **1**, e64.
156. G. Priotto, S. Kasparian, W. Mutombo, D. Ngouama, S. Ghorashian, U. Arnold, S. Ghabri, E. Baudin, V. Buard, S. Kazadi-Kyanza, M. Ilunga, W. Mutangala, G. Pohlig, C. Schmid, U. Karunakara, E. Torreele and V. Kande, *Lancet*, 2009, **374**, 56-64.
157. E. Alirol, D. Schrumpf, J. A. Heradi, A. Riedel, C. de Patoul, M. Quere and F. Chappuis, *Clin. Infect. Dis.*, 2013, **56**, 195-203.
158. DNDi, *Human African Trypanosomiasis - Target Product Profile*, http://www.dndi.org/diseases-projects/diseases/hat/target-product-profile.html, (accessed 8th June, 2015).
159. M. Kaiser, L. Maes, L. P. Tadoori, T. Spangenberg and J. R. Ioset, *J. Biomol. Screen.*, 2015, **20**, 634-645.
160. P. Trouiller, P. Olliaro, E. Torreele, J. Orbinski, R. Laing and N. Ford, *Lancet*, 2002, **359**, 2188-2194.
161. B. Pedrique, N. Strub-Wourgaft, C. Some, P. Olliaro, P. Trouiller, N. Ford, B. Pecoul and J. H. Bradol, *Lancet Glob. Health*, 2013, **1**, e371-e379.
162. DNDi, *London Declaration on Neglected Tropical Diseases*, http://www.dndi.org/images/stories/press_kit/PressRoom/NTDs/NTD_Event_London_Declaration.pdf, (accessed 13th June, 2015).
163. P. H. Jakobsen, M. W. Wang and S. Nwaka, *PLoS Negl. Trop. Dis.*, 2011, **5**, e1221.
164. J. L. W. Thudichum, *Treatise on the Chemical Constitution of the Brain*, Bailliere, Tindall and Cox, London, 1884.
165. A. H. Merrill, M. D. Wang, M. Park and M. C. Sullards, *Trends Biochem. Sci.*, 2007, **32**, 457-468.
166. K. A. Karlsson, *Lipids*, 1970, **5**, 878-891.
167. C. Bure, J. L. Cacas, S. Mongrand and J. M. Schmitter, *Anal. Bioanal. Chem.*, 2014, **406**, 995-1010.
168. A. H. Merrill, *J. Biol. Chem.*, 2002, **277**, 25843-25846.
169. A. H. Merrill, *Chem. Rev.*, 2011, **111**, 6387-6422.
170. E. Fahy, S. Subramaniam, H. A. Brown, C. K. Glass, A. H. Merrill, R. C. Murphy, C. R. H. Raetz, D. W. Russell, Y. Seyama, W. Shaw, T. Shimizu, F. Spener, G. van Meer, M. S. VanNieuwenhze, S. H. White, J. L. Witztum and E. A. Dennis, *J. Lipid Res.*, 2005, **46**, 839-861.
171. Y. Hirabayashi, Y. Igarashi and A. H. Merrill, *Sphingolipid Biology*, Springer Science & Business Media, 2007.
172. W. Godchaux, III and E. R. Leadbetter, *J. Bacteriol.*, 1980, **144**, 592-602.
173. A. A. Hicks, P. P. Pramstaller, A. Johansson, V. Vitart, I. Rudan, P. Ugocsai, Y. Aulchenko, C. S. Franklin, G. Liebisch, J. Erdmann, I. Jonasson, I. V. Zorkoltseva, C. Pattaro, C. Hayward, A. Isaacs, C. Hengstenberg, S. Campbell, C. Gnewuch, A. C. J. W. Janssens, A. V. Kirichenko, I. R. Koenig, F. Marroni, O. Polasek, A. Demirkan, I. Kolcic, C. Schwienbacher, W. Igl, Z. Biloglav, J. C.

M. Witteman, I. Pichler, G. Zaboli, T. I. Axenovich, A. Peters, S. Schreiber, H. E. Wichmann, H. Schunkert, N. Hastie, B. A. Oostra, S. H. Wild, T. Meitinger, U. Gyllensten, C. M. van Duijn, J. F. Wilson, A. Wright, G. Schmitz and H. Campbell, *PLoS Genetics*, 2009, **5**, e1000672.
174. J. T. Hannich, K. Umebayashi and H. Riezman, *Cold Spring Harb. Perspect. Biol.*, 2011, **3**, a004762.
175. W. H. Wilson, D. C. Schroeder, M. J. Allen, M. T. G. Holden, J. Parkhill, B. G. Barrell, C. Churcher, N. Harnlin, K. Mungall, H. Norbertczak, M. A. Quail, C. Price, E. Rabbinowitsch, D. Walker, M. Craigon, D. Roy and P. Ghazal, *Science*, 2005, **309**, 1090-1092.
176. D. A. Brown and E. London, *J. Biol. Chem.*, 2000, **275**, 17221-17224.
177. B. Ramstedt and J. P. Slotte, *FEBS Lett.*, 2002, **531**, 33-37.
178. F. J. Alvarez, L. M. Douglas and J. B. Konopka, *Eukaryot. Cell*, 2007, **6**, 755-763.
179. D. A. Brown and E. London, *J. Memb. Biol.*, 1998, **164**, 103-114.
180. K. Simons and E. Ikonen, *Nature*, 1997, **387**, 569-572.
181. M. D. Ledesma, K. Simons and C. G. Dotti, *Proc. Natl. Acad. Sci. USA*, 1998, **95**, 3966-3971.
182. D. A. Brown, *Int. J. Med. Microbiol.*, 2002, **291**, 433-437.
183. D. W. Shi, X. D. Lv, Z. Zhang, X. F. Yang, Z. C. Zhou, L. Zhang and Y. Zhao, *J. Biol. Chem.*, 2013, **288**, 12605-12614.
184. I. A. Prior and J. F. Hancock, *J. Cell Sci.*, 2001, **114**, 1603-1608.
185. E. E. Prieschl and T. Baumruker, *Immunol. Today*, 2000, **21**, 555-560.
186. Y. Li, S. Li, X. Qin, W. Hou, H. Dong, L. Yao and L. Xiong, *Cell Death Dis.*, 2014, **5**, e1245.
187. A. Huwiler, T. Kolter, J. Pfeilschifter and K. Sandhoff, *Biochim. Biophys. Acta*, 2000, **1485**, 63-99.
188. Y. A. Hannun and L. M. Obeid, *Nat. Rev. Mol. Cell Biol.*, 2008, **9**, 139-150.
189. N. Bartke and Y. A. Hannun, *J. Lipid Res.*, 2009, **50**, S91-S96.
190. R. Tidhar and A. H. Futerman, *Biochim. Biophys. Acta Mol. Cell Res.*, 2013, **1833**, 2511-2518.
191. M. F. Rutti, S. Richard, A. Penno, A. von Eckardstein and T. Hornemann, *J. Lipid Res.*, 2009, **50**, 1237-1244.
192. R. Berkey, D. Bendigeri and S. Y. Xiao, *Front. Plant Sci.*, 2012, **3**, a22.
193. L. A. Cowart and L. M. Obeid, *Biochim. Biophys. Acta Mol. Cell Biol. Lipids*, 2007, **1771**, 421-431.
194. Z. Li, T. K. Hailemariam, H. Zhou, Y. Li, D. C. Duckworth, D. A. Peake, Y. Zhang, M.-S. Kuo, G. Cao and X.-C. Jiang, *Biochim. Biophys. Acta Mol. Cell Biol. Lipids*, 2007, **1771**, 1186-1194.
195. M. Koval and R. E. Pagano, *Biochim. Biophys. Acta*, 1991, **1082**, 113-125.
196. P. W. Denny, H. Shams-Eldin, H. P. Price, D. F. Smith and R. T. Schwarz, *J. Biol. Chem.*, 2006, **281**, 28200-28209.
197. R. L. Lester and R. C. Dickson, *Adv. Lipid Res.*, 1993, **26**, 253-274.
198. N. H. Georgopapadakou, *Exp. Opin. Invest. Drugs*, 2000, **9**, 1787-1796.
199. K. Takesako, K. Ikai, F. Haruna, M. Endo, K. Shimanaka, E. Sono, T. Nakamura, I. Kato and H. Yamaguchi, *J. Antibiot.*, 1991, **44**, 919-924.
200. S. A. Heidler and J. A. Radding, *Antimicrob. Agents Chemother.*, 1995, **39**, 2765-2769.
201. T. Hashida-Okado, A. Ogawa, M. Endo, R. Yasumoto, K. Takesako and I. Kato, *Mol. Gen. Genet.*, 1996, **251**, 236-244.

202. M. M. Nagiec, E. E. Nagiec, J. A. Baltisberger, G. B. Wells, R. L. Lester and R. C. Dickson, *J. Biol. Chem.*, 1997, **272**, 9809-9817.
203. S. A. Heidler and J. A. Radding, *Biochim. Biophys. Acta Mol. Basis Dis.*, 2000, **1500**, 147-152.
204. D. W. Waggoner, J. Xu, I. Singh, R. Jasinska, Q. X. Zhang and D. N. Brindley, *Biochim. Biophys. Acta Mol. Cell Biol. Lipids*, 1999, **1439**, 299-316.
205. S. M. Mandala, R. A. Thornton, J. Milligan, M. Rosenbach, M. Garcia-Calvo, H. G. Bull, G. Harris, G. K. Abruzzo, A. M. Flattery, C. J. Gill, K. Bartizal, S. Dreikorn and M. B. Kurtz, *J. Biol. Chem.*, 1998, **273**, 14942-14949.
206. S. M. Mandala, R. A. Thornton, M. Rosenbach, J. Milligan, M. Garcia-Calvo, H. G. Bull and M. B. Kurtz, *J. Biol. Chem.*, 1997, **272**, 32709-32714.
207. S. A. Young, J. G. Mina, P. W. Denny and T. K. Smith, *Biochem. Res. Int.*, 2012, **2012**, a248135.
208. P. G. M. Wuts, L. J. Simons, B. P. Metzger, R. C. Sterling, J. L. Slightom and A. P. Elhammer, *ACS Med. Chem. Lett.*, 2015, **6**, 645-649.
209. K. Huitema, J. van den Dikkenberg, J. Brouwers and J. C. M. Holthuis, *EMBO J.*, 2004, **23**, 33-44.
210. V. Mandlik, S. Shinde, A. Chaudhary and S. Singh, *Integr. Biol.*, 2012, **4**, 1130-1142.
211. M. A. Goren, B. G. Fox and J. D. Bangs, *Biochemistry*, 2011, **50**, 8853-8861.
212. J. G. M. Mina, PhD Thesis, Durham University, 2010.
213. Y. J. Sigal, M. I. McDermott and A. J. Morris, *Biochem. J.*, 2005, **387**, 281-293.
214. J. G. Mina, J. A. Mosely, H. Z. Ali, P. W. Denny and P. G. Steel, *Org. Biomol. Chem.*, 2011, **9**, 1823-1830.
215. F. G. Tafesse, P. Ternes and J. C. M. Holthuis, *J. Biol. Chem.*, 2006, **281**, 29421-29425.
216. A. K. Tanaka, V. B. Valero, H. K. Takahashi and A. H. Straus, *J. Antimicrob. Chemother.*, 2007, **59**, 487-492.
217. J. G. Mina, S.-Y. Pan, N. K. Wansadhipathi, C. R. Bruce, H. Shams-Eldin, R. T. Schwarz, P. G. Steel and P. W. Denny, *Mol. Biochem. Parasitol.*, 2009, **168**, 16-23.
218. P. M. Adcock, P. Pastor, F. Medley, J. E. Patterson and T. V. Murphy, *J. Infect. Dis.*, 1998, **178**, 577-580.
219. S. Buffet-Bataillon, P. Tattevin, M. Bonnaure-Mallet and A. Jolivet-Gougeon, *Int. J. Antimicrob. Ag.*, 2012, **39**, 381-389.
220. S. M. Paul, D. S. Mytelka, C. T. Dunwiddie, C. C. Persinger, B. H. Munos, S. R. Lindborg and A. L. Schacht, *Nat. Rev. Drug Disc.*, 2010, **9**, 203-214.
221. J. Y. Chien, S. Friedrich, M. A. Heathman, D. P. de Alwis and V. Sinha, *AAPS J.*, 2005, **7**, e544-e559.
222. M. Hay, D. W. Thomas, J. L. Craighead, C. Economides and J. Rosenthal, *Nat. Biotechnol.*, 2014, **32**, 40-51.
223. J. Bibette, *Proc. Natl. Acad. Sci. USA*, 2012, **109**, 649-650.
224. G. Takatsky, *Kiserl. Orvostud.*, 1950, **5**, 393-397.
225. J. W. Noah, *Int. J. High Throughput Screen.*, 2010, **1**, 141-149.
226. BioTek, *BioTek History Timeline*, http://www.biotek.com/about/timeline.html, (accessed 13th June, 2015).
227. T. Ferragamo and M. J. Wildey, *J. Biomol. Screen.*, 1999, **4**, 175.
228. SLAS, *For Microplates - Footprint Dimensions*, http://www.slas.org/default/assets/File/ANSI_SLAS_1-2004_FootprintDimensions.pdf, (accessed 13th June, 2015).

229. SLAS, *For Microplates - Height Dimensions*, http://www.slas.org/default/assets/File/ANSI_SLAS_2-2004_HeightDimensions.pdf, (accessed 13th June, 2015).
230. SLAS, *For Microplates - Bottom Outside Flange Dimensions*, http://www.slas.org/default/assets/File/ANSI_SLAS_3-2004_BottomOutsideFlangeDimensions.pdf, (accessed 13th June, 2015).
231. SLAS, *For Microplates - Well Positions*, http://www.slas.org/default/assets/File/ANSI_SLAS_4-2004_WellPositions.pdf, (accessed 13th June, 2015).
232. B. Lloyd, J. Burrin, P. Smythe and K. Alberti, *Clin. Chem.*, 1978, **24**, 1724-1729.
233. E. W. Holmes, J. Fareed and E. W. Bermes, *Clin. Chem.*, 1981, **27**, 816-818.
234. P. Hodder, R. Mull, J. Cassaday, K. Berry and B. Strulovici, *J. Biomol. Screen.*, 2004, **9**, 417-426.
235. L. M. Mayr and D. Bojanic, *Curr. Opin. Pharmacol.*, 2009, **9**, 580-588.
236. R. P. Hertzberg and A. J. Pope, *Curr. Opin. Chem. Biol.*, 2000, **4**, 445-451.
237. J. A. Frearson and I. T. Collie, *Drug Disc. Today*, 2009, **14**, 1150-1158.
238. R. Brenk, A. Schipani, D. James, A. Krasowski, I. H. Gilbert, J. Frearson and P. G. Wyatt, *ChemMedChem*, 2008, **3**, 435-444.
239. J. A. Frearson, S. Brand, S. P. McElroy, L. A. T. Cleghorn, O. Smid, L. Stojanovski, H. P. Price, M. L. S. Guther, L. S. Torrie, D. A. Robinson, I. Hallyburton, C. P. Mpamhanga, J. A. Brannigan, A. J. Wilkinson, M. Hodgkinson, R. Hui, W. Qiu, O. G. Raimi, D. M. F. van Aalten, R. Brenk, I. H. Gilbert, K. D. Read, A. H. Fairlamb, M. A. J. Ferguson, D. F. Smith and P. G. Wyatt, *Nature*, 2010, **464**, 728-732.
240. J. Inglese, R. L. Johnson, A. Simeonov, M. Xia, W. Zheng, C. P. Austin and D. S. Auld, *Nat. Chem. Biol.*, 2007, **3**, 466-479.
241. G. M. Keseru and G. M. Makara, *Nat. Rev. Drug Disc.*, 2009, **8**, 203-212.
242. C. Delvecchio, J. Tiefenbach and H. M. Krause, *Assay Drug Dev. Technol.*, 2011, **9**, 354-361.
243. J. Lee, D. W. Jung, W. H. Kim, J. I. Um, S. H. Yim, W. K. Oh and D. R. Williams, *ACS Chem. Biol.*, 2013, **8**, 1803-1814.
244. S. C. Baraban, M. T. Dinday and G. A. Hortopan, *Nat. Comm.*, 2013, **4**, a2410.
245. J. L. Shepard, J. F. Amatruda, H. M. Stern, A. Subramanian, D. Finkelstein, J. Ziai, K. R. Finley, K. L. Pfaff, C. Hersey, Y. Zhou, B. Barut, M. Freedman, C. Lee, J. Spitsbergen, D. Neuberg, G. Weber, T. R. Golub, J. N. Glickman, J. L. Kutok, J. C. Aster and L. I. Zon, *Proc. Natl. Acad. Sci. USA*, 2005, **102**, 13194-13199.
246. I. Gashaw, P. Ellinghaus, A. Sommer and K. Asadullah, *Drug Disc. Today*, 2011, **16**, 1037-1043.
247. R. Macarron and R. P. Hertzberg, *Mol. Biotechnol.*, 2011, **47**, 270-285.
248. J. A. Frearson, P. G. Wyatt, I. H. Gilbert and A. H. Fairlamb, *Trends Parasitol.*, 2007, **23**, 589-595.
249. A. C. Cheng, R. G. Coleman, K. T. Smyth, Q. Cao, P. Soulard, D. R. Caffrey, A. C. Salzberg and E. S. Huang, *Nat. Biotechnol.*, 2007, **25**, 71-75.
250. P. Schmidtke and X. Barril, *J. Med. Chem.*, 2010, **53**, 5858-5867.
251. T. Liu and R. B. Altman, *CPT Pharmacometrics Syst. Pharmacol.*, 2014, **3**, e93.
252. T. A. Halgren, *J. Chem. Inf. Model.*, 2009, **49**, 377-389.
253. I. Moraes, G. Evans, J. Sanchez-Weatherby, S. Newstead and P. D. S. Stewart, *Biochim. Biophys. Acta Biomembranes*, 2014, **1838**, 78-87.
254. W. Faulkner and L. Borella, *J. Immunol.*, 1970, **105**, 786-790.

255. N. Miyazaki, H. Ohkura, N. Kajimura and N. Okazaki, *Human Cell*, 1993, **6**, 114-120.
256. K. Steger, J. Brady, W. L. Wang, M. Duskin, K. Donato and M. Peshwa, *J. Biomol. Screen.*, 2015, **20**, 545-551.
257. J. H. Toney, A. Ogawa, M. Blair and Y. W. Park, *Assay Drug Dev. Technol.*, 2003, **1**, 521-525.
258. E. England, P. Newton, F. Neal, L. Kitching, C. Colley and C. J. Rossant, *J. Biomol. Screen.*, 2015, **20**, 536-544.
259. C. Eggeling, L. Brand, D. Ullmann and S. Jager, *Drug Disc. Today*, 2003, **8**, 632-641.
260. R. Sink, S. Gobec, S. Pecar and A. Zega, *Curr. Med. Chem.*, 2010, **17**, 4231-4255.
261. N. Thorne, D. S. Auld and J. Inglese, *Curr. Opin. Chem. Biol.*, 2010, **14**, 315-324.
262. A. Simeonov, A. Jadhav, C. J. Thomas, Y. H. Wang, R. L. Huang, N. T. Southall, P. Shinn, J. Smith, C. P. Austin, D. S. Auld and J. Inglese, *J. Med. Chem.*, 2008, **51**, 2363-2371.
263. R. Hopkins, D. Esposito and W. Gillette, *J. Struct. Biol.*, 2010, **172**, 14-20.
264. S. Schlegel, A. Hjelm, T. Baumgarten, D. Vikstrom and J. W. de Gier, *Biochim. Biophys. Acta Mol. Cell Res.*, 2014, **1843**, 1739-1749.
265. S. L. McGovern, E. Caselli, N. Grigorieff and B. K. Shoichet, *J. Med. Chem.*, 2002, **45**, 1712-1722.
266. R. M. Reguera, E. Calvo-Alvarez, R. Alvarez-Velilla and R. Balana-Fouce, *Int. J. Parasitol. Drugs Drug Resist.*, 2014, **4**, 355-357.
267. D. C. Swinney and J. Anthony, *Nat. Rev. Drug Disc.*, 2011, **10**, 507-519.
268. K. S. Schroeder and B. D. Neagle, *J. Biomol. Screen.*, 1996, **1**, 75-80.
269. P. Coward, S. D. H. Chan, H. G. Wada, G. M. Humphries and B. R. Conklin, *Anal. Biochem.*, 1999, **270**, 242-248.
270. K. L. Whiteaker, S. M. Gopalakrishnan, D. Groebe, C. C. Shieh, U. Warrior, D. J. Burns, M. J. Coghlan, V. E. Scott and M. Gopalakrishnan, *J. Biomol. Screen.*, 2001, **6**, 305-312.
271. S. M. Gopalakrishnan, B. Mammen, M. Schmidt, B. Otterstaetter, W. Amberg, W. Wernet, J. L. Kofron, D. J. Burns and U. Warrior, *J. Biomol. Screen.*, 2005, **10**, 46-55.
272. J. Qian, C. H. Zhou, Z. Qian, F. J. Nan and Q. Z. Ye, *Acta Pharmacol. Sin.*, 2001, **22**, 821-826.
273. F. M. Balis, *J. Natl. Cancer Inst.*, 2002, **94**, 78-79.
274. J. Drewe and S. X. Cai, *Exp. Opin. Drug Disc.*, 2010, **5**, 583-596.
275. T. Spangenberg, J. N. Burrows, P. Kowalczyk, S. McDonald, T. N. C. Wells and P. Willis, *PLoS One*, 2013, **8**, e62906.
276. I. Pena, M. P. Manzano, J. Cantizani, A. Kessler, J. Alonso-Padilla, A. I. Bardera, E. Alvarez, G. Colmenarejo, I. Cotillo, I. Roquero, F. de Dios-Anton, V. Barroso, A. Rodriguez, D. W. Gray, M. Navarro, V. Kumar, A. Sherstnev, D. H. Drewry, J. R. Brown, J. M. Fiandor and J. J. Martin, *Sci. Rep.*, 2015, **5**, a8771.
277. J. Oeljeklaus, F. Kaschani and M. Kaiser, *Angew. Chem. Int. Ed.*, 2013, **52**, 1368-1370.
278. W. Zheng, N. Thorne and J. C. McKew, *Drug Disc. Today*, 2013, **18**, 1067-1073.
279. Y. Fang, A. G. Frutos and R. Verklereen, *Comb. Chem. High Throughput Screen.*, 2008, **11**, 357-369.

280. R. Zhang and X. Xie, *Acta Pharmacol. Sin.*, 2012, **33**, 372-384.
281. A. E. Eakin, R. Nievesalicea, R. Tosadoacevedo, M. S. Chin, C. C. Wang and S. P. Craig, *Antimicrob. Agents Chemother.*, 1995, **39**, 620-625.
282. W. J. Netzer and F. U. Hartl, *Nature*, 1997, **388**, 343-349.
283. P. W. Denny and P. G. Steel, *J. Biomol. Screen.*, 2015, **20**, 56-63.
284. T. Munder and A. Hinnen, *Appl. Microbiol. Biotechnol.*, 1999, **52**, 311-320.
285. R. D. Klein, M. A. Favreau, S. J. AlexanderBowman, S. C. Nulf, L. Vanover, C. A. Winterrowd, N. Yarlett, M. Martinez, J. S. Keithly, M. R. Zantello, E. M. Thomas and T. G. Geary, *Exp. Parasitol.*, 1997, **87**, 171-184.
286. E. Bilsland, P. Pir, A. Gutteridge, A. Johns, R. D. King and S. G. Oliver, *PLoS Negl. Trop. Dis.*, 2011, **5**, e1320.
287. E. Bilsland, A. Sparkes, K. Williams, H. J. Moss, M. de Clare, P. Pir, J. Rowland, W. Aubrey, R. Pateman, M. Young, M. Carrington, R. D. King and S. G. Oliver, *Open Biol.*, 2013, **3**, a120158.
288. S. Kurtz, G. X. Luo, K. M. Hahnenberger, C. Brooks, O. Gecha, K. Ingalls, K. I. Numata and M. Krystal, *Antimicrob. Agents Chemother.*, 1995, **39**, 2204-2209.
289. O. Middendorp, C. Ortler, U. Neumann, P. Paganetti, U. Luthi and A. Barberis, *Biochim. Biophys. Acta*, 2004, **1674**, 29-39.
290. J. L. Norcliffe, E. Alvarez-Ruiz, J. J. Martin-Plaza, P. G. Steel and P. W. Denny, *Parasitology*, 2014, **141**, 8-16.
291. M. Klumpp, A. Boettcher, D. Becker, G. Meder, J. Blank, L. Leder, M. Forstner, J. Ottl and L. M. Mayr, *J. Biomol. Screen.*, 2006, **11**, 617-633.
292. L. M. Mayr and P. Fuerst, *J. Biomol. Screen.*, 2008, **13**, 443-448.
293. O. Motabar, Z. Shi, E. Goldin, K. Liu, N. Southall, E. Sidransky, C. P. Austin, G. L. Griffiths and W. Zheng, *Anal. Biochem.*, 2009, **390**, 79-84.
294. S. Isken, A. Derks, P. F. G. Wolffs and J. A. M. de Bont, *Appl. Environ. Microbiol.*, 1999, **65**, 2631-2635.
295. I. Coma, L. Clark, E. Diez, G. Harper, J. Herranz, G. Hofmann, M. Lennon, N. Richmond, M. Valmaseda and R. Macarron, *J. Biomol. Screen.*, 2009, **14**, 66-76.
296. C. B. Maddox, L. Rasmussen and E. L. White, *J. Assoc. Lab. Autom.*, 2008, **13**, 168-173.
297. Shayne, Cox and Gad, *Development of Therapeutic Agents Handbook*, Wiley, 2011.
298. D. J. Urban, W. Zheng, O. Goker-Alpan, A. Jadhav, M. E. LaMarca, J. Inglese, E. Sidransky and C. P. Austin, *Comb. Chem. High Throughput Screen.*, 2008, **11**, 817-824.
299. J. H. Zhang, T. D. Y. Chung and K. R. Oldenburg, *J. Biomol. Screen.*, 1999, **4**, 67-73.
300. M. S. Rogers, L. M. Cryan, K. A. Habeshian, L. Bazinet, T. P. Caldwell, P. C. Ackroyd and K. A. Christensen, *PLoS One*, 2012, **7**, e39911.
301. PerkinElmer, *Scintillation Proximity Assay (SPA): Custom Assay Development and Membrane Validation*, http://www.perkinelmer.co.uk/content/featured/gpcrnews/200803/PE_SPA_AppNote_r4.pdf, (accessed 19th June, 2015).
302. P. J. Brescia Jr. and P. Banks, *Automation of a Generic Fluorescent Methyltransferase Activity Assay*, http://www.biotek.com/assets/tech_resources/Transcreener_EPIGEN_App_Note.pdf, (accessed 19th June, 2015).
303. B. Neumann, M. Held, U. Liebel, H. Erfle, P. Rogers, R. Pepperkok and J. Ellenberg, *Nat. Methods*, 2006, **3**, 385-390.

304. J. H. Zhang, T. D. Y. Chung and K. R. Oldenburg, *J. Comb. Chem.*, 2000, **2**, 258-265.
305. Z. Wu, D. Liu and Y. Sui, *J. Biomol. Screen.*, 2008, **13**, 159-167.
306. C. Brideau, B. Gunter, B. Pikounis and A. Liaw, *J. Biomol. Screen.*, 2003, **8**, 634-647.
307. T. Y. Shun, J. S. Lazo, E. R. Sharlow and P. A. Johnston, *J. Biomol. Screen.*, 2011, **16**, 1-14.
308. F. Parham, C. Austin, N. Southall, R. Huang, R. Tice and C. Portier, *J. Biomol. Screen.*, 2009, **14**, 1216-1227.
309. R. Hamid, Y. Rotshteyn, L. Rabadi, R. Parikh and P. Bullock, *Toxicol. In Vitro*, 2004, **18**, 703-710.
310. W. M. Lee, *New Engl. J. Med.*, 2003, **349**, 474-485.
311. B. K. Park, N. R. Kitteringham, J. L. Maggs, M. Pirmohamed and D. P. Williams, *Annu. Rev. Pharmacol. Toxicol.*, 2005, **45**, 177-202.
312. C. A. Lipinski, F. Lombardo, B. W. Dominy and P. J. Feeney, *Adv. Drug Del. Rev.*, 1997, **23**, 3-25.
313. T. I. Oprea, A. M. Davis, S. J. Teague and P. D. Leeson, *J. Chem. Inf. Comp. Sci.*, 2001, **41**, 1308-1315.
314. R. W. Spencer, *Biotechnol. Bioeng.*, 1998, **61**, 61-67.
315. R. Macarron, *Drug Disc. Today*, 2006, **11**, 277-279.
316. J. Hert, J. J. Irwin, C. Laggner, M. J. Keiser and B. K. Shoichet, *Nat. Chem. Biol.*, 2009, **5**, 479-483.
317. S. Fox, S. Farr-Jones, L. Sopchak, A. Boggs and J. Comley, *J. Biomol. Screen.*, 2004, **9**, 354-358.
318. A. M. Davis, D. J. Keeling, J. Steele, N. P. Tomkinson and A. C. Tinker, *Curr. Top. Med. Chem.*, 2005, **5**, 421-439.
319. F. E. Koehn, *Prog. Drug Res.*, 2008, **65**, 210.
320. J. G. Mina, J. A. Mosely, H. Z. Ali, H. Shams-Eldin, R. T. Schwarz, P. G. Steel and P. W. Denny, *Int. J. Biochem. Cell Biol.*, 2010, **42**, 1553-1561.
321. J. G. Mina, Y. Okada, N. K. Wansadhipathi-Kannangara, S. Pratt, H. Shams-Eldin, R. T. Schwarz, P. G. Steel, T. Fawcett and P. W. Denny, *Plant Mol. Biol.*, 2010, **73**, 399-407.
322. E. S. Sevova, M. A. Goren, K. J. Schwartz, F. F. Hsu, J. Turk, B. G. Fox and J. D. Bangs, *J. Biol. Chem.*, 2010, **285**, 20580-20587.
323. Agilent, *pESC Yeast Epitope Tagging Vectors*, http://www.chem.agilent.com/Library/usermanuals/Public/217451.pdf, (accessed 7th August, 2015).
324. W. M. Wang, X. H. Yang, S. Tangchaiburana, R. Ndeh, J. E. Markham, Y. Tsegaye, T. M. Dunn, G. L. Wang, M. Bellizzi, J. F. Parsons, D. Morrissey, J. E. Bravo, D. V. Lynch and S. Y. Xiao, *Plant Cell*, 2008, **20**, 3163-3179.
325. J. D. Boeke, J. Trueheart, G. Natsoulis and G. R. Fink, *Methods Enzymol.*, 1987, **154**, 164-175.
326. N. Wansadhipathi-Kannangara, PhD Thesis, Durham University, 2011.
327. K. Sato, Y. Noda and K. Yoda, *Mol. Biol. Cell*, 2009, **20**, 4444-4457.
328. P. A. Aeed, C. L. Young, M. M. Nagiec and A. P. Elhammer, *Antimicrob. Agents Chemother.*, 2009, **53**, 496-504.
329. V. J. Cid, A. M. Alvarez, A. I. Santos, C. Nombela and M. Sanchez, *Yeast*, 1994, **10**, 747-756.
330. F. del Rey, T. Santos, I. Garciaacha and C. Nombela, *J. Bacteriol.*, 1979, **139**, 924-931.
331. *US Pat.*, US20060293354A1, 2006.

332. *US Pat.*, US20100048639A1, 2010.
333. P. G. Lord and A. E. Wheals, *J. Cell Sci.*, 1981, **50**, 361-376.
334. T. Schneider-Poetsch, J. H. Ju, D. E. Eyler, Y. J. Dang, S. Bhat, W. C. Merrick, R. Green, B. Shen and J. O. Liu, *Nature Chem. Biol.*, 2010, **6**, 209-217.
335. D. A. Abbott, R. M. Zelle, J. T. Pronk and A. J. A. van Maris, *FEMS Yeast Res.*, 2009, **9**, 1123-1136.
336. J. M. Alvarez-Pez, L. Ballesteros, E. Talavera and J. Yguerabide, *J. Phys. Chem. A*, 2001, **105**, 6320-6332.
337. IDBS, *ActivityBase Suite: Successful, Proven, Trusted Data Management*, http://www.idbs.com/pdfs/IDBS%20ActivityBase%20Suite%2010_lo.pdf, (accessed 24th July, 2015).
338. P. D. Leeson and B. Springthorpe, *Nat. Rev. Drug Disc.*, 2007, **6**, 881-890.
339. D. Butina, *J. Chem. Inf. Comput. Sci.*, 1999, **39**, 747-750.
340. B. Page, M. Page and C. Noel, *Int. J. Oncol.*, 1993, **3**, 473-476.
341. M. De Rycker, I. Hallyburton, J. Thomas, L. Campbell, S. Wyllie, D. Joshi, S. Cameron, I. H. Gilbert, P. G. Wyatt, J. A. Frearson, A. H. Fairlamb and D. W. Gray, *Antimicrob. Agents Chemother.*, 2013, **57**, 2913-2922.
342. R. H. Glew, A. K. Saha, S. Das and A. T. Remaley, *Microbiol. Rev.*, 1988, **52**, 412-432.
343. J. J. Castilla, M. Sanchezmoreno, C. Mesa and A. Osuna, *Mol. Cell. Biochem.*, 1995, **142**, 89-97.
344. W. W. Zhang, L. I. McCall and G. Matlashewski, *Eukaryot. Cell*, 2013, **12**, 70-77.
345. D. P. Aden, A. Fogel, S. Plotkin, I. Damjanov and B. B. Knowles, *Nature*, 1979, **282**, 615-616.
346. J. Sahi, S. Grepper and C. Smith, *Curr. Drug Disc. Technol.*, 2010, **7**, 188-198.
347. L. Ballell, R. H. Bates, R. J. Young, D. Alvarez-Gomez, E. Alvarez-Ruiz, V. Barroso, D. Blanco, B. Crespo, J. Escribano, R. Gonzalez, S. Lozano, S. Huss, A. Santos-Villarejo, J. J. Martin-Plaza, A. Mendoza, M. J. Rebollo-Lopez, M. Remuinan-Blanco, J. L. Lavandera, E. Perez-Herran, F. J. Gamo-Benito, J. F. Garcia-Bustos, D. Barros, J. P. Castro and N. Cammack, *ChemMedChem*, 2013, **8**, 313-321.
348. R. J. Young, D. V. S. Green, C. N. Luscombe and A. P. Hill, *Drug Disc. Today*, 2011, **16**, 822-830.
349. A. Moreau, M. Le Vee, E. Jouan, Y. Parmentier and O. Fardel, *Fundam. Clin. Pharmacol.*, 2011, **25**, 743-752.
350. S. Tsuchiya, M. Yamabe, Y. Yamaguchi, Y. Kobayashi, T. Konno and K. Tada, *Int. J. Cancer*, 1980, **26**, 171-176.
351. M. Castagna, Y. Takai, K. Kaibuchi, K. Sano, U. Kikkawa and Y. Nishizuka, *J. Biol. Chem.*, 1982, **257**, 7847-7851.
352. W. Chanput, J. J. Mes and H. J. Wichers, *Int. Immunopharmacol.*, 2014, **23**, 37-45.
353. S. Patterson and S. Wyllie, *Trends Parasitol.*, 2014, **30**, 289-298.
354. K. Zhang, M. Showalter, J. Revollo, F. F. Hsu, J. Turk and S. M. Beverley, *EMBO J.*, 2003, **22**, 6016-6026.
355. P. W. Denny, D. Goulding, M. A. J. Ferguson and D. F. Smith, *Mol. Microbiol.*, 2004, **52**, 313-327.
356. E. P. A. Neve, E. Eliasson, M. A. Pronzato, E. Albano, U. Marinari and M. Ingelman-Sundberg, *Arch. Biochem. Biophys.*, 1996, **333**, 459-465.
357. F. P. Guengerich, *Chem. Res. Toxicol.*, 2008, **21**, 70-83.

358. L. A. McLaughlin, M. J. I. Paine, C. A. Kemp, J. D. Marechal, J. U. Flanagan, C. J. Ward, M. J. Sutcliffe, G. C. K. Roberts and C. R. Wolf, *J. Biol. Chem.*, 2005, **280**, 38617-38624.
359. C. Bissantz, B. Kuhn and M. Stahl, *J. Med. Chem.*, 2010, **53**, 5061-5084.
360. S. Gupta and Nishi, *Ind. J. Med. Res.*, 2011, **133**, 27-39.
361. A. Nieto, G. Dominguez-Bernal, J. A. Orden, R. De La Fuente, N. Madrid-Elena and J. Carrion, *Vet. Res.*, 2011, **42**, e13.
362. D. J. Bradley and J. Kirkley, *Trans. R. Soc. Trop. Med. Hyg.*, 1972, **66**, 527-528.
363. S. Brand, N. R. Norcross, S. Thompson, J. R. Harrison, V. C. Smith, D. A. Robinson, L. S. Torrie, S. P. McElroy, I. Hallyburton, S. Norval, P. Scullion, L. Stojanovski, F. R. C. Simeons, D. van Aalten, J. A. Frearson, R. Brenk, A. H. Fairlamb, M. A. J. Ferguson, P. G. Wyatt, I. H. Gilbert and K. D. Read, *J. Med. Chem.*, 2014, **57**, 9855-9869.
364. J. K. Singh, A. Solanki and V. S. Shirsath, *J. Drug. Metab. Toxicol.*, 2012, **3**, e1000126.
365. P. R. O. de Montellano, *Chem. Rev.*, 2010, **110**, 932-948.
366. L. M. Hjelmeland, L. Aronow and J. R. Trudell, *Biochem. Biophys. Res. Comm.*, 1977, **76**, 541-549.
367. V. Yardley and S. L. Croft, *Int. J. Antimicrob. Agents*, 2000, **13**, 243-248.
368. M. Wenzel, *J. Label. Compd. Radiopharm.*, 1989, **27**, 1143-1155.
369. D. J. Kushner, A. Baker and T. G. Dunstall, *Can. J. Phys. Pharmacol.*, 1999, **77**, 79-88.
370. H. Z. Ali, C. R. Harding and P. W. Denny, *Biochem. Res. Int.*, 2012, **2012**, 691363-691363.
371. F. F. Fleming, L. H. Yao, P. C. Ravikumar, L. Funk and B. C. Shook, *J. Med. Chem.*, 2010, **53**, 7902-7917.
372. S. L. Cockroft, J. Perkins, C. Zonta, H. Adams, S. E. Spey, C. M. R. Low, J. G. Vinter, K. R. Lawson, C. J. Urch and C. A. Hunter, *Org. Biomol. Chem.*, 2007, **5**, 1062-1080.
373. E. Couplan, R. S. Aiyar, R. Kucharczyk, A. Kabala, N. Ezkurdia, J. Gagneur, R. P. St Onge, B. Salin, F. Soubigou, M. Le Cann, L. M. Steinmetz, J.-P. di Rago and M. Blondel, *Proc. Natl. Acad. Sci. USA*, 2011, **108**, 11989-11994.
374. X. Q. Zhang, D. L. Smith, A. B. Merlin, S. Engemann, D. E. Russel, M. Roark, S. L. Washington, M. M. Maxwell, J. L. Marsh, L. M. Thompson, E. E. Wanker, A. B. Young, D. E. Housman, G. P. Bates, M. Y. Sherman and A. G. Kazantsev, *Proc. Natl. Acad. Sci. USA*, 2005, **102**, 892-897.
375. O. Ceyhan, K. Birsoy and C. S. Hoffman, *Chem. Biol.*, 2012, **19**, 155-163.
376. Y. G. Shi, *Cell*, 2014, **159**, 995-1014.
377. Y. J. Jia, M. Kai, I. Wada, F. Sakane and H. Kanoh, *FEBS Lett.*, 2003, **552**, 240-246.
378. J. W. Newman, C. Morisseau, T. R. Harris and B. D. Hammock, *Proc. Natl. Acad. Sci. USA*, 2003, **100**, 1558-1563.
379. L. Oster, S. Tapani, Y. Xue and H. Kack, *Drug Disc. Today*, 2015, **20**, 1104-1111.
380. J. M. Figueiredo, W. B. Dias, L. Mendonca-Previato, J. O. Previato and N. Heise, *Biochem. J.*, 2005, **387**, 519-529.
381. M. M. Bradford, *Anal. Biochem.*, 1976, **72**, 248-254.

Appendix A

Assay Optimisation Matrices

1. Galactose Concentration

		Sugar Concentrations / %												
	Raffinose:	1	1	1	1	1	1	1	1	1	0	0	0	
	Galactose:	10	5	2.5	1.25	0.63	0.31	0.16	0.08	0	0	0	0	
	Glucose:	0	0	0	0	0	0	0	0	0	2.5	5	10	
Test Compound Concentration / µM	0													H
	0													G
	0.010													F
	0.039													E
	0.156													D
	0.625													C
	2.5													B
	10													A
		1	2	3	4	5	6	7	8	9	10	11	12	

The layout of the 96-well plates used to determine the optimal galactose concentration, with sugar concentration gradients across the columns and compound concentration gradient down the rows. Row H is a control row with no yeast cells.

2. FDGlu and Culture Concentration (12 by 12)

Starting Culture Concentration / OD_{600}	FDGlu Concentration / µM												
	20.0	16.0	12.8	10.2	8.2	6.6	5.2	4.2	3.4	2.7	2.2	1.7	
0.125													A
0.100													B
0.080													C
0.064													D
0.051													E
0.041													F
0.033													G
0.026													H
0.021													I
0.017													J
0.013													K
0.011													L
	1	2	3	4	5	6	7	8	9	10	11	12	
	13	14	15	16	17	18	19	20	21	22	23	24	

The layout of the matrix to determine the optimal FDGlu and starting yeast culture concentrations, with an FDGlu gradient across the columns and a starting culture concentration down the rows. The matrix was prepared in duplicate in low volume 384-well plates, with the matrix in A1−L12 and repeated in A13−L24.

3. FDGlu and Culture Concentration (5 by 5)

Starting Culture Concentration / OD_{600}	FDGlu Concentration / µM					
	20	10	5	2.5	0	
0.125						A
0.063						B
0.031						C
0.016						D
0.000						E
	1	2	3	4	5	
	11	12	13	14	15	

The layout of the second matrix to determine the optimal FDGlu and starting yeast culture concentrations, with an FDGlu gradient across the columns and a starting culture concentration down the rows. The matrix was prepared in duplicate in low volume 384-well plates, with the matrix in A1−E5 and repeated in A11−E15.

4. Z′ Optimisation

Starting Culture Conditions		Conditions tested across entire row	
20/0.031	-		A−D
	AmB		E−H
	Cycloheximide		I−L
			M−P
10/0.063	-		Q−T
	AmB		U−X
	Cycloheximide		Y−BB
		1−48	

Starting Culture Conditions		Conditions tested across entire row	
20/0.031	-		A−D
	Suloctidil		E−H
	Clemastine		I−L
			M−P
10/0.063	-		Q−T
	Suloctidil		U−X
	Clemastine		Y−BB
		1−48	

The layout of the plates to determine which conditions produced the optimal Z′ for the HTS assay. Each set of conditions was tested across 4 rows, resulting in 192 data points. Each plate was tested using both fresh and frozen yeast culture. AmB and cycloheximide were tested at 10 µM, as this was shown to be effective in the assay to determine optimal galactose concentration, whilst suloctidil and clemastine, which were previously untested against yeast, were tested at 100 µM.

Appendix B

L. major Growth Curves

1. *L. major* FV1 24 hours

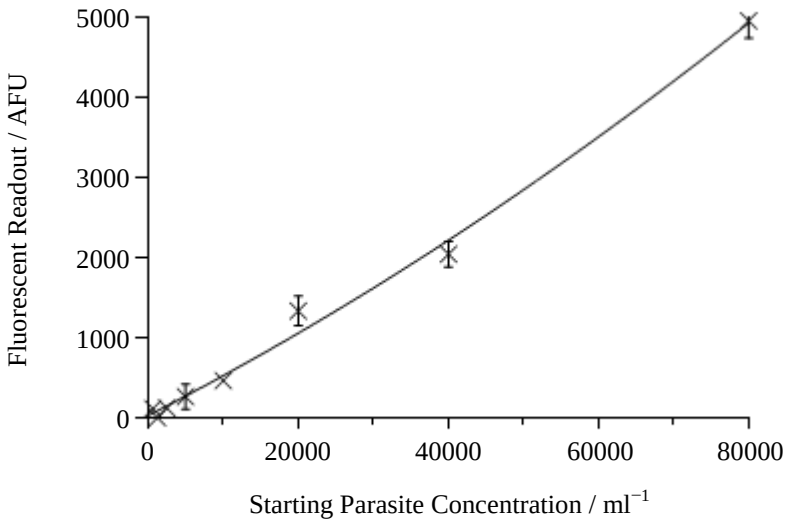

The fluorescence readout produced by various starting concentrations of *L. major* FV1 parasites following a 24 hour incubation period and 4 hours treatment with AlamarBlue®. Error bars show the standard error of the mean for an octuplet set of data.

2. *L. major* FV1 48 hours

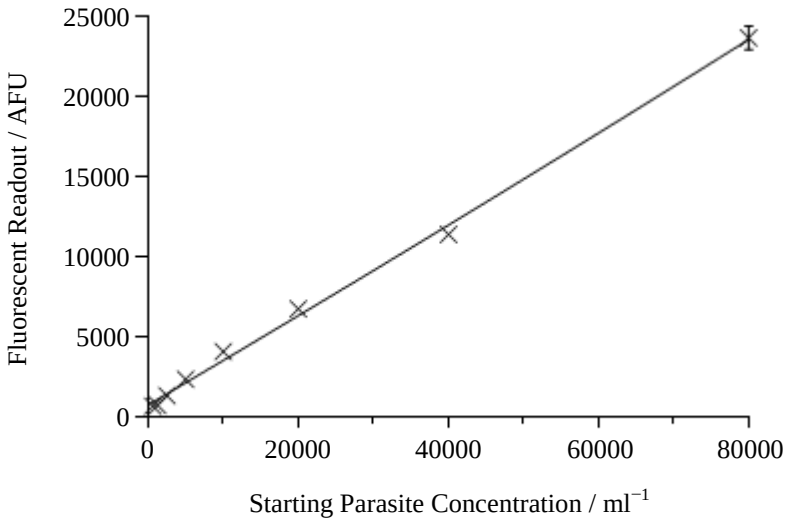

The fluorescence readout produced by various starting concentrations of *L. major* FV1 parasites following a 48 hour incubation period and 4 hours treatment with AlamarBlue®. Error bars show the standard error of the mean for an octuplet set of data.

3. *L. major* FV1 72 hours

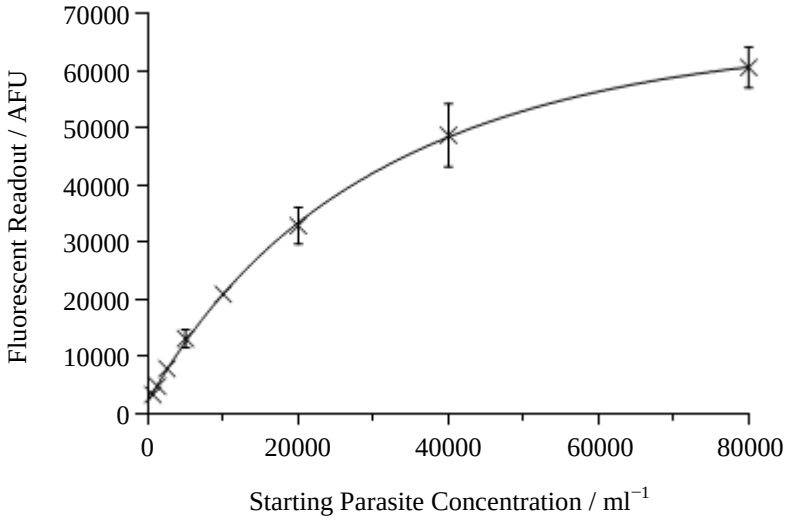

The fluorescence readout produced by various starting concentrations of *L. major* FV1 parasites following a 72 hour incubation period and 4 hours treatment with AlamarBlue®. Error bars show the standard error of the mean for an octuplet set of data.

4. *L. major lcb2Δ* 72 hours

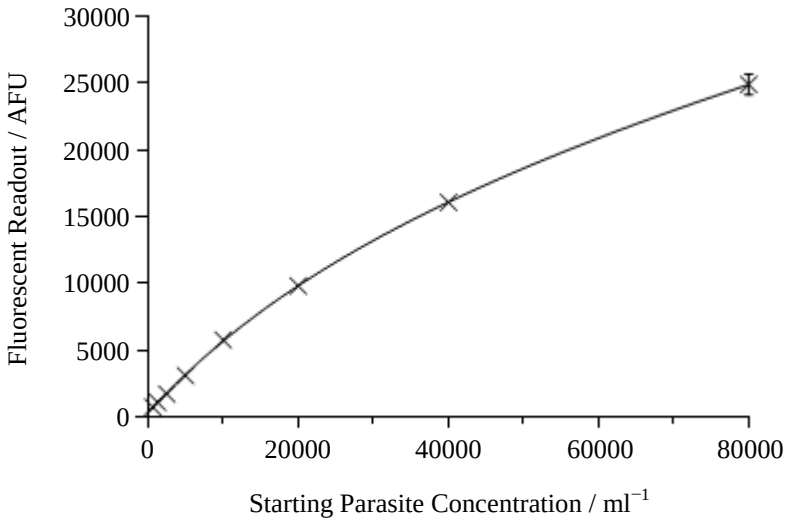

The fluorescence readout produced by various starting concentrations of *L. major lcb2Δ* parasites following a 72 hour incubation period and 8 hours treatment with AlamarBlue®. Error bars show the standard error of the mean for an octuplet set of data.

Appendix C

Benzazepane SAR Data

Compound Code	Thesis Number	Structure	Biochem pIC_{50}	*L. major* FV1 pED50	*L. major* *lcb2Δ* pED_{50}	*L. donovani* InMac pED_{50}	THP-1 pED_{50}	pSI (InMac over THP-1)	PFI
SB-762123-AAA	**29**	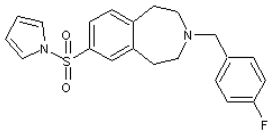	6.1	5.8	5.7	5.0	4.6	0.4	11.0
VAPT/8555/172/3	**30**	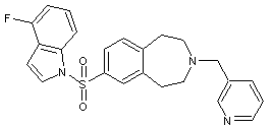	5.7	5.7	5.4	4.7	4.5	0.2	10.7
VAPT/8576/13/3	**34**	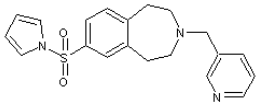	4.2	5.6	5.1	6.3	5.0	1.3	8.4
VAPT/8555/173/1	**35**	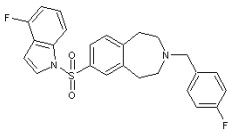	6.0	5.7	≤ 5.0	4.7	≤ 4.3	0.4	12.8
VAPT/8559/99/2	**36**	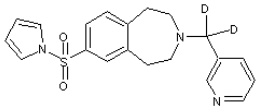	4.2	5.7	5.2	6.4	5.0	1.4	8.3
CS100138-022A11	**37**	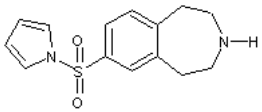	≤ 4.0	≤ 5.0	≤ 5.0	5.3	≤ 4.3	1.0	4.1
VAPT/8559/137/1	**38**	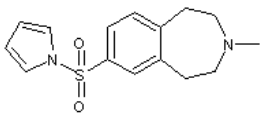	4.6	≤ 5.0	≤ 5.0	5.7	5.0	0.7	5.6

Compound Code	Thesis Number	Structure	Biochem pIC_{50}	*L. major* FV1 pED50	*L. major* *lcb2Δ* pED_{50}	*L. donovani* InMac pED_{50}	THP-1 pED_{50}	pSI (InMac over THP-1)	PFI
VAPT/8559/131/1	**39**	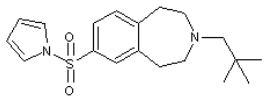	4.2	5.7	5.1	6.1	≤ 4.3	1.8	11.4
VAPT/8576/45/1	**40**	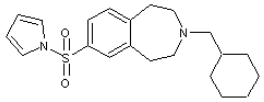	5.5	6.3	5.6	5.7	5.0	0.7	11.2
VAPT/8576/59/1	**41**	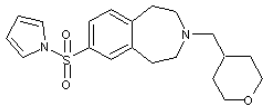	≤ 4.0	6.1	≤ 5.0	5.7	5.2	0.5	8.1
VAPT/8559/135/1	**42**	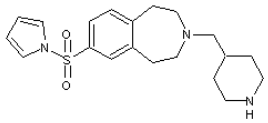	4.9	5.5	5.9	6.9	5.2	1.7	N/A
CS100462-069A11B15	**43**	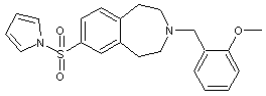	≤ 4.0	≤ 5.0	≤ 5.0	6.2	4.7	1.5	10.2
CS100462-069A11B24	**44**	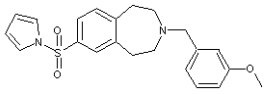	≤ 4.0	≤ 5.0	≤ 5.0	5.2	4.4	0.8	10.6
CS100462-069A11B18	**45**	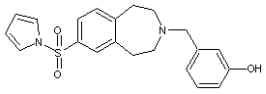	≤ 4.0	≤ 5.0	≤ 5.0	7.0	4.5	2.5	8.7

Compound Code	Thesis Number	Structure	Biochem pIC_{50}	*L. major* FV1 pED50	*L. major* *lcb2Δ* pED_{50}	*L. donovani* InMac pED_{50}	THP-1 pED_{50}	pSI (InMac over THP-1)	PFI
CS100462-069A11B23	**46**	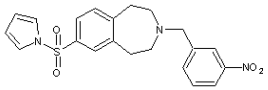	4.4	6.0	5.2	5.2	≤ 4.3	0.9	10.5
CS100462-069A11B17	**47**	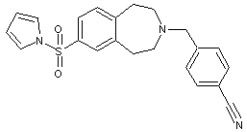	≤ 4.0	6.6	5.8	7.3	≤ 4.3	3.0	10.1
CS100462-069A11B11	**48**	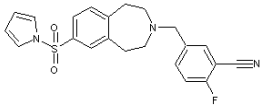	≤ 4.0	6.1	5.3	6.5	4.6	1.9	10.3
VAPT/8559/141/1	**49**	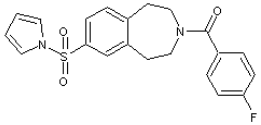	≤ 4.0	≤ 5.0	≤ 5.0	4.9	≤ 4.3	0.6	8.7
VAPT/8559/143/1	**50**	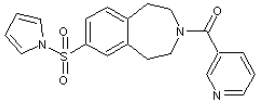	≤ 4.0	≤ 5.0	≤ 5.0	5.4	4.8	0.6	7.0
VAPT/8559/175/1	**51**	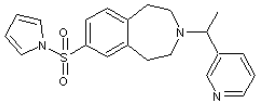	≤ 4.0	5.4	5.6	5.0	5.2	−0.2	9.0
VAPT/8559/153/2	**52**	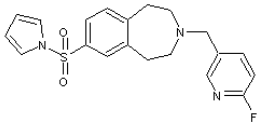	≤ 4.0	6.4	5.5	6.0	5.1	0.9	9.4

Compound Code	Thesis Number	Structure	Biochem pIC_{50}	*L. major* FV1 pED50	*L. major* *lcb2Δ* pED_{50}	*L. donovani* InMac pED_{50}	THP-1 pED_{50}	pSI (InMac over THP-1)	PFI
VAPT/8559/155/1	**53**	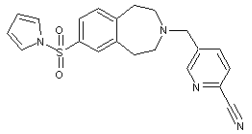	≤ 4.0	6.1	6.1	6.9	5.1	1.8	9.2
CS100462-069A11B3	**54**	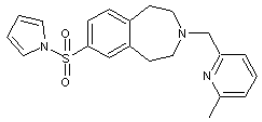	≤ 4.0	≤ 5.0	≤ 5.0	5.4	≤ 4.3	1.1	9.2
VAPT/8559/159/3	**55**	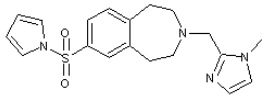	≤ 4.0	5.8	6.4	6.4	5.1	1.3	7.8
VAPT/8559/165/4	**56**	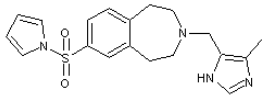	≤ 4.0	5.7	6.1	6.8	5.4	1.4	6.2
CS100462-069A12B9	**57**	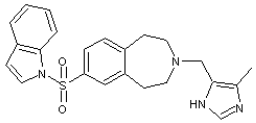	≤ 4.0	5.7	6.1	6.6	4.4	2.2	8.2
CS100462-069A15B9	**58**	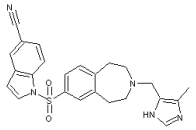	≤ 4.0	5.6	6.1	5.7	4.4	1.3	7.9
CS100462-069A14B1	**59**	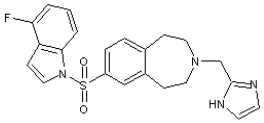	≤ 4.0	5.5	5.6	5.2	4.5	0.7	9.0

Compound Code	Thesis Number	Structure	Biochem pIC_{50}	*L. major* FV1 pED50	*L. major* *lcb2Δ* pED_{50}	*L. donovani* InMac pED_{50}	THP-1 pED_{50}	pSI (InMac over THP-1)	PFI
CS100462-069A20B1	**60**	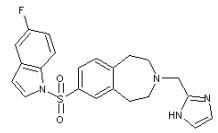	≤ 4.0	5.3	5.4	5.1	4.7	0.4	8.8
VAPT/8576/67/2	**61**	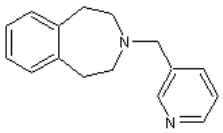	≤ 4.0	≤ 5.0	≤ 5.0	≤ 4.3	≤ 4.3	0.0	6.7
JS49295-116A1	**62**	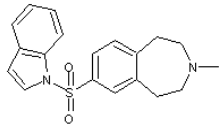	≤ 4.0	≤ 5.0	≤ 5.0	4.7	≤ 4.3	0.4	7.8
DS204111-095A8B2C2	**63**	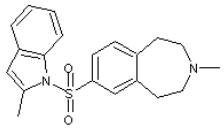	≤ 4.0	≤ 5.0	≤ 5.0	6.4	4.9	1.5	8.5
ED101676-149A1	**64**	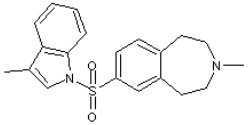	≤ 4.0	≤ 5.0	≤ 5.0	5.7	4.6	1.1	8.5
CR102479-047A1	**65**	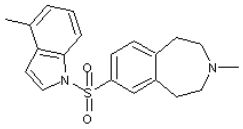	≤ 4.0	≤ 5.0	≤ 5.0	5.5	4.6	0.9	8.5
CR102479-047A2	**66**	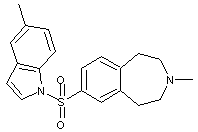	≤ 4.0	≤ 5.0	≤ 5.0	5.5	4.7	0.8	8.6

Compound Code	Thesis Number	Structure	Biochem pIC_{50}	*L. major* FV1 pED50	*L. major* *lcb2Δ* pED_{50}	*L. donovani* InMac pED_{50}	THP-1 pED_{50}	pSI (InMac over THP-1)	PFI
DS204111-095A12B2C2	**67**	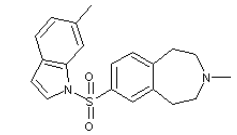	4.9	≤ 5.0	≤ 5.0	6.2	4.8	1.4	8.5
DS204111-095A11B2C2	**68**	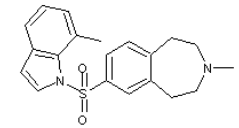	≤ 4.0	6.0	5.2	6.0	4.7	1.3	8.5
ED101676-193A1	**69**	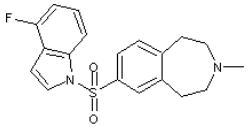	≤ 4.0	≤ 5.0	≤ 5.0	5.7	4.7	1.0	8.4
VAPT/8576/41/1	**70**	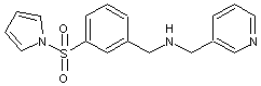	≤ 4.0	≤ 5.0	≤ 5.0	≤ 4.3	≤ 4.3	0.0	7.1
VAPT/8562/139/1	**71**	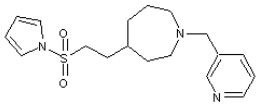	≤ 4.0	6.1	5.4	6.3	≤ 4.3	2.0	6.0

Appendix D

Publication

The utility of yeast as a tool for cell-based, target-directed high-throughput screening

J. L. NORCLIFFE[1], E. ALVAREZ-RUIZ[2], J. J. MARTIN-PLAZA[2], P. G. STEEL[1]* *and* P. W. DENNY[1,3]*

[1] *Department of Chemistry and School of Biological Sciences, Biophysical Sciences Institute, University Science Laboratories, South Road, Durham, DH1 3LE*
[2] *GlaxoSmithKline, Platform Technologies and Science, Parque Tecnologico de Madrid, 28760 Tres Cantos, Madrid, Spain*
[3] *School of Medicine, Pharmacy and Health, Durham University, Queen's Campus, Stockton-on-Tees, TS17 6BH, UK*

(*Received 28 December 2012; revised 12 March 2013; accepted 23 March 2013; first published online 24 April 2013*)

SUMMARY

Many Neglected Tropical Diseases (NTDs) have recently been subject of increased focus, particularly with relation to high-throughput screening (HTS) initiatives. These vital endeavours largely rely of two approaches, *in vitro* target-directed screening using biochemical assays or cell-based screening which takes no account of the target or targets being hit. Despite their successes both of these approaches have limitations; for example, the production of soluble protein and a lack of cellular context or the problems and expense of parasite cell culture. In addition, both can be challenging to miniaturize for ultra (u)HTS and expensive to utilize. Yeast-based systems offer a cost-effective approach to study and screen protein targets in a direct-directed manner within a eukaryotic cellular context. In this review, we examine the utility and limitations of yeast cell-based, target-directed screening. In particular we focus on the currently under-explored possibility of using such formats in uHTS screening campaigns for NTDs.

Key words: Yeast, HTS, NTDs.

INTRODUCTION

Over the last few decades high-throughput screening (HTS) has become one of, if not the most important strategy for the discovery of new drug leads. HTS can be undertaken on a number of levels, ranging from individual proteins through unicellular systems, e.g. yeast, to multicellular organisms such as zebrafish embryos and nematode worms. Each has their benefits and in this review we will discuss the utility of yeast-based approaches in HTS, with special focus on their potential to be used in the search for much needed novel anti-parasitics, including those for so-called Neglected Tropical Diseases (NTDs) such as leishmaniasis and other kinetoplastid infections, Human African Trypanosomiasis (Sleeping Sickness) and Chagas Disease (WHO, 2012*a*).

HIGH-THROUGHPUT SCREENING – A BRIEF OVERVIEW

One of the major technological advances arising from the advent of genomics and combinatorial chemistry approaches to drug discovery was the development of HTS. This is a process in which large numbers of compounds are rapidly ($\geqslant$ 100 000/day) tested for biological activity. In general HTS assay formats can be divided into two types, *in vitro* biochemical and cell-based assays. The former are generally simpler and more specific whilst the latter more challenging but give greater content and context (An and Tolliday, 2010).

For automated HTS, *in vitro* biochemical assays must negate the need for substrate-product separation and produce a readily detectable and quantifiable signal (fluorescence, radiochemical etc). This requires purified, active and soluble protein. In contrast, cell-based platforms do not require purified target protein and can be engineered to produce a simple, measurable readout of cellular processes for HTS (Barberis *et al*. 2005). Furthermore, in these formats the activity of any compound against a specific target is analysed in a cellular context that more closely resembles the *in vivo* scenario, for example the requirement of an inhibitor to cross the plasma membrane and reach an intracellular target. Finally, a well controlled cell-based HTS can identify those compounds that are generically cytotoxic or may exhibit problems with stability or solubility *in vivo*. As such, and compared with *in vitro* biochemical assay platforms, cell-based assays have the potential to identify compounds with drug-like properties which are ready for further development. See Table 1 for a summary of the advantages and disadvantages for each approach.

* Corresponding authors: Department of Chemistry, Biophysical Sciences Institute, Durham, DH1 3LE, UK. Tel: +44 (0)191 334 3983. Fax: +44 (0)191 334 2051. E-mail: p.w.denny@durham.ac.uk, E-mail: p.g.steel@durham.ac.uk. Tel: +44 (0)191 324 2131.

doi:10.1017/S0031182013000425

Table 1. The advantages and disadvantages of the screening platforms employed for anti-parasitic drug discovery.

Platform	*In vitro* HTS	Cellular HTS (parasites)	Yeast-based HTS
Advantages	Possibility of simple, specific and sensitive assay system Facilitates SAR based on molecular recognition of the target	Does not require purified target Provides specific cellular context allowing early selection of drug-like compounds Naïve approach challenging all targets at once in an unbiased manner	Does not require purified target Provides axenic eukaryotic cellular context allowing early selection of drug-like compounds Ease of manipulation and speed of growth Straightforward genetic manipulation for generic assay platform Ease of discrimination of false positive hits Low cost of culture
Disadvantages	Requires purified target, limiting assay of hard to purify/assay targets such as transmembrane enzymes Expensive due to necessity for protein purification etc Requirement for suitable substrates	Relatively insensitive due to drug pumps and membrane barriers Expensive or inability to culture relevant lifecycle stages Limitations in genetic manipulation for assay platform Assays currently rely on non-target specific, phenotypic output SAR is not assisted by target knowledge. Target deconvolution is approached *a posteriori*	Relatively insensitive due to drug pumps, membrane barriers and the thick cell wall Reliant on the ability of an heterologous protein to be functional in an axenic system Target protein is tested in a non-native cellular milieu

To replicate physiological conditions as accurately as possible cell-based assays should ideally be performed using the target cell of interest, for example protozoan pathogens for NTDs or mammalian cells for anti-cancer agents (Simon and Bedalov, 2004). However, protozoan parasites can be both difficult and expensive to culture and genetically manipulate compared to model eukaryotes (Limenitakis and Soldati-Favre, 2011). Mammalian cells can pose similar problems and, in addition, the redundancy of processes can confound the read-out of HTS for a specific inhibitor (Barberis *et al*. 2005). Yeast, *Schizosaccharomyces pombe* and particularly *Saccharomyces cerevisiae*, have been established as simple, tractable, highly characterized model eukaryotes (Castrillo and Oliver, 2011). As well as being accessible through a highly developed genetic tool kit, yeast are also relatively fast growing in simple, low-cost (liquid or solid) media with a doubling time of approximately 90 minutes. These features make both of these model species ideal candidates to be employed in HTS for anti-fungals (Hughes, 2002). However, many functions of yeast, protozoan and human cells are conserved, allowing straightforward orthologous expression, complementation by replacement and functional analyses in a simplified system. In addition, processes not found in yeast can be constituted in a heterologous cell by taking advantage of these model systems' wide variety of genetic tools (Munder and Hinnen, 1999). Both of these approaches have been successfully utilized in drug discovery programmes and here we will examine the strengths and limitations of yeast as a screening tool, with particular emphasis on their use for NTD drug discovery (Table 1).

YEAST AS A SUBSTITUTION PLATFORM

Many yeast cell-based assay platforms rely on the substitution of an essential yeast gene with an orthologue from the system of interest (Fig. 1) to constitute a simple growth assay for inhibition. The generation of such hybrid yeast relies on the conservation of protein function between distantly related eukaryotes. This approach has been widely used in the study of parasite (Klein *et al*. 1997; Sibley *et al*. 1997; Bilsland *et al*. 2011) and mammalian proteins (Munder and Hinnen, 1999) through the constitution of phenotypic screening assays. One recent example involved the development of an HTS assay to identify inhibitors of the human acetyl-CoA carboxylase 2 (AAC2) with a view to discovering potential agents for the treatment of obesity (Marjanovic *et al*. 2010). In this example, the *S. cerevisiae* AAC was replaced using homologous recombination by orthologous human AAC 1 and 2, as well as by the corresponding wheat and protozoan (*Toxoplasma gondii*) AACs. Selection of complemented yeast cells was facilitated by placing the inserted AAC under the control of a GAL10 promoter, thereby making the yeast galactose-dependent. Following validation using known AAC inhibitors

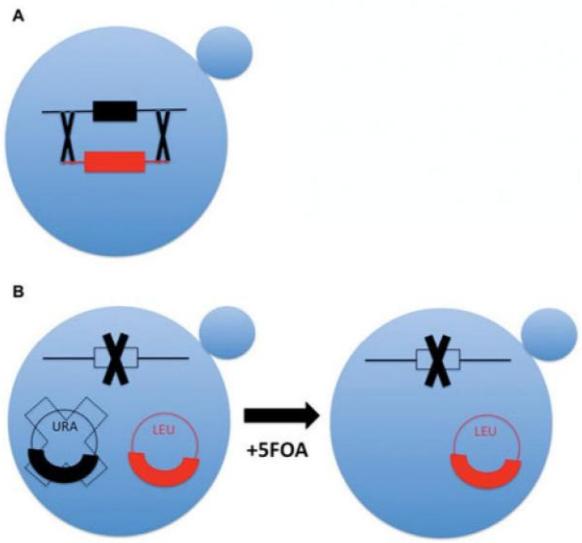

Fig. 1. Substitution platform. In these cases the yeast open reading frame (black) is replaced with a foreign open reading frame (red) encoding an orthologous protein. This can be easily achieved by either direct substitution via homologous recombination incorporating a selectable marker/inducible promoter (A) or, for example, by plasmid shuffle in a knockout yeast line reliant on expression of an essential protein from a uracil selectable plasmid (B). In the presence of 5FOA the ura marker will be selected against allowing a plasmid encoding a functional orthologue of the essential protein to replace it. In both of these cases, for an HTS platform to be constructed, the yeast-encoded protein must be essential and a functional orthologue must be present in the system of interest. A counter-screen, for example against wild type yeast or, better, yeast complemented with the native protein, is essential to identify off target effects causing generic cytotoxicity.

these yeast strains, dependent on human AAC1 and 2, were screened with 34 000 compounds from three libraries in a 96-well plate format where growth was monitored by measuring turbidity at 580–620 nm. The hit rate of this primary screen varied from 0·02% to 3·5% depending on the library source. Some of these were non-selective for AAC2 whilst, importantly, others were shown to be generically toxic in a screen employing wild-type yeast. These counter-screens are vital to maximize target specificity. In addition, Marjanovic *et al.* employed a secondary enzymatic screen to further validate the specificity and selectivity of their hits and identify a small subset of AAC2 specific inhibitors that conform to Lipinski's rule of five criteria for drug-like characteristics (Lipinski *et al.* 2001).

This simple approach of screening for phenotypic changes in a complemented *S. cerevisiae* strain has also been used to identify a novel human K^+ channel inhibitor (Zaks-Makhina *et al.* 2004). An HTS assay was designed where the K^+-dependent growth phenotype of K^+ channel mutants was rescued by mammalian Kir2.1 channel expression. In a 96-well plate format, using turbidity as a growth measure, Zaks-Makhina and colleagues screened a 10 000 compound library selecting those that inhibited Kir2.1-dependent yeast growth at low but not high K^+. This assay allowed the identification of compounds showing non-specific toxicity, as evidenced by inhibition in the presence of both low and high K^+. Through this process, 42 compounds with inhibition >50% and toxicity <20% were selected. As in the example above, a secondary screen was then undertaken to analyse specificity for Kir2.1 over other human and plant K^+ channels. Inhibition of K^+ channels by one of the selected compounds was demonstrated in mammalian cells and this inhibitor was also shown to confer neuroprotection in cultured neuronal cells. This combination of screens, from a large primary effort to a neuronal assay via biochemical and cellular assay, demonstrated the step-wise process that can be employed for lead identification. Starting from a large library, it is possible using a yeast-based approach to quickly identify robust, contextualized hits that can then be rapidly triaged using other, perhaps more labour-intensive, assays.

YEAST AS A LETHAL EXPRESSION PLATFORM

Not all mammalian and protozoan proteins and pathways have functional equivalents in yeast. However, in some cases heterologous expression of these completely foreign proteins in yeast induces measurable phenotypes which can be measured in HTS (Munder and Hinnen, 1999; Simon and Bedalov, 2004). For example, over-expression of influenza virus ion-channel forming protein M2 in *S. cerevisiae* results in growth impairment. Inhibition of M2 rescues this phenotype and this positive readout growth assay has been used in a 96-well plate based assay to identify a novel inhibitor from a library screen that demonstrated anti-viral activity in cell culture (Kurtz *et al.* 1995).

Similarly, using the fission yeast *S. pombe*, the pro-apoptotic HIV-1 protein Vpr has been formatted into 96- and 384-well yeast-based screens (Benko *et al.* 2010). As for the M2 assay, toxic expression was controlled via an inducible promoter and restoration of growth was measured using optical density in a very simple 'mix-and-measure' primary assay requiring no complicated preparation, centrifugation, filtration or extraction (Kurtz *et al.* 1995; Benko *et al.* 2010). Significantly, these yeast constructs were also suitable for the necessary secondary assays. Initially an agar plate-based, semi-quantitative colony-forming test showing dose-dependent effects, and subsequently a fluorescence-based LIVE/DEAD yeast viability assay was utilized as an indicator of the desired anti-apoptotic effect. Whilst agar plate-based systems do not easily lend themselves to high-volume applications, the fluorometric readout of the latter assay could potentially be formatted for HTS.

By the cut-off criteria set by the research team, a screen of a small 2000 compound library gave a single hit from the primary screen. This drug, benfotiamine, showed a dose response effect and suppressed apoptosis in secondary assays, however further analyses are required to fully verify the mode of action (Benko *et al*. 2010).

The two examples above were studies focused on the discovery of anti-viral agents against influenza and HIV respectively. However, the majority of screening programmes employing yeast-based approaches have been directed at human cellular processes (Simon and Bedalov, 2004; Barberis *et al*. 2005). For example, phosphatidylinositol 3-kinase (PI3K) pathway mediates cell transduction via the generation of the second messenger phosphatidyl-3,4,5-*tris*phosphate and inappropriate activation of this pathway is associated with oncogenesis (Wu, 2010). Over-expression of PI3K in *S. cerevisiae* is lethal and, as in the viral examples above, this phenotype was used in an agar plate-based rescue screen – this time against 9600 natural product extracts (Fernandez-Acero *et al*. 2012). Amongst the barriers to the deployment of yeast in HTS is the presence of extremely effective drug efflux systems (Barberis *et al*. 2005). Interestingly Fernandez-Acero and colleagues exploited the genetic tractability of yeast to improve the sensitivity of their platform. Deletion of the efflux pump Snq2 enhanced sensitivity 2-fold in the semi-quantitative assay developed, demonstrating the potential of engineering yeast to optimize their use in HTS. Furthermore, Fernandez-Acero *et al*. found that non-lethal disruption of the plasma membrane through the addition of small quantities (0·0003%) of sodium dodecyl sulphate to the media had a similar 'sensitizing' effect, although the general utility of such chemical approaches in HTS is unclear.

Clearly, the measurement of growth on agar plates (Fernandez-Acero *et al*. 2012) can only be semi-quantitative and most studies measure turbidity of liquid culture in a microtitre plate via optical density. For example, rescue of toxic expression of human p38α, a kinase with major implications in oncogenesis and inflammatory disease (Muller and Knapp, 2010), in *S. cerevisae* was quantified in this way and used in a phenotypic rescue HTS to identify 2 compounds, from a library of 40 000, that restored growth. Both of these inhibited activity in *in vitro* and in mammalian cell secondary assays (Friedmann *et al*. 2006).

In a rather different approach, a heat-sensitive yeast mutant (*fmc1Δ*) has been used to screen 12 000 compounds for entities that reversed an inability to grow with glycerol as the sole carbon source. This relates to a defect in the ATP synthase assembly and as such serves as an effective model for certain mitochondrial diseases e.g. NARP (neuropathy, ataxia and retinitis pigmentosa) (Couplan *et al*. 2011). In their assay platform Couplan and colleagues used filters spotted with each compound to identify those that induced an enhanced halo of growth when placed on solid glycerol medium spread with the yeast strain of interest. This approach was modelled on one developed for yeast-based screening for inhibitors of prion toxicity (Bach *et al*. 2003, 2006). However, here the researchers utilized a yeast prion model which, due to a stop codon read through phenotype, are able to metabolize exogenous adenine. Inhibitors of the formation of the toxic prion protein (PrP^{Sc}, insoluble Sup35p in yeast) lead to the yeast being unable to metabolize adenine and the colonies on the solid media obtained a dark red colour distinguishable from the usual white appearance. Again, these approaches, monitoring growth on solid-media, appear unlikely to lend themselves to true (ultra) HTS for 100 s of thousands of compounds.

These data (Bach *et al*. 2003, 2006; Couplan *et al*. 2011) show that for some processes, the conservation between yeast and the target organism is close enough to allow direct, informative screening against the model system. In addition, it is important to recognize that in all these cases of phenotypic rescue the possibility of generically toxic false positives is removed greatly simplifying the generation and interpretation of data.

YEAST AS A TRANSACTIVATION PLATFORM

In all cases discussed so far the HTS read-out has relied on phenotypic changes, either positive or negative growth, directly resulting from inhibition of a specific function mediated by a specific protein. However, the genetic tractability of yeast allows cells to be engineered so that the HTS read-out is the result of transactivation of another process. A good, and extensive, example of this is provided by the work of the Hoffman laboratory (Boston College) towards the identification of inhibitors of mammalian phosphodiesterases (PDEs) (Demirbas *et al*. 2011). Tissue-specific PDEs (in mammals approximately 100 isoforms encoded by 21 genes) convert cAMP to 5′AMP and cGMP to 5′GMP, serving to regulate the levels of these cyclic secondary messengers which influence a wide variety of cellular processes in a tissue specific manner. Selective inhibition of PDE enzymes has therapeutic potential for a wide range of diseases (Bender and Beavo, 2006; Conti and Beavo, 2007). The basis of the assay designed by Hoffman and colleagues is fission yeast, *S. pombe*, which unlike *S. cerevisiae* can tolerate loss of function mutations of its adenylyl cyclase. These yeast-based assay lines were also engineered to express controllably the selectable marker *ura4*. In the absence of adenylyl cyclase and PDE (Csg2 in yeast) exogenous cAMP or cGMP activates Protein Kinase A (PKA) and *ura4* expression is repressed. Under these conditions the yeast are able to grow in the presence of 5-fluoroorotic

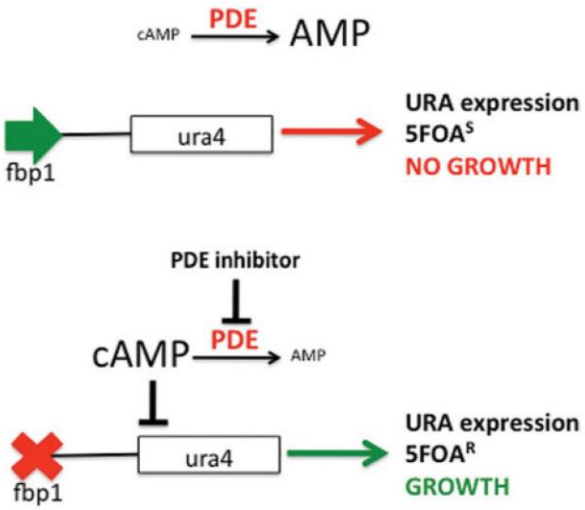

Fig. 2. Transactivation platform. Expression of the fbp1-ura4 reporter in the yeast screening strain is repressed by Protein Kinase A, which is activated by the addition of cAMP (or cGMP) to the media. Hydrolysis of cAMP (or cGMP) by either yeast or human (or protozoan) PDE allows ura4 expression leading to a FOA^S growth phenotype (upper frame). PDE inhibition causes cAMP (or cGMP) to accumulate repressing ura4 expression leading to a $5FOA^R$ phenotype (lower frame). This positive growth readout negates the need for a yeast cytoxicity control as compounds inhibiting growth through off target effects will not be rescued by PDE inhibition.

acid (5FOA), which is converted to toxic fluoro-orotidine monophosphate in the presence of URA4 (Fig. 2). However, expression of either yeast PDE (Csg2) or heterologous (e.g. human) PDE leads to the conversion of cAMP to 5′AMP or cGMP to 5′GMP, expression from *ura4* and 5FOA sensitivity ($5FOA^S$) (Demirbas *et al*. 2011). This system provides an elegant positive selection platform for PDE inhibitors, with inhibition of the enzyme conferring 5FOA resistance ($5FOA^R$) on the yeast (Fig. 2). This robust assay system, measuring growth by optical density in 384-well plates, has been utilized for HTS of compound libraries against several human PDEs. A small subset of compounds (3120, including known PDE inhibitors) were screened against human PDE2A, PDE4A and PDE4B and yeast Cgs2 (Ivey *et al*. 2008). In addition to the known inhibitor controls, several specific inhibitors were identified, with the assay having a hit rate of 0·8% to 3·2%. In a secondary screen, a subset of these compounds demonstrated the ability to raise the level of cellular cAMP, indicating PDE inhibition (Ivey *et al*. 2008). PDE7 has been similarly screened, this time with a library of nearly 50 000 compounds (Alaamery *et al*. 2010). This HTS identified two compound classes conferring the highest growth, i.e. PDE inhibition and rescue. A subset of these demonstrated PDE7 selectivity and activity in an *in vitro* secondary screen. Importantly, one of these potently suppressed TNFα release by LPS-stimulated model macrophage cells indicating a possible anti-inflammatory effect of PDE7 inhibition (Alaamery *et al*. 2010). More recently, a 200 000 member compound collection was screened against PDE11 expressing yeast (Ceyhan *et al*. 2012). Using data from previous screening campaigns to remove non-specific hits, 39 compounds were selected for secondary selectivity and dose-dependency assays; this identified four compounds as potent and highly selective. One of these compounds induced high cAMP levels in a mammalian cell-based assay and the same compound induced cortisol production (associated with PDE11 inactivation) in these cells (Ceyhan *et al*. 2012). Collectively these studies present the largest body of work in the literature describing the use of yeast for cell-based, target-directed HTS. Furthermore, other studies have employed a similar transactivation platform for HTS. Like Hoffman and colleagues, Grozinger *et al*. utilized $5FOA^S$/$5FOA^R$ selection in a screen for inhibitors of *ura3* repression by the yeast transcriptional repressor Sir2p, a NAD-dependent deactylase. However, this study used a negative growth screen in which hits from a small 1600 compound collection were scored for their ability to confer $5FOA^S$, i.e. inhibit Sir2p, to *S. cerevisiae* (Grozinger *et al*. 2001). General cytotoxicity was established against yeast grown without FOA and three compounds were further assessed for their ability to selectively inhibit the activity of the human orthologue, SIRT2.

A direct screen for inhibitors of mammalian protein function, using an alternative transactivation system, is illustrated by a HTS against human β-secretase expressed in *S. cerevisiae* (Middendorp *et al*. 2004). This enzyme drives the production of the Aβ peptides thought to be associated with Alzheimer's disease and therefore inhibitors could have significant medicinal value. Screening was undertaken using a modified yeast strain in which invertase is engineered to only be active and released upon cleavage by human β-secretase (an enzyme not found in yeast). Without intervention the yeast cannot grow in histidine-depleted media with sucrose, as released invertase cleaves sucrose to form glucose which represses the expression of a *HIS3* selectable marker. However, on β-secretase inhibition invertase is not released and the cells are rescued in this positive screen (Middendorp *et al*. 2004). Similarly, again in brewers' yeast, an orphan human G-protein-coupled receptor (GPCR) was coupled to histidine prototrophy. In this case, stimulation of the GPCR facilitated growth in the absence of histidine and a positive read-out assay was then formatted to identify peptide agonists (Klein *et al*. 1997).

Two-hybrid screens also fall into this transactivator class of platform, and although they have not been extensively employed in HTS, they have been used to identify modulators of protein-protein interactions.

The interaction of human calcium channel subunits α1B and β3 has been coupled to a marker conferring cycloheximide sensitivity (Young *et al*. 1998). A screen of >150 000 compounds identified 10 compounds that rescued growth of the α1B and β3 strain, but not a control strain in the presence of cycloheximide. These were subsequently assessed for their ability to modulate calcium channels. Whilst in this screen of calcium channels Young *et al*. monitored growth on agar plates, all the other screens using transactivation systems discussed here employed turbidity measurements which is a more quantitative approach that allows the robustness of the assay to be assessed accurately as discussed below.

YEAST-BASED SCREENING FOR ANTI-PARASITICS

NTDs are caused by a diverse group of 17 infections, 11 of which are caused by protozoan or helminth parasites (WHO, 2012*a*). They are almost exclusively diseases of poverty, affecting a staggering 2·7 billion people who live on less than $2/day. NTDs are endemic in tropical and sub-tropical regions of the developing world, with Africa, Asia and Latin America carrying 90% of the disease burden. In the absence of vaccines many of these parasitic diseases lack adequate therapeutic regimes, with many of the few current drugs being not widely available, costly, and/or exhibiting unacceptable side effects (WHO, 2012*a*). Recently, public-private initiatives have lead to increased focus on NTDs and a renewed drive to discover new and better therapeutic agents (Allarakhia and Ajuwon, 2012; WHO, 2012*b*). Both *in vitro* biochemical (Frearson *et al*. 2010) and parasite cell-based (Siqueira-Neto *et al*. 2012) screening technologies have been deployed in this effort. However, both have limitations and cost implications as discussed above (Table 1). To overcome these and accelerate the process of NTD drug discovery the use of yeast as a screening vehicle may become more prevalent. Examples of all the strategies described above are possible although all the reported approaches, described below, rely on using yeast as a substitution platform.

In 1997, Klein *et al*. described an HTS assay utilizing a *S. cerevisae* ornithine decarboxylase (ODC) mutant complemented by expression of ODC from the nematode worm *Haemonchus contortus*, a major parasite of ruminants (Klein *et al*. 1997). ODC is a key regulatory enzyme in the biosynthesis of polyamines (PA) in eukaryotes, which has been established as an anti-protozoal target with the inhibitor difluoromethylornithine (DFMO; eflornithine) a key treatment for Human African Trypanosomiasis (Heby *et al*. 2007). In contrast to the ODC mutant parent strain, an *H. contortus* ODC-complemented yeast line was able to grow in the absence of exogenous PA (Klein *et al*. 1997). This complemented yeast cell line was utilized in a 96-well plate-based assay to screen 90 000 compounds for their ability to inhibit cell growth (quantified using Alamar Blue) in the absence of PA. The approximate 1% hits of this primary screen were subsequently retested against the same yeast line grown in the presence of PA, when ODC is redundant. This counter-screen identified those compounds that demonstrated general toxicity leaving a single, target-specific hit, stilbamidine isethionate. However, this compound showed no activity against the helminth ODC *in vitro* and was hypothesized to inhibit yeast *S*-adenosylmethionine decarboxylase (SAMdc), an enzyme required for spermidine and spermine synthesis (Klein *et al*. 1997). This exemplifies, in this simple eukaryotic model, the issue of process redundancy discussed above in relation to more complex mammalian cell-based screening.

Until very recently this was the only published yeast-based HTS for anti-parasitics, although the potential of these platforms for this purpose has been recognized with respect to the protozoal acetyl-CoA carboxylase (Marjanovic *et al*. 2010). However, drug sensitivity yeast mutants have been used to identify the primary targets and possible toxic effects of the anti-malarials quinine (Khozoie *et al*. 2009), St. John's Wort (McCue and Phang, 2008) and artemisinin (Li *et al*. 2005). In addition, the use of *S. cerevisiae* as a vehicle for anti-protozoal drug discovery has been explored with drug targets from the causative agent of malaria *Plasmodium falciparum*. *P. falciparum* dihydrofolate reductase (DHFR, essential for thymidine, histidine and methionine synthesis) and topoisomerase II (decatenation of DNA) have both been used to complement corresponding yeast mutants (Sibley *et al*. 1997). This work was recently further developed by Bilsland *et al*. in an exploration of mutant *S. cerevisiae* complemented with DHFR from *P. falciparum, Plasmodium vivax, Leishmania major* (a causative agent of leishmaniasis), *Trypanosoma brucei brucei* (an animal pathogen serving as a model for Human African Trypanosomiasis), *T. cruzi* (Chagas Disease), *Schistosoma mansoni* (schistosomiasis) and *Homo sapiens* (Bilsland *et al*. 2011). In an agar plate-based assay, the well characterized antimalarial pyrimethamine was able to inhibit the growth of yeast complemented with *Plasmodium* DHFR as expected. Notably, complementation with drug-resistant *Plasmodium* DHFR conferred pyrimethamine resistance thus confirming target specificity. All of the other complemented strains demonstrated lower sensitivity to the drug, although sensitivity became more evident on suppression of DHFR expression. Deletion of the major multidrug export pump encoded by *PDR5* also increased the sensitivity of the *T. brucei* DHFR strain to pyrimethamine. This platform was further developed and utilized in HTS applications for specific inhibitors of parasite DHFR, *N*-myristoyltransferase (NMT)

and phosphoglycerate kinase (PGK) (Bilsland *et al.* 2013). Here DHFR, NMT and PGK mutant *S. cerevisiae* were complemented by expression of the fluorescently-tagged parasite orthologues. By using fluorescent protein tags with non-overlapping spectra the assay was multiplexed, allowing for multiple readings to be taken from a single well. This platform was then used, utilizing an automated 384-well protocol, to screen the Maybridge Hitfinder Library (14400 chemically diverse compounds) to identify parasite-specific hits (i.e. those not affecting yeast dependent on expression of the human orthologue). Of the 36 specific hits identified against the kinetoplastid protozoan enzymes (*T. b. brucei, T. cruzi, L. major*), 18 were cytotoxic for *T. b. brucei* in cell culture.

S. cerevisiae have also been employed in the study of the *Leishmania* inositol phosphorylceramide (IPC) synthase, a putative anti-protozoal drug target (Denny *et al.* 2006; Mina *et al.* 2009). Exploiting public-private partnership we have developed and deployed a robust yeast-based, 1536-well formatted assay for ultra (u)HTS (Norcliffe *et al.* unpublished). The uHTS campaign involved the screening of the GSK compound collection, 1·8 million compounds, and is, to the best of our knowledge, the largest yeast-based screen reported to date. IPC synthase is a membrane-bound enzyme with six transmembrane domains that drives the formation of IPC, a non-mammalian phosphosphingolipid and a major component of the parasite plasma membrane. Preliminary studies had led to the development of a 96-well plate-based enzyme assay system that was utilized to define the mode of action of the *Leishmania* IPC synthase (Mina *et al.* 2010) and investigate its substrate binding requirements (Mina *et al.* 2011). However, the complexity of this microsomal assay, with a requirement to separate lipid substrate and product, precluded its employment as a true HTS platform. To facilitate a high volume approach a yeast-based assay was formatted in *S. cerevisiae*, utilizing the ability of the protozoan enzyme to complement for the absence of its functional orthologue AUR1p (Nagiec *et al.* 1997), in which growth could be coupled with a fluorometric output enabling on- and off-target effects to be discriminated. The primary screen was successfully executed with, following initial dose response secondary assays, >500 potent and selective hits identified (0·03% hit rate). Secondary screening is currently underway and the full results of this yeast-based uHTS will be reported in due course.

These results demonstrated the ability to engineer yeast to optimize a robust assay platform and exemplify the utility of this model eukaryote as a vehicle for drug analyses and screening in NTDs, for example with respect to the kinetoplastid protozoa. Consequently, the potential for yeast-based screens to assist in the search for new solutions for NTDs is now well established. Whilst only the substitution approach, in which orthologous enzymes are explored, has been used to date it can only be expected that, with time, the other approaches will become viable. Whilst the development of lethal expression systems for NTD pathogen target screening probably requires further functional analyses of protein function in many of these organisms, the application of transactivation approaches looks much closer. For example, co-expression of human cytomegalovirus (HCMV) protease with an engineered Trp1p enzyme has been used to identify HCMV protease inhibitors that prevent cleavage of Trp1p to stimulate growth in media lacking trytophan (Cottier *et al.* 2006). However, these transactivation technologies could readily to applied to parasite systems provided the knowledge base is there to indicate target protein function, interactions etc. In this respect, building directly on the work of the Hofmann group described above, protozoan PDE orthologues are widely characterized and shown to be essential, putative drug targets in several pathogenic species (Seebeck *et al.* 2011). Consequently there is every prospect of formatting these into the various assay platforms discussed to facilitate the search for novel, selective inhibitors which will act as lead compounds for anti-parasitic drug discovery.

DISCUSSION AND CONCLUSIONS

As evidenced by the results summarized above, yeast-based screening methodologies offer considerable benefits for HTS (Table 1). Cell-based, yet target-directed assays can be readily developed and their eukaryotic nature confers a relevant cellular context not available in highly tractable bacterial systems. Where determined and stated the Z-factors of yeast cell-based, target-directed screens lie well above the generally accepted threshold (0·5) for an excellent, robust assay (Benko *et al.* 2010; Demirbas *et al.* 2011; Fernandez-Acero *et al.* 2012). Most of these screens are relatively simple, using 'mix and measure' approaches with measurement achieved by monitoring yeast growth in liquid media via optical density. Higher content readouts are possible using colour or fluorometric responses and these will continue to add value in the future (Bilsland *et al.* 2013). Importantly, miniaturization is possible with a number of the assays being run in 384-well plate format (Benko *et al.* 2010; Demirbas *et al.* 2011; Bilsland *et al.* 2013); however, further miniaturization to a 1536-well format is desirable for uHTS. Therefore, as discussed, yeast can serve as a cheap, flexible and robust assay platform suitable for miniaturization to facilitate HTS and uHTS. Importantly, as outlined above, all yeast-based HTS must employ panels of counter-screens and secondary assays to rule out off-target effects. In particular, those platforms relying on growth inhibition read-outs are prone to identify

off-target hits and the Molecular Mode of Action (MMoA) must be corroborated (Marjanovic *et al.* 2010).

The ability to screen specifically for target inhibition in a well controlled cellular context, whilst reducing the challenge caused from confounding effects due to pathway redundancies, is further enhanced by the relatively rapid growth of yeast compared with higher eukaryotic cells. As described various assay platforms can be envisaged and the ability to screen 'hard to purify' or 'hard to assay' proteins (e.g. transmembrane enzymes involved in lipid biosynthesis) can be enhanced. However, as with all HTS assay platforms, yeast has limitations. Not least the ability to constitute or substitute heterologous protein function in another organism. In addition, the thick yeast cell wall may serve as a barrier to compounds in a screen and highly expressed efflux pumps may exclude these (Table 1). Whilst both of these can reduce the sensitivity of a given assay, it is evident that engineering the yeast to lack efflux pumps is a viable strategy to increase sensitivity (Bilsland *et al.* 2011; Fernandez-Acero *et al.* 2012).

In summary, it is clear that yeast can serve as a vehicle for HTS of human, viral and protozoan or helminth parasite proteins. In particular, yeast systems appear ideally suited for HTS and much needed drug discovery for the parasites that underlie many of NTDs. Given the robust and reproducible nature of these assay systems, and the facility to further engineer yeast strains to provide greater sensitivity, the use of such platforms is likely to become more commonplace.

AKNOWLEDGEMENTS

We would like to acknowledge the support of the Open Lab Foundation (PWD and PGS). These sponsors also provided financial support.

FINANCIAL SUPPORT

JLN is supported by a Durham Doctoral Fellowship.

REFERENCES

Alaamery, M. A., Wyman, A. R., Ivey, F. D., Allain, C., Demirbas, D., Wang, L., Ceyhan, O. and Hoffman, C. S. (2010). New classes of PDE7 inhibitors identified by a fission yeast-based HTS. *Journal of Biomolecular Screening* **15**, 359–367.

Allarakhia, M. and Ajuwon, L. (2012). Understanding and creating value from open source drug discovery for neglected tropical diseases. *Expert Opinion on Drug Discovery* **7**, 643–657.

An, W. F. and Tolliday, N. (2010). Cell-based assays for high-throughput screening. *Molecular Biotechnology* **45**, 180–186.

Bach, S., Talarek, N., Andrieu, T., Vierfond, J. M., Mettey, Y., Galons, H., Dormont, D., Meijer, L., Cullin, C. and Blondel, M. (2003). Isolation of drugs active against mammalian prions using a yeast-based screening assay. *Nature Biotechnology* **21**, 1075–1081.

Bach, S., Tribouillard, D., Talarek, N., Desban, N., Gug, F., Galons, H. and Blondel, M. (2006). A yeast-based assay to isolate drugs active against mammalian prions. *Methods* **39**, 72–77.

Barberis, A., Gunde, T., Berset, C., Audetat, S. and Luthi, U. (2005). Yeast as a screening tool. *Drug Discovery Today* **2**, 187–192.

Bender, A. T. and Beavo, J. A. (2006). Cyclic nucleotide phosphodiesterases: molecular regulation to clinical use. *Pharmacology Reviews* **58**, 488–520.

Benko, Z., Elder, R. T., Liang, D. and Zhao, R. Y. (2010). Fission yeast as a HTS platform for molecular probes of HIV-1 Vpr-induced cell death. *International Journal of High Throughput Screening* **1**, 151–162.

Bilsland, E., Pir, P., Gutteridge, A., Johns, A., King, R. D. and Oliver, S. G. (2011). Functional expression of parasite drug targets and their human orthologs in yeast. *PLoS Neglected Tropical Diseases* **5**, e1320.

Bilsland, E., Sparks, A., Williams, K., Moss, H. J., de Clare, M., Pir, P., Rowland, J., Aubrey, W., Pateman, R., Young, M., Carrington, M., King, R. D. and Oliver, S. G. (2013). Yeast-based automated high-throughput screens to identify new anti-parasitic leads. *Open Biology* **3**, 120158.

Castrillo, J. I. and Oliver, S. G. (2011). Yeast systems biology: the challenge of eukaryotic complexity. *Methods in Molecular Biology* **759**, 3–28.

Ceyhan, O., Birsoy, K. and Hoffman, C. S. (2012). Identification of biologically active PDE11-selective inhibitors using a yeast-based high-throughput screen. *Chemical Biology* **19**, 155–163.

Conti, M. and Beavo, J. (2007). Biochemistry and physiology of cyclic nucleotide phosphodiesterases: essential components in cyclic nucleotide signaling. *Annual Review of Biochemistry* **76**, 481–511.

Cottier, V., Barberis, A. and Luthi, U. (2006). Novel yeast cell-based assay to screen for inhibitors of human cytomegalovirus protease in a high-throughput format. *Antimicrobial Agents and Chemotherapy* **50**, 565–571.

Couplan, E., Aiyar, R. S., Kucharczyk, R., Kabala, A., Ezkurdia, N., Gagneur, J., St Onge, R. P., Salin, B., Soubigou, F., Le Cann, M., Steinmetz, L. M., di Rago, J. P. and Blondel, M. (2011). A yeast-based assay identifies drugs active against human mitochondrial disorders. *Proceedings of the National Academy of Sciences, USA* **108**, 11989–11994.

Demirbas, D., Ceyhan, O., Wyman, A. R. and Hoffman, C. S. (2011). A fission yeast-based platform for phosphodiesterase inhibitor HTSs and analyses of phosphodiesterase activity. In *Handbook of Experimental Pharmacology* (ed. Hoffmann, F. B.), pp. 135–149. Springer-Verlag, Germany.

Denny, P. W., Shams-Eldin, H., Price, H. P., Smith, D. F. and Schwarz, R. T. (2006). The protozoan inositol phosphorylceramide synthase: A novel drug target which defines a new class of sphingolipid synthase. *Journal of Biological Chemistry* **281**, 28200–28209.

Fernandez-Acero, T., Rodriguez-Escudero, I., Vicente, F., Monteiro, M. C., Tormo, J. R., Cantizani, J., Molina, M. and Cid, V. J. (2012). A yeast-based *in vivo* bioassay to screen for class I phosphatidylinositol 3-kinase specific inhibitors. *Journal of Biomolecular Screening* **17**, 1018–1029.

Frearson, J. A., Brand, S., McElroy, S. P., Cleghorn, L. A., Smid, O., Stojanovski, L., Price, H. P., Guther, M. L., Torrie, L. S., Robinson, D. A., Hallyburton, I., Mpamhanga, C. P., Brannigan, J. A., Wilkinson, A. J., Hodgkinson, M., Hui, R., Qiu, W., Raimi, O. G., van Aalten, D. M., Brenk, R., Gilbert, I. H., Read, K. D., Fairlamb, A. H., Ferguson, M. A., Smith, D. F. and Wyatt, P. G. (2010). N-myristoyltransferase inhibitors as new leads to treat sleeping sickness. *Nature* **464**, 728–732.

Friedmann, Y., Shriki, A., Bennett, E. R., Golos, S., Diskin, R., Marbach, I., Bengal, E. and Engelberg, D. (2006). JX401, A p38alpha inhibitor containing a 4-benzylpiperidine motif, identified via a novel screening system in yeast. *Molecular Pharmacology* **70**, 1395–1405.

Grozinger, C. M., Chao, E. D., Blackwell, H. E., Moazed, D. and Schreiber, S. L. (2001). Identification of a class of small molecule inhibitors of the sirtuin family of NAD-dependent deacetylases by phenotypic screening. *Journal of Biological Chemistry* **276**, 38837–38843.

Heby, O., Persson, L. and Rentala, M. (2007). Targeting the polyamine biosynthetic enzymes: a promising approach to therapy of African sleeping sickness, Chagas' disease, and leishmaniasis. *Amino Acids* **33**, 359–366.

Hughes, T. R. (2002). Yeast and drug discovery. *Functional and Integrative Genomics* **2**, 199–211.

Ivey, F. D., Wang, L., Demirbas, D., Allain, C. and Hoffman, C. S. (2008). Development of a fission yeast-based high-throughput screen to identify chemical regulators of cAMP phosphodiesterases. *Journal of Biomolecular Screening* **13**, 62–71.

Khozoie, C., Pleass, R. J. and Avery, S. V. (2009). The antimalarial drug quinine disrupts Tat2p-mediated tryptophan transport and causes tryptophan starvation. *Journal of Biological Chemistry* **284**, 17968–17974.

Klein, R. D., Favreau, M. A., Alexander-Bowman, S. J., Nulf, S. C., Vanover, L., Winterrowd, C. A., Yarlett, N., Martinez, M., Keithly, J. S., Zantello, M. R., Thomas, E. M. and Geary, T. G.

(1997). *Haemonchus contortus*: cloning and functional expression of a cDNA encoding ornithine decarboxylase and development of a screen for inhibitors. *Experimental Parasitology* **87**, 171–184.

Kurtz, S., Luo, G., Hahnenberger, K. M., Brooks, C., Gecha, O., Ingalls, K., Numata, K. and Krystal, M. (1995). Growth impairment resulting from expression of influenza virus M2 protein in *Saccharomyces cerevisiae*: identification of a novel inhibitor of influenza virus. *Antimicrobial Agents and Chemotherapy* **39**, 2204–2209.

Li, W., Mo, W., Shen, D., Sun, L., Wang, J., Lu, S., Gitschier, J. M. and Zhou, B. (2005). Yeast model uncovers dual roles of mitochondria in action of artemisinin. *PLoS Genetics* **1**, e36.

Limenitakis, J. and Soldati-Favre, D. (2011). Functional genetics in Apicomplexa: potentials and limits. *FEBS Letters* **585**, 1579–1588.

Lipinski, C. A., Lombardo, F., Dominy, B. W. and Feeney, P. J. (2001). Experimental and computational approaches to estimate solubility and permeability in drug discovery and development settings. *Advanced Drug Delivery Reviews* **46**, 3–26.

Marjanovic, J., Chalupska, D., Patenode, C., Coster, A., Arnold, E., Ye, A., Anesi, G., Lu, Y., Okun, I., Tkachenko, S., Haselkorn, R. and Gornicki, P. (2010). Recombinant yeast screen for new inhibitors of human acetyl-CoA carboxylase 2 identifies potential drugs to treat obesity. *Proceedings of the National Academy of Sciences, USA* **107**, 9093–9098.

McCue, P. P. and Phang, J. M. (2008). Identification of human intracellular targets of the medicinal Herb St. John's Wort by chemical-genetic profiling in yeast. *Journal of Agriculture and Food Chemistry* **56**, 11011–11017.

Middendorp, O., Ortler, C., Neumann, U., Paganetti, P., Luthi, U. and Barberis, A. (2004). Yeast growth selection system for the identification of cell-active inhibitors of beta-secretase. *Biochimica et Biophysica Acta* **1674**, 29–39.

Mina, J. G., Mosely, J. A., Ali, H. Z., Denny, P. W. and Steel, P. G. (2011). Exploring *Leishmania major* inositol phosphorylceramide synthase (LmjIPCS): insights into the ceramide binding domain. *Organic and Biomolecular Chemistry* **9**, 1823–1830.

Mina, J. G., Mosely, J. A., Ali, H. Z., Shams-Eldin, H., Schwarz, R. T., Steel, P. G. and Denny, P. W. (2010). A plate-based assay system for analyses and screening of the *Leishmania major* inositol phosphorylceramide synthase. *International Journal of Biochemistry and Cell Biology* **42**, 1553–1561.

Mina, J. G., Pan, S. Y., Wansadhipathi, N. K., Bruce, C. R., Shams-Eldin, H., Schwarz, R. T., Steel, P. G. and Denny, P. W. (2009). The *Trypanosoma brucei* sphingolipid synthase, an essential enzyme and drug target. *Molecular and Biochemical Parasitology* **168**, 16–23.

Muller, S. and Knapp, S. (2010). Targeting kinases for the treatment of inflammatory diseases. *Expert Opinion on Drug Discovery* **5**, 867–881.

Munder, T. and Hinnen, A. (1999). Yeast cells as tools for target-oriented screening. *Applied Microbiology and Biotechnology* **52**, 311–320.

Nagiec, M. M., Nagiec, E. E., Baltisberger, J. A., Wells, G. B., Lester, R. L. and Dickson, R. C. (1997). Sphingolipid synthesis as a target for antifungal drugs. *Journal of Biological Chemistry* **272**, 9809–9817.

Seebeck, T., Sterk, G. J. and Ke, H. (2011). Phosphodiesterase inhibitors as a new generation of antiprotozoan drugs: exploiting the benefit of enzymes that are highly conserved between host and parasite. *Future Medicinal Chemistry* **3**, 1289–1306.

Sibley, C. H., Brophy, V. H., Cheesman, S., Hamilton, K. L., Hankins, E. G., Wooden, J. M. and Kilbey, B. (1997). Yeast as a model system to study drugs effective against apicomplexan proteins. *Methods* **13**, 190–207.

Simon, J. A. and Bedalov, A. (2004). Yeast as a model system for anticancer drug discovery. *Nature Reviews Cancer* **4**, 481–492.

Siqueira-Neto, J. L., Moon, S., Jang, J., Yang, G., Lee, C., Moon, H. K., Chatelain, E., Genovesio, A., Cechetto, J., and Freitas-Junior, L. H. (2012). An image-based high-content screening assay for compounds targeting intracellular *Leishmania* donovani amastigotes in human macrophages. *PLoS Neglected Tropical Diseases* **6**, e1671.

World Heath Organization (2012*a*). http://www.who.int/neglected_diseases/diseases/en/.

World Heath Organization (2012*b*). www.who.int/neglected_diseases/London_Declaration_NTDs.pdf.

Wu, G. (2010). Recent progress in phosphoinositide 3-kinases: oncogenic properties and prognostic and therapeutic implications. *Current Protein and Peptide Science* **11**, 425–435.

Young, K., Lin, S., Sun, L., Lee, E., Modi, M., Hellings, S., Husbands, M., Ozenberger, B., and Franco, R. (1998). Identification of a calcium channel modulator using a high throughput yeast two-hybrid screen. *Nature Biotechnology* **16**, 946–950.

Zaks-Makhina, E., Kim, Y., Aizenman, E., and Levitan, E. S. (2004). Novel neuroprotective K + channel inhibitor identified by high-throughput screening in yeast. *Molecular Pharmacology* **65**, 214–219.